UNDERSTANDING THE PATHOLOGICAL EFFECTS OF EXOGENOUS MONOMERIC TAU PROTEIN AND THE DEVELOPMENT OF NOVEL TREATMENTS FOR ALZHEIMER'S DISEASE

Miranda A. Robbins

Department of Chemical Engineering and Biotechnology
University of Cambridge

This dissertation is submitted for the degree of
Doctor of Philosophy

Robinson College November 2019

DECLARATION

I hereby declare that my thesis entitled ‘Understanding the pathological effects of exogenous monomeric tau protein and the development of novel treatments for Alzheimer’s disease’ is the result of my own work and includes nothing which is the outcome of work done in collaboration except as declared in the Preface and specified in the text is not substantially the same as any that I have submitted, or, is being concurrently submitted for a degree, diploma or other qualification at the University of Cambridge or any other University or similar institution except as declared in the Preface and specified in the text. I further state that no substantial part of my dissertation has already been submitted, or, is being concurrently submitted for any such degree, diploma or other qualification at the University of Cambridge or any other University of similar institution except as declared in the Preface and specified in the text does not exceed the prescribed word limit.

Miranda A. Robbins

November 2019

ACKNOWLEDGEMENTS

I would like to acknowledge those who have provided theoretical, technical and moral support during my PhD research. Firstly, to my parents Barbara Sahakian and Trevor Robbins without whom I would never have entered a scientific research field, whom along with my sister Jacqueline Robbins have listened to repeated presentations and offered encouragement, support and lifelong mentorship. To my best friends Anabel Martinez, Jude Brady, Sahanika Ratnayake, Chris Valentine, and Andrew Stretton for offering laughter, relief, and spin class on a weekly basis. For mentorship, academic advice and enthusiasm I am greatly thankful to Ljiljana Fruk, Clemens Kaminki, and Ole Paulsen.

For the supervision I experienced, and openness to ideas I would like to thank my supervisor Gabi Kaminki whose attitude within and outside of the department has taught me a lot about resilience, perseverance and passion. I have also had the fortune to work with Amberley Stephens, Amanda Haack, Philippa Hooper, Chetan Poudel, Chris Rowlands, Nathan Curry, Marcus Fantham, Michelle Teplensky, Pedro Vallejo Ramirez and Olli Vanderpoorten all whom have offered me unique and excellent approaches to research that I expect to be invaluable in my future career in ways I cannot fully yet imagine.

During tough times, a quote from my 1st year daily supervisor Colin Hockings sums up the supportive attitude that has made the group a pleasure and privilege to work in for the past 3 years: *'The sooner you disprove your hypothesis the sooner we can all go to the pub'.*

ABSTRACT

Microtubule-associated protein tau (tau) is known to play a role in Alzheimer's disease (AD) through pathways resulting in the gradual formation of neurofibrillary tangles. The uptake of monomeric tau from the extracellular medium, and its aggregation at low pH inside of neurons has previously been shown by the group, but any pathophysiological effects of this aggregation remain unclear. Tau pathology has also been shown to be dependent upon synaptic activity, which hints to the role of neuronal activity in the pathway leading to toxicity. Synaptic impairment followed by synapse loss are thought to be the first points of pathology that are seen during AD and result in symptoms of memory loss.

This project aims to better understand the pathway through which aggregation of monomeric tau at low pH inside of endolysosomal compartments relates to pathology including impairment to synaptic function at the earliest stages of cytotoxicity. Through better understanding the pathways to aggregation and synaptic impairment, better therapeutic targets can be discovered. Alongside understanding tau pathology, this project aims to rescue symptoms by developing novel methods of treatment based on immunotherapies and neural stem cell prosthetics.

Through this project, a novel electrophysiological phenotype has been found. The uptake of monomeric tau taken into neurons results in an activity-dependent depression of synaptic transmission. The mechanisms through which this pathology occurs have been explored through studies investigating the relationship of tau aggregation to calcium ion concentration and different cell stimulation mechanisms. Technology including microfluidic culture chips and microelectrode arrays have been developed to further identify how tau protein affects spontaneous activity and evoked responses of neurons. Novel therapeutic methods including metal organic frameworks grafted with immunotherapy and biofunctionalised scaffolds for enhanced neural stem cell implantation have been developed. These may prove beneficial for early and late stage treatments of Alzheimer's disease.

NOVEL FINDINGS & CONTRIBUTIONS

In preparation

Omid Siddiqui**,** **Miranda A. Robbins**, Tanja Fuchsberger, Tijmen Euser, Clemens F. Kaminki, Ole Paulsen, Gabriele S. Kaminki Schierle. OptoGenie: an open-source, portable, and adaptable, optogenetic stimulation device.

- An inexpensive, open-source and easy to use method of optogenetic stimulation for use by the research community. The device can be made by proprietary components and readily assembled for use on any experimental system required. The device is ~1/10th the price of commercial systems and therefore aims to make optogenetics more accessible to researchers.

Miranda A. Robbins, Roberta Azzarelli, Venkat Pisupati, Antonina Kerbs, Sam Nehme, Roger Barker, Ljiljana Fruk, Gabriele S. Kaminki Schierle. Biofunctionalisation of bacterial cellulose for enhanced neural stem cell prosthetics.

- A fast and novel method of biopatterning coverslips
- The novel combination of BDNF and GDNF functionalisation of bacterial cellulose for use in enhanced neural prosthetics

Philippa J. Hooper, **Miranda A. Robbins**, Susanna B. Mierau, Tanja Fuchsberger, Timothy Sit, Chetan Poudel, Oliver Burton, Stephan Hoffman, Clemens F. Kaminki, Ole Paulsen, Antonio Lombardo, Gabriele S. Kaminki Schierle. Transparent graphene microelectrode array to combine electrophysiological measurements with fluorescence lifetime imaging.

- Helped to identify poly(methyl methacrylate) (PMMA) and Al_2O_3 as suitable encapsulation layers for a graphene MEA.
- Helped to show for the first time that Fluorescence lifetime imaging was achievable using a graphene MEA.

TABLE OF CONTENTS

LIST OF TABLES

LIST OF FIGURES

LIST OF COMMONLY USED ABBREVIATIONS

Ab	Antibody
AD	Alzheimer's disease
AFM	Atomic Force microscopy
AMPAR	α-amino-3-hydroxy-5-methyl-4-isoxazolepropionic acid receptors
BC	Bacterial cellulose
BDNF	Brain derived neurotrophic factor
$[Ca^{2+}]$	Calcium ion concentration
ChR2	Channelrhodopsin-2
Dextran-OG514	Oregon Green™ 514 dextran
Fab	Antigen-binding fragment
TCSPC-FLIM	Time-correlated single photon counting-Fluorescence lifetime imaging
FTD	Frontotemporal dementia
GDNF	Glial derived neurotrophic factor
IgG	Immunoglobulin G
ITO	Indium tin oxide
LTD	Long-term depression
LTP	Long-term potentiation
MEA	Multielectrode array
MOF	Metal organic framework
NMDAR	N-methyl-D-aspartate receptor
PDMS	Polydimethylsiloxane
PEDOT:PSS	Poly(3,4-ethylenedioxythiophene):poly(styrenesulfonate)
PMMA	Polymethyl methacrylate

PSD95	postsynaptic density protein 95
SV	synaptic vesicle
Tau	microtubule-associated protein tau

Compounds

EGTA	(ethylene glycol-bis(β-aminoethyl ether)-N,N,N′,N′-tetraacetic acid)
KCl	potassium chloride
NH_4Cl	ammonium chloride
OGB	Oregon Green 488 BAPTA-1

INTRODUCTION

1.1 Aim and Motivations

The aim of this project is to understand the link between the uptake and aggregation of exogenous monomeric tau by neurons and the symptoms that arise in Alzheimer's disease such as impairment to memory. This project will use these findings to develop methods of therapeutic intervention to help provide a novel and effective treatment.

1.2 Thesis structure

The introduction to this thesis discusses Alzheimer's disease (AD) and the current field with respect to the protein tau. Specific focus will be on recent literature looking at the physiological and pathological roles of tau at synaptic compartments and how this may influence synaptic activity relating to memory function. Previous work from the group looking at aggregation mechanisms of tau will also be described. The ultimate aim of this thesis, as previously discussed, is to link the aggregation of exogenous monomeric tau to pathophysiology that correlates with memory impairment seen in AD. Once better understood, this pathophysiology can then be rescued with novel treatments.

The results of this thesis can be considered as comprising of 3 main sections:

Section 1 – *Chapter 3*: Understanding the aggregation mechanisms of exogenous monomeric tau protein.

Section 2 – *Chapter 4 & 5*: Identifying a novel phenotype arising from the aggregation of exogenous monomeric tau protein.

Chapter 6 & 7: Developing novel technologies to better understand the tau-dependent pathophysiology following from Chapter 5.

Section 3 - *Chapter 8 & 9*: Developing novel therapeutic treatments to rescue tau pathology occurring in Alzheimer's disease.

Section 1, *Chapter 3* focusses on better understanding the causes and cell pathways involved in the aggregation of exogenous monomeric tau protein that is taken up by neurons. For understanding the contribution of different pathways towards the aggregation of tau, several variables are explored using fluorescence lifetime imaging to detect tau aggregation (Table 1).

Table 1 Factors predicted to have a role in the aggregation of tau. It was hoped that understanding the conditions that induced tau aggregation may help to map out pathways involved in synaptic impairment.

Variable	pH	[Ca^{2+}]	Neuronal stimulation
Hypothesis	Tau aggregation is dependent upon low pH	Increased calcium concentration increases tau aggregation	Neuronal stimulation increases tau aggregation
Method	Fluorescence lifetime microscopy Ammonium chloride Calibrate dextran lifetime sensor	Fluorescence lifetime microscopy Chemical treatment	Fluorescence lifetime microscopy Chemical treatment Optogenetics

Section 2 aims to find a pathological phenotype for tau aggregation inside of neurons treated with exogenous monomeric tau. *Chapter 4* investigates a mechanical phenotype and *Chapter 5* continues to link tau aggregation with the activity-dependence of tau pathology through electrophysiology. Hallmarks of pathology are explored from 2 diverse angles by using 'independent' cell properties as discussed in Table 2. *Chapter 6* and *7* help in the development of technology, namely microfluidic devices and microelectrode arrays, to continue with the work of *Chapter 5*.

Table 2 Pathological hallmarks of exogenous monomeric tau are investigated in Section 1. These are split into a phenotype related to mechanical changes versus a phenotype related to neuronal electrophysiology.

Phenotype	Mechanical	Electrophysiological
Hypothesis	Stiffness of neurons is decreased by tau aggregation	Tau aggregation is activity-dependent Activity-dependent impairment to synaptic function
Method	Atomic force microscopy (AFM)	Fluorescence lifetime microscopy Whole-cell patch-clamp recordings Optogenetics Microelectrode arrays
Novel technology developed	N/A	Microfluidic culture chips Optogenetic stimulation device Microelectrode arrays (contributed)

Section 3 aims to use the knowledge gained from **Section 2** to provide new and effective treatments for Alzheimer's disease (AD). Again, this is approached from two diverse angles: in *Chapter 8* using immunotherapy as an early stage treatment, or in *Chapter 9* using stem cell prosthetics as a late stage treatment, as discussed in Table 3.

Table 3. Novel therapies developed for the treatment of Alzheimer's disease based on immunotherapy and neural prosthetics.

Treatment	Metal-organic frameworks for anti-tau immunotherapies (MOF-Ab)	Biofunctionalisation of bacterial cellulose for neural stem cell prosthetics
Treatment method	Bind and remove exogenous monomeric tau protein	Cell replacement therapy with an enhanced local environment with growth factors BDNF and GDNF
Novel aspect	Therapeutic antibody grafted to a metal-organic framework (MOF-Ab)	Dual biofunctionalization onto bacterial cellulose to enhance differentiation and survival

On finishing this thesis, some areas of the project remain in progress, but key findings and future directions will be discussed in the conclusion *Chapter 10.*

1.3 Alzheimer's disease (AD) and the current field with respect to the protein tau

1.3.1 Alzheimer's disease

Alzheimer's disease (AD) is the most common form of dementia affecting 50 million people worldwide in 2018, a number predicted to triple by 2050 to affect over 152 million people. Alongside this, 25 % of hospital beds in the UK are occupied by people aged over 65 with dementia (Alzheimer's Research UK). Aging is the greatest risk factor for AD (Hasegawa et al., 1986; Evans *et al.*, 1989; Hofman *et al.*, 1991; Coria *et al.*, 1993; Gao *et al.*, 1998), which has some genetic and environmental risk factors. The pathophysiology of AD is complex and incompletely elucidated. AD is diagnosed histologically in *post mortem* by identifying 2 main forms of aggregated protein pathology. Extracellular senile plaques of amyloid-beta peptides and intracellular tangles of microtubule-associated protein tau (MAPT; tau) are both required for the diagnosis of AD. Due to these protein pathologies, the field was divided for a long time between people believing the amyloid-beta cascade versus tau pathology were causal to AD (Mudher and Lovestone, 2002).

Familial, early-onset AD (EOAD) cases and individuals with Down's syndrome have made the role of amyloid-beta apparent. In EOAD cases there is increased deposition of amyloid-beta through amyloid-precursor protein (APP) and, presenilin 1 or 2 mutations (Barton *et al.*, 1996; Lemere *et al.*, 1996; Mann *et al.*, 1996; Scheuner *et al.*, 1996). Down's syndrome represents overexpression of APP due to trisomy of chromosome 21 and results in early AD onset (Hock *et al.*, 2003). For cases of sporadic late-onset AD the main genetic risk factor is apolipoprotein-E4 allele, which is thought to act via increased production and deposition of amyloid-beta (Corder *et al.*, 1993; Schmechel *et al.*, 1993) but other lipid-transfer pathways may be involved, with membrane and synapse maintenance also being explored (Poirer, 2006). Interestingly, another allele, apolipoprotein-E2 appears to be neuroprotective (Conejero-Goldberg *et al.*, 2014).

Though there are multiple genes that increase the risk for Alzheimer's disease, these do not include mutations to *MAPT* itself, which can be mutated in over 40 locations to cause frontotemporal dementia with parkinsonism linked to chromosome 17 (FTDP-17; Desikan *et al.*, 2015; Doran *et al.*, 2007; Goedert and Jakes, 1990). Though mutant tau is not a risk for AD, high expression of tau has been shown to be detrimental, as seen in the H1 haplotype, and is a risk of AD and

Parkinson's disease (Kwok *et al.*, 2004; Desikan *et al.*, 2015). Overexpression of tau can result in its aggregation (Guo and Lee, 2011; d'Orange *et al.*, 2018a) and therefore experiments are usually designed to maintain a physiological level of tau in case overexpression induces a different aggregation pathway or results in a combination of variables not seen in AD pathology itself. Previous research from the group has found no effect of high concentration alone on the aggregation of tau *in vitro* without cellular uptake suggesting a cellular catalyst to induce aggregation even at high concentration (Michel *et al.*, 2014).

Though many questions remain unanswered about the complex genetics and the aetiology of AD, some progress in understanding the relationship between amyloid-beta and tau has been made. It has been shown that tau protein is necessary for the amyloid-beta cascade to exert its toxic effect. Tau has been shown as causal to induced neuronal excitotoxicity. Knockdown or knockout of *MAPT* rescues hyperexitability of neural networks and is neuroprotective against seizures and epileptiform activity, and reduces pathogenic outcome seen in the amyloid-beta pathway (Roberson *et al.*, 2007; Ittner and Götz, 2010; Leroy *et al.*, 2012; Holth *et al.*, 2013; Sarah L. DeVos *et al.*, 2013; Gheyara *et al.*, 2014). Recently it has been shown that tau-dependent depression of neuronal activity dominates over amyloid-beta-dependent neuronal hyperactivity. (Busche *et al.*, 2019). Support for the amyloid cascade has been put in question following the several unsuccessful high-profile immunotherapy trials that targeted the amyloid-beta cascade (Mullard, 2019). Though a recent reversed decision has suggested that aducanumab, an immunotherapy against a conformational epitope of amyloid-beta caused a dose-dependent reduction in brain amyloid and CSF phospho-Tau and may be granted regulatory approval (Biogen, Cambridge, USA).

Some research moved away from preventing amyloid-beta pathology, towards inhibiting tau pathology. The distribution and density of amyloid plaques is variable between neuropathological stages and not informative of cognitive status (Giannakopoulos *et al.*, 2003). Amyloid-beta pathology has been shown to arise preceding tau pathology and correlate with subsequent tau changes. Cognitive decline was most closely associated to tau changes (Hanseeuw *et al.*, 2019). The progression of tau between synaptically connected neurons is replicable between patients and was characterised as the 'Braak stages'. Symptoms of AD progress characteristically with disease and highly correlate with the progression of tau pathology as it invades the hippocampal formation

(Braak and Braak, 1991; Arriagada, Marzloff and Hyman, 1992a). The hippocampus is an anatomical region of the brain responsible for spatial-based learning and memory and it is one of the earliest and most drastically affected areas in AD. Impairment of this region results in the most diagnosable early symptoms of memory loss. The role of hippocampal neuron subtypes in learning and memory give them some special properties including characteristic calcium dynamics, a high degree of plasticity and synaptic remodelling into adulthood and until recent controversy (Sorrells *et al.*, 2018) it was believed a major source of adult neurogenesis (Altman and Das, 1965; Zhao, Deng and Gage, 2008; Kitamura *et al.*, 2009; Deng, Aimone and Gage, 2010). It is thought that these properties may impart the selective vulnerability of these cells at early stages of pathology whereby pathology drastically accelerates on reaching neurons in this region, particularly layer II stellate neurons of the Entorhinal Cortex (Gómez-Isla *et al.*, 1996).

1.3.2 Microtubule-associated protein tau

Microtubule associated protein tau (MAPT; tau) has long been described as a protein responsible for stabilising microtubules in the axons of neurons (Weingarten *et al.*, 1975). The conventional role of tau is as the glue that binds and stabilises microtubules in concert with other microtubule-associated proteins. Microtubule stability is important for cellular polarity and for antero- or retro-grade cellular transport of vesicles and organelles to occur. However, as the full interactome of tau was revealed, the ubiquity of tau's roles is being uncovered to connect tau with mitochondrial respiration, DNA protection, cell membrane processes, synaptic activity, and other numerous fundamental processes. For example, the binding of tau to Fyn, Src, presenilin 1, and calmodulin, in each case elicits a different function (Loomis *et al.*, 1990; Dehmelt and Halpain, 2005; Pooler *et al.*, 2012; Liu *et al.*, 2016). Tau is also present at lower concentrations in somatodendritic compartments, often considered to be related to pathological mechanisms. In the earliest stages of disease, tau is found in the somatodendritic compartment of neurons, as well as astrocytes and oligodendrocytes (Tashiro *et al.*, 1997; Ittner *et al.*, 2010; Padmanabhan *et al.*, 2019). As a single protein, the ability to bind and interact with such a diverse range of molecules, and differentiate between its roles, comes from tau's 6 splice variants post-translational modifications, and terminal truncations. 6 isoforms are present in the adult human central nervous system, though tau occurs as a larger isoform in the peripheral nervous system (Goedert, Spillantini and Crowther, 1992). Figure 1 shows the diversity of the 6 isoforms arises from alternative splicing of exons 2 and 3 as

N-terminus inserts resulting in 0N,1N or 2N as exon 3 is never inserted independently of exon 2; and exclusion or inclusion of exon 10 regions respectively resulting in 3 repeat (3R) or 4 repeat (4R) of microtubule binding repeat region (MTB) altogether providing 0N3R-, 0N4R-, 1N3R-, 1N4R-, 2N3R-, 2N4R- tau (Goedert *et al.*, 1989; M. Goedert *et al.*, 1989; Andreadis, Brown and Kosik, 1992). 2N4R-tau is a 441-amino acid protein used in this study referred to as hTau40. The N-terminus has also been found capable of binding to synaptic vesicles (Zhou *et al.*, 2017). During human foetal stages, tau is present only in its 0N3R form, however in adults the number of 3R:4R tau are equal but the 1N isoform is most common with 54% total tau, 0N as 37% and 2N as only 9% of total tau isoforms (Goedert *et al.*, 1989; Goedert and Jakes, 1990; Andreadis, Brown and Kosik, 1992). The proline-rich region and microtubule binding domain are also capable of polymerising F-actin (Fulga *et al.*, 2006; He *et al.*, 2009). Until recently the role of tau has focused on its axonal location, with other microtubule-associated proteins (MAPs), such as MAP2, having homologous roles in neuronal dendrites. Due to the multiplicity of MAPs, the knock-out of tau has shown only subtle effects on behavioural phenotypes in mice (Harada *et al.*, 1994), and it is assumed that there is some compensation between MAPs under these circumstances, at least in younger mice (Takashima, 2010). Tau and MAP2 are so evolutionarily conserved that it has been shown that a difference of only 2 amino acids prevents the incorporation of MAP2 into neurofibrillary tangles, but instead adopt a granular conformation (Xie *et al.*, 2015).

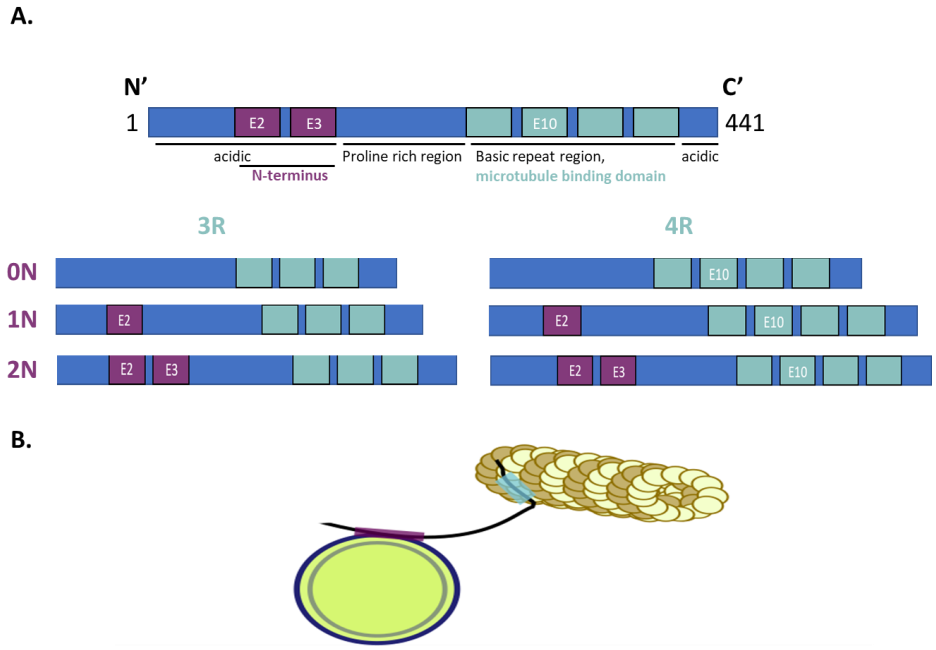

Figure 1. (A.) The basic structure of tau protein as annotated in the 2N4R (tau40) isoform of MAPT. The 6 splice isoforms vary dependent on inclusion of exon 2 and 3 (E2, E3) N-terminus regions resulting in 0N, 1N or 2N tau. The inclusion of exon 10 (E10) microtubule binding repeat results in 4-repeat (4R) tau. (B.) The N-terminus has been found capable of binding to synaptic vesicles (Zhou *et al.*, 2017). Repeats of exon E10 resulting in variations to the number of microtubule binding repeats. The repeat regions form the microtubule binding domain that also gives tau its aggregation propensity and forms the hydrophobic core of fibrillar structures (Fitzpatrick *et al.*, 2017).

Alongside the 6 isoforms of tau, truncation and post-translational modifications are other methods through which tau function is diversified. Debates about the roles of truncated forms of tau are also ongoing as to whether this is part of a physiological process of tau or whether truncation results from a pathogenic pathway that may contribute to disease pathology. A number of studies are attempting to intervene with the translocation of truncated tau between neurons to see if this inhibits the seeding of pathology. It has been shown that the major form of tau in the pre-synaptic compartment is C-terminal truncated and therefore lacking the aggregation-determining microtubule binding domain region (Sokolow *et al.*, 2015). The release of this truncated tau is increased upon synaptic activity (Kanmert *et al.*, 2015). However a study looking at changes to truncation in AD patient brain showed a relative increase in N-terminal truncation as compared with controls (Zhou *et al.*, 2018). This project uses the full-length form of human tau in the untruncated form, although it is possible that the protein is truncated once inside the cell or during cell-cell transfer. The link between phosphorylation and function, versus disease state, also remains unclear; phosphorylation of tau can occur through multiple kinases at 84 different phosphorylation sites and determines multiple functions of tau. These phosphorylation sites are also developmentally regulated, and transient phosphorylation occurs during intense periods of neuritic outgrowth and disappears during neurite stabilisation and synaptogenesis (Brion et al., 1993). Interestingly, microtubule-associated protein 1B (MAP1B) also has multiple isoforms that undergo phosphorylation, whereby the purpose of this is to alter their binding affinity for different proteins to influence the wave component in which they are targeted, and thereby velocity of transport (Ma *et al.*, 2000). This may be the case for many phosphorylation sites that may have physiological roles in some circumstances, but characterise pathological pathways when over-

represented, and change the local concentrations of tau to promote aggregation. In AD, tau appears hyperphosphorylated at characteristic locations, including Ser199, Ser202/205, Thr231 and Ser262, and these sites can therefore be used as diagnostics of paired helical filaments (PHF) formation in AD (Götz et al., 1995; Augustinack et al., 2002; Luna-Muñoz et al., 2007). It has also been hypothesised that the phosphorylation sites common to AD pathology may be part of a pathway cascade to induce conformational changes and further enzyme binding and posttranslational modification and incorporation into larger structure (Yoshida and Goedert, 2006; Noble et al., 2013). Unbound tau exposes the microtubule-binding domain sequence known to form the aggregate core, but not the 'fuzzy' terminal regions predicted to coordinate their β-sheet incorporation (Fitzpatrick *et al.*, 2017). Unbound tau is also more readily able to come into contact with factors known to be capable of inducing conformation change and aggregation including anionic lipids, fatty acids, nucleic acids, low pH, heparin sulfates, and other poly-anionic substances though the relevance of these *in vivo* are less known (King *et al.*, 1999; Barghorn and Mandelkow, 2002; Michel *et al.*, 2014). Initially, it was supposed that phosphorylation of tau that caused it to dissociate from microtubules and increase its concentration in the cytosol would correlate to the formation of insoluble PHFs, however the opposite has also been shown. Phosphorylation of tau at sites inducing microtubule unbinding can actually preclude the formation of PHFs, and are conversely protective and not pathological under these circumstances (Schneider *et al.*, 1999). The phosphorylation of tau to cause microtubule unbinding is also necessary to allow transport of cargo along microtubules where tau poses a physical obstacle for motor proteins, and therefore a balance is needed between unbinding and rebinding to prevent destabilisation (Kuret *et al.*, 2005; Ballatore, Lee and Trojanowski, 2007). The kinase-phosphatase cycle of tau must be tightly controlled to maintain axonal transport, microtubule stability, axonal flexibility by microtubule sliding, and prevent a high local concentration of unbound tau, which may promote aggregation (Ballatore, Lee and Trojanowski, 2007).

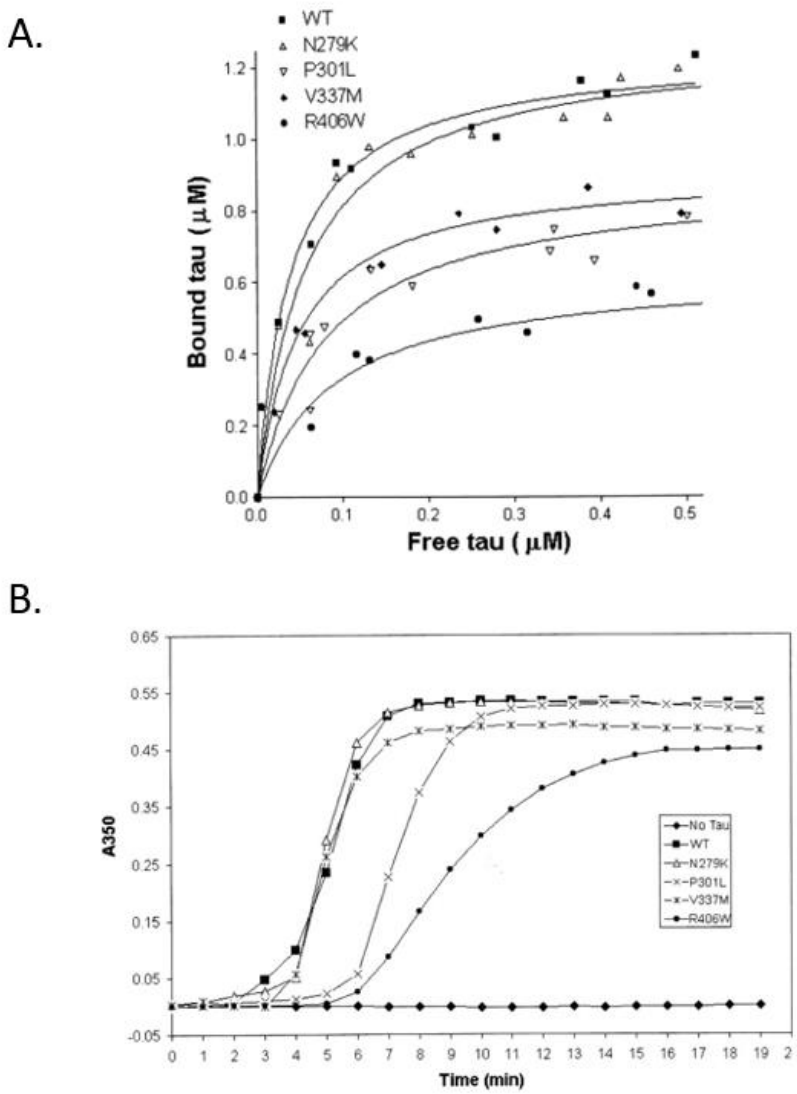

Figure 2. Mutations in tau alter its properties as a microtubule-associated protein. (A.) Mutations known to occur in FTD can result in decreased binding of tau to microtubules *in vitro*. Experiment was performed to determine bound and free tau using ^{125}I-labeled quantitative immunoblot analysis with the polyclonal antiserum to tau (17026). (B.) Missense mutations reduce the ability of tau to promote MT assembly *in vitro*. Experiments were performed using light-scattering assays. Reproduced: Hong *et al.*, 1998.

Mutant tau has also been shown to have changed affinity for microtubule binding and tubulin polymerisation *in vitro* (Figure 2; Hong *et al.*, 1998), though many of these effects are much lower in cell models (Dayanandan *et al.*, 1999; Vogelsberg-Ragaglia *et al.*, 2000). Mutations arising in

frontotemporal dementia with Parkinsonism linked to chromosome 17 (FTDP-17) are also used in models of tau pathology, including in Alzheimer's disease where mutations do not strictly occur, although there is often a large overlap between disorders (Dermaut *et al.*, 2005). Many studies in the tauopathy field use transgenic mice expressing tau with familial FTD mutations, commonly missense mutations such as P301L, P301S, V337M**,** R406W, and A152T (Tatebayashi *et al.*, 2002; K SantaCruz *et al.*, 2005; Yoshiyama *et al.*, 2007a; Warmus *et al.*, 2014; Decker *et al.*, 2016). These commonly used lines show differences in expression levels of tau protein compared to endogenous tau, different symptoms of age-dependent tau pathology, pathophysiology, synapse loss, cell death, and behavioral deficits. However, these mouse models are differentially used to show an overall correlation between neuronal dysfunction and cognitive decline with tauopathy. Alongside commonalities with FTD, tau has been shown to promote pathogenesis in the presence of mutations, or increased concentration of the pre-synaptic protein α-synuclein, the protein characteristic of Lewy bodies in Parkinson's disease. This aggregation occurs through a pathway involving phosphorylation of tau at Ser262 (Qureshi & Paudel, 2011). This close relationship of protein pathology is interesting due to 50 % of patients diagnosed with Dementia with Lewy bodies, from α-synuclein aggregates, having enough pathology for a co-diagnosis of Alzheimer's disease (Irwin and Hurtig, 2018). Along with the presence of tau with other proteins in FTD (Chornenkyy et al., 2019), it suggests perhaps there is interplay between mechanisms resulting in the aggregation of multiple proteins.

Although much focus has been put on the role of microtubule unbinding in disease pathogenesis (Hong *et al.*, 1998; Wang & Mandelkow, 2015), mutations that do not alter binding but instead affect the N-terminal hinge region of the protein so that tau loses its 'paperclip' conformation have also been highlighted. The paperclip conformation sequesters the N-terminal phosphatase-activating domain (PAD) of tau, known to be capable of activating activation of the PP1–GSK3 pathway, and inhibition of anterograde fast axonal transport (Kanaan *et al.*, 2011). Therefore, the initial location and structure of tau during pathology require further clarification. In the cytosol, tau remains as a highly soluble, intrinsically disordered protein, which gains secondary structure upon binding to microtubules. Tau is also capable of forming β-sheets in a cross-β/β-helix structure through intra-molecular interactions, as seen during the pathogenesis of AD and FTDP-17. The formation of these large fibril formations is dependent upon two hexapeptide sequences, ^{306}VQIVYK^{311} and ^{275}VQIINK^{280} in the MTB regions; though tau requires sequences outside of

these regions to form structures seen in AD as the 'K18' MTB-only sequence forms structurally different fibrils (Ganguly *et al.*, 2015; Li and Lee, 2006; Fitzpatrick *et al.*, 2017; Berriman *et al.*, 2003). In the characteristic pathway of proteinaceous pathology seen in AD, hyperphosphorylated monomeric tau forms soluble granular oligomeric structures. These oligomers are implicated as the toxic species in AD pathogenesis (Maeda *et al.*, 2006; Patterson *et al.*, 2011; Usenovic *et al.*, 2015; Busche *et al.*, 2019). Oligomers are seen as an intermediate structure capable of nucleating conformational induction of monomeric tau into stacked assembly of insoluble paired helical filaments (PHFs) that amalgamate into large neurofibrillary tangles (NFTs; Lasagna-Reeves *et al.*, 2010; Grundke-Iqbal *et al.*, 1986; Fitzpatrick *et al.*, 2017). The pathogenic versus protective role of larger, insoluble structures, that are less neurotoxic than soluble oligomers, but confine cell space and prevent intracellular trafficking as they grow in size, continues to be debated.

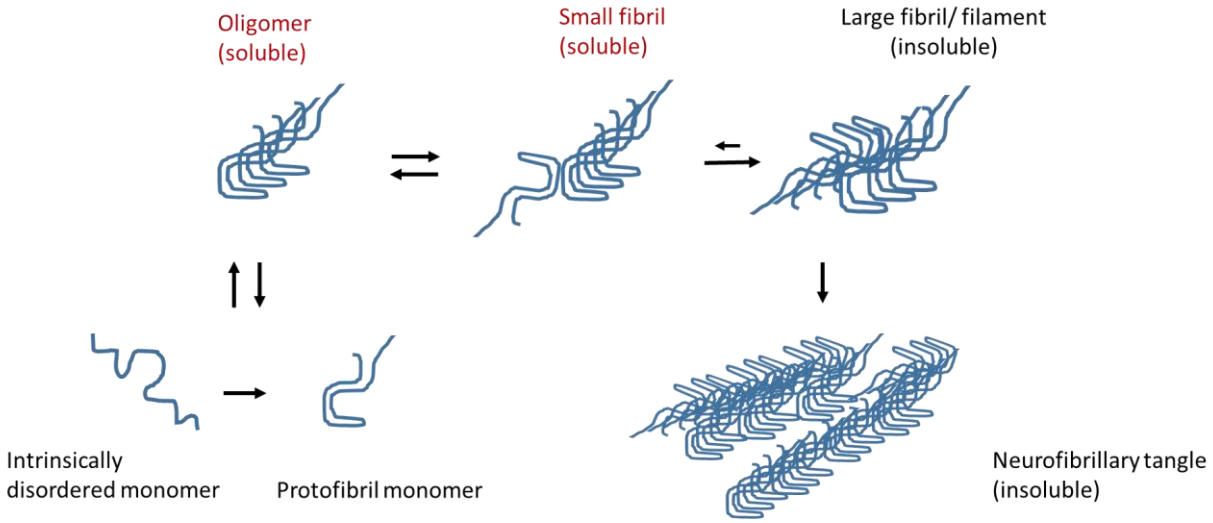

Figure 3. The formation of toxic tau multimers from monomers. Debates between which forms of tau protein are toxic have been ongoing. It is thought the soluble species of tau containing a β-sheet structure can confer toxicity. Insoluble fibrils are suggested to be protective by sequestering toxic soluble species, versus cytotoxic from invading cell space. Stages and functions of phosphorylation states are not well understood though tau is found hyperphosphorylated in neurofibrillary tangles.

Whether oligomeric tau has a functional role is still controversial, as although their formation occurs in physiological conditions, no beneficial effects of their actions have been found.

Conversely, oligomeric forms of tau have been shown to impair synaptic functioning, with synaptic dysfunction occurring as an early marker preceding fibril formation, synaptic loss, axonal retraction and cell death (Masliah *et al.*, 2001; Maeda *et al.*, 2006; Yoshiyama *et al.*, 2007b; Patterson *et al.*, 2011; Polydoro *et al.*, 2014; Fá *et al.*, 2016; Koss *et al.*, 2016). Commonalities exist between the amyloid-beta plaques and tau NFTs that are characteristic to AD. Both aggregates contain a β-sheet amyloid structure, where the monomers extend perpendicular to the fibril axis with parallel hydrogen bonding. Both proteins are thought to convey toxicity in soluble form (Kirschner et al., 1986; Fitzpatrick *et al.*, 2017). However, the location of these deposits do not clearly correlate, such that amyloid-beta plaques are found extracellularly across the brain, whereas tau NFTs are seen intracellularly and follow the defined Braak stages. How an axonally located microtubule-associated protein is able to targets synaptic function at early stages of pathology is unknown. Increasing interest is being transferred from its structural role as a microtubule-stabilising protein in the axon, to synaptic roles of tau including accelerating spine formation and dendritic elongation, and involvement in memory pathways (SantaCruz *et al.*, 2005; Sapir *et al.*, 2012; Kimura *et al.*, 2014; Zempel *et al.*, 2017).

Due to the correlation of tau pathology and symptom onset, this project aims to target the protein tau as both a protein with causal role of early symptoms in AD as well as a preventative therapeutic target. Monomeric, wildtype, human full-length tau (hTau40, 2N4R) without mimetic posttranslational modification is used. Due to the difference in fibril structure, and the fact that FTD or aggregate-prone mutants do not organically occur in AD, this study uses wildtype tau and hippocampal cells from wildtype rats or mice versus mutant tauopathy or overexpressing transgenics. Rodent neurons were deemed a physiologically relevant model. Although rodents do not develop AD or express all forms of the human tau isoforms, the same pathways for tau uptake and aggregation would exist between species. Plasticity induction protocols are the same between rodents and primates. This monomeric tau protein is added exogenously to neurons. Exogenous application could either represent the physiological release of tau from neurons that has been posited to have a role, potentially as a growth factor, and is increased upon neuronal activity (Chai, Dage and Citron, 2012; Pooler *et al.*, 2013; Yamada *et al.*, 2014; Sokolow *et al.*, 2015; Wu *et al.*, 2016). The conditions in which these mechanisms are physiological versus pathological are not yet understood. Alternatively, tau release could occur from a pathological mechanism such as lysosomal dysfunction (Mohamed *et al.*, 2015), or necrosis seen in traumatic brain injury (TBI),

which is a known risk factor for AD (Mortimer *et al.*, 1985; Roberts, 1988). In this project, exogenous monomeric tau is added to cells to question how this wildtype protein has the propensity to form β-sheet conformers and soluble multimers and fibrils that are capable of inducing synaptic dysfunction as an early hallmark of pathology. Gómez-Ramos *et al.*, (2006, 2008) showed that monomeric tau can have effects on cells through binding to M1 and M3 muscarinic receptors to raise intracellular calcium concentrations. There are fewer other studies working with wildtype monomeric tau that show any direct effects of monomeric tau on neurons, or mechanisms through which it may aggregate and result in a pathological phenotype related to symptoms seen in AD.

1.3.3 The role of pH in tau aggregation

pH-dependent effects of tau have been shown, possibly due to the protein's sensitivity to pH arising from various acidic and basic regions (Figure 1). The affinity for tau to microtubules is sensitive to intracellular pH. Acidification of the neuronal cytosol results in microtubule unbinding due to conserved histidine residues, and also increases its diffusion rate along microtubules (Hinrichs *et al.*, 2012; Charafeddine *et al.*, 2019). Much of this project is based on previous work from the group (Michel *et al.*, 2014) that has shown that exogenous monomeric tau can be taken into cells in monomeric form where it aggregates at low pH. Both full length human tau (hTau40) and the repeat region of the microtubule binding region of tau (K18 tau) were shown to be taken into cells whereby they formed sarkosyl-insoluble/SDS-soluble fractions that were able to recruit endogenous tau into aggregates. The work used fluorescence lifetime imaging measurements that were able to detect a decrease in fluorescence lifetime when tau monomers came in close contact during the formation on β-sheet aggregates (see Section 1.6.6. for detail). Michel et al., (2014) showed that in the extracellular space, without cellular uptake, tau remains in monomeric form as seen by a higher fluorescence lifetime. The protein is taken up by endocytosis, as uptake is mostly blocked at 4 °C, where it colocalises inside of vesicular markers. The aggregation is not due to high concentration alone, as 100x tau does not cause aggregation at physiological pH (7.2-7.4). However, incubation of 1x tau at pH 4.7 outside of cells for 24 hr resulted in aggregation, showing that pH is specifically responsible. The exogenous monomeric K18 tau was also capable of recruiting endogenous tau into aggregates that could be detected in cell lysate. These aggregates

were released into cell medium and when added to tau naïve cells was able to further seed aggregation of tau protein.

Figure 4. shows the hypothesised pathway through which exogenous monomeric tau is taken into cells and aggregates in endolysosomal vesicles at low pH. Aggregated tau may either recruit endogenous tau that enters endolysosomes into aggregates, or is released into the cytosol to recruit endogenous tau. From vesicles tau could be released by exocytosis, or from the cytosol from multiple methods can occur including free release.

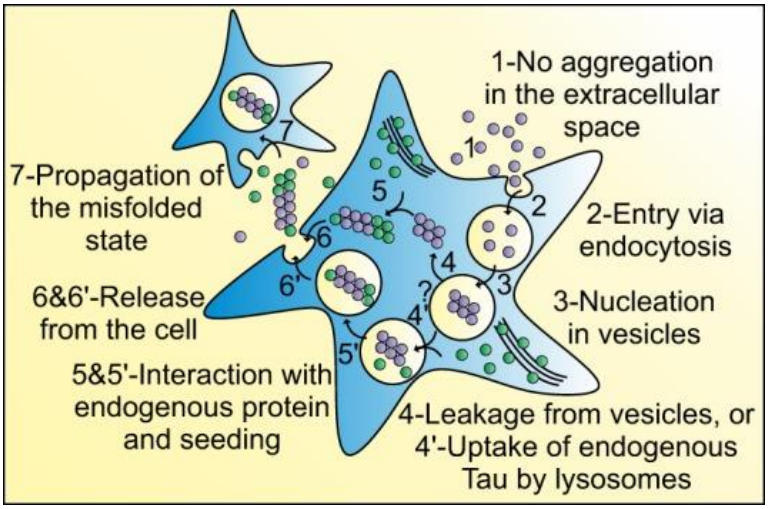

Figure 4. The model for the aggregation and trafficking of extracellular tau. Numbers show the hypothesised pathway through which exogenous monomeric tau enters cells and aggregates at low pH. Recruitment of endogenous tau could either happen inside of vesicles, or following escape into the cytosol followed by release into the extracellular space and reuptake by neighbouring cells. Reproduced: Michel *et al.*, 2014.

This work was novel as it was previously considered that tau was unable to cross the cell membrane in the monomeric form. Further studies have since confirmed the entry of monomeric tau into cells and two mechanisms have been described: 1) a fast dynamin-dependent mechanism of classic endocytosis and 2) a slow actin-dependent mechanism of micropinocytosis (Evans *et al.*, 2018).

However the timescale that tau has been shown to aggregate inside of neurons as compared with in PBS is at least 3x less (Michel *et al.*, 2014). Therefore, whether other mechanisms involved during cellular internalisation and endolysosomal transportation catalyse this aggregation are unclear, though as discussed, concentration inside of vesicles alone had been shown not to induce aggregation. For this reason, pH is explored in further detail using ammonium chloride (NH_4Cl), and a calibrated pH sensor. NH_4Cl is a weak base that is commonly used to neutralise endolysosomal compartments. NH_4Cl diffuses into acidic organelles and sequesters H^+ to form NH_4^+ causing deacidification (Boron and De Weer, 1976). However, NH_4Cl has also been shown to affect cellular calcium ion (Ca^{2+}) concentrations, and alongside this, lysosomes also contain a supply of Ca^{2+}, although less than the extracellular medium that tau will experience prior to uptake (Table 4). The loss of lysosomal pH gradient by V-ATPase inhibition or by bases such as NH_4Cl result in a drastic decrease of free lysosomal [Ca^{2+}] without further effecting cytosolic [Ca^{2+}](Christensen et al., 2002; Calcraft *et al.*, 2009; Coen *et al.*, 2012; Dickson *et al.*, 2012). Alongside this, NH_4Cl has a direct effect on cellular calcium ions, resulting in an increase of intracellular Ca^{2+} and a reduction of vesicle release (Lazarenko *et al.*, 2017). The contribution of pH and Ca^{2+} are not necessarily evident from previous studies, and whether there is a combinative effect remains unknown.

Table 4. The pH and calcium ion concentration in cellular environments.

Compartment	**pH**	**[Ca^{2+}]**	**Ref.**
Extracellular medium	7.2-7.4	~2 mM	
Intracellular, cytosol	~7.0	~100-1000 nM (resting vs activated)	(Berridge, Lipp and Bootman, 2000)
Endosome	~6.5-6.0 (early vs late)	3-500 µM (early vs late)	(Mellman, 1996; Gerasimenko *et al.*, 1998; Sherwood *et al.*,

			2007; Diering *et al.*, 2013)
lysosome	4.0-5.0	~400–600 µM	(Mellman, 1996; Christensen, et al., 2002)
Synaptic vesicles	~5.8	Assumed 2 mM-<<2 mM (early vs late) 5.4 mM in torpedo electric organ	(Israël *et al.*, 1980; Egashira *et al.*, 2016)

Key aspects of this project are therefore the understanding of the link between tau aggregation at low pH and the cellular dysfunction seen during the pathogenesis of AD, particularly the synaptic deficits that occur during the initial stages. This is important as previous studies have not shown a pathological phenotype for monomeric tau other than, as previously discussed, the addition of monomeric tau to cells results in an increase of intracellular [Ca^{2+}] due to direct tau binding of muscarinic M1 and M3 receptors (Gómez-Ramos *et al.*, 2006, 2008). It is therefore of interest whether monomeric tau can aggregate at low pH to form toxic structures. In particular, the activity-dependence of tau pathology has been clearly demonstrated (Wu *et al.*, 2016) but pathways relating this to initial aggregation mechanisms have not been established, or how this specifically leads to memory impairment. It is therefore important to understand the activity-dependent mechanisms that occur, particularly to induce plasticity in the selectively vulnerable cells of the hippocampus for the formation and maintenance of spatial forms of memory. Understanding these mechanisms may help understand the relationship between tau internalisation, aggregation, and synaptic deficits.

1.4 Activity-dependent synaptic plasticity mechanisms in the hippocampus

The lipid bilayer of a neuron is partially permeable and separates ion concentrations (charges) on the intracellular and extracellular membrane. Neurons have therefore been modelled as an RC capacitor for their ability to separate and store charge. Ion channels control the resistance of the membrane by their gating kinetics (Squire, 2012). When ion channels are open following electrical or chemical stimulation, ions flow across the membrane. As more channels open, there is an increased inward (Na^+) or outward (K^+) flow of ions which represents a decreased resistance, and increased conductance measured as a transmembrane current. The relationship between the membrane resistance (R), potential difference (V) and current (I) can be described by Ohm's law, V=I*R. The resting potential of the membrane is negative ~-70 mV; when ions pass through the membrane, across their electrochemical gradient, there is a redistribution of charges. If the distribution results in a small positive charge increase inside of the cell and a less negative membrane potential, this is called an excitatory post-synaptic potential (EPSP). If a larger positive charge occurs inside of the cell causing the membrane potential to increase above ~-10 mV, this can lead to the further opening of voltage-gated ion channels and spreading of membrane depolarisation from the soma down to the axon, known as an 'action potential'. These excitatory events are most associated with the neurotransmitter glutamate, acting at α-amino-3-hydroxy-5-methyl-4-isoxazolepropionic acid (AMPA) receptors and sometimes the concurrence of N-methyl-D-aspartate receptors (NMDARs). If negative ions enter the cell (eg. Cl^-), or positive ions exit the cell (eg. K^+), this can result in a further negative intracellular charge known as hyperpolarisation and results in an inhibitory post-synaptic potential (IPSP). These inhibitory events are most associated with the neurotransmitter γ-aminobutyric acid (GABA) and its corresponding receptors. Figure 5 shows a combination of EPSPs and IPSPs received by dendrites that are integrated in the soma. If the resulting membrane potential is below ~-10 mV there is no response, if the potential is depolarised above ~-10 mV there is a sudden opening of voltage sensitive ion channels along the axon to depolarise the entire neuron causing an action potential. Charges are redistributed back to a resting membrane potential by ATP-dependent transporters (Na^+/K^+-ATPase).

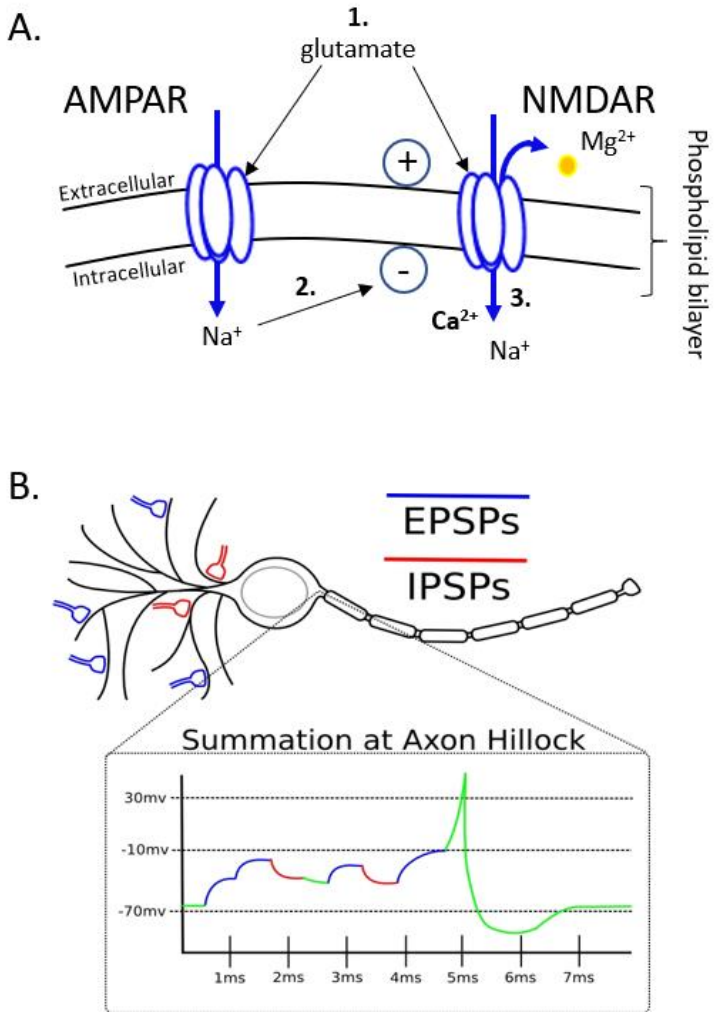

Figure 5. (A.) When activated, excitatory channels such as AMPA and NMDA receptors can result in excitatory postsynaptic potentials (EPSPs). This occurs through 1. glutamate binding and activation of AMPA receptors to allow entry of sodium ions resulting in 2. partial depolarisation of the phosphlipid bilayer that separates charged ions across the membrane until ion channels are activated. 3. This membrane depolarization releases magnesium ions blocking NMDA receptors to allow influx of calcium ions. (B.) The contribution of EPSPs (blue traces) and IPSPs (red traces) to generating action potentials (green traces). A schematic showing how excitatory and inhibitory post-synaptic potentials are integrated in the soma to result in a sub- or supra-threshold potential resulting in an all-or-nothing response from the neuron. Reproduced from: http://techlab.bu.edu.

Several factors can affect the input resistance of a neuron including the number of ion channels or the surface area of the membrane; a decreased input resistance results in a larger cell depolarisation (decreased V) for a steady current (V=I*R). A decreased input resistance is mostly determined by a smaller spherical surface area ($4\pi r^2$) but also by larger channel numbers (as determined by R_M = resistance/cm^2) as described in Figure 6.

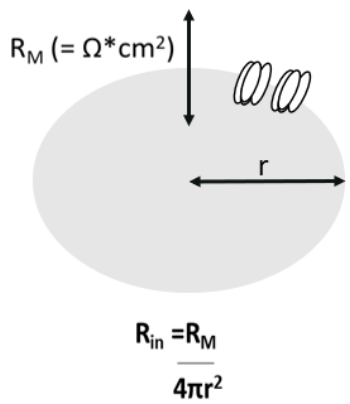

Figure 6. Factors affecting the input resistance of a neuron. The input resistance of a neuron (R_{in}) is decreased by increased ion channels (R_M) or decreased surface area ($4\pi r^2$). The smaller the input resistance the greater propensity for the depolarisation of a neuron.

Neuronal signalling can therefore occur through subthreshold (EPSP, IPSP) or suprathreshold (action potential) generation. Specific firing frequencies can also generate oscillatory activities linked with behaviour and/or signalling synaptic plasticity. Synapses were first proposed as the primary site of memory simultaneously with their discovery by Ramón y Cajal. The contribution of synaptic strengthening between pre- and post- synaptic partners was later discovered. (Hebb, 1949; Konorski, 1950). The neural basis of memory was believed to occur from long lasting responses from cells based on findings in spinal cells showing a transient increase in synaptic

conductance induced by high-frequency stimulation (Lloyd, 1949). The breakthrough occurred when Lømo (1966) discovered evoked responses to high frequency stimulation were found in the hippocampus that lasted for hours. Together with Bliss, they defined a number of properties of this activity known as 'long-term potentiation' (LTP). Key findings of this work included LTP involving an increase in both EPSP and neuronal spiking. Repeated post-synaptic firing was not necessary for LTP induction, the high frequency stimulation only evokes a population spike by the first stimulation in the series of input spikes. That LTP is input specific such that only synapses receiving stimulation can display LTP compared to unstimulated synapses of the same cell (Bliss & Gardner-Medwin, 1973; Bliss & Lømo, 1973; Bliss *et al.*, 2018). Induction of long-term potentiation can occur through several methods. A decade later, the molecular mechanisms underlying this phenomenon became discovered including the role of glutamate to bind NMDARs alongside postsynaptic depolarisation to relieve the Mg^{2+} voltage gating of these receptors (Collingridge, Kehl and McLennan, 1983; Mayer, Westbrook and Guthrie, 1984; Nowak *et al.*, 1984). Alongside LTP, its counterbalance that is induced by low frequency stimulation to decrease conduction of synapses, long-term depression (LTD), was also discovered (Staubli & Lynch, 1990). LTP and LTD have been heavily studied in the hippocampus where they coordinate spatial and declarative learning and memory (Milner et al., 1968; Mishkin, 1978; Cohen and Squire, 1980). Impairment to these forms of memory is seen as early symptoms in Alzheimer's disease, and correlate to tau pathology in the hippocampus (Braak and Braak, 1991; Arriagada et al., 1992b). The next question became what molecular mechanisms occur to maintain these enhanced synaptic responses in LTP. Though controversial, three mechanisms have consistent experimental evidence. The pre-synaptic mechanism increases the probability of neurotransmitter release by increasing the number of release sites, or the concentration of cleft glutamate. The post-synaptic mechanisms increase the single AMPAR conductance, including an increase in their mean open-time, or their opening probability on binding glutamate, through phosphorylation or exchange of subunits. Additionally, an increase channel number through insertion of receptor-containing vesicles to the plasma membrane or lateral diffusion from extrasynaptic regions can occur (Bliss & Collingridge, 2013). These mechanisms also involve cytoskeletal restructuring for stabilising synaptic densities, trafficking and tethering of required proteins and vesicles via cell membrane or recycling vesicles, and crude shrinkage or growth of synaptic volumes.

The term LTP includes a diverse range of plasticity-related mechanisms arising from multiple induction methods including tetanus-induced LTP, pairing-induced LTP, spike-timing dependent LTP and chemically-induced LTP. For each mechanism, the form through which LTP expression arises can be completely distinct, such as the involvement of particular channels, or protein-synthesis. Alongside induction methods, LTP can be induced over a range of developmental ages, different *in vitro* and *in vivo* preparations, and different anatomical networks with variations of cell subtype (Bliss et al., 2018). The hippocampus is a structurally and functionally complex formation with numerous neuronal subtypes to support its important roles in learning and memory. Multiple long-term plasticity mechanisms exist in the hippocampus, dependent upon location. A common form of plasticity involves LTP induction following high frequency stimulation causing postsynaptic activation of NMDARs or Ca^{2+} channels (Madison et al., 1991; Kauer et al., 1988). The increase in intracellular Ca^{2+} allows activation of protein kinases, such as CaMKII and PKA that instigate the phosphorylation signalling cascades required for plasticity (Lisman, 1997; Weisskopf *et al.*, 1994). Most LTP events at the CA3-CA1 synapse are NMDAR-dependent, however NMDA-independent forms of plasticity can also exist. An NMDAR-independent LTP occurs in mossy fibre axons of hippocampal dentate gyrus granule neuron synapses with CA3 pyramidal neurons; this form of LTP is induced and expressed pre-synaptically. Pre-synaptic LTP is dependent on Ca^{2+} entry at the granule cell somata, protein synthesis and microtubule-dependent fast axonal transport (Barnes *et al.*, 2010).

Experimentally, the first method discovered used high frequency (tetanic) electrical stimulation (100Hz frequency for 1-2s), which is not physiologically realistic of neuronal cells (Bliss and Gardner-Medwin, 1973). Since then, many other LTP induction protocols have been discovered commonly using other variations of high frequency stimulation to mimic burst discharges of hippocampal pyramidal neurons. A common example is theta burst stimulation using bursts at ~5 Hz frequency of the endogenous theta rhythm. This frequency blocks feed-forward inhibition via $GABA_A$ autoreceptors to result in an enhanced postsynaptic depolarization that can activate NMDARs (Larson et al., 1986). Less understood low frequency methods also exist. Alongside the physiological relevance of an induction mechanism, the limitations of the experimental procedure need to be considered. Optogenetic stimulation of neurons offers high precision for the spatial and temporal stimulation of neurons. However, for many 1st generation light-activated channels, the recovery time was too slow to respond to such high frequency light stimulation. Chemically

induced LTP is an alternative option, which though not physiologically-relevant as such, does use endogenous channel activity (For comparison of methods see Table 6.)(Aniksztejn and Ben-Ari, 1991; Hosokawa *et al.*, 1995; Musleh *et al.*, 1997; Lee *et al.*, 1998; Peineau *et al.*, 2007). The technique and stimulation protocol of inducing activity can also be important for revealing the role of the expression of specific phenotypes. For example, when investigating deficits in LTP in 12 month-old hTau, H1 haplotype, mice, a reduction in the release probability, and lack of LTP was seen from induction by high-frequency stimulation but not by theta burst stimulation (Polydoro *et al.*, 2009).

Several studies have tried to connect tau pathology with symptoms of memory impairment seen in AD. As LTP is a correlate of memory, there is much interest in whether tau has any influence on the induction or maintenance of LTP at early stages of pathology preceding stages of cell death. Figure 7. shows the processes in which tau could interfere with LTP induction; these include: channel activation or gating function for Ca^{2+} entry, calcium homeostasis, pre-synaptic vesicle cycling, cytoskeletal rearrangement, axonal-dependent synaptic transport, and post-synaptic vesicle cycling (ion channels/subunits etc.).

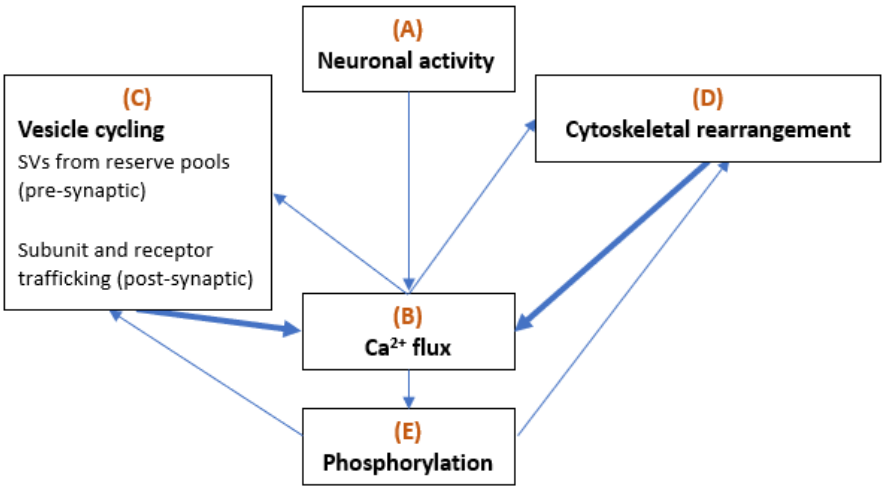

Figure 7. General factors related to the induction of long-term plasticity. Certain forms of neuronal activity result in the influx of Ca^{2+} into synapses. Ca^{2+} acts as a 2nd messenger and can result in phosphorylation-dependent signaling cascades causing structural alteration of the cytoskeleton,

the incorporation or alteration of channels and their subunits. These ultimately feedback to maintain an increased Ca^{2+} conductance. Each of these components (A-E) relate to the early stages of LTP and its induction and are discussed in terms of their links with tau pathology.

1.5 Relating tau pathology to memory impairment seen in AD

Tau has been detected at the pre- and post-synaptic compartments in human control brains where increased concentrations of phosphorylated tau are seen in AD post-mortem synapses (Fein *et al.*, 2008; Tai *et al.*, 2012). Pre- versus post- synaptic forms of pathology have been described without clear mechanistic links between the two (Ittner *et al.*, 2010; Polydoro *et al.*, 2014; Zhou *et al.*, 2017). There was originally some controversy as to whether the finding of tau in synapses is providing a healthy, physiological function, or is a hallmark of pathology. Tau inside of synaptic compartments is often associated with pathology (Ittner *et al.*, 2010; Tai *et al.*, 2012; Zempel *et al.*, 2017; McInnes *et al.*, 2018). Though a study expressing mutant P301L tau mice showed that although there was accumulation and aggregation of tau in the pre-synpatic compartment, this did not correlate to cognitive AD phenotypes (Harris *et al.*, 2012). Other papers have also shown that tau has functional roles in dendrites and synapses including dendritic growth, and pathways involved in learning and memory (SantaCruz *et al.*, 2005; Sapir *et al.*, 2012; Kimura *et al.*, 2014; Zempel *et al.*, 2017).

An obvious question for understanding the role of tau pathology in AD is whether it directly causes memory impairment, which occurs as an early symptom preceding large tangle formation and cell death to the hippocampal formation (Yoshiyama *et al.*, 2007b; Lasagna-Reeves *et al.*, 2011). Tau protein may influence the expression of the neural correlates of learning and memory, long-term potentiation (LTP) and long-term depression (LTD). Studies have also shown varying effects dependent on age, model, and protocol used when understanding how tau may alter electrophysiological properties of cells. *MAPT* knockout has also shown varied effects in plasticity such that in one study it resulted in a loss of LTD whereas LTP and basal transmission remained

unaffected (Kimura *et al.*, 2014a), and a role of tau in LTD has been previously shown (Regan *et al.*, 2015). In a different *MAPT* knockout study, the reverse was also shown, whereby short term potentiation and LTP were completely abolished without changes to LTD (Ahmed *et al.*, 2014). Endogenous tau may therefore have a physiological role in the induction or expression of long-term plasticity that interacts with amyloid-beta dysfunction. Endogenous wild-type tau expression, but not N296H FTD mutant form is required for amyloid-beta dependent impairment of LTP (Vargas-Caballero *et al.*, 2017), and impairment of LTP by tau oligomers is dependent upon amyloid precursor protein expression (Puzzo *et al.*, 2017). Table 6 shows the variability of outcome based on study method. The most consistent finding appears to be that exogenous oligomeric tau impairs LTP, with monomeric tau having no effect (Lasagna-Reeves *et al.*, 2012; Fá *et al.*, 2016; Suzuki and Kimura, 2017a). Extracellular oligomeric tau impairs memory LTP in mice (Lasagna-Reeves *et al.*, 2012; Polydoro *et al.*, 2009; Fá *et al.*, 2016; Puzzo *et al.*, 2017). Fá et al., (2016) showed a 20 min treatment of oligomeric 4R2N tau on CA3-CA1 hippocampal neurons before induction of LTP caused a marked reduction in its expression without affecting basal synaptic transmission. On the contrary, 4R1N monomeric tau did not reduce LTP. Polydoro et al., (2009) also predicted an impairment to the induction, versus expression, of LTP from their findings that high frequency but not theta burst stimulation failed to induce LTP in an hTau mouse model (Polydoro *et al.*, 2009). Another study in mice expressing mutant tau, rTgP301L mice, showed an impairment to both basal transmission *and* LTP (Hoover *et al.*, 2010) consistent with two similar studies using P301S or hTau mice (Yoshiyama *et al.*, 2007a; Polydoro *et al.*, 2009). One study has even shown improved cognitive performance and LTP in the dentate gyrus of young tau-P301L mice, and suggested hyperphosphorylation of tau as the pathogenic cause to synaptic impairment (Boekhoorn *et al.*, 2006). These results are concurrent at a behavioural level where small soluble aggregated tau species, before the formation of NFT, correlate with functional deficits during the progression of tauopathy (SantaCruz *et al.*, 2005; Berger *et al.*, 2007). Many other studies have also linked tau pathology with poor cognitive performance (Tatebayashi *et al.*, 2002; Arendash *et al.*, 2004; Ramsden *et al.*, 2005; Schindowski *et al.*, 2006; Sydow *et al.*, 2011; Van der Jeugd *et al.*, 2012), and the ability of suppressing tau expression with amelioration of symptoms (SantaCruz *et al.*, 2005; Sydow *et al.*, 2011).

Table 5. The changes to basal transmission and LTP measured in different mouse models expressing endogenous mutant, human or wildtype tau. Results show the large amount of variation

dependent upon the method but exogenous oligomeric tau consistently impairs LTP (Fá et al., 2016; Lasagna-Reeves *et al.*, 2012; Puzzo et al., 2017).

Study	**Model and tau expression**	**Basal transmission**	**LTP**
Boekhoorn *et al.*, (2006)	9-week tau-P301L mice. 2x expression level as compared with endogenous tau (controlled for in wildtype); Under Thy1 promoter.	No change	Increase
Schindowski *et al.*, (2006)	G272V and P301S (Thy22) mice. 4-6-fold expression level as compared with endogenous tau; Under Thy1.2 promoter.	Reduced	No change
Hoover et al., (2010)	TgP301L mice. ~13-fold-expression level as compared with endogenous tau; Under CaMKII promoter.	Reduced	Impaired induction
Yoshiyama et al., (2007)	P301S (PS) mice. 3-5-fold expression level as compared with endogenous tau (controlled for in wildtype); Under mouse prion (MoPrP) promoter.	Reduced	Impaired induction
Polydoro et al., (2009)	hTau mice. Expression not determined but higher than	Reduced	Impaired

	endogenous levels; Under tau promoter.		
Koch *et al.*, (2016)	Human AD patients	N/A	Impaired. Reversal of LTP toward LTD
Fá et al., (2016) Lasagna-Reeves *et al.*, (2012) Puzzo et al., (2017)	Oligomeric exogenous tau and wildtype mice	No change	Impaired
Maeda et al., (2016)	hTau-A152T mice. 3-5-fold expression level as compared with endogenous tau; Under CaMKII-tTA promoter.	Increased	No change
Decker et al., (2016)	hTau- A152T mice	Increased	No change

Although these papers did not explain a mechanism through which tau impaired the expression of LTP, Figure 7 describes cellular mechanisms involved in the induction and maintenance of early LTP. The relationship between tau pathology and these activity-dependent mechanisms will therefore be further explored in the following sections.

1.5.1 Activity-dependence of tau pathology in the hippocampus

As represented in Figure 7 (A). The release of soluble tau into the extracellular space has been shown to occur independently of cell death, but increased upon hyperphosphorylation or the expression of aggregate-prone tau (Chai et al., 2012; Karch et al., 2012) It is not known whether this soluble tau released is monomeric or oligomeric. The release of soluble tau from neurons, both *in vivo* and *in vitro*, can be regulated by neuronal activity, and is suggested to be a physiological process (Pooler *et al.*, 2013; Yamada *et al.*, 2014; Wu *et al.*, 2016). It was tested by Wu et al.,

(2016) whether neural activity could increase the rate of the propagation of pathology due to the rate of release showing activity-dependence. To test this hypothesis, cells that expressed mutant P301L hTau aggregates were stimulated with picrotoxin; approximately 45% of stimulated cells were shown to have internalised tau as compared with 20% of unstimulated cells. Similar results were seen *in vivo*, where hippocampal cells stimulated for 20 days showed greater accumulation of tau in cell bodies and hippocampal cell layer atrophy (Wu *et al.*, 2016). The study did not link increased pathology with behavioural deficits related to AD, to see whether the stimulation and tau pathology they induced also caused earlier or more pronounced symptom onset.

The interconnected relationship between neuronal activity and pathology is still in question. It is possible that there is a feedback mechanism whereby neuronal activity causes increased pathology of tau, which in turn results in impairments to neurotransmission, which feedforward to further tau aggregation and propagation etc. (Bright *et al.*, 2015) This could either be an age-dependent mechanism whereby neuronal activity over time causes pathological tau species, and their propagation. Activity could drive pathology by increased intracellular pathways that drive the formation of toxic tau species; alternatively, in our exogenous tau model, by high concentration of tau released into the medium by uncontrolled cell death or extreme secretion from hyperexcitable network activity. Alternatively, pathology could begin with aberrant tau species produced by selectively vulnerable population of cells that then alter their own electrophysiology to feedforward their rate of propagation. Both amyloid-beta and tau have shown to relate to hyperexcitability of neural, and tau has been linked to pro-convulsive effects (Roberson *et al.*, 2007, 2011; Ittner *et al.*, 2010; Holth *et al.*, 2013; S. L. DeVos *et al.*, 2013; Busche *et al.*, 2019). The high frequency of activity that occurs in the hippocampal formation due to its role in learning and memory, alongside other behaviour requiring spatial exploration, may explain the drastic advance of pathology on reaching these networks.

Although neuronal activity drives the propagation of tau species that are toxic to show an increase in tau pathology, there is no evidence that activity drives the formation of toxic species. It has been shown that neuronal activity increases the rate of transfer of tau aggregates but it is possible that neuronal activity both catalyses the toxic aggregation and rate of transfer of species to cause a pathogenic cascade effect. In this case, a key question about the activity-dependence of tau pathology is whether the aggregation of tau is an active or passive mechanism. An active

mechanism (Figure 8, A.) may relate to trafficking of proteins to synapses, plasticity mechanisms including cytoskeletal rearrangement or vesicle trafficking and could also present an opportunity for exogenous and endogenous tau to combine to cause pathology. A passive mechanism (Figure 8, B) would result from monomeric tau forming aggregates based upon the various environments that it is exposed to during extracellular uptake into endolysosomal vesicles such concentration changes in H^+ and Ca^{2+} ions. Endogenous and exogenous tau could coincidentally meet in degradation pathways. If tau conformation is affected by Ca^{2+}, this mechanism would take advantage of Ca^{2+} fluxes occurring during sustained neuronal activity in cells, and feedback to the finding that monomeric tau directly increases the concentration intracellular Ca^{2+} through binding and activation of muscarinic M1 and M3 receptors (Gómez-Ramos *et al.*, 2006, 2008).

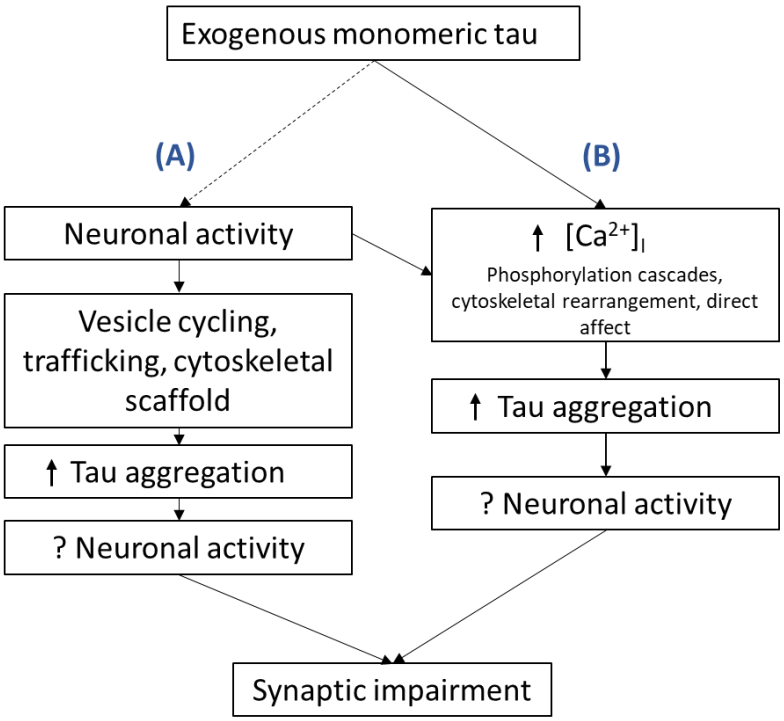

Figure 8. Disentangling the interaction neuronal activity may have with tau aggregation and the rate of pathology. A direct effect of neuronal activity on tau aggregation has not been shown, however there is an activity-dependent increase in pathology from the propagation of aggregates. The schematic shows active (A.) versus passive (B.) mechanisms that may influence the aggregation of monomeric tau protein.

1.5.2 Directly altering calcium concentrations inside of cells

As represented in Figure 7 (B). It is important to separate different aspects of neuronal activity to better understand which factors may result in an increased rate of tau aggregation inside of neurons, or whether it is solely due to an increased release of aggregates (Wu *et al.*, 2016). As previously discussed, many intracellular vesicles contain higher [Ca^{2+}] than endogenous tau would experience inside of the cytosol (Table 4). For this reason it was questioned whether increased Ca^{2+} alone, in the absence of excitotoxicity (Mattson, 1990) or an increase in neuronal activity, caused aggregation of tau protein such as through physically binding and inducing a conformational change. Following tau uptake into endocytic vesicles, the rate of vesicle cycling is dependent upon Ca^{2+} (Stevens & Wesseling, 1998; Hosoi et al., 2007) and therefore may directly affect the time tau is inside low pH compartments; this may provide the necessary time and environment to catalyse tau aggregation. Altering intracellular Ca^{2+} can therefore occur following neuronal activity or can also be artificially induced using pharmacological agents such as ionomycin, the Ca^{2+} ionophore, that has been shown to target the ER membrane causing release of Ca^{2+} stores when used at low concentrations (<1 μM) but can also affect other membranes at higher concentrations (e.g., 10 μM; Foyouzi-Youssefi *et al.*, 2000). As previously discussed, the treatment of cells with ammonium chloride has also been shown to cause the mobilisation of $Ca^{2+}$from intracellular stores. As this is a secondary effect to neutralising pH, it is worth considering the mobilisation of Ca^{2+} stores as a possible variable that influences the role of ammonium chloride to inhibit tau aggregation. Therefore, the direct effect of changing intracellular Ca^{2+} environments was considered a relevant measure for understanding the mechanisms of tau aggregation. To do this, molecules that affect intracellular Ca^{2+} stores were added to measure whether these treatments changed the aggregation of tau using TCSPC-FLIM (Section 1.6.6.). However, activity-dependent concentrations of Ca^{2+} are another consideration for aggregation mechanisms.

A key aspect of neuronal activity, particularly in hippocampal neurons that induce plasticity mechanisms, are calcium ion (Ca^{2+}) fluxes. Ca^{2+} has an important role as a second messenger inside of cells for the transformation of electrical to biochemical activity. for initiating signaling cascades including release of neurotransmitters, dendritic control of synaptic plasticity, gene

expression, and cell morphology (Katz and Miledi, 1968; Lisman, 1989; Nishiyama *et al.*, 2000; Gasque, 2015). This results in Ca^{2+} concentration fluxes that are tightly temporally and spatially regulated inside of cells to reduce undirected pathway activation. Fluxes can be specific to the level of single dendritic spines (Johenning *et al.*, 2015). Concentration of free intracellular Ca^{2+}($[Ca^{2+}]_i$) is maintained between ~10-1000 nM through potent Ca^{2+}pumps and Ca^{2+}-chelating buffering proteins such as parvalbumin, calbindin-D28k, or calretinin (Berridge et al., 2000; Schwaller, 2010). Ca^{2+} flux can arise through perturbations to $[Ca^{2+}]_i$ through release of Ca^{2+} from intracellular stores including the endoplasmic reticulum and mitochondria, or extracellular entry through voltage-gated calcium channels, ionotropic glutamate receptors, nicotinic acetylcholine receptors (nAChR), and transient receptor potential type C (TRPC) channels (Fucile, 2004; Vazquez *et al.*, 2004; Higley & Sabatini, 2008). Alongside Ca^{2+} entry into dendrites eliciting EPSPs and further Ca^{2+} release from stores, the backpropagating action potential plays an important role in plasticity and feeding back on VGCCs and endoplasmic reticulum Ca^{2+} to increase $[Ca^{2+}]_I$ in a spine-specific manner (Spruston *et al.*, 1995; Waters et al., 2005). Ca^{2+} regulation in the brain has been shown to deviate as a process of aging, which is the biggest risk factor of AD. Processes shown to be directly affected by aging include increased intracellular Ca^{2+} concentration, increased Ca^{2+} entry via voltage-dependent Ca^{2+} channels, mitochondrial buffering, and alterations of ryanodine and Ins(1,4,5)P_3-sensitive Ca^{2+} regulation, alterations to gene transcription related to Ca^{2+}signalling (Brown et al., 2004; Toescu et al., 2004; Emilsson et al., 2006; Murchison & Griffith, 2007). Tau has also been shown to cause calcium dysregulation at a systems level as well as a molecular level through the 'calcium dysregulation hypothesis' of Alzheimer's disease (Mattson and Chan, 2001; Khachaturian, 2006; Berridge, 2010). Several factors link calcium dysregulation with AD. Amyloid-beta and tau have both been shown to cause increases to $[Ca^{2+}]_i$ (Mattson and Chan, 2001; Gómez-Ramos *et al.*, 2006, 2008; Kuchibhotla *et al.*, 2008). The cells that are particularly vulnerable to neurofibrillary tangle formation are also high in NMDARs whilst proportionally low in Ca^{2+} buffering proteins, and enriched in type II calcium/calmodulin-dependent protein kinase (McKee *et al.*, 1990; Bezprozvanny & Mattson, 2008; Spät *et al.*, 2008). One study has shown a direct link between high cellular Ca^{2+} from the overactivation of glutamate receptors in hippocampal neurons, and the formation of ubiquitinated tau structures similar to NFTs (Mattson, 1990). This paper suggested a potential direct effect of large-scale calcium entry and tau aggregation, though many of the cells showed degeneration from

excitotoxicity and therefore tau aggregation may be a biproduct of cell death mechanisms rather than cytosolic Ca^{2+} directly. However, tau has also been shown to directly increase cytosolic Ca^{2+} either through binding of muscarinic M1 and M3 receptors, or indirectly by FTD mutant tau via a reduction microtubule stability. Microtubules have been shown to modulate cytosolic Ca^{2+} via voltage-dependent calcium channels (VDCC) whereby depolymerisation of MTs results in a decreased rundown of voltage-dependent calcium current (Furukawa *et al.*, 2003; Gómez-Ramos *et al.*, 2008). Neurons that are particularly vulnerable to neurofibrillary tangle formation are also rich in calcium-activated proteins, calpains, during pathogenesis (Nixon, 2003). Calpains have multiple roles and modulate further activity by selective proteolytic cleavage of signaling and structural molecules, and enzymes. Their roles are therefore diverse and include signal transduction, vesicular transport and cytoskeletal stabilisation (Nixon, 2003). However, the imbalance of their activation can tip the scale towards degeneration. Calpains can be activated by acute cell injury triggering a high Ca^{2+} influx (Bartus, 1997; Nixon, 2003). Although calpains are responsible for negotiating apoptotic pathways, during acute activation they also result in necrotic cell death (Lankiewicz *et al.*, 2000; Syntichaki *et al.*, 2002; Neumar *et al.*, 2003). During aging, calpain activation is increased, yet a further, chronic level of calpain activation occurs at an early stage of AD pathology (Saito *et al.*, 1993). mCalpain is activated before tau pathology is seen and later colocalises extensively with 'pre-tangle' granular structures, neurofibrillary tangles, neuritic plaques, and neuropil threads in brains of AD patients suggesting an early and long-term role (Grynspan *et al.*, 1997; Kurbatskaya *et al.*, 2016). Grynspan et al., (1997) conclude that early in AD, pathogenic activation of calpains that regulate kinases and phosphatases that control cytoskeletal and membrane skeletal proteins, can impair various intracellular signaling cascades including LTP and vesicular transport (Massicotte *et al.*, 1991; Nakamura *et al.*, 1992; Sato et al., 1995). Calpains have a role in clathrin-mediated endocytosis whereby they bind to membrane at coated pit regions and, following Ca^{2+}-dependent activation, facilitate endocytosis by cleavage of clathrin light chain, tubulins, and adaptins (Sato, Saito and Kawashima, 1995).

1.5.3 Tau in the synaptic endocytic vesicle cycle

As represented in Figure 7 (C). In the pre-synaptic compartment, tau has been shown capable of mediating toxicity specifically via interactions with synaptic vesicle proteins and the prevention of vesicle release. Wild-type, hyperphosphorylated, and mutant P301S tau bound the synaptic vesicle protein synaptogyrin-3 through their N-terminus with equal binding affinity (Zhou *et al.*, 2017). P301S tau binding to synaptogyrin-3 impaired vesicle release following 10 Hz stimulation over 10 minutes, resulting in decreasing excitatory junction potential (EJP) amplitudes. This reduced vesicle motility was hypothesised to occur through a mesh of immobilised vesicles formed by a crosslinking of tau and synaptogyrin-3 with F-actin networks. Tau was specifically capable of this crosslinking via its N-terminus vesicle binding domain attaching to synaptogyrin-3, whilst its proline-rich and MBD bound to F-actin networks. The reduced vesicle mobility could be rescued by knock-down of synaptogyrin-3 or depolymerisation of F-actin bundles (He *et al.*, 2009; Zhou *et al.*, 2017). Tau's effect on bundling F-actin has also been shown to cause degeneration in another study (Fulga *et al.*, 2006). The pathogenicity was therefore said to arise from the increased concentration of synaptic tau that was thought to occur due to lower affinity of P301S tau or phospho-mimetic for microtubules (McInnes *et al.*, 2018). It was suggested that in Alzheimer's disease where tau protein is wildtype, as opposed to a missense mutation seen in FTD, tau may inhibit vesicle release via hyperphosphorylation and oligomerisation of tau that may simultaneously bind multiple synaptic vesicles to restrict their motility (Zhou *et al.*, 2017; McInnes *et al.*, 2018). As mentioned (Table 5), the converse effect of tau has also been shown for vesicle release probability. The electrophysiological properties of the hippocampal formation in the 16 month mice using the Tet-OFF system to express P30lL tau in a subset of cells from the entorhinal cortex (rTgTauEC, de Calignon *et al.*, 2012) suggested an increased release probability in these cells (Polydoro *et al.*, 2014).

Alongside synaptogyrin-3, Figure 9 shows proteins that have functional roles inside of synaptic compartments, and have been shown capable of binding to monomeric tau by co-immunoprecipitation studies (Liu *et al.*, 2016). Many of these proteins appear to be related to clathrin-mediated endocytosis, and synaptic vesicle cycling pathways. The proteins have therefore been mapped onto synaptic compartments in relation to these pathways as possible physiological roles that endogenous tau facilitates. GluA2 and AMPARs are not a direct binding partner of tau, but have been added in as an indicator of a possible pathway tau modulates through its other binding partners such as PICK1.

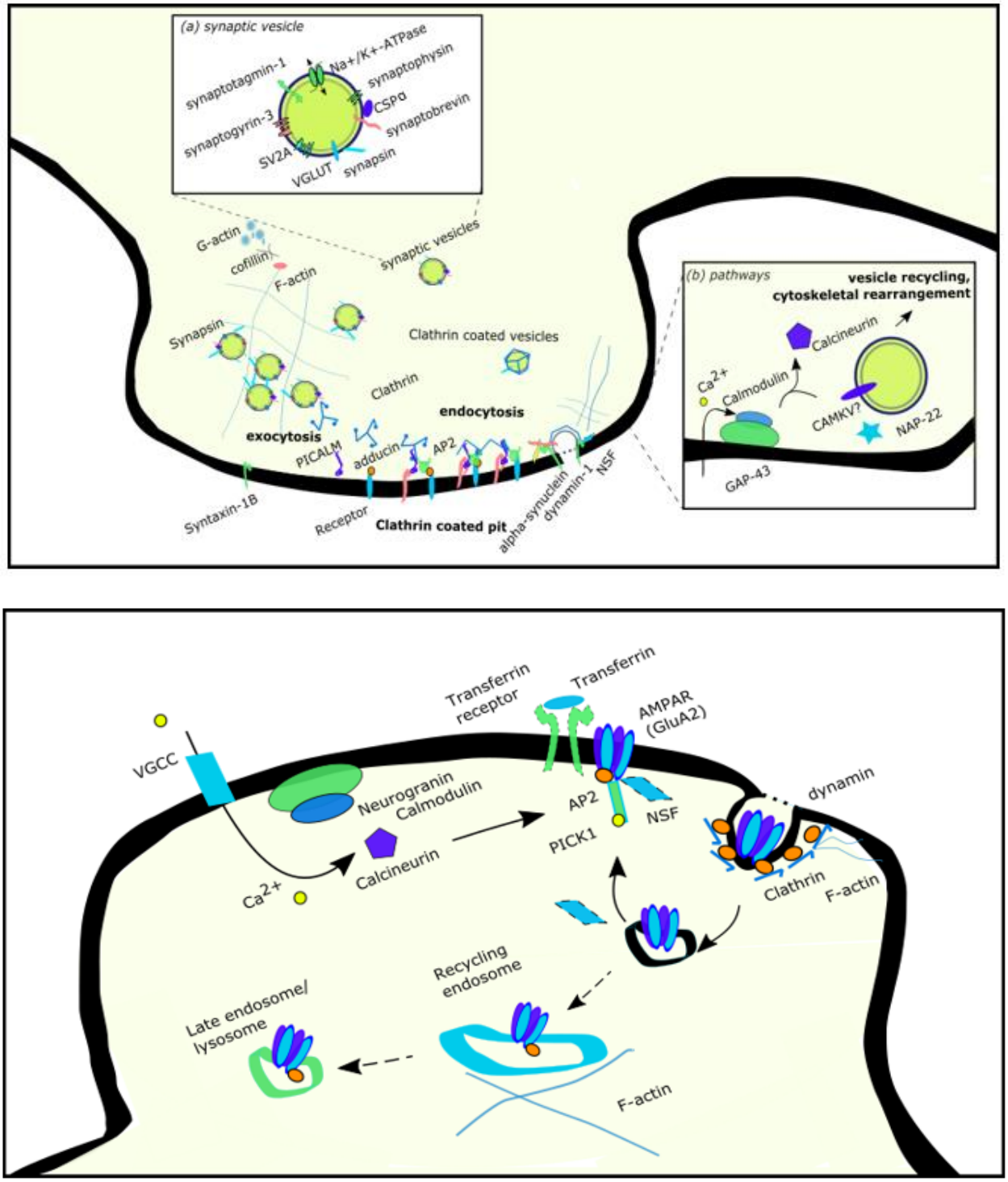

Figure 9. A schematic of possible pathways involving endogenous tau. The figure shows proteins that exist in the pre- or post- synaptic compartment and have been found capable (though not

necessarily functionally) of binding to tau. Many of these proteins appear to map to clathrin-mediated endocytosis of vesicle trafficking. Image based upon data from Liu *et al.*, 2016.

In the pre-synaptic compartment, tau has been shown to relocate to the plasma membrane, colocalised with synaptic vesicle protein, Cysteine string protein- α (CSPα), following neuronal stimulation by KCl (Zhou *et al.*, 2017). CSPα is essential for the high Ca^{2+}-sensitivity of exocytosis occurring in neurotransmission by mediating the release of anchored synaptic vesicles, but also regulates dynamin-1 binding in endocytosis (Ruiz *et al.*, 2008; Zhang *et al.*, 2012). CSP-KO has already been shown capable of inducing neurodegeneration and its decreased expression can result in synaptic deficits (Ruiz *et al.*, 2008). The role that CSP may play in tau-mediated neurodegeneration is being questioned following the finding that CSP expression is downregulated in tauopathy models at timepoints that correspond to impaired synaptic function. In these models, CSPα was also found to be neuroprotective, whereby increased expression reduced neuronal loss (Tiwari *et al.*, 2015). CSPα binds with DnaJ/Hsc70 complexes, which release tau protein from synapses in what is believed to be a physiological, activity-based mechanism (Fontaine *et al.*, 2016). Although the physiological relevance of this interaction is still not known, it will be interesting to see whether CSPα loss in tauopathies also reduces tau release, and whether this has any clear phenotype. Alongside CSPα binding, the presence of wildtype tau binding synaptogyrin-3 in control brain makes it is likely that this interaction has a role in physiological synaptic function, though the exact mechanism is still unknown (McInnes *et al.*, 2018). It is therefore of interest whether there are tau-dependent pathways that link neural activity and structural rearrangements, during synaptic plasticity, that require tau's ability to bind proteins including Fyn kinase and synaptogyrin-3; these pathways could be vulnerable during the aetiology of AD and act as a primary target for therapeutic intervention.

1.5.4 A cytoskeletal role for tau in the synapse?

As represented by Figure 7 (D)**.** The activity-dependence of the release, propagation of tau, and transport into synapses have questioned the relationship between tau protein and neuronal activity, and whether it could be a functional one under physiological circumstances (Pooler *et al.*, 2013;

Fá *et al.*, 2016; Wu *et al.*, 2016). It has been claimed that the localisation of tau in synapses is pathological and results from microtubule unbinding, either from reduced affinity from mutation (eg. FTDP-17) or phosphorylation (eg. AD)(Wang and Mandelkow, 2015). Amyloid-beta can provoke the missorting of tau in the dendritic regions to consequently cause spine loss, local Ca^{2+}-elevation, and microtubule depolymerisation (Zempel *et al.*, 2010). The translocation of tau into synapses by amyloid-beta prevents tau from being further translocated following neural stimulation, which could be detrimental to plasticity. Interestingly, from fluorescence recovery after photobleaching experiments, the dynamics of tau in spines have been shown to be variable depending on the signal for translocation of tau into synapses. Translocation, dependent on amyloid-beta oligomers, or electrical stimulation results in different turnover rates of synaptic tau, determined by specific phosphorylation sites (Frandemiche *et al.*, 2014). Different isoforms of tau have different roles in dendrite and spine formation, and it has been argued that the pathological missorting is dependent on the level of specific tau isoforms, though this may also just be driven by overexpression (Thies and Mandelkow, 2007; Zempel *et al.*, 2017). Although a small amount of tau has been detected at synapses in physiological conditions, due to the activity-dependence of tau translocation into synapses, it has been hypothesized that tau may have a supporting structural role during development and plasticity (Hoover *et al.*, 2010; Mondragón-Rodríguez *et al.*, 2012; Sapir *et al.*, 2012; Tai *et al.*, 2012; Frandemiche *et al.*, 2014; Suzuki and Kimura, 2017b). Tau has been suggested to coordinate microtubule and actin dynamics to allow structural alterations during activity. Tau could be delivered from microtubules which have been found to penetrate synaptic spines (Jaworski *et al.*, 2009; Merriam *et al.*, 2013). Tau has also been shown to bind F-actin with a physiological function (Fulga *et al.*, 2006; Yu and Rasenick, 2006; He *et al.*, 2009). A key component of plasticity is NMDAR-dependent actin rearrangement toward F-actin complex structures for modifying spine morphology (Star, Kwiatkowski and Murthy, 2002). This binding was therefore used to explain the correlation between increased synaptic tau following synaptic activity, via an increased demand for actin stabilisation. The stabilisation of filamentous actin by the drug jasplakinolide also results in a direct increase in synaptic tau (Frandemiche *et al.*, 2014). Tau is not the only MAP that has been shown to have roles in F-actin binding in the synapse; MAP1B is found in brain areas with significant activity and through F-actin binding is involved in morphological changes required for plasticity (Tortosa *et al.*, 2011). Tau has been shown to have roles on the morphology of spines in response to BDNF and can alter the size and shape of

synapses. Knockdown of tau reduced spine density in a manner that could not be reversed by BDNF, and was therefore suggested to have a vital role in cytoskeletal rearrangement following BDNF signalling (Chen *et al.*, 2012). Changes in dendritic complexity and spine morphology have also been noted in several other tau models and may be explained by tau's role in coordinating actin and acting as a scaffold for other synaptic proteins (Dickstein *et al.*, 2010; Rocher *et al.*, 2010; Chen *et al.*, 2012; Hoffmann *et al.*, 2013). The entry of tau into synapses is also thought to be connected to transporting synaptic proteins required following activity and structure, including Fyn kinase, GluA1 and PSD95 (Ehlers, 2003; Steiner *et al.*, 2008; Kessels and Malinow, 2009), following which tau may bind to F-actin.

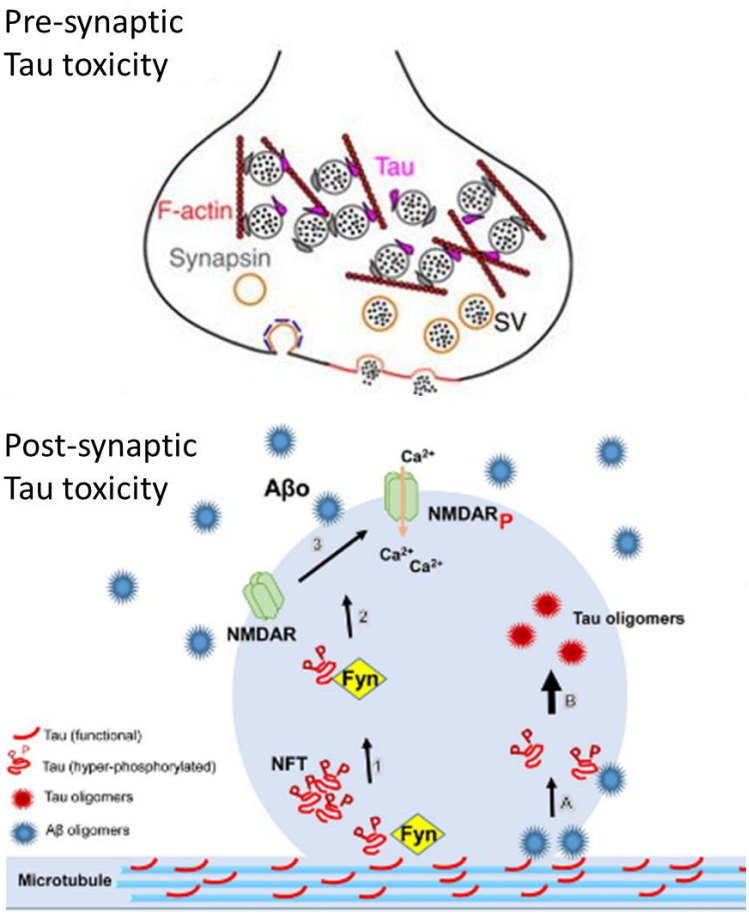

Figure 10. Examples of toxic roles tau has been shown to play at the pre- and post- synaptic compartments. A toxic role for tau protein may occur at either the pre-synaptic or post-synaptic

compartment; alternatively, a combination of these pathological effects could occur. Adapted from: Ittner *et al.*, 2010; Zhou *et al.*, 2017.

The role of tau as a post-synaptic scaffold protein has already been posed, and tau is known to interact with the signalling protein, tyrosine protein kinase Fyn (Lee *et al.*, 1998; Ittner and Götz, 2010; Ittner *et al.*, 2010). This interaction enhances phosphorylation of Fyn kinase of NMDAR subunit 2B (NR2B) to promote binding and stabilisation by postsynaptic density protein 95 (PSD-95). This has been implicated as the mechanism of amyloid-beta-induced excitotoxicity caused during AD pathology through activation of NMDARs (Salter and Kalia, 2004). Tau phosphorylation or mutation could enhance the tau-Fyn binding affinity, and thus neurotoxicity, dependent upon its MBD for entry of tau into dendrites. Conversely, tau knockout has been shown to be neuroprotective by ameliorating amyloid-beta induced excitotoxicity and causes exclusion of Fyn from the post-synaptic compartment (Ittner and Götz, 2010; Ittner *et al.*, 2010). Another recent paper has shown post-synaptic FTD-mutant tau has functional consequences through resulting in aberrant Fyn nanoclustering in hippocampal dendritic spines (Padmanabhan *et al.*, 2019b). Other studies have suggested that tau may have physiological roles in long-term depression (LTD) (Kimura *et al.*, 2014; Regan *et al.*, 2015).

1.5.5 Phosphorylation of synaptic proteins to instigate signaling pathways

As represented by Figure 7 (E). Tau hyperphosphorylation is an important step in the pathway of tau pathology. This project does not investigate the phosphorylation state of aggregated tau detected at low pH, and it is considered that phosphorylation may occur at later stages than timepoints used in our model. Therefore, links between tau phosphorylation and synaptic activity will only be briefly mentioned. Phosphorylation of tau can occur through many kinases that also have crucial roles in synaptic plasticity (eg. GSK3, CaKMII-α and PKA) (Wang *et al.*, 2005; Peineau *et al.*, 2007; Grey & Burrell, 2010; Jin *et al.*, 2015). Calpain activation or transient increases in $[Ca^{2+}]_i$ can both upregulate GSK3 activity and are thought to be linked to hyperphosphorylation (Hartigan & Johnson, 1999; Jin *et al.*, 2015). Calcineurin is the only Ca^{2+}-activated PP in the brain and responsible for regulating essential proteins for synaptic transmission

and neuronal excitability. Reduced calcineurin activity has been shown to increase extracellular phosphorylated tau (Karch et al., 2013). However, tau can be phosphorylated and unphosphorylated by dozens of kinases and phosphatases, many of which do not have key synaptic roles (Stoothoff and Johnson, 2005). Phosphorylation is known to influence tau interactions to membrane, the nucleus, axons or synapses (Mandell and Banker, 1996; Hoover *et al.*, 2010; Sultan *et al.*, 2011; Pooler *et al.*, 2012). A small amount of tau that is found in dendrites and spines under physiological conditions can be phosphorylated following NMDAR activation. This phospho-tau is able to facilitate the interaction of Fyn kinase, PSD95 and NMDARs to stabilise their position in the postsynaptic density (Götz *et al.*, 1995; Mondragón-Rodríguez *et al.*, 2012). Tau phosphorylation also has a vital physiological function inside of postsynaptic compartments to facilitate LTD via phosphorylation of residue serine 396 (Regan *et al.*, 2015). The distinct activity-dependent versus oligomeric amyloid-beta-dependent pathways through which tau can be translocated into the post-synaptic compartment are thought to be distinguished via phosphorylation profile (Allyson *et al.*, 2010; Mondragón-Rodríguez *et al.*, 2012; Frandemiche *et al.*, 2014). It has therefore been suggested that deregulated tau protein could play a role in altering synaptic function in AD, particularly through phosphorylation-dependent mechanisms that change protein interactions and synaptic scaffolding (Mondragón-Rodríguez *et al.*, 2012).

There are therefore multiple steps required for plasticity mechanisms involved in spatial memory and behaviour that could be impaired during early stages of AD by tau dysfunction. These stages have been summarised in Figure 7. and are explored in this thesis to try to relate tau aggregation with a pathological phenotype of synaptic impairment.

1.6 Methods for investigating tau pathology

Previous studies have shown that neural stimulation increases the rate of tau pathology *in vitro* and *in vivo* (Wu *et al.*, 2016), though the mechanism through which this occurs remains unknown. Alongside this, no clear relationship between the activity-dependence of aggregation to synaptic dysfunction and AD symptoms of memory impairment have been shown. This project aims to better understand the role of the uptake of exogenous monomeric tau protein by neurons and its

aggregation at low pH, to early stages of pathology seen in AD such as synaptic dysfunction (Yoshiyama *et al.*, 2007; Polydoro *et al.*, 2014). For carrying out this project a number or electrophysiological methods are employed to better understand the progression of tau pathology and neuronal dysfunction. Alongside using commercial electrophysiological technology, this project contributes towards the development of these technologies including a novel optogenetic stimulation device, and characterising optically transparent microelectrode arrays. Microscopy methods were also employed including fluorescence lifetime, and atomic force microscopy, along with colocalisation analysis on intensity imaging data.

1.6.1 A background to electrophysiology: intracellular and extracellular stimulation and recording techniques

Methods to improve electrophysiological stimulation and recordings have greatly progressed our ability to study the brain. Since the finding of the action potential (Hodgkin and Huxley, 1952), the field has discovered forms of hippocampal activity that correlate with learning and memory (Bliss and Gardner-Medwin, 1973; Bliss and Lømo, 1973), hippocampal population activity that govern forms of behaviour (Grastyán *et al.*, 1959; Vanderwolf, 1969), and hippocampal activity that allows us to sense our environment and our relationship to its space (O'Keefe, 1976). The ability to measure the electrical properties of neurons is important for understanding the most fundamental mechanisms of these processes, and developments to technology that enhance stimulation and recording methods are key to break-throughs in the neurosciences.

Controlling neuronal activity via pharmacology**,** optogenetic stimulation, intracellular electrodes, or extracellular bath or micro- electrodes is also possible. Table 7. shows a comparison of different methods that can be used to stimulate cells alongside experimental considerations for each of these techniques. There are different dis/advantages to each of these methods and therefore the choice of stimulation and recording should be based upon the requirements of the experiment. This project uses a combination of methods including chemical stimulation to better understand whether the rate of tau aggregation is specific to the pathway through which stimulation occurs such as activation of certain channel types or is nonspecific to neuronal depolarisation. Chemical methods

are compared with stimulating neurons using optogenetics, whereby a specific stimulation frequency can also be used on the order of hours. Chemical methods are less temporally precise and require wash-off which can cause damage to neurons if medium is replaced multiple times, or excitotoxicity if stimulants are left on for long time periods (Zhang and Bhavnani, 2006). Stimulation using an extracellular bath electrode for the nonspecific stimulation of all cells with high temporal precision for a short time period is carried out on a patch-clamp rig. Unlike chemical and optogenetic stimulation methods, the bath electrode requires cells to be placed on the electrophysiology rig and therefore cannot be incubated at 5 % CO_2 at 37 °C unless fresh medium is circulated and is therefore best suited for short-term experiments.

Recording of neurons is done by intracellular whole-cell patch-clamp technique, which allows single-cell resolution with high temporal precision. Characterisations of novel microelectrode technologies are also carried out for future use of optically transparent MEAs to stimulation and record from populations or slices of hippocampal neurons treated with tau protein.

Table 6. Methods to induce neuronal activity. Different methods can be used for different purposes though each has advantages and disadvantages either in its capabilities or in the practicalities of the method. Methods can be used in combination when more information is required than can be gained through one method alone.

Stimulation method	**Technique**	**Spatial resolution**	**Temporal resolution**	**Comments**
Chemical stimulation	Ion channel activators or inhibitors. Direct application of ions.	Low. Stimulates all cells in treated medium.	Low. Long-term or requires medium change. Order of seconds – minutes.	Requires no expert equipment or training. Chemicals are often inexpensive. Can target specific channels by drug used.

Electrical: **Intracellular**	Patch-clamp electrode (voltage or current clamp)	High. Single-unit stimulation or recording.	High. Electrical pulse stimulation. Stimulates and records on order of milliseconds.	Requires specialist equipment and skill. Slow as only records a single cell at a time. Limit to recording time before cell deteriorates.
Electrical: Extracellular	Microelectrode array	Medium. Stimulates populations of cells. Records cell populations; single-cell sorting of multi-unit activity possible.	High. Electrical pulse stimulation. Stimulates and records on order of milliseconds.	Requires specialist equipment and analysis pipeline. Non-invasive to cells.
Electrical: Extracellular	Extracellular bath electrode	Low. Electrode placed in cell medium and stimulates populations.	High. Electrical pulse stimulation. Stimulates and records on order of milliseconds.	Requires no expert equipment and training. Not a method of recording.
Optical: Light-induced channel activation.	Optogenetics	Medium. Populations (sometimes single cells dependent on configuration).	High. Precise optical control of stimulation. Recovery time of channels limits high frequency stimulation for conventional channels.	Requires light-activatable cells. Can require expensive or custom equipment. Often non-specific ion channel activation.

A simple and long-established method of stimulating neurons is using pharmacological agents, several of the chemicals used in the project are shown in Table 8. Chemical stimulation can occur using drugs that activate specific ion channels such as glutamate to directly activate glutamate receptors, allowing Na^+, K^+ or Ca^{2+} entry into neurons and resulting in depolarisation. Alternatively, bicuculline, an agonist of inhibitory $GABA_AR$ channels that allows entry of chloride ions (Cl^-), results in disinhibition of excitatory neurons. Other than targeting ionotropic receptors directly, altering ion concentrations can disrupt homeostasis and cause ion channel opening and neuronal depolarisation. Potassium chloride (KCl) results in two main effects including the depolarisation of neurons as described by the Nernst or Goldman equation and in parallel, an increased firing rate of cells (Holman, 1958). K^+-induced depolarisation of neurons occurs by increasing the $[K^+]_{extracellular}$, causing flow of K^+ into the cell resulting in a change in the equilibrium potential of the cell. This can also result in leakage of Na^+ back into the cell by activating some Na^+-channels. Overall, this results in more cations inside of the cell and therefore a less negative membrane resting potential. The extent of depolarisation is therefore directly related to the increased $[K^+]_{extracellular}$ (Casteels and Kuriyama, 1966); the anion (Cl^-) also has an effect as the more permeable it is, the ion can enter the cell and shift the membrane potential back towards resting potential by balancing out the cation charge (Weiss, 1975).

Table 2. Pharmacological agents used and the mechanisms through which these change cellular ion homeostasis for the depolarisation of neurons.

Pharmacological agent	**Target**	**Mechanism of depolarisation**
Glutamate	Agonist of AMPARs, NMDARs, kainite receptors. (Other secondary messenger channels not discussed)	Activation of ionotropic receptors results in nonspecific cation permeability (Na^+ and K^+, and in some cases small amounts of Ca^{2+}).
Bicuculline	Antagonist of $GABA_AR$	Disinhibition of excitatory neurons by preventing activation of Cl^- permeable

		$GABA_A$Rs and increases probability of action potential.
Potassium chloride (KCl)	$[K^+]_{extracellular}$	Entry of K^+ into cell and activation of Na^+ channels through a change in the equilibrium potential of the cell. Can result in opening of voltage-gated L-type calcium channels.

Calcium ions (Ca^{2+}) act as an intracellular second messenger following entry into neurons through multiple ion channels to transmit signals to the nucleus and regulate gene transcription. This signalling is an important property of plasticity and long-term memory pathways to initiate immediate early gene transcription (Worley *et al.*, 1993; Curran & Morgan, 1995; Johnson *et al.*, 1997). NMDARs s and L-type Ca^{2+} channels are two main Ca^{2+} channels in hippocampal neurons; these channels both transmit different signals to the nucleus following calcium influx. Ca^{2+}-entry stimulated by glutamate and bicuculline can lead to the activation of the same Ca^{2+} 2nd messenger pathways through NMDARs, however Ca^{2+}-entry stimulated by potassium chloride (KCl) has been shown to involve a distinct signalling pathway involving L-type Ca^{2+} channels (Bading et al., 1993). It is important to note that these 2 distinct Ca^{2+}-mediated pathways are not distinct in all neuron types, but is a property of hippocampal neurons (Macías *et al.*, 2001). Based on the hypothesis that Ca^{2+} may be directly responsible for the aggregation of tau, all three pharmacological methods of neuronal stimulation were used to test whether different ionotropic receptor pathways showed different effects on the aggregation of tau protein. Alternatively it could be possible that all forms of neuronal activity could non-specifically reproduce the finding of an activity-dependent rate of tau pathology (Wu *et al.*, 2016), and therefore these results would be replicated using optogenetic stimulation. A nonspecific channel suggesting that no single form of ionotropic receptor was directly responsible but an alternative mechanism occurring during depolarisation was responsible for tau aggregation (Figure 7).

Optogenetics was used in this project to stimulate cells on the order of hours, the time predicted from previous work in the group it would take tau protein to aggregate inside of cells. Optogenetic stimulation was selected over MEAs in the first instance such that cells could be plated on a

coverslip and recorded from on a patch-clamp rig post-stimulation. Optogenetic stimulation was selected over the use of the extracellular stimulating bath electrode on the patch-clamp rig as this required the devices to be placed in the patch-clamp rig during stimulation. Placement on the rig stage would require CO_2 buffering of the medium and an extra heating stage, or a continual flow of fresh cell medium which was not suitable due to the large amount of tau that would be used to keep this concentration at 1µM. Optogenetic stimulation was selected over chemical stimulation to provide specific stimulation frequencies and stimulate over long time periods without causing cell death.

For this project it was necessary to design a novel stimulation device for optogenetics that was able to be transferred between cell incubators for long-term stimulation of cells in a suitable environment, patch-clamp electrophysiology rigs for cell recordings, and optical microscopes for fluorescence lifetime imaging of tau aggregation. To make this device portable between these experimental set-ups, low cost, and flexible for stimulation area and frequency, it was necessary to design a custom device. A secondary aim of the device was to provide an open-source model made from proprietary parts such that researchers without experience with electronics and coding could easily purchase and assemble devices for their projects as necessary. The device was named 'OptoGenie'.

1.6.2 The stimulation of neurons with a custom developed optogenetic simulator device

The term 'optogenetics' was coined in the 2005 paper authored by Edward Boyden, showing the ability to excite neurons with millisecond precision using light (Boyden *et al.*, 2005; Boyden, 2011). Since then, optogenetics has become a key tool in the neurosciences that is used both *in vitro* and *in vivo* to noninvasively excite or inhibit neurons that express light-sensitive ion channels. Now multiple wavelengths of light can be used to activate a diverse number of designer proteins with different permeability and gating dynamics dependent upon the channel used (Nagel *et al.*, 2002, 2003; Govorunova *et al.*, 2015). Optogenetics using channelrhodopsin-2 works by incorporating these 7-transmembrane ionotrophic proteins into the membrane of cells such that they can be activated by blue light to allow nonspecific cation permeability (Figure 11). The light-

activation induces photoisomerisation of all-trans retinal into its contracted *cis* configuration, thereby increasing the channel size to ≈6 Å in diameter to allow ion entry (Nagel *et al.*, 2003).

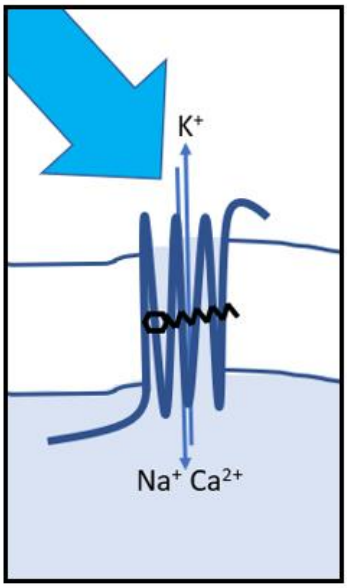

Figure 11. A schematic showing channelrhodopsin- 2 that is activated by blue light. The isomerisation of all-trans retinal causes the widening of the channel to result in nonspecific permeability to cations.

The spatiotemporal precision with which channelrhodopsins can be stimulated, and show a response, as compared with chemical and extracellular electrodes makes them highly popular for use in the neurosciences. However several further generations of ChR2 have been developed that have improve channel dynamics, such as faster gating closure time than ~10 ms of ChR2, that limits the rate of stimulation frequency that can be used, thereby preventing some tetanic forms of LTP induction (Table 8) (Gunaydin *et al.*, 2010).

Table 8. The properties and kinetics of channelrhodopsin-2. Adapted from: Lin *et al.*, 2009; Bamann *et al.*, 2008.

	Peak activation	**Light sensitivity/EC_{50}**	**Opening rate τ (ms)**	**Closing rate τ (ms)**
Channelrhodopsin-2	~470nm	~1.10 mW mm^{-2}	~0.2	~13.39 ±1.05 (for 10ms pulse)

The main limitations of optogenetic methods include the expression of the light-inducible protein by target cells, maximum stimulation frequency of ~40Hz for conventional channelrhodopsin-2 due to slow channel closing kinetics, and access to a flexible experimental set-up to achieve the full capabilities of these optogenetic models (Gunaydin *et al.*, 2010). Once DNA encoding the optogenetic gene(s) is delivered to the desired cells, the ability to activate these expressed proteins under the required experimental conditions needs to be optimised. This project contains multiple experimental set-ups for understanding the activity-dependence of tau pathophysiology including the use of a cell incubator for maintaining optimal conditions during the aggregation of tau protein, a patch-clamp rig for recording cell activity following tau treatment, and a fluorescence lifetime microscope for measuring the aggregation of tau protein. To be able to effectively combine these diverse experimental methods to provide an integrated understanding about the links between neuronal activity, tau aggregation, and synaptic impairment, a novel stimulation device was designed.

Although there are commercially-available devices on the market that can stimulate cells on a specific experimental set-up and wavelength of light, none offer portability, adaptability of activation area and frequency, and low cost (< £1000), within one device. Therefore, many labs take it upon themselves to design their own stimulation device on a per-experiment basis, however this often requires electronics expertise, prototyping costs and significant time to design and characterise the device. We therefore designed a device with the three key aims: (1) accessible: inexpensive and easy to assemble by researchers across all disciples to build from commercially

available components, including many that are common to laser laboratories (2) portable: flexible to use between incubators, electrophysiology rigs and optical microscopes such that the device can be passed between collaborators at multiple departments (3) adaptable: accommodating to researchers' needs so that alternative laser diode wavelengths, stimulation area or stimulation frequency can be used.

For demonstrating these three design aims, we look at common experimental set-ups in which highly precise neuronal stimulation may be commonly required. The optogenetic stimulation device was designed for the optical excitation of cells between: an incubator for long-term stimulation, on a patch-clamp rig, on an optical microscope for simultaneous stimulation and imaging, or microelectrode array device for cellular recordings.

Experiments requiring stimulation on the order of hours, or during long-term treatment in a protein or drug may need to occur within a maintained environment. Stimulation over a long period of time may therefore require cell incubator such that the humidity, temperature and partial pressures of gases do not perturb the cell physiology. These factors themselves can alter the electrophysiological properties of neurons and therefore if not tightly controlled can add variables to the experiment. For many commercial designs it is not convenient to transfer cells into and out of incubators whilst maintaining stimulation as required. This was therefore a primary consideration for the design of OptoGenie such that the device could be easily sterilised, placed onto a shelf and powered using a battery inside of a closed incubator.

In addition to incubation, many experiments looking at activity-dependent mechanisms will combine excitation with optical microscopy to detect fluorescent markers. This device can be easily placed onto any inverted optical microscope for simultaneous stimulation and imaging. This may be of use for combining neuronal excitation with calcium imaging, tracking of vesicles or proteins, or fluorescence lifetime measurements of protein aggregation.

Due to the broad range of experiments OptoGenie is intended to be suitable for, flexibility of stimulation between multiple experimental systems whilst reliably maintaining high temporal and spatial activation precision is vital. The OptoGenie's output intensity can be calibrated on an electrophysiology rig to measure the required intensity for cell stimulation before transferring the device to alternative set-ups. This is important to determine for each ChR2-expressing model used

as variation will arise between different transgenic lines, virally infected cells, and within different culture preparations of the same model. Differences in ChR2-expression will affect sensitivities to light stimulation. Although stimulating at the maximum intensity for each preparation is possible, this could result in toxicity when using long-term stimulation protocols. Therefore, as a first step it may be necessary to record the response to increasing light intensities until the minimum activating intensity is found. For this, the OptoGenie device can be easily mounted to a patch clamp set-up for adjustment of stimulation parameters to ensure repeatable action potential firing of neurons. Once the intensity and stimulation pattern parameters are validated, the programmed Arduino can be reliably used on any required experimental set-up including incubators and optical microscopes over a timescale of several hours, days, or weeks. Alternatively, researchers may be interested in using microelectrode arrays or patch-clamp electrophysiology to record from the neurons that are optogenetically stimulated. The ability to quickly change the excitation angle of the laser, spot size, and intensity of the light make OptoGenie easy to position onto a patch-clamp rig in any available space in the set-up.

Although experiments using a cell incubator, optical microscope of electrophysiology rig can occur in unison, OptoGenie offers the integration of these methods such that measurements can be done with this single device.

Optogenetics is an incredible method for stimulating cells with high spatial and temporal precision, however for recording responses from neurons it must be used in combination with another method. For recording the intracellular electrical responses from single cells whole-cell patch-clamp electrodes are most commonly used; for extracellular recordings of the activity from populations of neurons microelectrode arrays are an efficient method.

1.6.3 Whole-cell patch-clamp recordings

The electrochemical gradient across the neuronal membrane can be measured directly with an intracellular electrode that records the membrane potential. Whole-cell patch-clamp recordings are a highly sensitive intracellular method of measuring the currents of ion channels across the entire plasma membrane of a single neuron (Hamill *et al.*, 1981). The whole-cell method provides a tight

seal between the cell membrane and the electrode to result in minimal ionic leakage, and as such has become the most popular patch-clamp technique (Marty and Neher, 1995). Before this method was developed in the 1980s, previous 'sharp' microelectrodes formed seals between cells and the electrodes with lower resistance in the megaohms due to leakage at the seal site. The high giga-ohms resistances (10-100 GΩ) formed by suction inside of the pipette to rupture the patch membrane resulted in mechanically stable, tighter "giga-seals" which reduced the background noise of the recording by an order of magnitude (Sigworth and Neher 1980). The high resistant seal between the electrode and membrane allows even small fluxes from EPSPs to be resolved.

Figure 12 shows the set-up of the patch-clamp recording instrumentation. The intracellular electrode is composed of thin glass with a wide (~1-2 μm) tip, and therefore lower access resistance and noise level than previous sharp electrodes (Brette & Destexhe, 2012). The other end of the electrode contains a metal (usually silver) wire that works as an electrode with the electrolyte solution by exchanging electrons for ions. The wire is connected to the amplifier that measures the potential of the electrode relative to the reference electrode or can inject current into the cell. The amplifier is then connected to other electronic equipment e.g. an oscilloscope and computer to record the measurements or send commands such as controlling the current injection.

The standard procedure for whole-cell patch-clamp is as follows: 1) patch-clamp micropipettes are prepared and filled with a high-K^+, low-Ca^{2+} solution and pressed into contacted with a cell as detected by impedance changes. 2) to form a membrane seal at the point of contact a negative voltage below bath potential is applied to hyperpolarise the pipette and suction pulses are applied inside of the pipette. This causes rupture, or 'break-in' of the cell membrane at the patch site to form a direct connection between the inside of the pipette and the cytosol. Alternatively to suction, a voltage 'zap' can also be used to perforate the membrane and result in break-in of the cell (Figure 12)(Marty and Neher, 1995). At the time of rupture, a large increase in capacitive transients can be seen; the large increase in capacitance is due to contribution of the cell membrane capacitance to the recording now that the pipette is in connection to the cell. The high seal resistance allows high-resolution picoamp current measurements or application of voltages across the membrane. Recordings can then be taken over ~1 hr before cells begin to show signs that the cell's health is deteriorating.

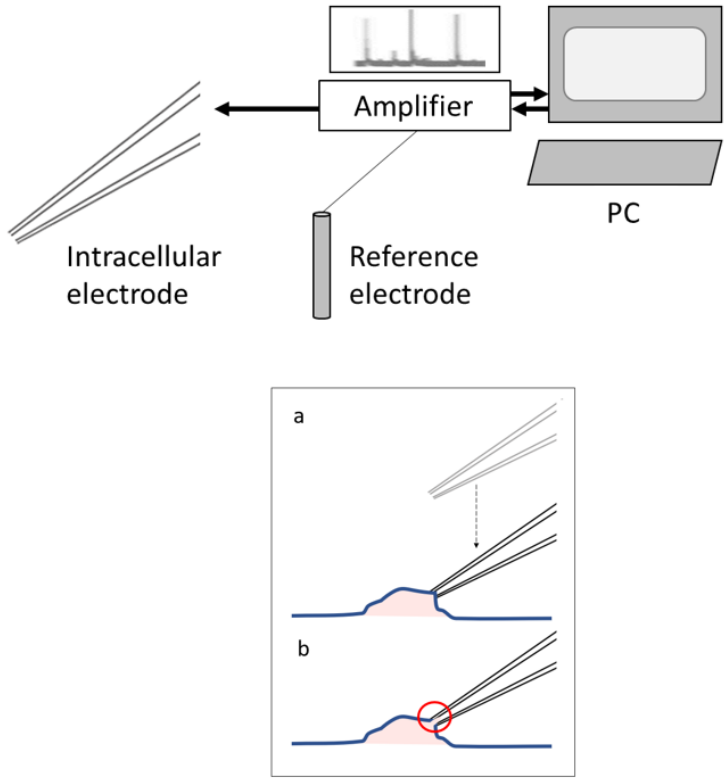

Figure 12. The set-up of the patch-clamp recording instrumentation and procedure. Top: configuration between the intracellular electrode with the amplifier and PC for recording cellular activity. Bottom: Schematic showing the stages of whole-cell patch-clamp technique. (a) 'giga-seal' formation when the patch-pipette is lowered to a cell of interest and the membrane at the pipette tip is puckered into the inside through negative pressure inside of the hyperpolarized pipette. (b) 'break-in' of the cell through a hyperpolarizing voltage applied to the pipette and pulses of suction until the membrane is ruptured such that the intracellular solution of the pipette is in direct connection to the cell cytosol.

Once contact has formed between the pipette and the cytosol, the cell measurement can be through 1-of-2 methods: voltage-clamp or current-clamp. Voltage-clamp causes the pipette potential to extend into the cell and clamp the plasma membrane to a constant voltage to study ionic currents across the membrane and through the intracellular electrode. Current-clamp mode can inject current through the amplifier and intracellular electrode into the cell for measurement of membrane potential changes such as for action potentials.

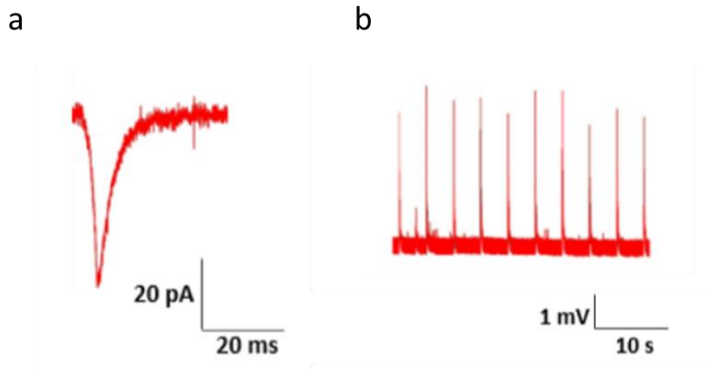

Figure 13. A comparison of voltage-clamp and patch-clamp recordings. (a) A single EPSP recorded in voltage clamp mode. (b) a sequence of EPSPs recorded in current clamp mode.

Whole-cell patch-clamp is the gold standard in electrophysiology for measuring the electrical activity of single neurons, particularly due to its capabilities to measure subthreshold events. In some studies, however, it is desired to record from populations of neurons over longer periods of time. For larger populations of cells, or recordings over the period through which the cells remain viable by using patch-clamp (>~1 hr) microelectrode arrays may be used to record action potentials and network activity.

1.6.4 Microfluidic culture chips

An introduction to microfluidic chip design and application

Soft lithography methods using polydimethylsiloxane (PDMS) are popular for cell culture chips as they can be made gas permeable, transparent, inexpensive, biocompatible and allow increased environmental control of cell culture conditions (Whitesides, 1998). The production steps of PDMS microfluidic chips are conducive to prototyping as during the design stages many iterations can be screened quickly and with relatively low financial expense. Figure 14 shows the stages of microfluidic chip design and fabrication. Initial designs are made using computer-aided design software which are printed to-scale onto a photomask. The mask is then aligned to a silicon wafer that has been coated in the negative photoresist SU-8 and exposed to UV. Depending on the desired

height of the features in the design, different SU-8 series and spin coating speeds are used. The SU-8 features that were exposed to UV remain crosslinked on the wafer following baking and development, whilst unexposed SU8 blocked from UV by the photomask is dissolved during the development process. The silicon wafer with SU-8 features now acts as a 1-layer master-mould for the microfluidic chips. The process must be repeated if multiple feature heights are required, with the smallest features on the bottom layer and taller features on layer-2 etc. This project, and the commercial Xona Microfluidic chips utilise 2-layers to allow the microchannel height to be thinner than cell bodies but the cell compartments to be larger (Figure 14). To make the chips, PDMS with curing agent are poured over the moulds and left to harden. Devices are then cut out and details such as cell compartments are cut or punched out from PDMS. The chip is then irreversibly plasma bonded to a glass coverslip and immediately coated with cell adhesion factors (ie. Laminin, poly-L-lysine) and kept moist until cell plating to prevent hydrophobicity of PDMS reoccurring. The gas permeability of PDMS, allows O_2 and CO_2 exchange during cell culture. Microfluidics, the ability to control microliter quantities of fluids, became popular for multiple reasons including the ability to investigate concentration gradients, pattern cells, and create fluidic isolation (Rhee *et al.*, 2005; Millet and Gillette, 2012). This is commonly done through a combination of microchannels connecting to small adjoining compartments that either store or mix solutions.

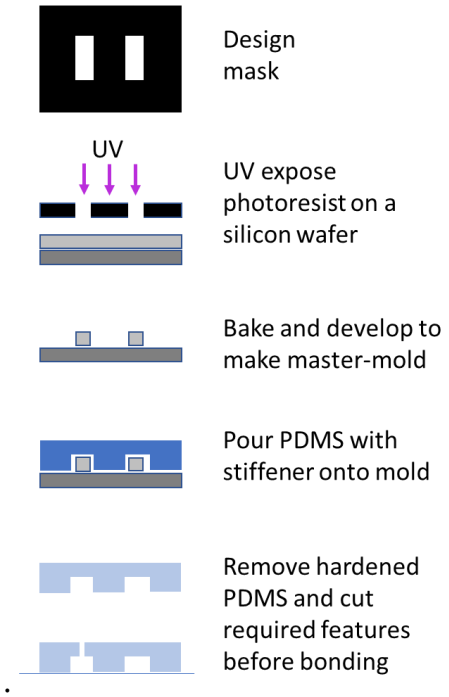

Figure 14. The stages for fabrication of PDMS chips from silicon master moulds. A photomask is designed using computer-aided design software. The mask is then used to expose specific regions of negative photoresist to UV light. Regions exposed to UV crosslink to result in microscale features following baking and developing. PDMS can then be added to the mold to make chips, which can be irreversibly bonded to coverslips for culturing cells to use for imaging or electrophysiology.

A popular commercial microfluidic device used for culturing neurons was developed by Xona Microfluidics that contains two compartments to plate cells, connected by microchannels (Figure 15). The devices consist of two layers (two-layer device) such that the microchannels are thinner than the cell reservoirs; in addition to this, cell plating wells are punched out of PDMS to pipette cells and medium during device plating. The microchannels are too thin for entry of cell bodies and are too long (>250 µm) for growth of dendritic protrusions but allow growth of axons through to connect the cell reservoirs. The microchannels also ensure fluidic isolation between the two cell

compartments through hydrostatic pressure difference when the compartments are filled to different volumes creating backflow from the higher to lower volume compartment (Figure 15).

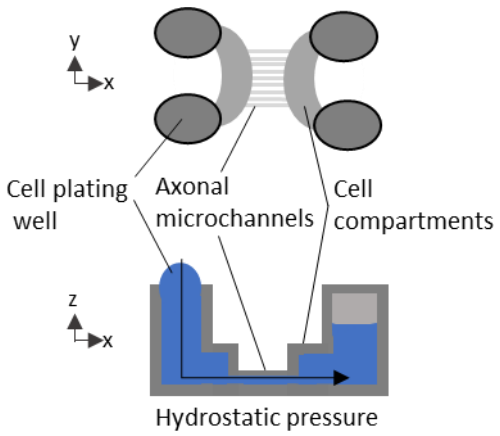

Figure 15. A schematic of the commercial Xona Microfluidics device. Fluidic isolation is achieved by adding more media in one of the reservoirs and the resulting higher hydrostatic pressure.

Fluidic isolation can be used to add a protein, or chemical treatment, to cells in one (smaller volume) compartment but prevent it from having a direct effect on cells in the 2nd (larger volume) compartment other than through contact with treated cells in the compartment-1. For better understanding the spread of aggregated tau, it is possible to treat cells in the 1st compartment with exogenous monomeric tau and observe its transport via axons to exogenous-tau naïve cells in the 2nd compartment. It is also possible to use fluidic isolation to test the phenotypic effect of the protein or drug on a single population of cells.

This project therefore aims to design microfluidic neuronal culture chips that can be used for fluidically isolating two populations of cells whilst performing patch-clamp electrophysiology. Three applications of these devices to understand the link between the uptake and activity-dependence of tau pathology have been mentioned as future aspects of this project.

For combining of microfluidic culture chips with patch-clamp electrophysiology, multiple design constraints must be considered. The chip design by Xona Microfluidics are not suitable for patch-

clamp electrophysiology due to a layer of PDMS that covers the cell compartment and therefore prevents access by patch-clamp pipettes. Figure 16 shows a mapping of the design constraints involved. The height of the device is limited to <2 mm due to the working distance of the dipping objective that is used for bringing the patch-pipette into contact with the cell membrane. The compartment length and width are determined by the angle required for the patch-clamp pipette to access cell bodies. The manipulator angle used on the rig was 22° with the possibility of increasing to 28° if required. The calculated width for the cell compartment was therefore 5 mm, however 6 mm was chosen to allow experimental room for error, allowing the manipulator to theoretically achieve access from 18° if required. The final requirement was the overall size of the chip to be ~ 2 cm x 2 cm to fit on the stage of the patch-clamp rig. The length of the cell compartment was designed to be 8 mm to allow an increased cell area and medium volume of the chips whilst maintaining ~6 mm of PDMS around the features to aid bonding onto coverglass. Alongside this, it is important that the evaporation of cell medium is considered since the volumes in the chips is small and the compartments have a large, exposed surface area.

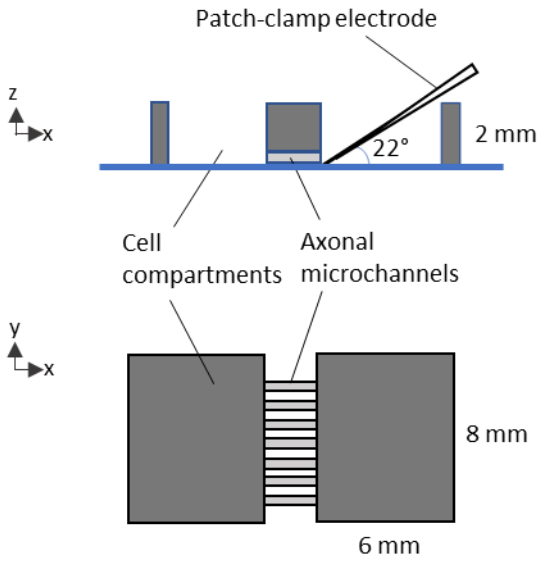

Figure 16. Constraints for the design of microfluidic chips for patch-clamp electrophysiology. The access angle of the patch electrode and working distance of the dipping objective limited the geometry and height of the cell compartments.

Synaptic activity is an important aspect of neuronal function, and as such, electrophysiology is a key tool in the neurosciences. The ability to stimulate and record from cells is important for this study as tau release and pathology have been shown to be related to neuronal activity (Pooler et al., 2013; Wu et al., 2016), and many hallmarks of pathology can be measured by recording neuronal activity. Figure 17 shows three applications for this project and its future directions requiring the ability to simultaneously stimulate and/or record from neurons whilst maintaining fluidic isolation. a) adding exogenous monomeric tau protein to cells in compartment-1 in the presence of optical stimulation whilst whole-cell patch-clamp recording cells in compartment-2 to detect any alterations to synaptic activity (Figure 17, a). b) screening the efficacy of therapeutic antibodies on cells in compartment-1 to rescue electrophysiological deficits following on from a) (Figure 17, b). c) plating neurons in compartment-1 and adding tau protein to compartment-2 to see whether pre-synaptic compartments are capable and sufficient for uptake and aggregation of tau. This can be repeated with optogenetic stimulation to determine whether this increases synaptic uptake of tau (Figure 17, c).

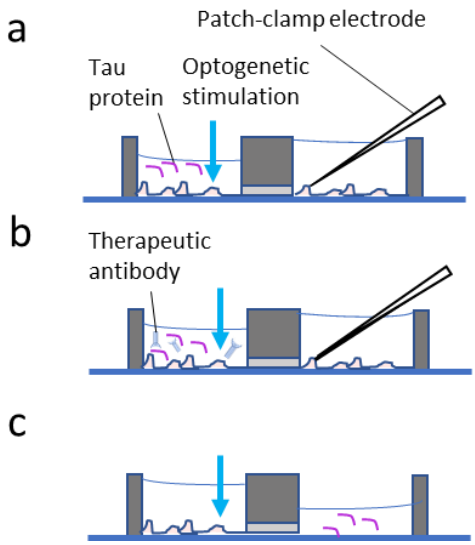

Figure 17. Possible experimental methods developed from this project that require the combination of fluidic isolation by the microfluidic chips and/or patch-clamp recording. Applications requiring electrophysiological recordings include a) recording of tau naïve cells that are fluidically isolated from tau treated cells receiving optogenetic stimulation to understand how this effects synaptic

communication. b) recording of neurons as in a) whilst tau treated cells receive therapeutic antibodies against exogenous monomeric tau. C) cell bodies receive optogenetic stimulation whilst presynaptic protrusions in a 2nd, fluidically isolated compartment are treated with tau and imaged to detect tau uptake.

1.6.5 Microelectrode arrays

The characterisation of custom developed optically transparent multielectrode array devices for improved simultaneous neuronal recordings and FLIM

An alternative method of measuring the activity of neurons is using microelectrode arrays (MEAs). This is a non-invasive method to record from multiple neurons over longer time periods. MEAs are an arrangement of electrodes (typically 60) placed equidistance apart to allow recording and stimulation at multiple sites of contact with a neuronal culture. As extracellular medium is conductive to the flux of ions from cells, and the resistance of the extracellular space is non-zero, a small voltage can be measured as results from Ohm's law (V = I*R). As MEAs are an extracellular method, they record the flux of ions as they are released from (source) or taken into (sink) cells. The measured voltage is therefore also inverse of intracellular recordings as it measures the opposite flux of ions. These extracellular effects occur on two timescales. The voltage changes occurring from the extracellular measurement of action potentials occur on fast (EAP; 300-3000 Hz) timescales and network oscillations of cell populations resulting in slower local field potentials (LFP; 1-300Hz). Figure 18 shows a comparison between the low pass (LFP + EAP) and high pass (EAP) filtered MEA trace as compared to the intracellular trace for the same cell. Although MEAs, as compared to intracellular patch-clamp recordings, can measure oscillatory rhythmic population activity, their signal-to-noise for action potential measurements is lower than intracellular recordings as they are not recording from single cells in direct seal with the cells.

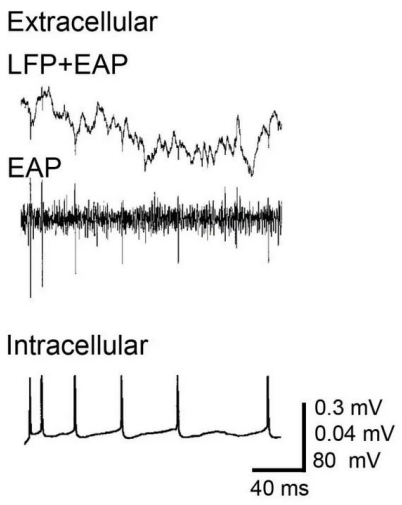

Figure 18. A comparative trace from the extracellular or intracellular recording of a cell. The extracellular trace can be low pass (top) or high pass (middle) filtered depending on the signal of interest. The intracellular trace (bottom) shows higher signal-to-noise but no population information. Reproduced: Henze *et al.*, 2000.

An MEA set-up requires four main components. The signal generator (cells), the biosensor (MEA), a filter amplifier and the recording hardware (MEA2100-Mini in this study), and software (MC_Experimenter, Multichannel systems, used in this study). The interface with the signal generator (cells) and electrode is an important consideration due to the small voltage that occurs in the extracellular space, a high signal-to-noise is required to detect lower activity levels (Multichannelsystems.com). As such MEAs with improved signal detection are constantly being developed and improved upon.

Figure 19 shows a schematic of neurons growing on a microelectrode array device. Neurons grow across the insulating layer that encapsulates the leads connecting the electrodes to the amplifier. Neurons can also grow on the conductive electrode layer where electrical activity can be stimulated or recorded from. A reference electrode is not used for stimulation or recording of cells but maintains a stable potential. At the far sides of the device are conductive pads that join each connecting lead and micro-electrode to the amplifier. When the MEA device is placed into the

MEA2100 headstage (containing the amplifier and recording hardware) metal contact pins in the lid of the amplifier are pressed onto the MEA contact pads as the headstage is closed to transfer the electrical signal between the MEA and headstage (Multichannelsystems.com).

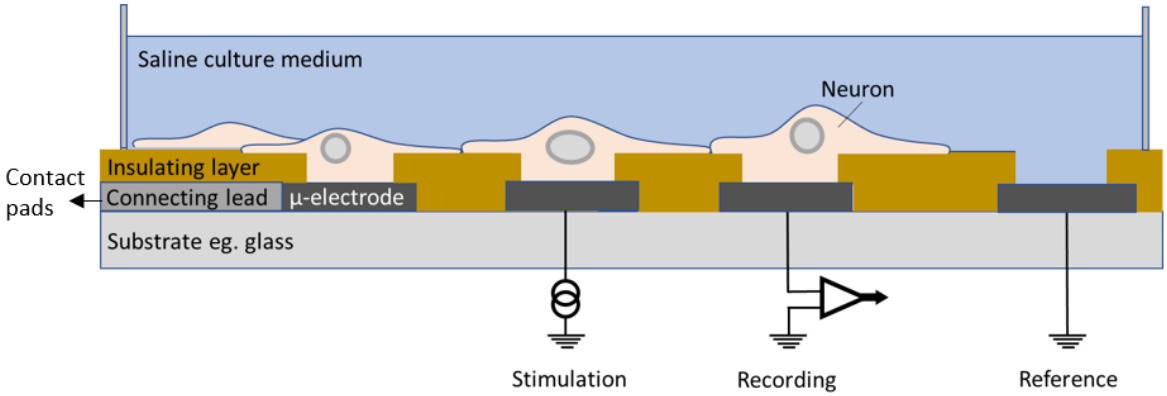

Figure 19. Schematic of neurons growing on a microelectrode array device. Neurons can be cultured across insulating and conducting layers. Microelectrodes (µ-electrodes) can be used to stimulate or record from neurons that are maintained in a conductive cell culture medium. The conducting layer includes the electrodes that are joined to the amplifier through gold contact pads that press onto the connecting leads. The insulating layer provides a barrier between the connecting leads and the conductive culture medium. Adapted: nmi-tt.de.

The ability to fabricate electrodes from biocompatible transparent conductors has led to the development of MEAs for correlative electrical stimulation/recording and optical imaging of neurons. To simultaneously record neuronal activity and image cells has a number of advantages over these techniques used separately; this combined approach allows us to directly correlate fluorescent signals, including calcium indicators, tau aggregation sensors and pH-sensors, with spontaneous or evoked electrical activity of specific population of neurons. Although commercial devices with transparent microelectrodes currently exist, many of these are based on the use of indium tin oxide (ITO) as the transparent conductive layer. ITO is the conventional transparent conductive material for a number of devices, but efforts have been made to find alternative transparent conductors for a couple of reasons. Indium is a relatively rare material and as such,

expensive (Ouyang, 2013). Alongside cost, although ITO has good electronic conductance, it is impermeable to ions. Thus, the impedance at physiologically relevant frequencies is significantly high. A high impedance (or more specifically a high resistance) causes increased electrode noise. Another problem is that following repeated stimulation ITO has been shown to oxidise causing an increase in impedance and decrease in transparency (Gross *et al.*, 1993). Increased impedance can result in an increase in noise levels and a reduced voltage window for safe stimulation (Bareket-Keren and Hanein, 2012). To compensate for these issues, an opaque platinum layer is normally coated over the active electrodes in ITO devices. It is therefore of interest whether alternative materials can be used in place of ITO that offer the same conductance and transparent properties but at lower cost and without showing increased impedance following repeated stimulation. Graphene is a 2-dimensional allotrope of carbon in the form of a plane of sp2-bonded atoms that form a hexagonal 'honey-comb' lattice. Graphene as a material has high thermal conductivity, high current, density, chemical inertness, optical transmittance. Though graphene has high transmittance of light at all wavelengths, the opacity increases by 2.3 % for each one-atom layer of graphene added, independent of wavelength (Bunch *et al.*, 2007). This project uses graphene with > 97 % monolayer coverage (grown by Oliver Burton). As a material for electrodes, graphene has already shown promising results (Kuzum *et al.*, 2014) however enhanced signal-to-noise measurements can continue to be developed upon with improvements to fabrication methods.

Alongside this, alternative ways to enhance electrophysiological recordings are being developed such as the use of conducting polymers as a surface coating to electrodes. An example of surface modification that has shown successful results is poly(3,4-ethylenedioxythiophene):poly(styrenesulfonate) (PEDOT:PSS) -coated MEAs (Jonas et al., 1995). PEDOT:PSS is transparent, and has high thermal stability and electrical conductivity. The mixed ionic and electronic conductance of PEDOT makes the impedance very low at 1 KHz frequency, as compared to other materials. PEDOT:PSS conductivity from unprocessed films from aqueous solution is below 1 S cm^{-1}, which is lower than that of ITO by several orders in magnitude (Ouyang, 2013). However with simple processing such as post-treatment such as methanesulfonic, dilute sulfuric acid, or in this study dodecyl benzene sulfonic acid (DBSA), the conductivity can increase to >3000 S cm^{-1} which is comparable to ITO (Xia et al., 2012; Ouyang, 2013). PEDOT:PSS-coating both offers a conductive coating with low reactivity to aqueous environments, and has been shown to produce stimulation to evoke much greater neuronal

responses as compared with stimulation by uncoated ITO electrodes (Nyberg, Shimada and Torimitsu, 2007). However electrodes made solely of PEDOT:PSS have not yet been published or widely used in the field. This project therefore aims to characterise PEDOT:PSS electrodes to show that they are effective for use in MEAs for the simultaneous recording of neuronal activity and optical microscopy.

Table 9. A comparison for properties indium tin oxide (ITO), graphene, and PEDOT:PSS. These are all optically transparent conductive materials that have been used for the electrode layer in microelectrode arrays.

Material	**Conductivity/ S cm^{-1}**	**Transmittance on glass**	**Structure**	References
Indium Tin Oxide (ITO)	~1x 10^4	90.31 % at 550nm	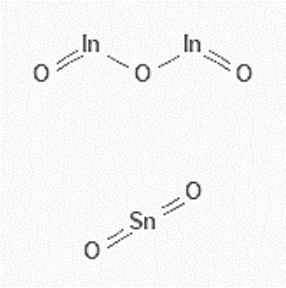	(Granqvist and Hultåker, 2002)(Askari *et al.*, 2014)(pubchem.ncbi.nlm.nih.gov)
Graphene	~1x 10^3	97.4 % (CVD monolayer) at 550nm	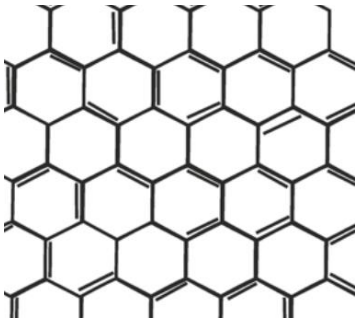	(Marinho *et al.*, 2012)(Zhu, Yuan and Janssen, 2014)(Bunch *et al.*, 2007)

PEDOT:PSS	~3x 10^3 (post-treatment)	87 % at 550 nm, 66nm thickness	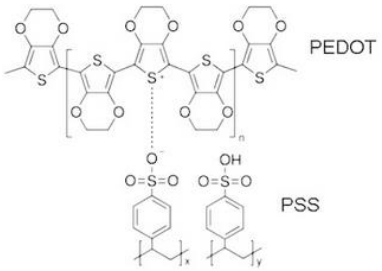	(Xia, Sun and Ouyang, 2012)(Karbovnyk *et al.*, 2016)

Although these materials are highly transparent to visible light, it is important to confirm that their chemical structures do not result in a measured fluorescence lifetime different to that of borosilicate glass coverslips as standard. Any difference in measurements compared to glass would result in false values compared to the majority of literature that uses glass substrates to calibrate the lifetime of dyes and their use for sensing applications. Parylene C and PDMS are common materials for the insulating layer of devices, however due to the typical patterning of parylene C and PDMS using an O_2 plasma, which also etches these materials, extreme care during lithographic processing or an alternative more practical material was explored. Preference was given to using 'careful lithographic processing' for the use of Parylene C as the insulating layer for PEDOT:PSS electrodes while etching by reactive ion etching with CF_4 and O_2. However, since graphene is only a single layer of atoms, any exposure to O_2 plasma would irreversibly damage the electrode, so an investigation into different insulating layers was undertaken. This project therefore tests the biocompatibility of insulating layer materials including aluminium oxide (Al_2O_3), negative photoresist SU-8, positive photoresist AZ5214E, silicon nitride (Si_3N_4), Poly(methyl methacrylate) (PMMA) and parylene C; conducting layer materials including ITO, graphene, PEDOT:PSS, and gold are also used. Biocompatible materials are then further characterised to determine whether the fluorescence lifetime of standard dyes is accurate on these substrates to confirm whether they are suitable materials for use as transparent microelectrode array.

The fabrication of improved optically transparent electrodes made of graphene or PEDOT:PSS is of particular interest to this project for two applications using correlative fluorescence lifetime imaging and recording of neuronal activity. Applications of the MEAs include 1) correlating calcium dynamics and tau aggregation with spontaneous neuronal activity to see the relationship

between neuronal activity and the aggregation rate of tau. 2) using the MEAs to repeat the optogenetic method used to stimulate neurons in the presence of tau to detect any changes to evoked neuronal activity as a second method to confirm these results.

1.6.6 Time-correlated single photon counting fluorescence lifetime imaging (TCSPC-FLIM)

Fluorescence lifetime is the average time that it takes for a fluorophore, on absorbing a photon, to decay from the excited to its ground vibrational and rotational energy state. Mathematically, it is the time constant of the fluorescence exponential decay function. The fluorescence lifetime is calculated from the slope of the decay curve as shown in Figure 20 and described by equation (1) showing the intensity, I, at time t, and fluorescence lifetime, τ.

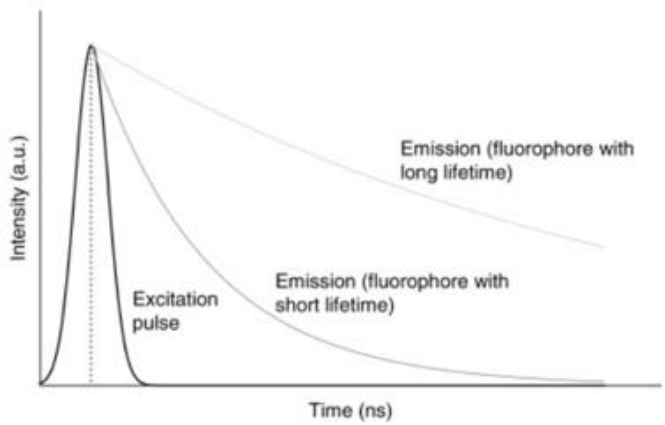

$$I = I_0 e^{-t/\tau} \qquad (1)$$

Figure 20. The decay of fluorescence intensity as a function of time is described by an exponential function (1) where *I* is the fluorescence intensity for a population of molecules excited by a pulse of light and measured at time *t*. Reproduced: Jain et. al., 2009.

The excited state decays due to both radiative and nonradiative processes depending on the environment around the fluorophore. Besides the radiative process of photon emission, the return to ground state can also occur through non-radiative processes like internal conversion into heat,

energy transfer to its molecular environment, or transient transfer to the longer-lived, and dark, triplet state before return (Lakowicz, 2006). A population of fluorophores can have fluorescence decay that is a single or multi- exponential function based on the mechanisms of return to ground state. The fluorescence lifetime can also be written as the reciprocal sum of the rate constants of these radiative and non-radiative return paths (k_r and k_{nr}) from excited to ground state (equation (2)).

$$\tau = \frac{1}{(k_r + k_{nr})} \qquad (2)$$

Fluorescence lifetime imaging therefore differs from intensity-based imaging methods which are concentration dependent. The fluorescence decay function of a fluorophore is environment-dependent and thereby acts as a sensor for environmental conditions, molecule conformations, or interactions with neighbouring fluorophores. Fluorescence lifetime is a key parameter for biological samples as the fluorescence decay function correlates best to molecular or environmental changes of a fluorophore in biological specimens. In time-domain FLIM, the fluorescence decay function is measured by exciting fluorophores with short laser pulses and measuring the resulting fluorescence intensity at nano- or pico-second scale. The most popular of the time-domain FLIM implementations is called time-correlated single photon counting (TCSPC-FLIM), where the sample is scanned with a high-frequency pulsed laser. Single emitted fluorescent photons are detected based on x,y spatial location of the laser scan on the sample, and time-correlated by the photon arrival-time relative to the excitation laser pulse. From these measurements a three-dimensional array can be created with x,y,t; each x,y spatial coordinate contains a large number of t, photon arrival times, following the excitation pulses. These pixel-based histograms of photon arrival times are then used to determine a fluorescence lifetime for each pixel and subsequently the entire image (Becker, 2012).

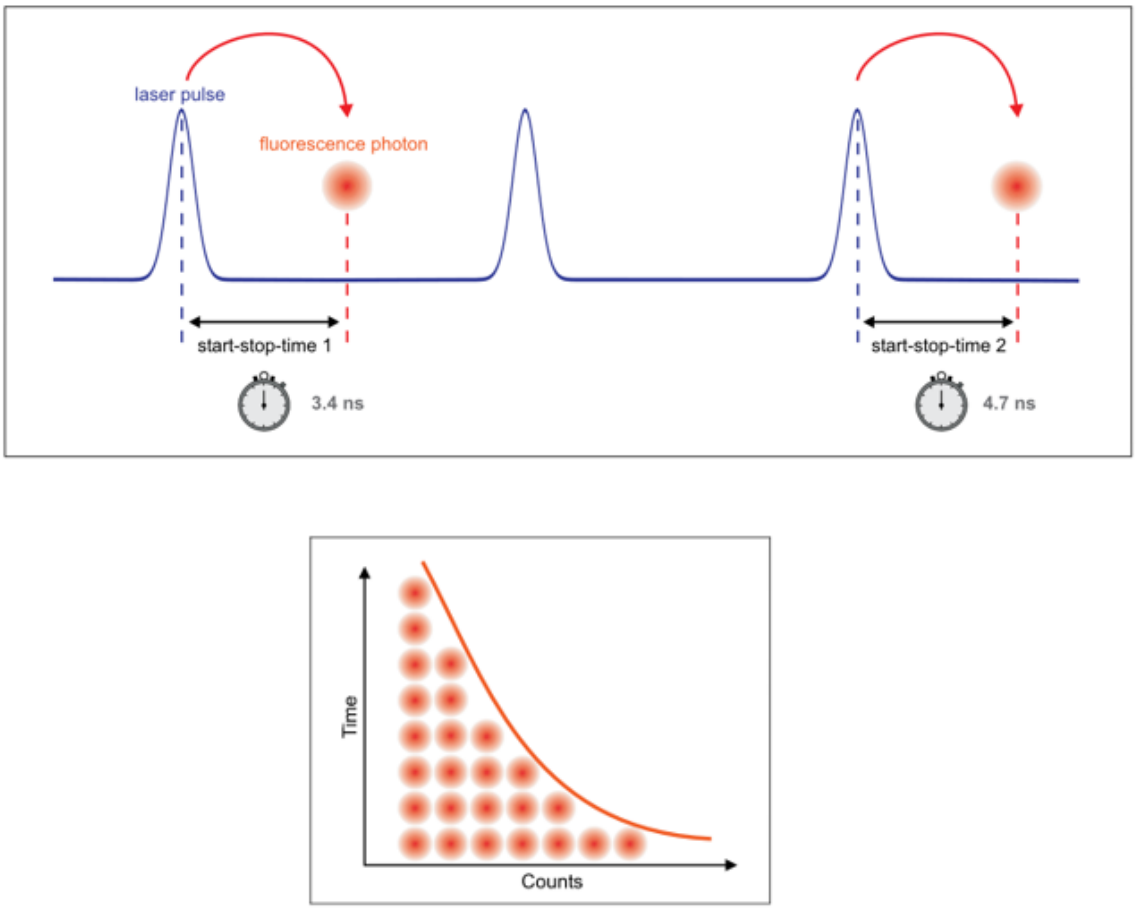

Figure 21. The time-correlated method of measuring fluorescence lifetime counts the arrival time of single photons in relation to excitation pulses from a laser. Top: a laser is pulsed many times and the arrival times of the first detected photon for each pulse are counted for each x,y spatial coordinate of the sample. Bottom: the arrival times of single photons following multiple laser pulses are time-binned to form a histogram of photon arrival times (technical notes_TCSPC, Picoquant).

A key disadvantage of TCSPC-FLIM is the relatively long acquisition time on the scale of minutes, which limits the temporal resolution that can be achieved and also requires spatially constant fluorophores during the measurement. Unlike intensity based imaging that only requires tens of photons per image pixel to produce a reliable measurement, FLIM requires >100 photons per pixel to make accurate fluorescence lifetime measurements (Gerritsen et al., 2002). As a technique, TCSPC-FLIM is therefore a relatively low throughput method. The rates of environmental changes

that the fluorescence lifetime sensors measure are unable to discriminate within the ~ 3 min imaging time, and practically require averaging of multiple images for accurate measurements. In this project, many of the lifetime sensors are therefore measured on the scale of an hour and the data are pooled for analysis.

Alongside this, TCSPC count rates are limited by three effects: dead-time of timing electronics resulting in count loss; pulse overlap caused by dead-time of the detector resulting in count loss; and classic TCSPC photon 'pile-up'. Although important to detection sensitivity, photon loss has no direct impact on the measured lifetime and is a property of the electronic design and will therefore not be further described. Photon pile up however is an important consideration for the design and parameters of each experiment; pile up is lost information of the photon arrival time and therefore can directly misestimate the fluorescence lifetime. Pile up is caused as only one photon can be measured per excitation period. Photon pile-up occurs because detectors are typically configured to detect only one photon per laser pulse. Therefore, a photon arriving later than the first photon may not contribute to the histogram of photon arrival times, resulting in an under-representation of higher lifetimes to give an incorrect, shorter lifetime than accurate (Arlt *et al.*, 2013).

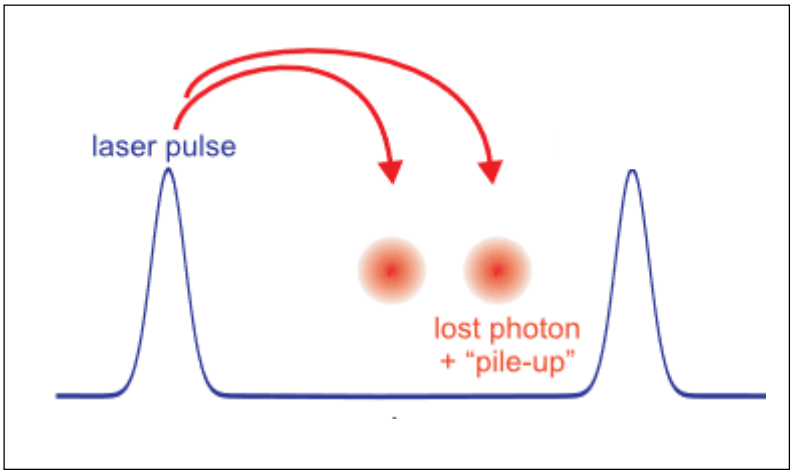

Figure 22. A representation of how photon pile-up results in under-representation of higher lifetimes resulting in an inaccurately short measured fluorescence lifetime (adapted: technical notes_TCSPC, Picoquant).

To avoid photon pile-up, experimental measure can be made to attempt to capture one photon per 20-100 excitation pulses ie. The count rate should be 1-5 % of the excitation rate. Another consideration for time resolution of TCSPC is the instrument response function (IRF). The IRF arises from the combination of the laser not having an infinitely sharp excitation pulse and the detector not having an infinitely sharp response time on detection of a photon. This results in a broadening of the IRF which in the ideal case would be infinitely narrow. For experiments, the IRF of the system must be measured as the fluorescence decay of a sample, and is made up of the exponential decay curve of the 'ideal' physical process convolved with the IRF. Through deconvolution that is carried out during analysis that accounts for the lifetime shift due to the IRF, it is therefore possible to obtain a more accurate measurement (O'Connor et al., 1979; Warren et al., 2013).

Once histograms of the decay curves have been collected across all pixels for the sample, and adjusted for the IRF, the relevant analysis method must be selected. Analysis methods can be selected using pixel-wise, or image-wise with global binning, depending on the information to be extracted. Image-wise sampling can be useful if comparisons are being made between samples of different conditions, such as drug treatments. Here, the lifetimes across the entire image are binned and compared with those of another image. This method of analysis was used for labelled tau as an aggregation sensor whereby the comparison was made between cell populations given different treatments. Alternatively, pixel-wise analysis can be useful when making comparisons within an image. Pixel-wise analysis is useful for spatial binning of lifetime histograms as compared to averaging across all pixels. When looking at pH and calcium dynamics, pixel-wise analysis allowed spatial heterogeneities in the lifetime within the same image to be compared and not averaged out as in the case of image-wise binning. This was important for pH such that different endolysosomal vesicles could be distinguished or correlating between two variables to understand their relationship such as pH or calcium concentration effects on tau aggregation.

A number of fluorophores are used throughout this project to measure different environmental conditions or molecular conformations. Environmental sensors include pH sensor, Oregon Green™-514 that is bound to dextran for cellular uptake through fluid-phase endocytosis. Oregon Green™-514 is pH sensitive such that its fluorescence decreases with pH within a certain range (Lin, Herman and Lakowicz, 2003). Oregon Green™ 488 BAPTA- 1 (OGB1) is used as a high-

affinity calcium sensor to detect calcium concentration changes in cells via calcium ion chelator, BAPTA. OGB-1 fluorescence lifetime is sensitive to calcium concentrations between 10-500 nM and shows ~10x FL increase upon calcium binding. The analysis of OGB-1 also requires double-exponential decay fitting due to a fast component of the free dye, and the slow component of the Ca^{2+}-dye complex (Wilms & Eilers, 2007).

Monomeric tau protein is conjugated via a maleimide reaction to AlexaFluor®-488 or -594. This acts as a molecular conformation sensor as when the monomers come in close contact as they form aggregates, the proximity of the fluorophores results in self-quenching, which reduces their fluorescence lifetime. Through this mechanism, aggregation can be measured by the reduction of measured fluorescence lifetime (Michel *et al.*, 2014). Figure 23 shows the use of fluorescently-labelled tau as an aggregation sensor. In PBS solution, tau is stable as a monomeric protein exhibiting a lifetime of 3686 ± 16 ps. Following addition and entry to low pH cellular compartments, tau forms aggregates, whereby the fluorophores come in close enough proximity to self-quench. The self-quenching of fluorophores reduces the fluorescence lifetime by ~500 ps to 3154 ± 56 ps for hTau40-488 over 8 hr, and therefore can measure the aggregation state of tau (Michel *et al.*, 2014).

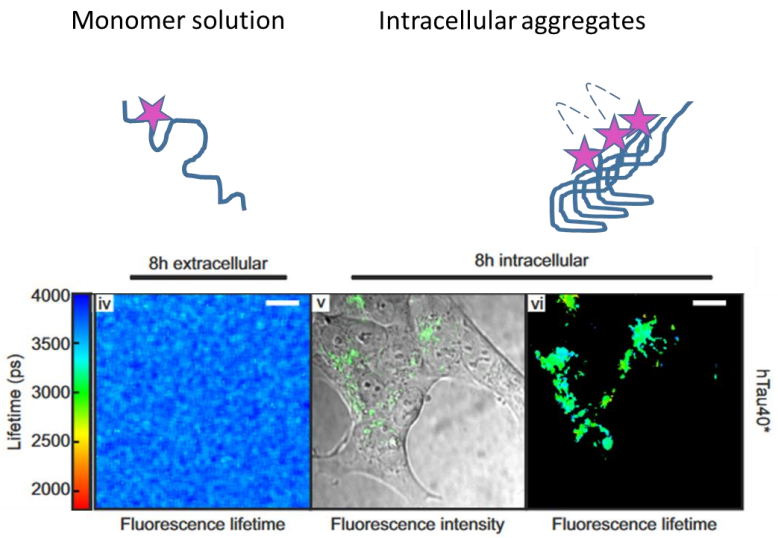

Figure 23. Fluorescently-labelled tau protein can be used as a sensor for aggregation. The fluorescence lifetime of monomeric tau in solution decreases by ~500 ps due to self-quenching of

fluorophores on entering low pH compartments inside of cells and aggregating. Adapted from Michel et al., 2014.

1.6.7 Intensity imaging and colocalisation analysis

Alongside imaging methods based on fluorescence lifetime measurements to detect molecular or environmental changes of a fluorophore in biological specimens, fluorescence intensity-based methods can also be employed. Unlike fluorescence lifetime measurements, intensity measurements are dependent upon fluorophore concentration. The average intensity of pixels in an image is useful when quantifying the distribution of a fluorescently-labelled protein of interest to make comparisons between samples. This study uses average intensity measurements of images to quantify whether a protein of interest is taken into cells. Therefore, the pixel intensity in a cell with protein uptake would be expected to be significantly higher as compared to controls exhibiting no uptake. Average intensity measurements can be difficult to reproduce due to changes between samples such as differences in intrinsic background fluorescence, small changes in dye concentration, and instrumental variations such as fluctuations in laser power. Even though these differences may allow comparisons within datasets, they often greatly alter intensity measurements between datasets, even though the same exposure times, laser powers and dye concentrations are used, and therefore may need normalisation to adjust for effects. An important advantage of intensity-based measurements is the ability to quantify the spatial relationship between two (or more) fluorescently-labelled molecules through colocalisation analysis. Several different approaches to correlate the fluorescence-intensities of two proteins have previously been explored, commonly using correlation coefficients to measure the linear relationship between two variables eg. Fluorescence intensity of pixels in colour channel A versus colour channel B. Pearson's correlation coefficient, PCC, is one of the original methods for analysing covariance of two channels (Manders et al., 1992). PCC measures the pixel-by-pixel covariance of intensity in two images. The mean intensity is subtracted from each pixel so that the method is independent of variations in pixel intensities and background. It is also simple and relatively unbiased to use as images do not require any form of pre-processing. However, a disadvantage of this method is the requirement for both channels to show similar number densities detected in each channel, and it can become inaccurate in the presence of many low intensity background pixels, which are falsely

identified as colocalised and lead to non-biologically relevant results. PCC is therefore recommended for use within individual cells to avoid extracellular background. To improve upon aspects this method, the 'Manders overlap coefficient'(Manders et al., 1993) was developed, which omits the mean intensity subtraction of pixels thereby preventing negative values. As such, the MOC is a measure of the fraction of pixels with correlating positive values in both channels, independent of their intensity (Dunn et al., 2011). However, an alternative to intensity correlation coefficient-based methods (such PCC and MOC) are object-based methods using intensity centres or the overlap approach. Intensity correlation coefficient-based methods rely on coincidence of individual pixels as opposed to specific structures. Object-based colocalisation first segment areas of the images into *objects*, and then compares between these *objects* in the channels, which are more resistance to background noise. Figure 24 shows the steps taken for colocalisation analysis using object-based methods. Two steps are required before coincidence detection between the two channels is performed. 1) A threshold is applied to try to remove low intensity noise; 2) edge detection is performed, resulting in defined objects (Figure 24, A). The intensity-centre of these objects is located and the distances between the centres are measured between the two channels (Figure 24, B). Objects are defined to colocalise if their distance is below the optical resolution of the imaging system (Figure 24, C). However, this method can result in the underestimation of colocalised objects, as seen by Figure 24 (C) showing 50 % less colocalised objects that Figure 24 (D). Therefore Lachmanovich et al., (2003) developed an 'overlap approach' of this object-based method. The overlap approach accounts for objects being larger than the optical resolution or difference in their size between the two colour channels, which results in underestimation in the distance between centroids method. For the overlap approach, centroids from channel A are said to colocalise if they fall into the area covered by an object of channel B (Figure 24, D). The degree of colocalisation is calculated by the percentage of object centroids in channel A that colocalise with object areas of interest in channel B. A second percentage of overlap is also calculated from the percentage of object centroids in channel B that colocalise with object areas of interest in channel A. Whether one of these percentages provides more useful information will depend on the question being asked.

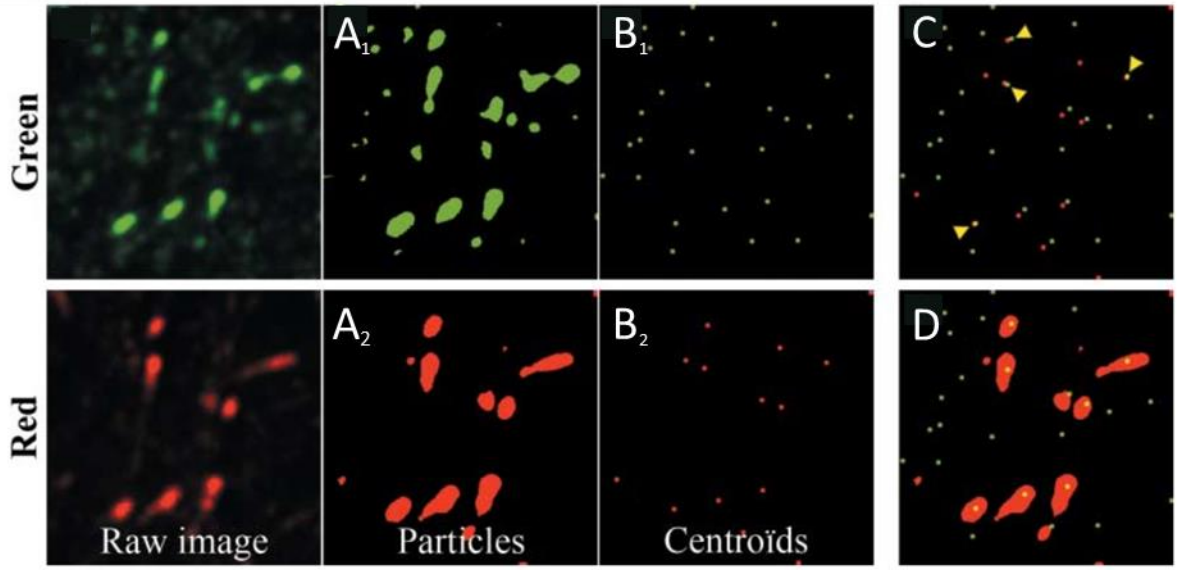

Figure 24. The stages required for colocalisation analysis using object-based methods. (A) An intensity threshold and edge detection are performed on the raw images. (B) The intensity centre is calculated from the object to result in centroids. (C) Either the overlap of these centroids can be used to define colocalisation if their distance is less than the resolution of the technique used, or (D) an overlap approach can be used to define colocalisation of the centroid from channel A within the area of channel B (vice versa). Reproduced: Bolte & Cordelières, 2006.

This project uses colocalisation analysis to better understand the relationship between 1) tau and different synaptic markers in unstimulated versus optogenetically stimulated cells 2) the colocalisation of antibody with tau protein internalised by cells. To optimise a method for these studies, multiple tests were carried out including Manders overlap coefficient and the 'overlap approach' object-based method. These methods were tested using two-colour (561 nm/ 647 nm) Tetraspeck beads. For negative 'no overlap' control, images were randomly translated and flipped. For moderate overlap, beads were analysed as imaged. For positive 'complete overlap' controls, chromatic aberration correction was performed before colocalisation analysis was performed (Results can be found in Appendix A.4). The overlap object-based method performed best for the calibration samples and was therefore selected for use with the *JACoP* plugin which is capable of performing pixel-intensity based and object-based analysis (Bolte & Cordelières, 2006). A consideration for this method is that apparently colocalising objects are counted and compared to

total objects, which means that it can vary substantially depending on whether there are many or few objects in the segmented image (Moser et al., 2017). Test samples were then imaged and compared to the values measured for the degree of colocalisation in the bead calibration samples.

1.7 Determining whether exogenous monomeric tau is capable of exerting toxic effects using two independent measures.

A common feature of Alzheimer's Disease is the progression of pathological tau in a pattern following synaptically-connected neurons. This spread of tau from the Locus Coeruleus to the hippocampal formation is closely correlated to the onset of AD symptoms, yet the specific processes through which tau exerts its toxicity remain elusive (Braak and Braak, 1991). Previous studies in the group have shown that monomeric tau in the extracellular medium is taken up by neurons and can aggregate in low pH environments, such as endosomes (Michel *et al.*, 2014). This tau is also capable of spreading between fluidically isolated cells. However, the functional consequences of this uptake and whether it may actually cause pathology are little understood. The current opinion of the field is that soluble (and therefore low n-number) oligomers and fibrils are responsible for synaptic loss and eventual cell death. The toxicity of these species is dependent upon their propensity to form β-sheets (d'Orange et al., 2018; Kopeikina et al., 2012; Polydoro et al., 2014). Monomeric tau, in its native form, has only been found to cause toxicity by one group that show its ability to bind to M1 and M3 muscarinic receptors to cause an increase of intracellular calcium (Gómez-Ramos et al., 2008; Gómez-Ramos et al., 2006). There are therefore many remaining questions regarding monomeric tau in the pathway to synaptic pathway, and whether this results from its uptake and aggregation inside of endolysosomes.

To investigate whether exogenous monomeric tau taken into cells, leading to its aggregation, had any pathogenic phenotypes, two independent measures were explored. The first measure was the electrophysiological properties of tau pathology; this property was an attempt to unify how tau pathology may result in memory impairments seen as symptoms of AD, prior to mass cell death. The activity-dependence of tau release and increased rate of pathology are not currently fully understood. Although the rate of tau pathology has been found to be activity-dependent, there is

still little understanding of how tau, in the process of pathology, may impair neuronal activity to illicit impairment to memory. Therefore, an initial question was, can neuronal-activity induce impairment to the neural correlates of memory (LTP or LTD) that would explain how tau at a molecular level could express as the AD symptom behavioural deficits of impaired spatial and episodic memory at initial stages.

The second measure is the mechanical properties of tau pathology. Mechanical properties were proposed to be relevant due to the role of tau as a microtubule stabilising protein, and the concept in the field that endogenous tau is recruited to aggregates (Alonso et al., 1996; Alonso et al., 1994; Iqbal et al., 2008). It was therefore of interest whether this endogenous tau may be recruited from microtubules and result in their depolymerisation which could be measured as a loss of cell stiffness. A depolymerisation of microtubules might be able to explain the impairment, followed by retraction of synapses preceding axonal degeneration in the stages of cell death seen in AD (Selkoe, 2002). Therefore, synaptic and cell stiffness were considered relevant mechanical properties that may be a possible pathological phenotype following treatment with extracellular monomeric tau.

1.8 A Nanomechanical Approach to Understanding Tau Pathology in Alzheimer's Disease

It has been suggested that during the process of fibril formation, endogenous tau unbinds from microtubules for incorporation into seeds; this unbinding is thought to compromise microtubule integrity via destabilisation of tubulin subunits (Alonso et al., 1996; Alonso et al., 1994; Iqbal et al., 2008; Duan et al., 2012). Conversely, the stabilisation of microtubules by pharmacological agents including epothilone D and paclitaxel have been found to improve CNS axonal integrity, MT density and cognitive performance in mice overexpressing human tau (Tg mice) (Zhang *et al.*, 2005; Hampton *et al.*, 2010). This study uses nanomechanical methods, namely atomic force microscopy (AFM), to measure cytoskeletal integrity reflected through changes to cell stiffness following treatment with exogenous tau. In previous nanomechanical studies, increasing stiffness has been correlated with cytoskeletal maturation (Curry et al., 2017; Lee et al., 2015) with the main contributing structure being microtubules (Ouyang et al., 2013). We therefore employ this

technique to compare changes to cellular stiffness, a measurement primarily dependent upon the contribution of microtubules to cytoskeletal structure (Ouyang, Nauman and Shi, 2013), after the application of exogenous tau to primary hippocampal neurons. Understanding the mechanical changes that occur to cell stiffness via alterations to the cytoskeleton during neurodegeneration may help to understand mechanisms of tau-induced pathology, synapse deterioration and neurite retraction preceding cell death (Selkoe, 2002).

For this study, a number of treatments are used as controls to understand whether exogenous monomeric tau may have toxic effects to cells. As positive controls, a toxic concentration of DMSO is used, alongside a low concentration comparable to that used as vehicle. Nocodazole is a molecule that binds to a microtubule (MT) subunits, β-tubulin, and prevents polymerisation into MTs and therefore results in a destabilisation of the MT network. Due to MTs providing the main contribution to cell stiffness it could be expected that nocodazole would result in decreased cell stiffness (Ouyang, Nauman and Shi, 2013).

1.8.1 Measuring the stiffness of cells using quantitative nanomechanical mapping with Atomic Force Microscopy

Atomic force microscopy (AFM) is a scanning probe method of microscopy. Therefore, unlike optical methods which involve a light source and magnifying lenses, AFM uses a nanometer scale probe tip on a spring-like cantilever that physically traces a sample to provide a topographical image. A laser deflects off the reflective coating of the back of the cantilever at different angles as the probe tip interacts with the sample and is detected by a photodetector that reconstructs a topographical image from these interactions. AFM is therefore only able to map structures that come into physical contact with the tip, and therefore on the exterior of the cell. The many contact sites that are required to map an image also means that AFM is a relatively slow method, on the order of 10s of minutes, such that cell viability and rate of process imaged must be taken into account. Peak Force Tapping mode (Bruker, proprietary) is an intermittent contact mode method of scanning that produces force curves at point of contact; thereby, as well as topographical representations of the cell, quantitative nanomechanical measurements can be simultaneously

gained. These data are gained from the force-distance curves from each tip-sample interaction point. Figure 25 shows the mechanical properties taken into account for measuring the stiffness of a cell, as defined by its propensity to deformation.

$$\text{Young's Modulus (E)} = \frac{\text{tensile stress } (\sigma)}{\text{extensional strain } (\varepsilon)} = \frac{F / A_o}{\Delta L / L_o} = \frac{F L_o}{A_o \Delta L}$$

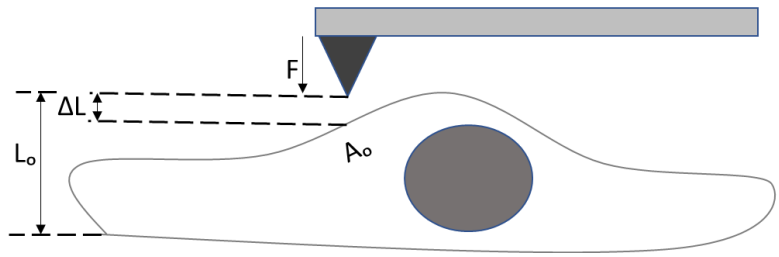

Figure 25. The Young's Modulus gives a stiffness measurement as calculated by the force-distance curves gained when the probe tip interacts with the cell surface where the force is applied (A_o). This is calculated from the change of distance (ΔL, change of length, L_o, original length of cell) the tip moves when a force (F) is exerted on the cell with the tip.

For reconstruction, the shape and size of the probe tip must also be considered as this will change the interaction properties of the tip with the cell surface area. The Hertzian cone-sphere model is used, such that the force gained from the measured force-distance curves are fitted with the model shown in Figure 26 (PeakForce-QNM Advanced Applications Training 2014, Bruker).

$$F = \frac{4}{3} \frac{E}{(1 - \nu^2)} \sqrt{R\delta}^{\,3/2}$$

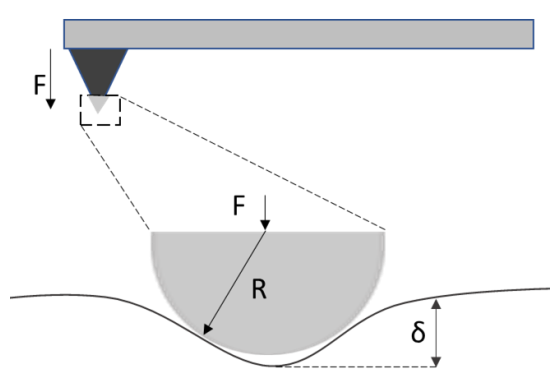

Figure 26. For fitting of force(F)-distance curves, the probe tip dimensions must be considered. The Hertzian model is used which estimates the tip as a cone/sphere with radius, R. A homogenously elastic indentation (δ) is assumed, though in biological samples this may not be strictly true. The Poisson ratio (ν) is a material property of the sample accounted for in the model.

1.9 Novel treatment methods for tau pathology

1.9.1 Metal-organic frameworks for anti-tau immunotherapies

Immunotherapy treatments for Alzheimer's disease have entered numerous clinical trials with various levels of success. Many initial attempts targeted amyloid-beta proteins at different epitopes and stages of the amyloid pathway. Amyloid-beta was thought a key target due to success immunisation in cell culture and *in vivo* models preventing amyloid-beta induced toxicity (Schenk *et al.*, 1999; Janus *et al.*, 2000; Fu *et al.*, 2010). However, in translational studies, although immunotherapy resulted in amyloid-beta clearance, trials showed poor outcome for patient safety and alleviation of synaptic symptoms and disease progression (Boche et al., 2010; Schenk, 2002). For this reason, many clinical researchers turned towards targeting tau in early stages of pathology, to attempt to prevent the progression to later Braak stages, which correlate more closely than amyloid-beta pathology with AD symptoms.

Mechanisms of anti-tau immunotherapy prevent the process of phosphorylation, seeding and spread of toxic tau species. The aim is to neutralise forms of tau before they become capable of forming pathogenic conformers that may alter cell physiology and cause synaptic impairment. Tau immunotherapy has already been shown effective both *in vitro* and *in vivo* (Nobuhara et al., 2017; Yanamandra et al., 2013). Treatments have also been taken to clinical trials to target AD at early stages (NCT02880956, NCT03289143, NCT03056729). Therapeutic antibodies have shown different efficacies depending on the epitope they target. Deciding on a relevant epitope may dramatically affect the efficacy of immunotherapies, particularly is targeting truncated forms of tau. In some studies, C-terminus targeting antibodies have been suggested to be less effective, which is at least in part predicted to be due to C-terminal truncations during different processes and cell-transfer stages, and accumulation of C-terminal truncated tau accumulating in the pre-

synaptic compartment (Florenzano *et al.*, 2017). For this reason some therapies target N-terminal and mid-domain regions which prevent neuronal uptake of tau (Nobuhara *et al.*, 2017). However there have been mixed results as to which extracellular forms of monomeric tau may relate to AD or merely be released as a biproduct. Although C-terminal truncated tau has been shown to occur in the CSF of AD patients (Kanmert *et al.*, 2015) and accumulate in pre-synaptic terminals, N-terminal truncated tau can also cause pre-synaptic pathology and alterations to synaptic activity (Florenzano *et al.*, 2017). This study aims to use a novel method of tau immunotherapy as compared to previous literature in this area. Although C-terminal truncation can occur in human AD (Meredith Jr. *et al.*, 2013), other physiological (Pooler et al., 2013) and pathophysiological (Kim et al., 2010), extracellular forms of tau are full length. Alongside this, neuronal injury induced by amyloid-beta protein increases the release of full-length, C-terminal containing, tau into the media (Kanmert *et al.*, 2015). This project investigates whether the aggregation of full-length monomeric tau taken up by cells can result in any form of cytotoxicity and aims to offer therapeutic avenues to prevent it. For this reason, an antibody targeting extracellular full-length, and not truncated tau, appears to be a suitable therapeutic target.

The project uses a monoclonal antibody against the C-terminal of tau (425-441, MedImmune, Figure 27) to remove full-length tau in the extracellular space before it is taken up by neurons and aggregate or modified by phosphorylation or truncation. The project therefore uses an antibody previously characterised for its binding properties by Chen et al., (2019), but with humanised scaffold from the previous mouse monoclonal form. The humanised scaffold and modified Fc-region to reduce effector function are both implemented to reduce the likelihood of inducing immune responses following administration to humans. The full-size IgG has been engineered with a triple mutation in the Fc region to decrease the affinity for Fc gamma-receptor type IIIA and to suppress antibody-dependent cellular toxicity (Oganesyan et al., 2008; Sondermann et al., 2000).

Figure 27. Schematic showing the binding epitope on tau protein of the immunotherapeutic antibody used in this study. Adapted: Chen et al., 2019.

An alternative design to preventing the neuronal uptake and propagation of exogenous tau protein is to graft the antibody to a structure that is too large to be uptaken by cells following tau binding. The use of metal organic frameworks (MOFs) is highly suitable for this function due to their biocompatibility and controllable properties via the metal ions and organic linkers selected. MOFs consist of metal ions or clusters interconnected by organic ligands forming a defined framework of repeated units with high pore volumes (Figure 28).

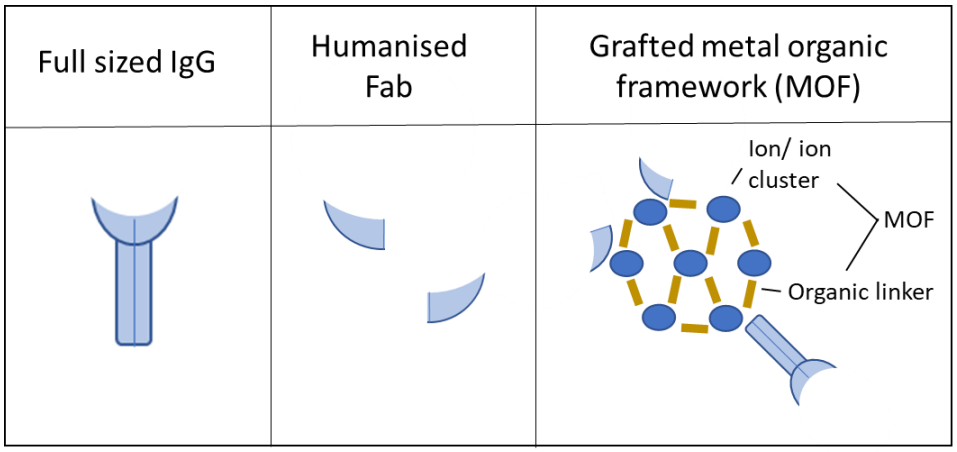

Figure 28. Three forms of immunotherapy will be tested for efficacy against the neuronal uptake and aggregation of exogenous monomeric tau. The main differences between forms of antibody is their size, which may have effects on cellular uptake, delivery, and clearance from the brain. The forms include the full-sized IgG antibody, the antigen-binding fragment (Fab), and a metal organic framework with either the IgG or Fab proteins grafted to it in high density.

For this project, the aim is to target exogenous monomeric tau extracellularly. Methods that prevent cellular tau uptake through MOF-immunotherapy versus conventional immunotherapy

using microglial and lysosomal clearing of tau will be used to compare the most effective and viable treatment option. Antibodies grafted to MOFs too large to enter cells are expected to bind tau with high affinity and be cleared away in the extracellular space to prevent tau uptake into low pH intracellular compartments to form aggregates capable of toxicity. Smaller antigen-binding fragments (Fab) may capture tau in non-aggregated form and be taken into cells and be cleared by lysosomes or microglial phagocytosis (Congdon et al., 2013), preventing further aggregation. These Fabs will be compared with the full-sized IgG antibody, which is larger but also possesses 2 Fabs to each protein (Figure 28).

A previous study by Evans et al., (2018) investigating the uptake mechanisms of tau into neurons has looked at the ability of an anti-tau antibody to prevent tau uptake into cells. This was based on the hypothesis that the increased molecular size of tau following complex formation with the antibody may either block an uptake recognition site or delay uptake through direct competition for vesicle cargo space. The study shows that IgG is taken into neurons following binding to monomeric tau protein; the overall amount of tau protein that enters cells is reduced through antibody-binding. These findings are relevant to this project as the aim is to prevent the uptake of antibody and tau, to allow extracellular clearance and prevent the possibility of synaptic impairment following uptake, aggregation and neuronal activity. In practice this therefore requires a) prevention of the uptake of antibody-tau complex and b) reduced overall uptake of tau protein into neurons. However, the previous study also had key differences to this project that may cause variation in the uptake of antibody and tau protein that was shown. Differences including the use of inducible pluripotent stem cell-derived human neurons (iPSCs) as opposed to primary rat neurons, the use of P301S mutant tau found in FTD-17 versus wildtype tau in AD, polyclonal anti-tau IgG versus monoclonal forms of IgG and the use of the fab alone.

Key initial question before the continuation of the project are therefore a) whether antibody is taken up by neurons once bound to tau; b) whether the antibody is taken up by neurons in IgG or Fab form in its unbound state c) whether the IgG or fab reduce the overall amount of exogenous tau taken into cells. For a). It has also been shown that antibody uptake into neurons is mainly by clathrin-dependent Fcγ receptor endocytosis (Congdon *et al.*, 2013). Although it has been shown that antibody entry to cells occurs via the Fc-region, it was considered that on binding to tau, IgG or Fab would enter the cell. Since the paratope binds to the far C-terminal of tau, it was possible

that antibody entered cells by hijacking the tau uptake pathway. This had been shown to occur a small amount in a study where tau-bound IgG was capable of entering into the cell. Whether this was possible for tau-bound Fab, and whether the smaller size of the Fab causes more tau-complex entry is not known (Evans *et al.*, 2018). For b) (whether the antibody is internalised by neurons in its unbound state), it was not certain whether this would occur, however it could be predicted not to occur when the antibody was used at lower concentration that reduce nonspecific binding of the antibody. The modified Fc-region should prevent recognition and uptake by extracellular receptors. It has been shown that IgG proteins are not taken into neurons unless they have a functional Fc-region and only accumulate in cells if they have a specific neuronal targeting epitope; this therefore excludes the uptake of Fab proteins (Greenlee *et al.*, 2016). Alongside this, it was considered important to understand c) whether the antibodies prevented the endocytosis of exogenous tau protein into neurons before being grafted to the MOF. This again was based on work by Evans et al., (2018) showing that tau IgG reduce uptake and are carried into neurons by tau. However, this again was only shown for polyclonal IgG form of antibody and not (monoclonal and) fab forms which could have different abilities to seclude tau from endocytosis or micropinocytosis.

Therefore, as a first crucial step, this study identifies whether anti-tau antibody is internalised by cells in its unbound state; following on, antibody is incubated with monomeric tau to detect whether this induces its uptake into neurons via hijacking tau uptake pathways. Should the antibody not be internalised in bound form, it would no longer be necessary to graft a MOF-Ab that prevents uptake of tau species as the antibody in Fc-modified form would be sufficient to exclude tau from entering cells and the possibility of its aggregation. Finally, the amount of tau taken into neurons in the presence of each form of antibody is measured to determine whether the antibody alone is capable of preventing tau uptake. As it has been previously shown, anti-tau antibody reduces the amount of tau taken into neurons (Evans *et al.*, 2018), and it will be of interest whether this varies between IgG and fab, and whether the MOF-Ab decreases overall tau entry.

1.9.2 Biofunctionalisation of cellulose for neural stem cell prosthetics

This project aims to biopattern growth factors onto coverslips to show that it is possible to locally direct the differentiation of neural stem cells into a neuronal lineage with high efficiency. This method removes the requirement to add additional growth factors to the cell culture medium, which is one of the most expensive reagents for cell culture. The method also helps better understand the function of growth factors during stages of development and differentiation. Following success of biopatterning coverslips, bacterial cellulose sheets are modified as a scaffold for neural prosthetics as a treatment avenue for Alzheimer's Disease. Currently stem cell therapy is not available as a treatment for AD even though the benefits of stem cell implantation, particularly through paracrine function to release neurotrophic factors such as BDNF, have been demonstrated in multiple studies (Blurton-Jones *et al.*, 2009; Zhang *et al.*, 2014). This project offers a powerful tool for enhancing neural prosthetics to better control stem cell differentiation into mature neurons to make implants replicable. Scaffolds also provide a local environment that promotes survival through functionalised growth factors for implantation into diseased tissue lacking healthy signalling.

1.9.2.1 Biopatterning methods and applications

Biofunctionalisation, the adhesion of biomolecules to a substrate, has become popular to target specific binding partners onto a surface to serve biological function or stimulus. These methods can often also be used for polynucleotide or protein binding using the same functional groups, such as for assays and diagnostics. Alternatively, the methods can be used with cell culture by binding antibodies or adhesion proteins onto a surface to target specific extracellular proteins or cell subtypes. Biofunctionalisation can be combined with biopatterning to add an extra element of control to the environment. Biopatterning restricts the binding of molecules to defined locations of interest on the substrate. Purposes of biopatterning for cell culture include localising cells or structures to specific locations on a coverslip to aid with imaging, create distinct subpopulations by cell types, understanding binding interactions, or direct the growth of cell networks. Previous work has used biopatterning to induce the formation of pre- or post- synaptic-like compartments ('hemisynapses') to spots on coverglass (Czöndör *et al.*, 2013). The adhesion of SynCAM1 or neurexin1β to coverglass allows the local environment to determine the location of the formation of pre- or post- synaptic compartments respectively. This method helps to better understand the processes involved in synaptic differentiation as well as adhering synapses within the range of

imaging for increased contrast TIRF microscopy. However, there are several disadvantages to the method including a noncovalent attachment of proteins using poly-L-lysine. Noncovalent binding of proteins can result in elution following media exchange, lateral diffusion, or an inhomogeneous coating surface depending on the immobilisation efficiency; overall this can result in transient immobilisation or high-background (Rusmini et al., 2007). Additionally, the method required commercial coverslips (CYTOO SA) that use photolithography to form cytophobic coating other than the spot patterns of poly-L-lysine. Photolithography methods involve using photoresist and a photomask to expose some areas of a substrate for biofunctionalisation whilst blocking other regions until a chemical stripping step to remove the photoresist. Photolithography involves multiple long procedural steps, expensive tools, clean room access, and the chemicals involved can be destructive to biomolecules (Kheyraddini Mousavi *et al.*, 2012). The advantages and disadvantages of other biopatterning options are discussed in Table 11. Ink-jet printing methods which deposit microdroplets (100–200 μm) on a polyethylene glycol-coated substrate is a highly precise method, though offers lower resolution than other methods. Recent ink-jet methods have also made improvements on the resolution to achieve micron-scale precision, however this requires more specialist or custom-built printing equipment (Sanjana and Fuller, 2004). Another approach is 'microphotopatterning'. Microphotopatterning requires a two-photon confocal microscope with ROI patterns generated using software for photoablation of a hydrogel coating; this method allows many different types of geometries but also requires access to a two-photon microscope and can result in adsorption versus covalent protein adhesion (Doyle et al., 2009). Photoactivation methods of biopatterning also exist, which use laser induced photolysis or enzyme activation in restricted areas of the coverslip (Cai et al., 2019; Carrico et al., 2007; Mosiewicz et al., 2013).

Table 3. A comparison between biopatterning methods. Many methods require specialist equipment or reagents making them less accessible to researchers desiring a fast, inexpensive, and easy biopatterning option.

Method	**Main advantage**	**Main disadvantages**

Commercial photolithographic coverslips	Easy to use (after photolithography steps)	Limited flexibility over pattern and substrate Noncovalent bonding
Ink-jet printing	High precision	Limited resolution ~100 μm unless custom-made or specialist equipment
Microphotopatterning	1-step method	Can damage protein function Often limited to hydrogels and noncovalent bonding
Photoactivation	High temporal and spatial control Covalent	Requires modified chemicals and/or proteins Multistep
Soft lithography microcontact printing eg. PDMS stamps	Easy to use Relatively inexpensive	Heterogeneous protein distribution

Other work has used stamps made of PDMS for microcontact printing (Kumar and Whitesides, 1994; Mrksich *et al.*, 1996). This offers a relatively inexpensive and convenient method for biopatterning, though it has been commented that these methods often require multistep reactions or modified functional groups on the protein (Rozkiewicz et al., 2006; Sullivan et al., 2004). This project makes use of the advantages of microprinting by developing a method using PDMS stamps that is accessible to researchers who want inexpensive and simple procedures to pattern on a benchtop within hours. The pattern can be designed to any dimensions within the limits of soft lithography (as explained in Section 1.6.4). Figure 29 shows two grid designs used during the optimisation of the biopatterning process; Figure 29 (right) has small features compatible with the microelectrode array dimensions and Figure 29 (left) has larger patterning surface area for testing the effect of biopatterning for neural stem cell.

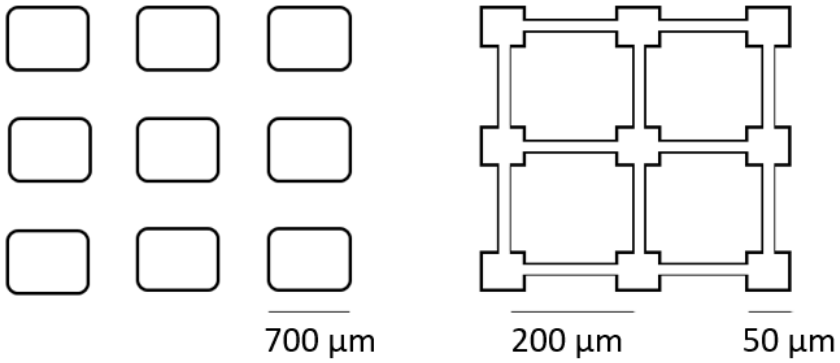

Figure 29. The PDMS stamp designs used for the microcontact printing in this project. Both stamps produce grid shapes of the applied substance with larger (left; designed by Amanda Haack) or smaller (right; designed by Jane Fojas) patterned regions.

Once the pattern has been designed and PDMS stamps have been produced, the method of biopatterning is simple. A chemical of interest is added onto the stamp pattern which is then pressed onto the surface of interest to induce transfer of the chemical to reproduce the stamp pattern (Figure 30).

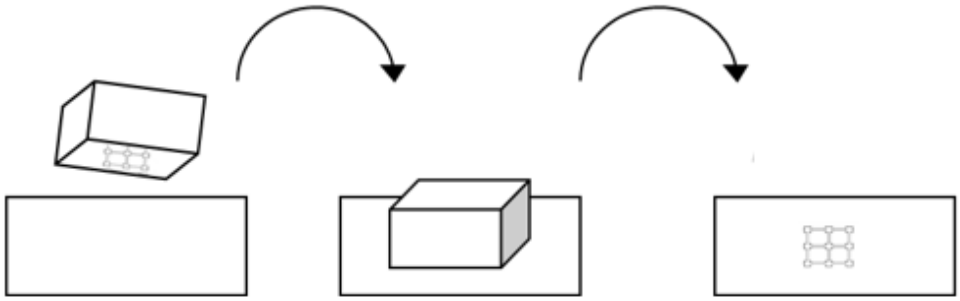

Figure 30. A schematic of microcontact printing using a PDMS stamp. A chemical of interest is places on the pattern of the stamp and placed onto the substrate of interest under pressure.

A number of chemicals were tested to optimise the stamping method including amino-silanes and epoxy-silanes to induce covalent linkages. Although amino-silanes are commonly used for functionalisation methods, they require post-modification activation for protein immobilisation, an additional chemical linker step to the protein or silane, such as p-phenyldiisothiocyanate to link to amino groups. Epoxysilanes however can provide a one-step biofunctionalisation process and do not require specific protein modification as they can react with free amine groups of lysine residues' primary amine group, or alternatively free hydroxyl groups. This method involves the covalent binding of amine groups in the protein-of-interest to the silicon oxide coverslip surface via (3-glycidoxypropyl)trimethoxysilane (GPTMS) (Figure 31). Although the amine group of the protein's lysine that reacted with GPTMS are nonspecific, and therefore result in random orientation, this can be accounted for by increasing the density of protein coating to increase the likelihood of protein in the required orientation for binding partner. The benefit of the non-specificity of the reaction to free amine groups was that no additional functional groups needed to be added to the protein.

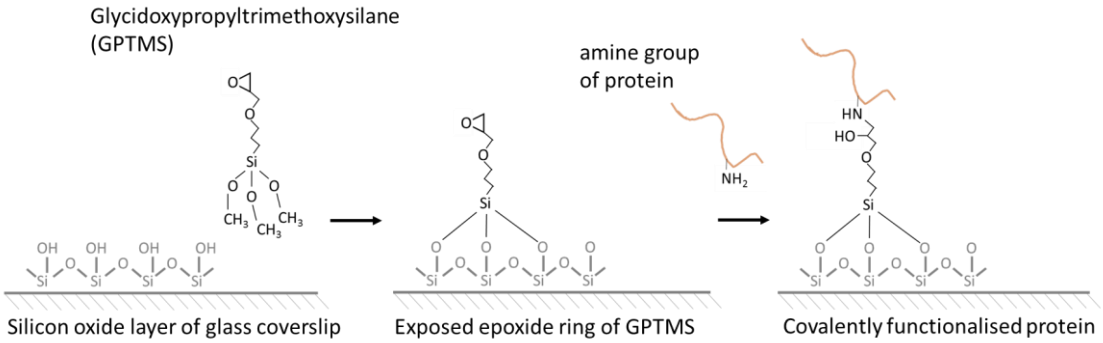

Figure 31. The reaction mechanism between an amine group of a protein and GPTMS to covalently bind it to the silicon oxide coverslip surface.

1.9.2.2 Neural stem cells for neural prosthetics

Human neural stem cells (hNSCs) are the precursors of differentiated cells in the CNS including astrocytes, oligodendrocytes, microglia and neurons. This gives them applications for stem cell-based therapy to treat disorders such as Alzheimer's disease (AD), Parkinson's disease, stroke or spinal cord injury. hNSCs can be gained from the foetal, neonatal or adult brain, or from directed differentiation of pluripotent stem cells.

Stem cell therapies can act through three main mechanisms: 1) cell replacement therapy to directly replace a subgroup of cells 2) provision of trophic support to remaining cells 3) modulating immunity including immunosuppression (Table 12; Lindvall & Kokaia, 2010). The introduction of stem cells into the brain may be able to counteract the cognitive decline that has been shown to correlate to decreased neurogenesis and decreased survival of progenitor cell proliferation that occurs due to aging (Siwak-Tapp et al., 2007; Wati et al., 2006). Conversely, new neurons have been shown to enhance cognition; cognition can be enhanced by neurogenesis arising through an enriched environment, drug treatment, or stem cell transplantation (Qu et al., 2001; Rockenstein et al., 2007; Deng et al., 2006; Wolf et al., 2006). Stem cell implantation has shown mixed results; there is a trend in the literature between neurogenesis and cognition whereby implantation of stem cells into the hippocampus has shown enhanced cognition (Qu *et al.*, 2001). The opposite has also been shown whereby aged rats that maintain cognitive function also show pronounced reductions in hippocampal neurogenesis (Bizon et al., 2005). These discrepancies may be due to the variability of stem cell treatment. Problems include the quality and number of cells required, and the long-term survival of cells following transplantation, resulting in unpredictable patient outcome (Table 12.; Lindvall & Kokaia, 2010).

Table 4. Benefits and challenges of stem cell therapies. Therapies based on stem cells offer promising treatment avenues (left column) however a number of problems in the field must be overcome to produce reliable therapies and consistent patient outcome (right column). Based on: Lindvall & Kokaia, 2010b.

Key benefits of stem cell therapies	**Key problems for stem cell therapies**
(A) Direct replacement of diseased cells	(D) Long-term cell survival
(B) Provision of trophic support and signalling	(E) Diseased local microenvironment (i) poor trophic and signaling support (ii) vulnerable to amyloid seeds
(C) Modulate immune response	(F) Reproducibility of cell differentiation and patient outcome

Cell replacement therapy (Table 12 (A)) is a newly establishing field in disorders where there is a profound decrease in neurotransmitter, neuromodulator, or trophic support that results in cell loss or cognitive dysfunction such as in neurodegeneration (Lindvall et al., 2004). A clear and successful example of cell replacement therapy is in Parkinson's disease, where patients have 50 % fewer dopaminergic neurons in the midbrain compared to normal brains, resulting in loss of motor control (German et al., 1989). Clinical trials using transplantation of human foetal dopaminergic neurons has offered a source of cells to replace a lost population and provide long-lasting aid to tremor, dyskinesia and loss of postural control (German et al., 1989; Lindvall & Kokaia, 2010; Wang et al., 2011).

An alternative approach (Table 12 (B)) to providing a specific differentiated neuronal subtype is to directly provide neural stem cells that promote neurogenesis and neurotrophic paracrine support. Neurotrophic factors are large polypeptides that help the growth and maintenance of structures in the central and the peripheral nervous systems. Their roles include regulating the growth development, differentiation and survival of cell populations and their adaptation to the

environment. Brain-derived neurotrophic factor (BDNF) is the most commonly occurring neurotrophin in the central nervous system; it is essential for synaptic plasticity, increased dendritic length and complexity, neuronal survival, and cognitive function (Waterhouse and Xu, 2009; Diniz and Teixeira, 2011). BDNF transcription is regulated by membrane depolarisation such as NMDAR activation resulting in release from dense-core vesicles in the pre-synaptic compartment for anterograde signalling (Dieni *et al.*, 2012). As such, increase in dendritic growth elicited by BDNF requires spontaneous activity, synaptic transmission, or L-type calcium channels. Neurons must be therefore be healthy and active enough to release and receive neurotrophic aid by BDNF (Hofer and Barde, 1988), which this study has shown (Chapter 4) may not always be the case. Following release BDNF has an essential role in memory formation, consolidation and storage through multiple mechanisms (Heldt et al., 2007). BDNF-TrkB signalling increased release and vesicle cycling of neurotransmitter pre-synaptically and increases opening of ionotropic glutamate receptors postsynaptically, including through relieving the Mg^{2+} block on NMDARs (Xu *et al.*, 2000; Kramár *et al.*, 2012). Further downstream of neuronal activity BDNF acts as a late stage mediator for long-term plasticity to influence local protein synthesis, spine remodelling, or gene transcription (Park & Poo., 2013; Sasi et al., 2017; Bramham & Messaoudi, 2005)

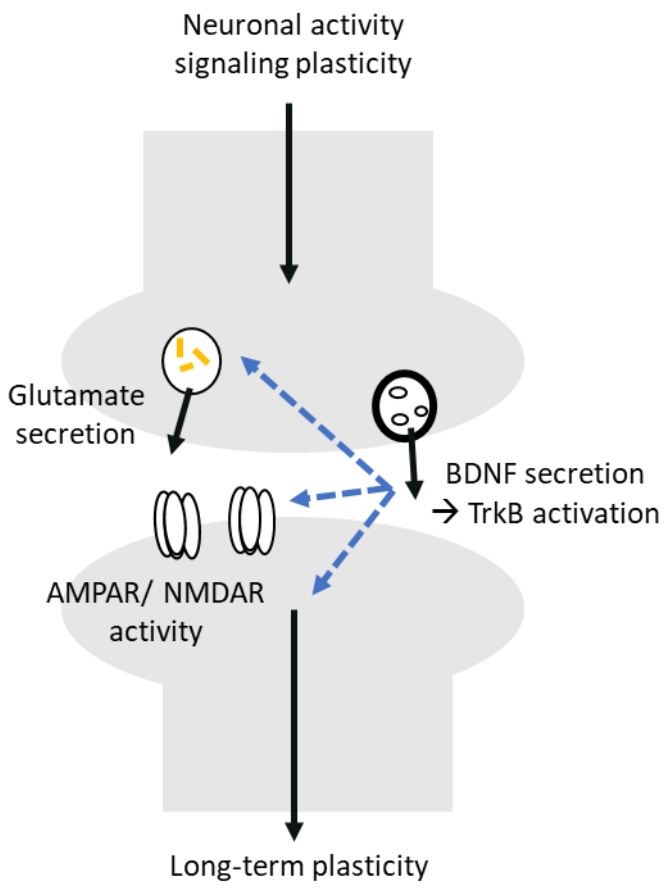

Figure 32. A schematic showing the roles of BDNF release and signalling mechanisms for modulating stages of long-term plasticity. The release of BDNF and activation of TrkB pathway (blue dotted lines) has affects at early stages of plasticity including glutamate secretion and receptor activation as well as affects at later stages of plasticity and gene transcription.

BDNF has also been shown to exert neuroprotective effect in multiple neurodegenerative diseases. In pathologies with amyloid-beta-induced neuronal cytotoxicity, BDNF has been shown to reverse these effects alongside other neurotrophins, IGF-1 and GDNF (Kitiyanant et al., 2012). Conversely amyloid-beta-toxicity can downregulate BDNF, and BDNF is also decreased in postmortem human AD brains compared with controls. In a rat *in vivo* CNS trauma model, injection of BDNF enhanced neuronal survival by activating the TrkB pathway and inhibited caspase-3-induced apoptosis (Noble et al., 2011). The relationship between BDNF enhancing

neuronal survival in traumatic brain injury (TBI) models could be of interest due to the increased association of AD linked to TBI (Blennow *et al.*, 2016; Washington, Villapol and Burns, 2016; Mendez, 2017).

In AD, the replacement of cells producing neuromodulators to replace degenerating cells have also shown success in rodent models, alongside the direct role of trophic support by stem cells. In two studies, spatial memory was restored in an AD rodent model following transplantation of NSCs that had been differentiated into cholinergic neurons (Moghadam *et al.*, 2009; Fujiwara *et al.*, 2013). In another study, NSCs improve cognition via brain-derived neurotrophic factor (BDNF) in a transgenic rodent model of Alzheimer disease. Although in this study the amyloid-beta and tau pathology remained the same, there was an enhancement of hippocampal synaptic density and restoration of hippocampal-dependent cognition due to BDNF. These improvements could be replicated by using recombinant BDNF and lost using BDNF knockdown in transplanted NSCs (Blurton-Jones *et al.*, 2009). Another study using P301L mice (a mouse model of tauopathy) showed reduced BDNF levels in CSF. By restoring BDNF levels through a viral vector they were able to attenuate behavioural deficits, prevent neuronal loss, and alleviated synaptic degeneration and was suggested as 'a promising treatment for tau-related neurodegeneration for AD and other neurodegenerative disorders with tauopathy' (Jiao *et al.*, 2016). Interestingly, like the previous study, the BDNF treatment showed improvements to cognitive deficits but not the tau pathology load, suggesting that it is not capable of curing neurons but may be effective to reduce future pathology and alleviate symptoms. However a negative correlation for BDNF immunoreactivity and tau pathology has been seen in neurons (Murer *et al.*, 1999); it appears that amyloid-beta toxicity reduces BDNF levels before the formation of tau and amyloid-beta aggregates.

Table 5. Stem cell therapies or direct BDNF expression used to improve cognition in rodent models of neurodegeneration. Adapted: Bali et al., 2017.

Type/ source of stem cell used	**Route of Administration of Stem Cells**	**Results/Outcome**	**Animal Model Used**	**References**
Neural stem cells	Intra-hippocampus	Ameliorated loss in spatial memory	Triple transgenic mice	(Blurton-Jones *et al.*, 2009)

		and learning by BDNF Increase in synaptic density	(3xTg-AD) that express PS-1, tau and APP	
Neural precursor cells	Cortical infarct cavity	Increased endogenous neurogenesis.	Focal cerebral ischemia in rat model	(Jin *et al.*, 2011)
Transdifferentiated human Wharton's jelly mesenchymal stem cells into neuron-like cells	Bilateral hippocampus injection	Improvement in cognitive functions. Reduced amyloid-beta load by increase in microglial activation	AβPP/PS1 transgenic mice model	(Yang *et al.*, 2013)
Neural stem cell	Intra-hippocampus	Increased expression of synaptic protein i.e. synaptophysin and GAP-43. Ameliorate cognitive impairment	APP + PS1 transgenic (Tg) mice	(Zhang *et al.*, 2014)
Choline acetyltransferase expressing human NSC	CA3 region in hippocampus	Differentiated into neurons and improved cognitive function of learning deficit model rats with hippocampal injury by increasing ACh level.	AF64A-cholinotoxin induced learning deficit rat model	(Park *et al.*, 2012)

AAV-BDNF alone	Intralateral ventricle injection	Attenuated behavioural deficits, prevented neuron loss, alleviated synaptic degeneration.	P301L mice	(Jiao *et al.*, 2016)
Astrocytic differentiation of grafted Neural Precursor Cells	Inilateral focal transplantation of NPCs	Neuroprotective effect of superficial cortical neurons	P301L mice	(Hampton *et al.*, 2010)

The main problems with stem cell therapies have been the quality and number of cells required, and the long-term survival of cells following transplantation, resulting in variability of patient outcome (Lindvall and Kokaia, 2010a). By better controlling the fate and local environment of transplanted NSCs, some of these problems may be overcome. The directed differentiation of neural stem cells has been previously investigated such as the use of BDNF (Blurton-Jones et al., 2009; Horne et al., 2010; Liu et al., 2014). A previous study has tried to capture the ability to differentiate cells using BDNF by aminolysation onto nanofiber scaffolds as a superior method to direct NSCs towards oligodendrocyte and neuronal fate than culturing in soluble BDNF. However, in this study the polymer polycaprolactone was used, which degrades slowly over time, has poor cell adhesion, wettability and mechanical properties and is more commonly used for bone tissue engineering (Hajiali et al., 2018). Alongside this, although BDNF provides an avenue to promote directed differentiation into neurons and enhance dendrite growth, BDNF does not act as a survival factor to increase survival of these cells (Blurton-Jones *et al.*, 2009; Liu *et al.*, 2014). Pre-treatment of NSCs with GDNF has previously been shown to increase cell survival following transplantation in a rodent Parkinson's disease model (Bizon et al., 2004). Alongside this, GDNF treatment has been shown to promote differentiation of cortical neural progenitor cells, even in the presence of the self-renewal-promoting factor, FGF2 (Bonafina et al., 2018).In combination with BDNF, this may enhance differentiation versus proliferation of neural stem cells, to increase the efficiency of cells produced for implantation. However once transplanted into the brain, it is difficult to maintain

external trophic support to these cells as neighboring cells in the pathological brain may be unable to provide healthy signaling and providing these factors regularly into a patient's brain is not a practical solution.

1.9.2.3 Human neural stem cell culture: self-renewal versus differentiation into mature neurons

Different factors promote the self-renewal versus differentiation of human NSCs. EGF and FGF2 are common mitogens used in neural stem cell cultures. The first four weeks after cells are plated from foetal tissue is known as derivation; cells adhere to laminin substrates and proliferate in the presence of both EGF and FGF2 in cell culture medium. At this stage cells do not survive without EGF and FGF2 (Figure 33. Pollard et al., 2006; Sun et al., 2008).

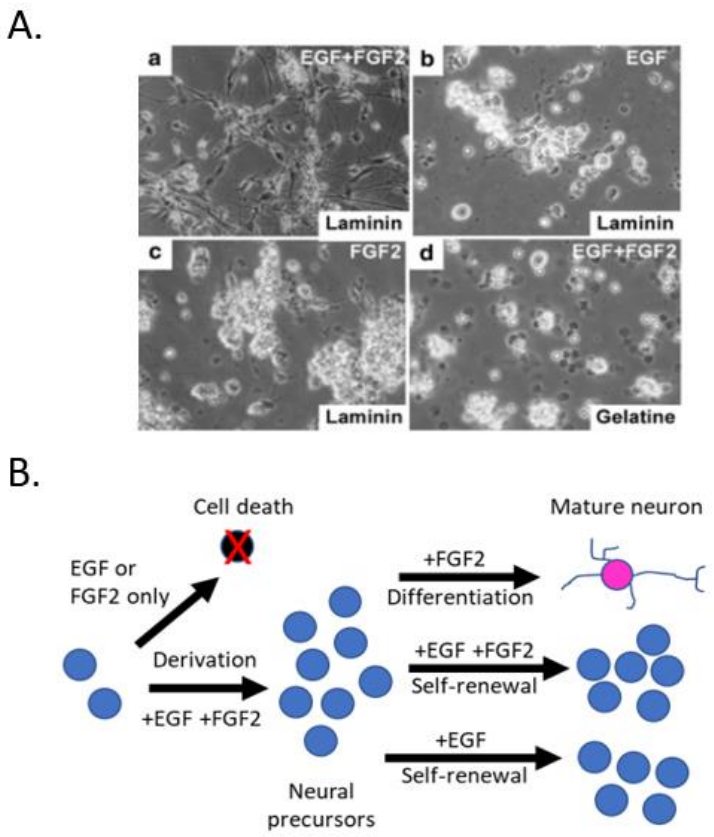

Figure 33. The growth of stem cells into mature neurons. A. EGF and FGF2 are both required for cell survival during the derivation but not expansion stage of hNSC culture (a-c). Even in the presence of EGF and FGF2, cells require laminin for adhesion and growth as cells grown on gelatin do not proliferate (d). Reproduced: Sun et al., 2008. B. Following derivation FGF2 is no longer required for self-renewal of cells. Removal of EGF results in differentiation via FGF2. Reproduced: Pollard et al., 2006.

Beyond derivation, EGF can be removed from the medium and cells will begin to differentiate in FGF2 alone and proliferation is inhibited. If FGF2 is removed, cells will continue to self-renew in EGF alone, and FGF2 is no longer required though the proliferation rate is much slower with a doubling time of 3–4 days (Figure 33; Sun et al., 2008).

To induce differentiation of neural stem cells into mature neurons, cells can be treated with FGF2 for two weeks, followed by 2-3 weeks maturation in basal medium with no exogenous growth factors. Only during weeks 3-4 of the maturation stage is the mature neuronal marker (Tuj1+) expressed (Figure 34, F). However, as shown by proportion of neural precursors (Nestin+) the differentiation is not fully effective. At this stage, BDNF is added to differentiated cell culture medium (Sun *et al.*, 2008).

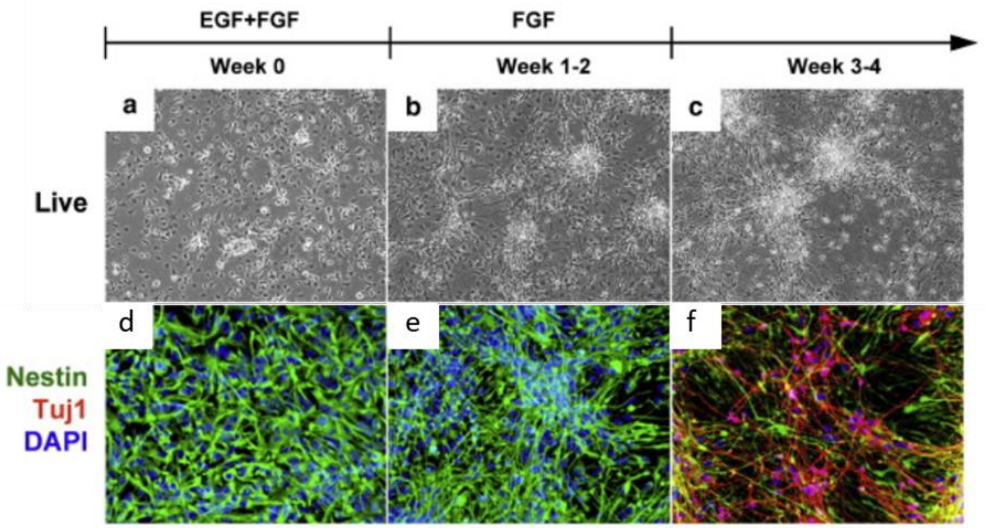

Figure 34. EGF and FGF2 are removed during stages of stem cell differentiation over four weeks. (Brightfield, a-c) cells are shown to proliferate and mature over 3-4 weeks. D-F show an increase of cells into mature neurons over 3-4 weeks, as shown by marker Tuj1, with a reduction in the neural stem cell marker, Nestin. DAPI shows nuclei of all cells. Adapted: Sun et al., 2008.

The pathway of plating cells from human foetal tissue to the formation of mature neurons takes a total of 7-8 weeks. At this timepoint, only a proportion of cells are differentiated into postmitotic neurons (Figure 34, f,Tuj1+). Alongside this, the addition of expensive proteins are required during medium replacements such as the mitogen FGF during maturation, and BDNF once cells are differentiated. We therefore aim to simplify the differentiation process with three key improvements. (1) differentiation can occur within a shorter time period, (2) efficient differentiation into mature neurons, and (3) requires less expensive proteins added to the medium

both to reduce costs and mimic a diseased brain environment where we assume any trophic support would be generated by the scaffold or implanted cells themselves.

1.9.2.4 Modification of bacterial cellulose for neural prosthetics

As a final step of the project, it is hoped that a biocompatible scaffold material can be used to provide an enriched environment, through biofunctionalisation, for neural stem cell prosthetics. Cell scaffolds provide a three-dimensional biomimetic environment for cells and tissue to grow on, and require three main properties: 1) a highly porous and permeable matrix in which nutrients and metabolic waste can be exchanged during cell growth 2) biocompatible with suitable surface chemistry that allows cell adhesion and differentiation, and a level of biodegradability required for its purpose, 3) mechanical properties closely matching the tissues at the site of implantation to increase cell integration and decrease chances of rejection (Hajiali et al., 2018).

Cellulose is considered to be the most abundant biopolymer in nature. Alongside its prominence in plants, cellulose is also found in some species of algae, fungi, or produced by certain bacterial strains. The *Gluconacetobacter hensenii* strain was used in this research offering a high yield of bacterial cellulose (BC). Some bacteria naturally produce cellulose from carbon and nitrogen sources to offer a protective cell coating. In nature, the carbon source for BC is often fruits, vegetables and alcoholic vegetables that offer high sources of glucose or glycerol. BC is produced as a 1% w/v thin film that rises to the air-liquid interface such that aerobic bacteria can trap themselves inside and remain in contact with oxygen. Bacterial cellulose (BC) and plant cellulose have the same chemical structure of $(C_6H_{10}O_5)_n$. BC has higher purity, and its well-spaced nano- and microfibrils with hydrogen bonds between fibrillar units result in higher strength, moldability and increased water holding ability as compared with plant cellulose(Jonas & Farah, 1998; Czaja et al., 2006). This unique cellulose structure is produced when hundreds-to-thousands of cellulose chains are extruded from pores on the cell envelope. These chains combine through hydrogen bonding into microfibrils and further combine into cellulose ribbons that make up the macrostructure of cellulose pellicles. A cellulose sheet is formed, which is a well-spaced 3D mesh

of ribbons is formed that is highly porous and offers plenty of space for hydration by water and bacteria to integrate into the matrix (Figure 35).

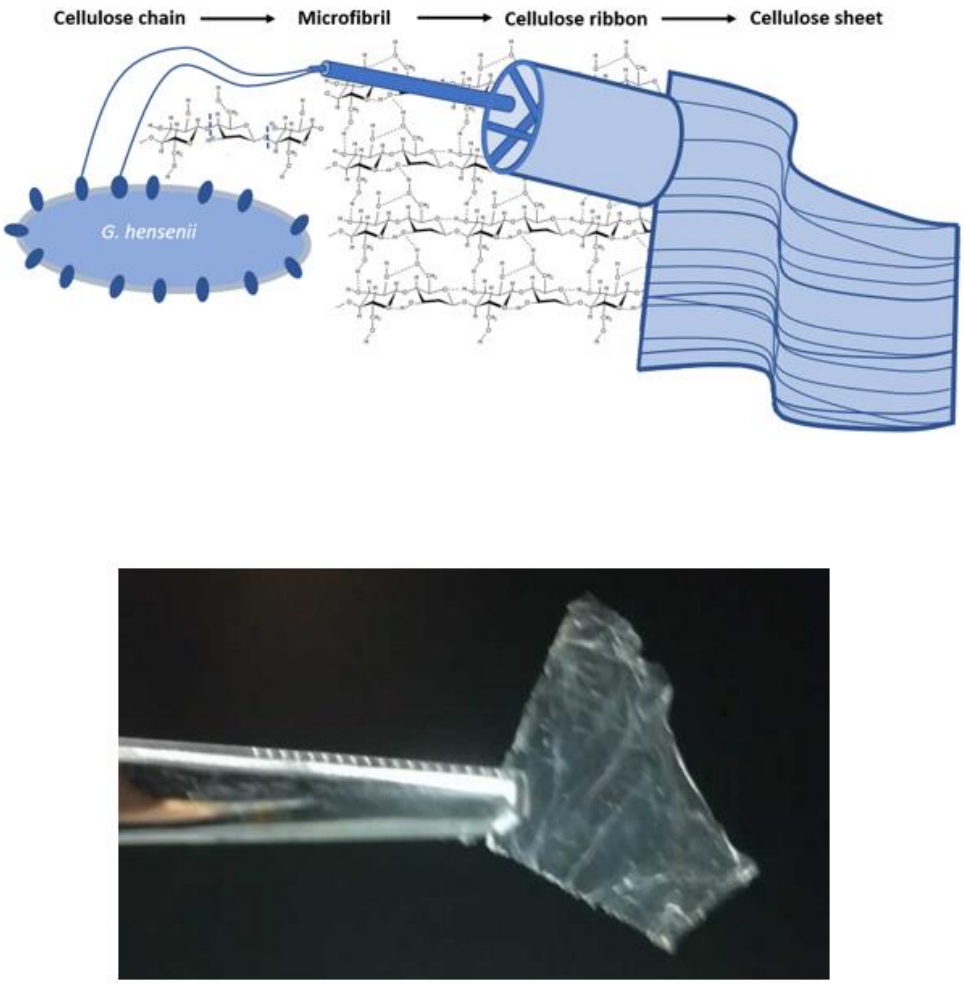

Figure 35. The structure of bacterial cellulose. Top: the production of bacterial cellulose initially from cellulose chains that hydrogen bond into microfibrils and form larger well-spaced ribbon/nanofibers and ultimately cellulose sheets. Adapted from: Lustri et al., 2015. Bottom: a piece of freeze-dried cellulose sheet after overnight PBS dehydration.

The biocompatibility, vapor permeability, molding ability, structural integrity and high water holding capability of cellulose has interested researchers in the medical applications of BC. Alongside this, the ribbons of bacterial cellulose microfibrils are structurally similar to native

extracellullar matrices that mammalian cells produce. Current medical applications include wound coating, tissue engineering and guided tissue regeneration (Czaja et al., 2007). For tissue engineering and regeneration, cell scaffolds are often used to support cell integration by providing an interface for cells whilst they form cell-cell connections and their own extracellular matrices. Some research is based on biodegradable scaffolds that disintegrate once the introduced cells have integrated and are capable of supporting themselves; however, the importance of the integrity of this scaffold to remain until this is the case has also highlighted the possibility of permanent scaffolds. The use of BC has already been shown to seed fibroblasts and/or keratinocytes to provide a monolayer of cells that can be directly placed into wounds to promote tissue regeneration. In these cases, BC is soaked in serum and electrolytic solutions such as sodium hydroxide, or adsorbed of collagen to promote cell adhesion (Watanabe *et al.*, 1993; Czaja *et al.*, 2007). BC can also act as an interfacing neural substrate that can be modified to allow conductivity, as shown by its use in microelectrode array fabrication. The ability to grow neurons on BC cellulose is highly advantagous due to the increased biocompatibility and reduced rigidity of BC as compared with other commonly used synthetic polymers including parylene C, PDMS and Poly(methyl methacrylate) (PMMA). Alongside this, BC has a similar stiffness to brain, and more robust mechanical properties and thermostability compared with other naturally derived polymers including Matrigel, collagen and silk (Figure 36) (Yang *et al.*, 2018). A major application for BC is therefore in neural prosthetics.

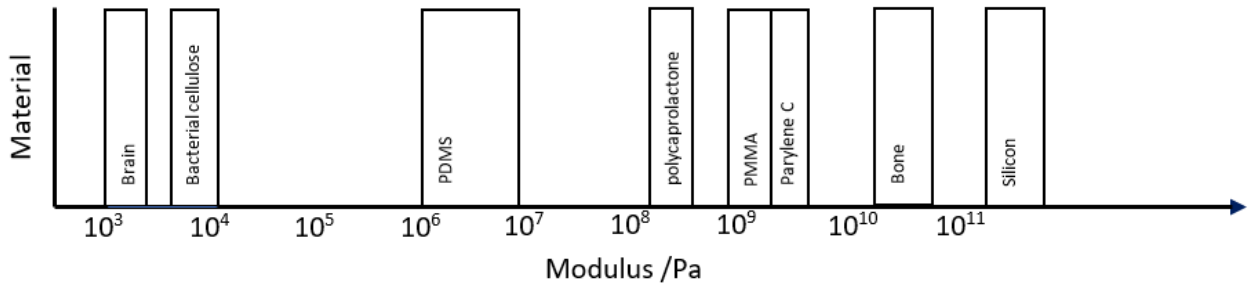

Figure 36. The modulus of materials widely used for fabrication of medical devices due to high biocompatibility. It is immediately apparent that BC is of most similar softness to the brain and therefore an optimal interfacing device where prosthetics require molding to brain regions. Adapted from Yang et al., 2018.

1.9.2.5 Key aims in the biofunctionalisation of cellulose for neural prosthetics

It is therefore of interest whether it is possible to functionalise proteins to cellulose that both direct the differentiation of neural stem cells and that promote their survival following transplantation. The first step requires adhesion of cells to the cellulose membrane, which has previously been done by serum treatment, which would promote glial versus neuronal growth in our conditions. The second step requires the ability of cells to grow and differentiate in an environment lacking trophic and signaling support due to dramatic cell loss in the transplantation region. The third step required long term survival of cells once transplanted and the ability to maintain signaling and trophic support. For this we combine BDNF to promote differentiation, with GDNF to promote survival, and laminin to aid adhesion. By removing growth factors from the cell culture medium, we mimic an environment that may occur in diseased brain to determine whether the cells are capable of maintaining their survival on the biofunctionalised cellulose graft alone.

METHODS

2.1 Ethics statement

All animal work conformed to guidelines of animal husbandry as provided by the UK Home Office. Animals were bred and supplied by Charles River UK Ltd., Scientific, Breeding and Supplying Establishment, registered under Animals (Scientific Procedures) Act 1986, and AAALAC International accredited, and sacrificed under schedule 1; procedures that do not require specific Home Office approval.

2.2 E18 rat primary hippocampal cultures

Sprague Dawley pregnant rats were obtained from Charles River (Margate, UK), and sacrificed by animal technicians under schedule 1 procedure. Day 18 embryos (E18) were dissected in HBSS ([-Ca] [-Mg] Sigma-Aldrich, St Louis, USA) to remove the hippocampi which were kept in DMEM (Sigma-Aldrich) on ice whilst the remaining hippocampi were dissected. Following isolation, hippocampi were incubated for 20 min at 37°C in 0.1 % trypsin (Worthington Biochemical Corporation, Lakewood, USA) and 0.05 % DNAse (DN25 Sigma-Aldrich, St Louis, USA) in DMEM (Sigma-Aldrich) to cleave the extracellular matrix. Hippocampi were washed 4x in 500 µL 0.05 % DNAse in DMEM. Cells were dissociated using a p200 pipette (Gilson, Middleton, USA) in DMEM with 10 % fetal bovine serum (FBS) to neutralise the trypsin. 8-well Nunc® Lab-Tek® (Sigma-Aldrich) were coated with 0.01% poly-L-lysine solution (Sigma-Aldrich, St Louis, USA) and kept in Neurobasal medium ([-phenol red], Gibco, Thermo Fisher Scientific, Waltham, USA), 0.25 % glutaMAX (Thermo Fisher Scientific, Waltham, USA) and 2 % B27 (Thermo Fisher Scientific) (E18 medium). Cell were kept in an incubator at 37°C, 5 % CO_2 and 100 % humidity and unless otherwise specified were experimented on between 14-18 days *in vitro* (DIV14-DIV18).

2.3 Production of monomeric human full length (htau40) tau protein

This work was performed by Na Yu, Dr. Colin Hockings, and Dr. Amberley Stephens

The protein was made using the full-length 2N4R human sequence of microtubule-associated protein tau (tau). Ile260 was replaced by a cysteine for labelling the protein via a maleimide reaction to Alexa Fluor® 488, 594 or 647 (Invitrogen, Thermo Fisher Scientific). The mutations C291A and C322A were used to remove native cysteines in the sequence to allow single residue labelling. Previous work has shown that cysteine residues 291 and 322 are required for heparin-dependent dimerization into fibrils (Bhattacharya *et al.*, 2001), however use of these residues does not appear to inhibit aggregation in our studies (Michel *et al.*, 2014). The use of Ile260 avoids situating a fluorescent dye in regions that may disrupt the aggregation of monomers such as in the β-promoting repeat regions.

The pET29b:Tau plasmid was added for final a concentration of 190 μg/μL in 20μl BL21 (DE3, New England Biolabs, Ipswich, MA) chemical competent cells which had been thawed on ice for ~2 min from -80 °C. The cells were kept on ice for 20 min with the plasmid, heat shocked at 42 °C for 35 s, and put back on ice for 35 s. 500 μL Lysogeny broth (LB) was added and the cells were incubated at 37 °C for 1 hr with shaking. The cell suspension was centrifuged at 3000 rpm, 3 min and the pellet was resuspended in 50 μL of LB. Cells were spread with a cell spreader onto LB Agar plates with 50 μg/mL Ampicillin and incubated overnight at 37 °C. 2 colonies were selected and added to 50 mL LB and 100 μg/ml ampicillin in a 250 mL flask; the cells were left to grow overnight in a shaking 37 °C incubator. The cell suspension was divided into 12L LB (1L/2Lflask) with 100 μg/mL Ampicillin and kept in a 220 revolutions per minute (rpm) shaking 37 °C incubator until the optical density (OD) of the bacteria solution of 0.7 at 600 nm was reached. Cells were induced with 0.5 mM Isopropyl β-D-1-thiogalactopyranoside (IPTG), for 3 hr at 37 °C before harvesting. Cells were centrifuged at 4000 rpm, 15 min, and the pellet was resuspended in 200 mL re-suspension buffer (20 mM 2-(N-morpholino)ethanesulfonic acid (MES), 1 mM ethylene glycol-bis(β-aminoethyl ether)-N,N,N′,N′-tetraacetic acid (EGTA), 0.2 mM $MgCl_2$, 5 mM dithiothreitol (DTT), pH 6.8 using NaOH). The cells were then

lysed in 0.1 mM phenylmethylsulfonyl fluoride (PMSF) using a sonicator with a cycle of 30 s on and 30 s off until the suspension turned from opaque to clear (~ 4 min).

High salt, 0.5 M NaCl, was added to the cell lysate to induce the precipitation of most proteins other than tau. Cell lysate was boiled in a water bath at 90 °C, 20 min. Once cooled, lysate was put into dialysis tubing overnight to remove high salt from the protein solution to allow binding with the ion exchange column. Tubing was submerged in dialysis buffer (20 mM MES, 1 mM EGTA, 1 mM $MgCl_2$, 2 mM Dithiothreitol (DTT), 0.1 mM PMSF, pH 6.8 using NaOH) stirred at 100 rpm, 4 °C.

A HiTrap SP HP column (GE Healthcare Life Sciences, Uppsala, Sweden) was used for cation exchange. The protein solution was loaded onto the column in buffer A (20 mM MES, 1 mM EGTA, 1 mM $MgCl_2$, 2 mM DTT, pH 6.8 using NaOH) and eluted in buffer B (20 mM MES, 1mM EGTA, 1mM $MgCl_2$, 2 mM DTT, 250 mM NaCl, pH 6.8 using NaOH). The different ion exchange elution fractions separated by sodium dodecyl sulfate–polyacrylamide gel electrophoresis (SDS PAGE) to identify tau. Ion exchange fractions containing tau were concentrated using a Vivaspin20 (GE Healthcare Life Sciences,) protein concentrator. Tau was further purified by size exclusion chromatography (SEC) on a Superdex® 75 pg 10/300 GL column or a HiLoad 16/60 Superdex 200 pg column (GE Healthcare Life Sciences, Marlborough, USA) in SEC buffer (PBS with 1 mM DTT, pH 7.4). The extinction coefficient of full length 2N4R tau protein, 7575 M-1cm-1 or Absorbance 0.1% (1g/L) = 0.165, was used to calculate its concentration. General protein yield was ~10 mg/L. Samples were also sent for liquid chromatography mass spectrometry (LCMS) at the Department of Chemistry, University of Cambridge to verify the protein identity.

2.3.1 Protein labelling

Alexa Fluor® 488, 594 or 647 maleimide (Molecular Probes by Thermo Scientific, Waltham, USA) were dissolved in dimethyl sulfoxide (DMSO) at 10 mM. A 10-fold molar excess of dye was added to the protein solution (108 µM protein with 1 mM dye) and incubated at 4 °C overnight for the maleimide labelling reaction to occur. Remaining free fluorophores were removed from the covalently labelled protein using SEC on a

Superdex® 75 pg 10/300 GL column with PBS. Protein labelling efficiency was determined using analytical reversed phase chromatography. This was performed on an Agilent 1260 Infinity High Performance Liquid Chromatography (HPLC) system (Agilent Technologies, Santa Clara, USA) equipped with an autosampler and a diode-array detector using an analytical C18 Discovery BIO Wide Pore C18, 15 cm x 0.46 cm, 5 µm column (Sigma-Aldrich) with a gradient of 5 % to 95 % acetonitrile with 0.1 % trifluroacetic acid (TFA) and 95 % water and a 1 mL/min flow rate over 40 min. The protein labelling efficiency was shown to be ~100 %. The protein concentration was calculated from measurements of the absorbance at 280 nm and the fluorophore absorbance maximum (see Table 13). Tau protein was frozen at -80 °C until use. The labelling was shown not to interfere with tau aggregation (Michel et al., 2014).

The protein concentration was calculated from measurements of the absorbance at 280 nm and the fluorophore absorbance maximum (Table 13). Tau protein was frozen at -80 °C until use.

Table 13. The concentration of labelled protein was calculated by measuring the absorbance at 280nm and that of the fluorophore absorbance maximum.

	Absorbance Maximum (λ_{max})	Extinction Co-efficient at λ_{max}	Extinction Co-efficient at 280 nm
Alexa Fluor 488	494 nm	203,000 $cm^{-1}M^{-1}$	22,330 $cm^{-1}M^{-1}$
Alexa Fluor 594	590 nm	73,000 $cm^{-1}M^{-1}$	40,880 $cm^{-1}M^{-1}$
Alexa Fluor 647	650 nm	203,000 $cm^{-1}M^{-1}$	7,170 $cm^{-1}M^{-1}$
Tau (cys)	-	0 $cm^{-1}M^{-1}$	7,450 $cm^{-1}M^{-1}$

All studies use this form of human full-length 2N4R monomeric tau protein (hTau40). Where labelled tau is used, the proportion of labelled: unlabelled protein, and the fluorophore tag used will be included.

2.4 FLIM-TCSPC

All samples were assayed on a home-built, confocal-based FLIM platform using time-correlated single photon counting (TCSPC). The equipment is a modified version of a published multiparametric imaging system (Frank et al., 2007) and equipped with a 100x objective lens (UPLS Apo, 60x oil, 1.4NA, Olympus, Germany). A pulsed supercontinuum source (WL-SC-400-15, Fianium Ltd., UK, pulse width 6 ps, repetition rate 40 MHz) was used for excitation in conjunction with a tuneable filter (AOTFnC-400.650, Quanta Tech, New York, USA), an excitation filter FF01-560/25, and an emission filter FF01-624/40 (both from Semrock Inc., New York, USA). Photons were recorded in time-tagged, time-resolved mode that permits sorting photons from each pixel into a histogram according to the arrival times after the last laser pulse. The data were recorded by SPC-830 (Becker and Hickl GmBH, Germany). Photons were acquired for 3 min to make a single 256 x 256 FLIM image. A reference dye Erythrosin B with a very short lifetime of 90 ps was used to capture the instrument response function. For labelled-tau data, the TCSPC histograms were fitted with a single exponential decay function using FLIMfit (Warren et al., 2013). Statistical analysis was carried out using one-way ANOVA followed by Dunnett's multiple comparisons test in Prism6.0 software (Graphpad, La Jolla, California, USA).

2.5 Treatment of cells with tau protein and ammonium chloride solution

8-well LabTek dishes (Thermo Fisher Scientific) were plated with 50,000 cells/well in 200 µL Neurobasal medium ([-phenol red], Gibco, Thermo Fisher Scientific, Waltham, USA), 0.25 % glutaMAX (Thermo Fisher Scientific, Waltham, USA) and 2 % B27 (Thermo Fisher Scientific) (E18 medium). At DIV14-18 the cells were used for experimentation.

For tau treatment, 1 µM tau protein (0.3 µM labelled Alexa Fluor®594: 0.7 µM unlabelled) was added to cells in 100 µL of E18 medium. For cells treated with ammonium chloride (NH_4Cl), 10 mM was added to cells in 100 µL E18 medium prior to the addition of tau protein (Poole & Ohkuma, 1981). Cells were incubated for 4 hr, at which time tau has been shown to enter cells through endocytosis and aggregate inside of cells at low pH (Michel et al., 2014). After 4 hr, cells were incubated with trypsin to remove tau that had not been taken up by cells from the media to reduce background fluorescence during imaging. Trypsin incubation consisted of the addition of 1x wash MEM (Sigma-Aldrich), 1 min incubation in 1:5 0.01 % Trypsin (0.05 % trypsin-EDTA) in MEM, 5 min incubation in MEM with 10 % FBS, 2 min in MEM. For cells incubated in NH_4Cl, 10 mM was added to each wash and imaging step to prevent aggregation during these steps. Samples were then transferred to an OKOLab StageTop Incubation chamber (Okolab Inc., Ottaviano, Italy) for imaging cells at 37°C and 5 % CO_2 using FLIM-TCSPC as previously described (Section 2.4).

2.6 Calibrating a pH lifetime sensor and its use in cell cultures

2.6.1 Preparation of cells and buffer solutions

Dextran Oregon green™ 514 70,000 MW (dextran-OG514) was calibrated for use as a sensor of pH using fluorescence lifetime imaging (FLIM-TCSPC). A protocol was developed based on Lin et al., (2003) with advice from Dr. Michelle Teplensky. A dextran-OG514 stock solution of 5 mg/mL was made using HBSS. For calibration studies, Human embryonic kidney 293T (HEK-293T) cells were plated at 30 000 cells in 0.4 mL per well of an 8-well LabTek dish (Thermo Fisher Scientific) for a ~18 hr seed. The media was removed and replaced with 200 µL of fresh HEK medium (DMEM with 10 % FBS and 1 % glutaMAX (Thermo Fisher Scientific). 50 µL of dextran-OG514 was added for a working concentration of 1mg/mL in which the cells were incubated for 2 hr. The solution was changed to 400 µL of fresh HEK medium for a 1 hr incubation. Following this, the media was removed and replaced with a buffer of measured pH for calibration of the probe.

The extracellular 2-(N-morpholino)ethane sulfonic acid (MES) buffer consisted of 5 mM glucose, 20 mM MES, 1 mM $CaCl_2$, 1 mM $MgCl_2$, 130 mM NaCl, and 10 mM KCl. The buffer was pH adjusted to 3.98, 4.45, 5.45, 5.34 or 6.45 using HCl and NaOH solutions. The lysosomal pH was clamped to that of the extracellular buffer pH through addition of nigericin and monesin (Biorad, Hercules, USA). The pH clamping is achieved through nigericin which causes the equilibration between the external and internal pH through exchanging internal K^+ for external H^+ (Thomas *et al.*, 1979). This process is accelerated through use of the Na^+/H^+ ionophore, monensin. Final concentrations of 20 µM nigericin and 10 µM monesin (Biorad) prepared in absolute ethanol, were added to the relevant pH buffer and imaged within 10 min to maintain cell viability.

2.6.2 Measuring pH in neuronal cultures

Hippocampal neurons were plated at 50 000 cell/well and incubated until DIV14-21. In 100 µL of E18 medium, cells were treated with 1 µM of tau protein with 30 % tau-AF594. After 1 hr, 2 µL (0.04 mg/mL) dextran-OG514 was added, higher concentrations were found to be cytotoxic. Cells were incubated for a further 1.5 hr before medium was replaced with 100 µL conditioned E18 medium and cells were imaged immediately without further 1 hr incubation as for HEK-293T cells. For NH_4Cl condition, 10 mM was added before the addition of tau, and again following medium replacement. The samples were imaged for up to 1 hr, at which point dextran-OG514 signal-to-noise became low.

2.6.3 TCSPC-FLIM imaging and analysis

Imaging and analysis in HEK-293T cells was performed by Chetan Poudel. Sample preparation of HEK-293T and primary neurons, imaging and analysis of primary neurons was performed by the author.

The samples were imaged on a custom-built confocal-based time-correlated single photon counting fluorescence lifetime imaging microscope (TCSPC-FLIM) that uses a

supercontinuum source. The tunable filter was set to 510 nm with additional excitation filter FF01- 542/27, and emission filter FF01-560/25 (both from Semrock Inc.). In addition, an excitation filter FF01-560/25, and an emission filter FF01-624/40 (both from Semrock Inc.) were used for imaging tau. For analysis, FLIMFit (Warren *et al.*, 2013) software was used, and the TCSPC histograms for each pixel were fitted using a monoexponential decay function.

2.6.4 Correlative analysis of two-colour FLIM images

Performed by Chetan Poudel.

FLIM images from the two channels (Tau- Alexa Fluor®594 and Dextran-OG514) were analysed independently in FLIMfit v4.12.1 (Warren *et al.*, 2013). Analysed FLIM images were exported from FLIMfit as tiff images and were imported in MATLAB. A custom MATLAB script was written to pair together the fluorescence lifetime of Tau-Alexa Fluor®594 and the fluorescence lifetime of dextran-OG514 for each pixel in the image set. Pixels where both lifetime values were not present were discarded from the correlation analysis. Each image set was plotted as an xy plot with the lifetime of dextran-OG514 on the x-axis and Tau-Alexa Fluor®594 on the y-axis. Data from n=3 biological repeats were pooled to create a single xy plot for each treatment condition (control and NH_4Cl). Each biological repeat had at least three sets of two-channel images.

2.7 Understanding the timescale at which exogenous tau aggregates inside of primary hippocampal neurons.

Neurons were plated 500 000 cells/well in an 8-well LabTek dish (Thermo Fisher Scientific). At DIV14-18, neurons were treated with 1 µM tau protein (0.3 µM labelled Alexa Fluor®594: 0.7 µM unlabelled). Timeseries of images were taken between 30 – 50 min using FLIM-TCSPC as previously described (Section 2.4) and data were pooled for analysis.

2.8 Altering calcium ion concentrations in cells to determine the effect of calcium ions on tau aggregation

Neurons were plated 500 000 cells/well in an 8-well LabTek dish (Thermo Fisher Scientific). At DIV 14-18, neurons were treated with 1 µM tau protein (0.3 µM labelled Alexa Fluor®594: 0.7 µM unlabelled) and treated with either 1.2 µM ionomycin ('high calcium'), 1.2 µM ionomycin + 10 mM KCl (Sigma-Aldrich) ('high calcium + stimulation'), or 1.2 µM ionomycin + 2 mM EGTA (Sigma-Aldrich) ('low calcium'). Cells were imaged at 3-4 hr or continuously between 30 – 50 min using FLIM-TCSPC as previously described (Section 2.4).

2.9 The pH and calcium ion concentration dependence of tau aggregation in the presence of synaptic vesicles

2.9.1 Synaptic vesicle isolation

Performed by Dr. Amberley Stephens

Isolation of synaptic vesicles (SVs) from rat brains of 6-8 week old mice was performed as previously described (Ahmed *et al.*, 2013). Brains were removed from two euthanized Sprague-Dawley rats and washed in ice cold homogenising buffer (320 mM sucrose, 4 mM 4-(2-hydroxyethyl)-1-piperazineethanesulfonic acid (HEPES), EDTA-free complete protease inhibitor, at pH 7.4). The brains were placed in 9 mL homogenising buffer in a glass-Teflon homogenizer and were homogenised for 10 strokes at 900 rpm. The homogenate was centrifuged at 1000 x g for 10 min at 4 °C and supernatant was further centrifuged at 15, 000 x g for 15 min at 4 °C. The supernatant was decanted and stored on ice and the pellet resuspended in 1 mL homogenising buffer. To release SVs from the synaptosomes, the resuspended pellet was homogenised in an added 9 mL ice cold ddH2O with EDTA free c0mplete protease inhibitors for three strokes at 2000 rpm. 50 µL of 1 M HEPES (NaOH) was immediately added. To remove contaminating proteins and

membranes, the homogenate was centrifuged at 17, 000 x g for 15 min at 4 °C. The resulting supernatant was combined with the supernatant kept on ice and centrifuged at 48, 000 x g for 25 min at 4 °C. The supernatant was decanted and homogenised for five strokes at 2000 rpm. The solution was triturated with a 30-gauge needle to disperse vesicle clusters. 5 mL of this solution was gently pipetted onto 5 mL 0.7 M sucrose cushion. The sucrose cushions were centrifuged at 133,000 x g for 1 hr at 4 °C. Starting at the top of the gradient 500 µL fractions were collected for the whole gradient; to identify SV (synaptotagmin) versus non-SV (proteasome; Regulatory particle triple-A ATPase 4 (Rpt4)) proteins by a dot blot, 5 µL of each fraction was pipetted onto a methanol soaked PVDF membrane. Rpt4 (Abcam, Cambridge, UK, AB22639, 1:1000) and the vesicle protein synaptotagmin (SYSY, Goettingen, Germany, 105103 1:1000) were probed using the anti-mouse IgG (GE Healthcare, Chicago, USA, 1:1000) and anti-rabbit IgG (GE Healthcare, Chicago, USA, 1:100) secondary antibodies. Fractions 12-20 were positive for synaptic vesicles and negative for proteasomes, and were pooled and centrifuged at 300,000 x g for 2 hr. Size-exclusion chromatography was performed as a final purification step. The vesicle pellet was resuspended in 1 mL column buffer (100 mM Tris-HCl, 100 mM KCl, at pH 7.6) and homogenised in a 1 mL glass-teflon homogeniser for ten strokes at 900 rpm. The vesicles were gently triturated 3x through a 30-gauge needle. Vesicles were loaded onto a pre-prepared Sephacryl S-1000 column and a peristaltic pump with a flow rate of ~6 mL hr^{-1}, 4°C overnight. After 10 or 11 hr SVs should be eluted from the column, and 0.7 mL fractions were collected and analysed at 280 nm on a Nanodrop to determine the location of vesicle elution. Two peaks were shown on the graph of protein concentration (absorbance at 280 nm), the vesicles resided in the second peak. The fractions from the second peak were pooled and centrifuged at 300,000 x g for 2 hr; SVs formed a clear pellet on the tube wall and the supernatant was removed and vesicles were resuspended to a concentration of 3.6 mg/mL protein in PBS.

2.9.2 Investigating the effect of pH and calcium ions on tau aggregation through incubation with synaptic vesicles

To test whether cell membrane was required to catalyse the aggregation of tau, 0.3 µL synaptic vesicles (of 3.6 mg/mL protein stock) were added to 30 µL HBSS ([-Ca] [-Mg] Sigma-Aldrich) in wells of rubber gaskets on a coverslip. The HBSS was adjusted to pH 5.3 or 7.2 using 4 M NaOH and 1 M HCl to compare acidic versus physiological pH conditions. $CaCl_2$ (Sigma-Aldrich, St Louis, USA) was added to investigate the effects of 100 µM, 2 mM, or 10 mM concentration of calcium ions on tau aggregation for both pH conditions. A condition without calcium was also used for each pH. An Hanks' Balanced Salt Solution (HBSS) control without vesicles at pH 7.2 was used as tau would not be expected to readily aggregate at physiological pH in this time period as previously shown (Michel *et al.*, 2014). 1 µM tau protein (0.3 µM labelled Alexa Fluor®594: 0.7 µM unlabelled) was added to each well and incubated for 4 hr at 37°C (ambient CO_2). 10.8 µg synaptic vesicles (3 µL from 3.6 mg/mL protein in PBS stock) were added to all conditions except for the negative control. Small petri dishes of water were places around the coverslips to reduce evaporation during incubation. At 4 hr, coverslips were imaged using FLIM-TCSPC, as previously described (Section 2.4), to determine the fluorescence lifetime of labelled tau protein as a correlate of its aggregation state.

2.9.3 Investigating the effect of pH 5.3 and calcium ions on tau aggregation

To determine whether tau was capable of aggregating at pH 5.3 over 4 hr or 24 hr, three conditions were explored. 1 µM tau protein (0.3 µM labelled Alexa Fluor®594: 0.7 µM unlabelled) was added to 30 µL HBSS ([-Ca] [-Mg] Sigma-Aldrich). HBSS was pH adjusted to pH 5.3 with 1 M HCl, or kept at physiological pH 7.2 for ‘monomer solution’ negative control. 2 mM $CaCl_2$ (Sigma-Aldrich) was added in the presence or absence of 10.8 µg synaptic vesicles (3 µL from 3.6 mg/mL protein in PBS stock). Solutions were incubated in PCR tubes for 4 hr or 24 hr at 37°C (ambient CO_2). Samples were imaged using FLIM-TCSPC (Section 2.4) to determine the fluorescence lifetime of labelled tau protein as a correlate of its aggregation state.

2.10 Measuring cell stiffness using atomic force microscopy

E18 rat primary hippocampal neurons were plated in glass-bottom dishes (WilCo Wells B.V., Amsterdam, Netherlands) suitable for atomic force microscopy (AFM). 200 µL of poly-L-lysine (Sigma-Aldrich) was added to the centre of the dish for a minimum of 40 min, and washed 3x in HBSS (Sigma- Aldrich). Cells were plated at a density of 50 000 cells/dish initially in only 200 µL of E18 medium overnight to keep the cells concentrated to the centre of the dish, before adding another 2 mL of medium once cells adhered.

Stiffness of control cells was measured in E18 medium. To test the effects of tau on the stiffness of cells, 1 µM of monomeric tau protein (unlabeled) was added to the medium of DIV 14 hippocampal neurons. The cells were incubated for 4 hr at 37 °C prior to stiffness measurements. To test the effects of microtubule depolymerisation on the stiffness of cells, 70 nM nocodazole was added to cell medium for 2 hr at which point stiffness measurements were taken. To control for the use of DMSO as vehicle, which is known to have an effect on cell membrane integrity at higher concentrations, 0.04 % DMSO was added to cell medium for 2 hr before measurements. As a positive control, 0.2 % DMSO was added to cell medium for 2 hr to test that a change in stiffness could be found during cell death using this method. During stiffness measurements cells remained incubated in E18 medium in their treatment, or control condition. After 1 hr measurements were stopped to limit evaporation of medium and cell death from acidity of cell medium.

Dishes were placed on the AFM (Bruker, Bioscope RESOLVE) low magnification stage heated to 37°C; PeakForce QNM-Live Cell probes were used for the measurements (PFQNM-LC, Bruker AFM probes). 25 μm^2 fields of view were selected (256 × 256) in areas of lowest cell density. NanoScope software (Bruker) was used to gain nanomechanical measurements over specific cell regions. For each cell, 3x 1 μm^2 areas were selected, and mean stiffness values were calculated as an estimate of the cone-sphere modulus taking into account the AFM tip size, shape and deflection sensitivity (Curry *et al.*, 2017). Second order flattening was applied to AFM topography images to remove tilt and bow. Data were analysed in Prism6.0 (GraphPad) using a one-way ANOVA and Tukey test for multiple comparisons between the group means.

2.11 The activity-dependent aggregation and pathological phenotype of tau protein

2.11.1 The stimulation of neurons with a custom developed optogenetic device, OptoGenie

The design and implementation of an optogenetic stimulation device in collaboration with Omid Siddiqui. Design objectives, modularity of device, laser diode selection and use of Arduino were by the Author. Circuit design and housing were selected or fabricated by Omid Siddiqui and the Electronics workshop of the Department of Physics.

OptoGenie is made of two core components, the laser diode head, and the metal mount that houses it. The laser diode head contains the electronics board and the mounting cage. The electronics of the laser diode was based on several commercial components that can be given to departmental electronic workshops or sent to commercial printed circuit board (PCB) prototype manufacturing companies for integration into a functional circuit. Components include: a 6 x 6 cm electronics board with a ~ 31 mm hole in each corner, surface mount resistors, a MOSFET (9V and up to 500mA), A 450 nm wavelength laser diode (TO38, PL 450B, Osram) with peak wavelength measured at 458 nm, a standard rotary potentiometer.

The laser diode head collimates and determines the spot size of the light. This is recommended for increased control of the spot size and intensity. Once the laser diode electronics were mounted to the board, 30 mm cage posts were screwed to the hole in each corner of the electronics board. A lens with focal length 4 mm (C610TME-A, Thorlabs Inc., Newton, USA) was screwed into a 30 mm XY translator cage (CX1Y1, Thorlabs Inc.) to collimate the laser light. The XY cage was then threaded through the 30 mm posts in the laser diode board until the lens was ~ 4 mm from the diode. The laser should then be turned on at low power to test whether the light is collimated. This was determined by measuring the size of a light spot on the wall to ensure that it remained constant whilst the laser head was moved closer and further from the wall. The XY cage was screwed securely to this position by tightening the inbuilt screws. The laser can be centred using the XY thumb screws on translator cage. Alternatively, a collimated package can be purchased though

this is a more expensive option. An adjustable aperture (SM1D25, Thorlabs Inc.) was screwed to a threaded standard cage plate (SM1SP2OM, Thorlabs Inc.). This was inserted into the 30 mm cage posts and secured.

For mounting onto an optical bread board (MB1015/M, Thorlabs Inc.) for housing the laser diode head, a ½" post was screwed onto the XY cage and a 2nd ½" post was screwed onto the optical breadboard. These were connected via an RA90 angled bracket.

Depending on the length of the experiment and placement of the system, the OptoGenie can be powered by a 9 V battery or connected to mains power supply through a power cable supplied to the Arduino Uno (Arduino.cc). The stimulation protocol was loaded to the Arduino using the Arduino IDE (code can be found in Appendix A.3) and equates to 3 x 10 ms light pulses each separated by 33 ms (33 Hz), followed by a 10 s interval repeated on a loop.

2.11.2 Characterisation of the OptoGenie device: intensity measurements and long-term stimulation

The stimulation power was changed manually by an analogue variable resistor, and the stimulation spot area could be changed manually with an adjustable iris. To ensure intensity remained above threshold required for cell stimulation whilst powered by the 9 V battery, intensity was measured over 2.5 hr. The spot diameter was set to 6 mm and the laser power diode to 9.38 mW for mains power recordings and maximal power of 44.8 mW for battery recording. After 2.5 hr, a 2nd battery-powered recording was made using 8.71 mW starting power from the laser diode for another 2.5 hr. The stimulation pulse was determined with an Arduino Uno and set using the Arduino IDE for 600 ms pulse each 200 s. Data were logged using 'Thorlabs Optical Powermeter Utility' software and PM100D power meter (Thorlabs Inc.). Data were plotted in Prism6.0 (Graphpad).

2.11.3 Neuronal culture

Performed by Dr. Tanja Fuchsberger

Postnatal day 0 or 1 (P0/P1) primary hippocampal neurons were prepared from brains of mice that express channelrhodopsin-2/EYFP fusion protein following exposure to Cre recombinase (Ai32) through the hippocampal specific Glutamate Ionotropic Receptor Kainate Type Subunit 4 (Grik4) promoter (Grik4-Ai32 mice). Hippocampi were dissected and placed into PBS containing papain (Thermo Fisher Scientific) in a 37°C water bath for 25 min to cleave the extracellular matrix. Cells were rinsed in 97.5 % Neurobasal Plus Medium (Gibco, Thermo Fisher Scientific), 0.25 % glutaMAX (Gibco, Thermo Fisher Scientific) and 2 % B27 plus (Gibco, Thermo Fisher Scientific) (P1 medium) containing 10 % fetal bovine serum (FBS). The tissue was then triturated with a pipette to dissociate the cells into single-cell suspension. Cells were then centrifuged for 10 min at 0.4 relative centrifugal force (rcf). The supernatant was removed from the pellet, and the cells were re-suspended in P1 culture media. Cells were plated at 50, 000 cells/well in poly-L-lysine coated 8-well LabTek (Thermo Fisher Scientific) dishes for imaging studies, or pre-coated with poly-D-lysine and laminin coverslips for electrophysiology studies. Cultures were incubated at 37°C, 5 % CO_2. Neurons on coverslips were plated in 500 µL of P1 medium in a 12-well plate and 24 hr after plating, 500 µL of P1 medium was added to each well to bring the total volume to 1 mL. Every 2nd day 330 µL of P1 medium from each well was replaced with 330 µL of fresh P1 medium. Recordings and imaging were carried out after 14-21 days of culture depending on the expression levels of YFP (DIV14-21).

2.11.4 Whole-Cell Patch Clamping recordings for validating the optogenetic stimulation of cells

Performed by Dr. Tanja Fuchsberger

Cells were superfused in artificial cerebrospinal fluid (aCSF) (126 mM NaCl, 3 mM KCl, 26.4 mM NaH_2CO_3, 1.25 mM NaH_2PO_4, 2 mM $MgSO_4$, 2 mM $CaCl_2$, and 10 mM glucose,

pH 7.2 and osmolarity 270–290 mOsm L^{-1}). The aCSF solution was continuously infused with carbogen gas (95 % O_2/5 % CO_2), and circulated at 2 mL/min with a peristaltic pump. Patch pipettes were made from borosilicate glass capillaries (0.68 mm inner diameter, 1.2 mm outer diameter) (Wold Precision Instruments, Hitchin, UK) using a P-97 Flaming/Brown Micropipette Puller (Sutter Instrument Co., Novato, USA) with tip resistances of 3-6 MΩ. Pipettes were filled with intracellular recording solution (IC) (110 mM potassium gluconate, 4 mM NaCl, 40 mM HEPES, 2 mM ATP-Mg, 0.3 mM GTP, pH 7.2 adjusted with 1 M KOH, and osmolarity to 270 mOsm L−1 with ddH2O). Whole cell patch-clamp recordings were carried out in current clamp mode. Cells were visualised using infrared differential interference contrast (DIC) microscopy (BX51WI Olympus). A U-RFL-T mercury light source (Olympus) with excitation filter 490-550 nm was used to select for cells expressing YFP. Only cells with a starting resting membrane potential of between −55 mV and −70 mV were used for recordings, and cells were kept at this resting membrane potential without the application of a current through the recording electrode. Voltage signals were low-pass filtered at 2 kHz using an Axon Multiclamp 700B amplifier (Molecular Devices, Sunnyvale, USA). Data were acquired at 5 kHz via an ITC18 interface board (Instrutech, Port Washington, New York, USA), and visualised using the Igor Pro software (WaveMetrics, Lake Oswego, USA).

2.11.5 Optogenetic stimulation of cells treated with monomeric tau

Cells were treated with 1 µm tau protein (0.3 µM labelled AlexaFluor®-594: 0.7 µM unlabelled). Following 20 min incubation with tau, cells were optically stimulated with pulses of 3x 10 ms light, each separated by 33 ms, followed by a 10 s interval without stimulation repeated on a loop for 2.5 hr at 37 °C, 5 % CO_2. It was determined that for a 6 mm spot size diameter, the power required to stimulate cells was 9 mW.

2.11.6 Whole-Cell Patch Clamping recordings for of cells treated with monomeric tau

Performed by Dr. Tanja Fuchsberger

The method is the same as for Section 2.11.4 Whole-Cell Patch Clamping recordings for validating the optogenetic stimulation of cells. Differences include that whole cell patch-clamp recordings were carried out in voltage clamp mode measured at -60mV holding potential. Pipettes were filled with intracellular recording solution (IC) (120 mM CsCH3SO3, 20 mM CsCl, 0.2 mM EGTA, 10 mM HEPES, 10 mM QX-314, 4 mM ATP-Mg, 0.3 mM Mg-GTP, pH 7.2-7.3 adjusted with 1 M KOH, and osmolarity to 285-300 mOsm L−1 with ddH2O). The evoked response of cells was generated using an external electrode as compared with optogenetic stimulation.

2.11.7 Simultaneous stimulation and FLIM-TCSPC imaging of neurons

Cells were treated with 1 µM tau protein (0.3 µM labelled AlexaFluor®-594: 0.7 µM unlabelled). Cells were transferred to an OKOLab StageTop Incubation chamber (Okolab Inc.) at 37 °C and 5 % CO_2 on the FLIM-TCSPC, for 20 min incubation prior to optical stimulation. The laser diode was set to 9 mW using a power meter (PM100D, Thorlabs Inc.,), taking into account the chamber (Okolab Inc.) and LabTek (Thermo Fisher Scientific) lids. Cells were optically stimulated with pulses of 3x 10 ms light, each separated by 33 ms, followed by a 10 s interval without stimulation repeated on a loop for 2.5 hr. Following 30 min stimulation (50 min total tau incubation) cells were simultaneously imaged and optically stimulated to measure the lifetime of tau protein imaging of tau protein by FLIM-TCSPC as previously described (Section 2.4). To compare with non-stimulated cells, cells treated with 1 µM tau were imaged from 50 min without optical stimulation. Cells were imaged for a total of 2.5 hr.

2.11.8 Immunofluorescence of neuronal synapses and colocalisation analysis

Following experiments, neurons were treated in 1:5 Trypsin solution (0.1 % trypsin, Worthington Biochemical Corporation) in E18 medium for 1 min to remove extracellular tau to reduce background. Cells were washed 1x in 37°C HBSS and fixed in 37°C PBS

solution containing 4 % paraformaldehyde and 0.1 % gluteraldehyde for 10 min at room temperature. Cells were washed 3x in 37°C PBS. Cells were incubated in blocking solution composed of PBS with 0.2% Triton-X and 4% normal goat serum (NGS) for 1 hr at 4°C. Primary antibody was added 1:200 into blocking solution either anti-bassoon (ab82958, Abcam) or anti-PSD-95 (NB300-556, Novus Biologicals, Littleton, USA) for 2 hr at room temperature. Samples were washed in 3x blocking solution before the addition of 1:500 Goat anti-Mouse IgG (H+L) Secondary Antibody, Alexa Fluor® 647 (Thermo Fisher Scientific, Waltham, USA) for 1 hr, room temperature. Samples were washed 3x in blocking solution, 1x in PBS before imaging in PBS. Samples were imaged using a custom-made widefield microscope with an Olympus frame (Olympus 1X71) and automated stage (ASI 2000M). 500mW 561nm and 647nm diode lasers (Cobolt Samba) were used with 600/37 nm emission filter for AlexaFluor®-594 conjugated tau or 676/29 nm emission filter for Secondary Antibody, Alexa Fluor® 647 respectively (both Semrock). Background subtraction and intensity thresholding was performed in ImageJ (Rueden *et al.*, 2017). Chromatic aberration correction was performed based on imaging of two-colour (561 nm/647 nm) TetraSpeck™ (Thermo Fisher Scientific) bead samples, using Detection of Molecules (DoM) plugin for ImageJ (Cell Biology Group, Utrecht University). The JaCoP plug-in for ImageJ was used on corrected images for Object-based colocalisation (Bolte & Cordelièrs, 2006). As sets of data were not completed to N=3 due to poor breeding of Grik4-Ai32 mice and inability to access laser labs during a departmental flood, no further statistical measures were carried out.

2.11.9 Chemical stimulation of neurons

Neurons were plated 500 000 cells/well in an 8-well LabTek dish (Thermo Fisher Scientific). At DIV14-18, neurons were treated with 1 µM tau protein (0.3 µM labelled: 0.7 µM unlabelled). For stimulation, 20 µM L-glutamate (Sigma-Aldrich), 20 µM bicuculine, 40 mM KCl (Sigma-Aldrich) were used. For stimulation method I, to determine whether the stimulation method effects the rate of tau aggregation at an earlier timepoint, stimulant was added at 20 min and cells were imaged after 30 min of stimulant treatment

(50 min tau incubation) for 1 hr. For method II, to determine whether the stimulation method effects the aggregation state of tau at 4 hr, cells were incubated for 3 hr before treatment with stimulant for 30 min before imaging for a further 1 hr. Cells were imaged using FLIM-TCSPC and data were analysed as previously described (Section 2.4).

2.12 Microfluidic culture chips for patch-clamp electrophysiology

Multiple prototypes were used during the initial attempts to make functional culture chips, (described in Section 1.6.4.) however only the final version will be described. Initial attempts used one-layer master mould methods that resulted in chips where the cell plating compartment and the channels were the same height. These chips showed air-blocked or hydrophobic microchannels between compartments and therefore a two-layer master mould was designed.

2.12.1 Two-layer Master mould fabrication

The final mask was designed by the author. The master mould fabrication was based on the protocol from initial prototypes using a one-layer method developed with Amanda Haack. With thanks to Philippa Hooper and Oliver Vanderpoorten for fabrication of the master mould in clean room facilities using this protocol. The protocol uses standard soft lithography methods.

Masks for photolithography were designed using AutoCAD software (Autodesk Inc., San Rafael, USA) and printed as a high-resolution film acetate photomask with negative features (MicroLithography Services Ltd, Chelmsford, UK). The mask was used with a 3 inch silicon wafer as the substrate for the master mould. To fabricate the 4 µm height axonal microchannels, 3 mL of SU-8 3005 series (MicroChem Corp., Westborough, USA) negative epoxy photoresist was added to the silicon wafer for the first layer of features. Based on instructions on the MicroChem SU-8 3000 series datasheet, the spin-coater was

set to 500 rpm for 7 s followed by 4000 rpm for 30 s. The wafer was then soft baked on a hot plate at 65°C for 1 min, then at 97°C for 2 min. The mask was then placed on top and exposed to a 1400 mW UV-LED (M365LP1, Thorlabs) for 15 s (the time of exposure is dependent on the UV source power). For post-bake/hard bake, the wafer was put on a 65°C for 1 min, 97°C for 1 min. The silicon master was soaked and rinsed in propylene glycol monomethyl ether acetate (PGMEA) developer (Sigma-Aldrich) for 1 min. The master was rinsed with isopropanol and dried using compressed nitrogen gas before addition of the next layer.

To fabricate the 100 µm cellular compartments, 3 mL SU8-3050 was added to the silicon wafer. This was placed on the spin coater at 500 rpm for 45 s followed by 1000 rpm for 60 s. The master was then soft baked at 65 °C for 5 min, then at 95 °C for 45 min. The mask was then aligned to the first layer using a micrometric XYZ and rotation stage, for placement under the UV-LED for 45 s. The master was then post-bake/hard baked at 65 °C for 1 min, 95 °C for 10 min. The silicon master was soaked and rinsed in PGMEA developer (Sigma-Aldrich) for 15 min before final wash in isopropanol and drying under nitrogen gas (Table 14).

Table 14 The protocol for a master mould. Simplified protocol for the production of a 2-layer master with the 1st layer consisting of 4 µm height features, and the 2nd layer consisting of 100 µm height features.

4 µm height axonal microchannels	
SU-8 type	3005
Spin coated speed	500 rpm, 7 s 4000 rpm, 30 s
Soft bake	65 °C for 1 min, then at 97 °C for 2 min
UV-LED exposure (power dependent)	15s
Hard bake	65 °C for 1 min, 97 °C for 1 min
Develop in PGMEA	1 min
100 µm height cellular compartments	
SU-8 type	3050
Spin coated speed	500 RPM, 45 s 1000 RPM, 60 s
Soft bake	65 °C for 5 min, 95 °C for 45 min

UV-LED exposure (power dependent)	45 s
Hard bake	65 °C for 1 min, 10 min 95 °C
Develop in PGMEA	15 min

2.12.2 PDMS imprinting of neural cell culture chips using the two-layer master mould

PDMS elastomer and curing agent Sylgard 184 (Dow, Midland, USA) were mixed vigorously in a 10:1 w/w ratio. This used ~6 g of elastomer to re-fill the mould to ensure the final chip height was < 2 mm to allow the chip's cellular compartments to be in working distance of the patch-clamp objective. The master was placed under vacuum for > 45 min to remove air bubbles occurring from mixing. The master was then placed in an oven at 65 °C for ~4 hr for curing of the PDMS mixture to occur. Once solidified, the regions of PDMS over the master features were cut out into rectangles containing the chip features. The 100 µm height cellular compartments were punched out using a specially designed punch that did not interfere with the microchannel features. Debris PDMS was removed from the devices using Scotch tape. For covalent bonding of the PDMS surface to the glass coverslide, an oxygen plasma bonder was set to 40 s at 40 % power (Diener electronic GmbH + Co. Ebhausen, German). Coverslides no larger than 22 x 22 mm were used to ensure the chips fit into the patch-clamp stage.

2.13 The characterisation of custom developed optically transparent multielectrode array devices for improved simultaneous neuronal recordings and FLIM

2.13.1 The fabrication of graphene electrodes

The selection and fabrication of substrates to test as materials for graphene microelectrode devices was by Philippa Hooper. Monolayer graphene was grown by Oliver Burton.

Substrates were prepared on borosilicate glass coverslips for biocompatibility and fluorescence lifetime characterisation tests. Gold (Au, 50 nm) coating to be used for connecting leads and contact pads was fabricated by thermal evaporation. Monolayer

graphene (>97 %) with grain size >100 μm was grown at ambient pressure, 1070 °C on a copper foil with methane (g) as the carbon supply, argon (g) for dilution, and hydrogen (g) for activating carbon binding to the copper foil surface. Graphene was transferred using a wet transfer method. PMMA, negative photoresist SU-8, and positive photoresist AZ5214E were added directly to the coverslip by spin coating. ITO coverslips were made commercially (SPI Supplies®, West Chester, USA). Si_3N_4 was deposited by electron beam evaporation directly into the coverslip. Al_2O_3 was deposited by atomic layer deposition.

2.13.2 The fabrication of PEDOT:PSS electrodes

Performed by Sagnik Middya

The devices were fabricated using standard lithographic procedures for a three-layer device. The 1st (bottom) layer consisted of Au connecting leads and contact pads which were fabricated by a standard lift-off process. The pattern was defined using a contact mask aligner followed by deposition of Titanium (Ti; 5 nm thick) and Au (100 nm thick) in an electron beam evaporator. The 2nd layer was made of PEDOT: PSS for the electrode region. This included the ~ 1.5 mm central region of each electrode which was made of only PEDOT: PSS such that it was optically transparent. The PEDOT:PSS layer extended above the Au layer until the outside of the Au contact pads. A dispersion of PEDOT:PSS and H_2O was chemically modified with 5 % (v/v) ethylene glycol and ~100 μL of dodecyl benzene sulfonic acid (DBSA). 1 % (v/v) GOPS was also added just before use. This chemically modified PEDOT:PSS was layered by spin coating (600 nm thickness). After spin coating, the PEDOT: PSS coated substrates were baked for 1 hr and soaked overnight in dH_2O in order to remove excess PSS. A thick photolithography etch mask was used, and reactive ion etching with CF_4 and O_2 patterned the PEDOT: PSS layer. The 3rd (top) layer consisted of the insulation layer and was made by chemical vapour deposition of ~ 500 nm Parylene C. A thick photolithography etch mask was used to remove parylene C at the electrodes and Au contact pads. Reactive ion etching with CF_4 and O_2 was used.

2.13.3 Viability of neurons grown on substrates

Performed by the author

Biocompatibility studies were carried out during initial stages of device design to ensure that primary E18 hippocampal neurons would grow on the devices. Borosilicate glass coverslips were coated with ITO, graphene, AZ5214E, SU-8, Au or PMMA as previously described were sterilised overnight using UV light. Coverslips were coated with 20 µL of 0.01 % poly-L-lysine (Sigma-Aldrich) for ~40 min and washed 3x in PBS. E18 primary hippocampal neurons were plated at 50 000 cells/ coverslip in 200 µL of cell medium. Coverslips were imaged at DIV14-17 to qualitatively assess whether neurons had survived and grown connecting axons, clustered with few axonal protrusion, or rounded and died.

2.13.4 Measuring the fluorescence lifetime of substrates

Performed by the Author

To ensure the insulating or conductive substrate coated on the coverslip did not affect the fluorescence lifetime of the sample measured, in initial tests for selecting an insulting layer material the calcium indicator Oregon Green 488 BAPTA-1 was used as a reference dye. Oregon Green 488 BAPTA-1 was excited at 485 nm using an acousto-optic tuneable filter and excitation light was further filtered with FF01-474/27 and fluorescence emission with FF01- 525/39 (bandpass filters from Semrock). Each image was acquired for 3 min to collect enough photons for accurate measurement of fluorescence lifetimes in each pixel. The fluorescence decays were processed using FLIMfit (Warren *et al.*, 2013) and fitted with double exponential decay functions (Lattarulo *et al.*, 2011). The images were analysed using 7 x 7 (B & H) binning with image-wise binning of fluorescence lifetimes in each pixel.

Once insulating substrate materials had been selected, the lifetimes of these materials (PMMA or parylene C) were compared to the electrode layer substrates (graphene or PEDOT:PSS) and borosilicate glass coverslips by pipetting ~10^{-5} g/mL rhodamine 6G onto each substrate. The fluorescence lifetime was measured using TCSPC-FLIM as previously described (Section 2.4). The tuneable filter was set to 510 nm with additional

excitation filter FF01- 525/39, and emission filter FF01-542/27 (both from Semrock Inc., New York, USA). Fluorescence lifetimes were compared to rhodamine 6G on an uncoated borosilicate glass coverslip. Data were analysed using FLIMFit (Warren *et al.*, 2013) software, and the TCSPC histograms for each pixel were fitted using a monoexponential decay function. The images were analysed using 7 x 7 (B & H) binning with image-wise binning of fluorescence lifetimes in each pixel.

2.13.5 Laser scanning and voltage recording cross-talk

Performed by the author

To determine whether the confocal line scanning laser affected the voltage that was recorded by the electrode, a 488nm laser was continually scanned across a single electrode of the PEDOT:PSS MEA device containing PBS for conduction. The voltage was recorded using a Multichannel System MEA-2100-Mini amplifier (Multichannel Systems, Reutlingen, Germany). Recordings were taken using MCS_Experimenter (Multichannel systems) by repeatedly switching between 1 s with laser off and 1 s with laser on to detect any changes to the voltage due to the laser, or at the time of switch. Data of the 1 s voltage traces were analysed in Prism6.0 (GraphPad).

2.14 Novel treatment methods for tau pathology

2.14.1 Metal-organic frameworks for anti-tau immunotherapies

All forms of antibody were produced and modified by Elise Siouve with AstraZeneca (formerly MedImmune LLC) and will be described in brief. Cell work and imaging was performed by the author.

The antibody paratope was designed based on the previously published antibody TauAB (425-441, MedImmune) (Chen *et al.*, 2019). The variable sequences of the mouse antibody were inserted into a humanized scaffold. A free cysteine was inserted at the C terminal for

both the full-size IgG and the antibody fragment (Fab). This free cysteine enabled the insertion of the fluorophore at this specific conjugation site via maleimide conjugation.

For Alexa Fluor®-647 (AF647) conjugation the free cysteine was reacted with a maleimide-DBCO payload. This DBCO-conjugated protein was conjugated to the AF647-Azide by click chemistry. The DBCO method was used instead of a direct maleimide reaction to the fluorophore for future grafting of the Fab or IgG to the metal organic framework by click chemistry using this same DBCO-conjugated protein.

2.14.2 Internalisation of tau-bound antibodies

The method as adapted from a paper (Evans *et al.*, 2018) was used to determine the uptake of tau-bound antibody. Excess of 10x antibody-AF647 (250 nM): monomeric tau-AF488 (25 nM) were incubated for 30 min in cell medium. For IgG-AF647, 4x concentration (1 µM) was used as the labelling efficiency was ~25%. This medium was then added to DIV 14-21 hippocampal neurons for 4 hr. At 4 hr, cells were trypsin washed with 1:5 0.01 % Trypsin (0.05 % trypsin-EDTA) to remove excess protein from the cell membrane. Medium was replaced with fresh E18 medium and cells were imaged immediately using a stage-top cell incubator (Okolab, Italy) and widefield microscope (60x, oil objective, Olympus). Images were analysed using average intensity in ImageJ (Rueden *et al.*, 2017) and compared to control samples of 'antibody control' treated with anti-Fc IgG control, Goat anti-Mouse IgG Alexa Fluor®-647, added at 0.04 mg/mL and 25 nM tau-AF488, or 'background' controls with no added dye to measure autofluorescence from laser excitation alone. For colocalisation analysis of the antibody with tau, the JaCoP plug-in for ImageJ was used for object-based colocalisation (Bolte & Cordelièrs, 2006).

2.14.3 Internalisation of tau protein

The method as adapted from a paper (Evans *et al.*, 2018) was used to determine the uptake of tau-bound antibody. Excess of 10x unlabelled antibody (250 nM): monomeric tau-

AF647 (25 nM) were incubated for 30 min in 100 µL cell medium. This medium was added to DIV 14-21 hippocampal neurons for 4 hr. At 4 hr, cells were trypsin washed with 1:5 0.01 % Trypsin (0.05 % trypsin-EDTA) to remove excess protein from the membrane. Medium was replaced with fresh E18 medium and cells were imaged immediately using a stage-top cell incubator (Okolab, Italy) and widefield microscope (60x, oil objective, Olympus). Images were analysed using by average intensity in ImageJ (Rueden *et al.*, 2017) and compared to control samples of 'antibody control' treated with anti-Fc IgG control, Goat anti-Mouse IgG Alexa Fluor®-488, added at 0.04 mg/mL and 25 nM tau-AF647, or 'background' controls with no added dye to measure autofluorescence from laser excitation alone. For figure preparation, images were corrected with +40 % contrast +40 % brightness in PowerPoint (Microsoft Corporation).

2.14.4 Internalisation of antibodies in tau-free medium

For investigating the uptake of the full-size IgG and the antibody fragment (Fab) into cells, unbound to tau protein, neurons were washed in fresh E18 medium to remove extracellular tau in the culture medium from cell death or free release from cells. 220 nM of AF647-conjugated IgG or Fab was added to the cell medium of DIV 14-17 hippocampal neurons for 1.5 hr to reduce tau that may enter the medium during incubation. After incubation, medium was replaced and cells were imaged using a stage-top cell incubator (Okolab, Italy) for widefield imaging (60x, oil objective, Olympus). As controls, an anti-Fc IgG control, Goat anti-Mouse IgG Alexa Fluor®-647, was added at 0.04 mg/mL to cell medium, or background control cells with no dye added were also imaged to determine the background autofluorescent signal from the 647 nm laser alone.

2.15 Developing an improved biopatterning method for the selective differentiation of neural stem cells

Culturing and immunofluorescence of human neural stem cells was performed by Dr. Roberta Azzarelli. The production of cellulose was performed by Sam Nehme. Advice on initial methods was given by Dr. Antonina Kerbs. Biofunctionalisation and analysis were performed by the author.

2.15.1 Conventional GPTMS method for functionalising glass coverslips with protein

The initial method was based on previous literature to test if this could be repeated successfully with AlexaFluor®-linked proteins. A silicon borohydride glass slide was incubated in 1 % v/v (3-Glycidyloxypropyl)trimethoxysilane (GPTMS) (>98 %, Sigma) in toluene overnight in an argon-filled falcon tube. The glass slide was washed 1x in acetone and dried with argon. Anti-Mouse IgG, Alexa Fluor® 647 conjugate (Thermo Fisher Scientific) was immediately added at stock concentration of 2 mg/mL for ~ 4 min and the glass slide was washed 3x in PBS to remove physically absorbed protein before imaging (Tsukruk et al., 1999; Luzinov et al., 2000).

2.15.2 A simplified final method for functionalising and patterning a coverslip with protein

The initial method was adapted to reduce the time and reagents required. Biopatterning was introduced to direct the functionalisation of protein to specific locations. For biopatterning, master molds to make polydimethylsiloxane (PDMS; Sylgard® 184, Dow Corning, USA) stamps with grids of 200 x 200 µm, or 700 x 500 µm were designed and fabricated by Jane Fojas or Amanda Haack. The method for design and fabrication of PDMS features is described in Section 2.12.1. 2 µL of GPTMS (>98%, Sigma-Aldrich) was added to the pattern of the PDMS stamp which was firmly pressed onto a polyvinylchloride plastic coverslide (Fisherbrand™ unbreakable cover slips) and kept

under argon for 5 hr. After 5 hr, the stamp was removed whereby the residue of excess GPTMS could be removed with a 1x acetone wash and drying with argon. This step was occasionally omitted as by 5 hr little residue remained, acetone could dissolve certain cell culture dish glue/plastics, and acetone residue appeared to stunt cell growth in several trials even following 3x PBS washes. 2 µL protein was pipetted on the GPTMS pattern for ~ 3 min followed by 3x wash in PBS. For control conditions, protein was added to untreated coverslips in parallel to test the effects of residual protein that may be adsorbed in this time. The stages of biofunctionalising protein to a substrate through patterning epoxysilane on PDMS stamps are depicted in Figure 37.

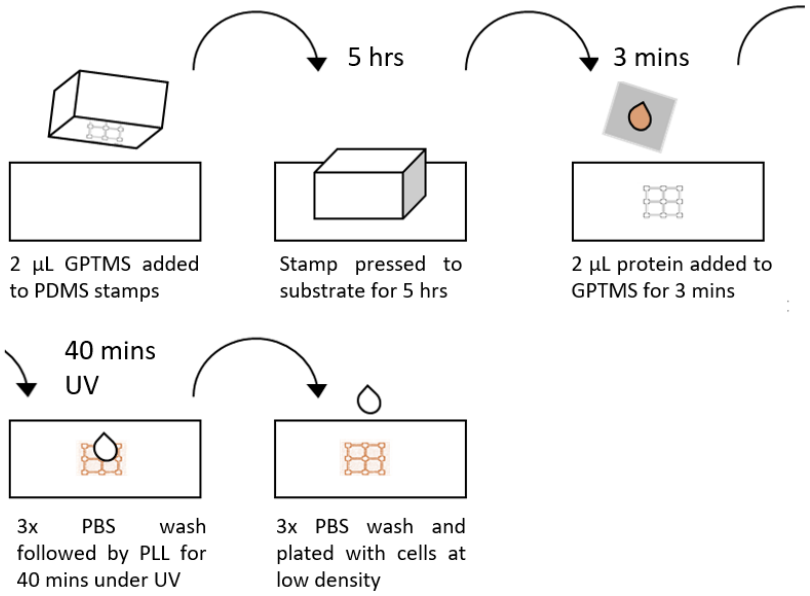

Figure 37. A schematic diagram depicting the stages of biofunctionalising protein to a substrate through patterning epoxysilane on PDMS stamps.

During initial stages of method validation, for proof of concept studies to show the ability of GPTMS to covalently link any protein with exposed amine or hydroxyl groups a selection of fluorescently labelled proteins were used. 2 µL of 200 µg/mL anti-DAT-ECD Alexa Fluor® 488 conjugate (fl-n17, ATSbio, San Diego, USA), 2 µL of 2 mg/mL goat anti-mouse IgG, Alexa Fluor® 647 conjugate (Thermo Fisher Scientific), 2 µL of 2 mg/mL goat anti-mouse IgG, Alexa Fluor® 488 conjugate (Thermo Fisher Scientific), or 2 µL of 1.5 mg/mL Alexa Fluor® 488 Affinipure donkey anti-human IgG, Fcγ fragment specific (Jackson Immunoresearch, Ely, UK), to qualitatively determine the protein binding

efficiency and location. Following a ~4 min incubation in the protein to be functionalised, the samples were washed 3x in PBS to remove physically absorbed protein. Coverslips were coated with poly-L-lysine for 40 min under UV light for sterilisation. Following coating, dishes were washed 3x in PBS and plated with E18 rat primary cortical neurons at a low density of 5 000 cells/coverslip, limited to the pattern region.

As the stiffness of substrates is also known to affect the growth of cells, the biopatterning of goat anti-mouse IgG, Alexa Fluor® 647 conjugate (Thermo Fisher Scientific) was used as a control. BDNF (Sigma-Aldrich) was used at 8 µg/mL, GDNF (Sigma-Aldrich) was used at 4 µg/mL, laminin was used at 300 µg/mL. For controls, laminin was added to a coverslip overnight at 10 µg/mL to ensure that cells grew healthily on the unmodified plastic coverslips; alternatively, laminin was added to GPTMS patterned coverslips at 300 µg/mL to show the laminin could be functionalised to the coverslip within the ~4 min incubation and cells were able to grow.

2.15.3 Preparation of cellulose from bacterial cultures

This work was carried out by Sam Nehme in the group of Dr. Ljiljana Fruk based on the thesis of Leire Urbina Moreno.

In this work the bacterium strain *Gluconacetobacter hensenii* wildtype was used, the method is based on Hestrin & Schramm (1954). For the preparation of bacterial cultures, 500 mL Hestrin and Schramm (H-S) medium was made in H_2O containing (w/v): 0.5 % yeast extract, 0.5 % peptone, 0.27 % Na_2HPO_4 dibasic, 0.15 % citric acid, and 2 % glucose (added following autoclaving), at pH6. For culturing in liquid, 5 mL of H-S medium was added to a 50 mL falcon flask; triplicates of *G. hensenii* culture were selected and kept at 30 °C for 7 days. For cellulose production, 100 µL of bacterial culture was added to a petri dish of 5 mL H-S medium and incubated at 30 °C for 2 weeks.

For cleaning, cellulose was removed from the cell solution and washed several times with dH_2O. Cellulose was then purified with 0.1-1M NaOH at 70ºC for 2 hr during which time

the cellulose became off-white/colourless. Cellulose was washed with dH_2O until the pH reached pH 7. The cellulose was freeze-dried and stored in dH_2O or PBS (Schramm and Hestrin, 1954).

2.15.4 Functionalising protein on cellulose for neural prosthetics

Freeze-dried cellulose in PBS was provided by Sam Nehme. Cellulose was spread and dried on parafilm overnight to form a single layer sheet. Squares of cellulose dried onto parafilm were cut out to keep the structure of cellulose during the functionalisation process. Due to previous silanisation methods of cellulose having used 'never-dried' or nanofiber forms of cellulose, as opposed to freeze-dried macrosheets used for this project, two methods of silanisation were tested. Both methods appeared successful whereby the second method was selected as the conventional 'curing' method resulted in hornification and temporary shrinkage during heating which may have resulted in cracking of the protein layer during rehydration in PBS.

The 'conventional' method, as modified in Salon et al., 2007, was composed of two steps. 1) Hydrolysis of 5 % GPTMS (>98%, Sigma) in 80:20 v/v isopropanol: water for 2 hr at room temperature. After 10 min the cellulose was added, and the mixture was placed on a shaker. This allowed adsorption of the silanol through acid-base bonding to the hydroxyl groups of cellulose. 2) chemical condensation through heating to 120°C using a hot plate until dry (~ 5 min) to result in siloxane bridges. The protein for functionalisation can then be placed in contact with the dried, cooled cellulose surface for ~4 min before washing 3x in PBS.

The 'aqueous one-pot silanisation' method, as developed by Beaumont et al., 2018 can also be successfully used. This method is composed of two steps, 1) cellulose was placed on a shaker in H_2O; acidification with 1 % v/v 0.5 M HCl was used to hydrolyse the 0.5 % v/v GPTMS (>98%, Sigma-Aldrich) for 30 min. 2) 2 % v/v 0.5 M NaOH was added for a further 2 hr to induce condensation. Cellulose was removed and washed 1x in acetone and

briefly dried under nitrogen before the addition of protein. After ~5 min, excess protein was removed using 3x wash in PBS.

2.15.5 *Culturing of human neural stem cells*

This work was performed by Dr. Robera Azzarelli

Human foetal neural stem cells were cultured based on Sun et al., (2008). Briefly, human foetal neural tissue at embryonic 50–55 days was dissociated in Neurobasal medium (Invitrogen) with accutase (Sigma-Aldrich). Cells were cultured at 2×10^4/ well of a 24 multiwell plate on 1 µg/mL laminin coating in serum-free medium supplemented with 20 ng/mL N2, B27, and propagated in the presence of 10 ng/mL EGF, and FGF-2. Due to our interest in whether BDNF and GDNF could be sufficient to induce the differentiation and survival of human NSCs into mature neurons, during differentiation, cells were plated in medium without EGF and FGF2. For immunofluorescence, fixation used 4 % PFA for 10 min followed by permeabilization in 0.1% TritonX10 in PBS for 10 min, and blocking in 10 % donkey serum 0.01% PBS Triton. Primary antibodies were added in 5% donkey serum and 0.01 % PBS TritonX10 and included DAPI, chicken anti-MAP2 (1:1000), mouse anti-Tuj1 (1:1000) were used with Alexa-Fluor® secondary conjugates (Invitrogen).

Analysis of cell growth and differentiation was performed by the author in ImageJ (Rueden *et al.*, 2017). An intensity threshold was applied across each image to segment cell bodies and protrusions using Tuj1 immunofluorescence. The percentage area of these regions was measured from the total image area. The percentage area of Tuj1 was compared between bacterial cellulose biofunctionalized with BDNF, GDNF and laminin versus laminin-only using Prism 6.0 (GraphPad).

2.16 Statistical measures

Data visualisation and statistical analysis were performed with GraphPad Prism 6.0 software (Graphpad, La Jolla, USA). All numerical data are expressed as mean ± standard deviation (SD) unless stated otherwise. Results ($n \geq 3$ in all cases, unless stated otherwise) were analysed by unpaired, two-tailed t-tests for 2 experimental groups, or by one-way analysis of variance (ANOVA) with multiple comparisons for 3+ groups of data. P-values < 0.05 were considered statistically significant:

P >= 0.05	ns
P < 0.05	*
P < 0.01	**
P < 0.001	***
P < 0.0001	****

CHAPTER 3

3.1 Fluorescence lifetime measurements to determine the factors that influence the aggregation of monomeric tau protein.

This chapter aims to follow on from the founding work in the group to better understand the contribution of low pH in endolysosomal compartments to the aggregation of the protein tau. Previous work in the group used fluorescently labelled tau protein as an aggregation sensor by measuring its fluorescence lifetime. In an aggregated state, the fluorescence lifetime of tau protein was found to decrease as compared with monomeric solutions of tau protein (Michel *et al.*, 2014). Although this work has been investigated at in SH-SY5Y cells, the timescale of aggregation inside of primary hippocampal neurons is unknown. Alongside this, it is known that the rate of stimulation increases the rate of tau aggregation (Wu *et al.*, 2016), though the mechanisms of how this occurs are not known. Studies looking at whether there is a direct role of calcium ions in aggregation aim to answer whether this is the link between neuronal activity and aggregation. As well as calcium ions, tau has been found aggregated with synaptic vesicle protein synaptogyrin-3 and actin (McInnes *et al.*, 2018), and synthetic vesicles (Ait-Bouziad *et al.*, 2017). Therefore, it is tested whether synaptic vesicles can directly aggregate monomeric tau protein.

3.2 Ammonium chloride solution prevents the aggregation of tau protein by neutralising lysosomal pH

Previous findings in the group showed that the uptake of exogenous monomeric tau protein into low pH compartments in cells resulted in its aggregation (Michel *et al.*, 2014). It was therefore of interest whether neutralising low pH would be sufficient to prevent tau aggregation. Following the addition of 10 mM the weak base ammonium chloride (NH_4Cl) and tau protein, the aggregation of tau was shown to be significantly reduced as compared to controls. Figure 38 (bottom panel) shows the fluorescence lifetime images of the neurons treated with tau in the presence or absence of NH_4Cl. The differences between aggregation state are visually apparent between the two conditions; The NH_4Cl treated cells show less aggregated states of tau (blue pixels high fluorescence lifetime), as compared to more aggregated state tau (yellow pixels, lower

fluorescence lifetime) in cells treated with tau in the absence of NH_4Cl. The data for each group appears as two populations due to development work taking place on the FLIM system before N=3 data measurements, resulting in lower lifetime for this dataset (Appendix A.1).

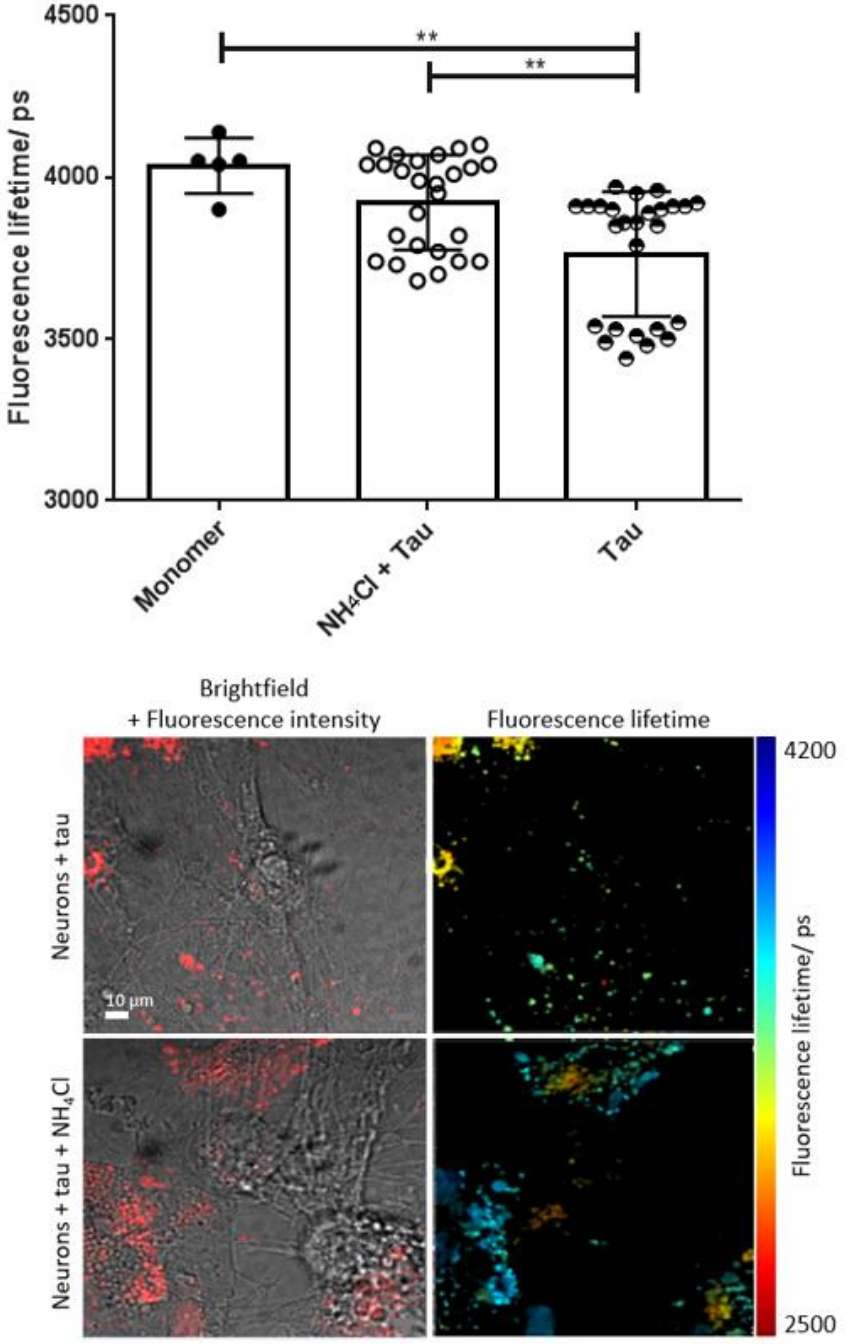

Figure 38. The neutralisation of endolysosomal compartments in hippocampal neurons using NH_4Cl results in a significant reduction of tau aggregation as compared with the positive control of tau treated neurons, and negative control of tau monomer in HBSS

without neurons (one-way analysis of variance (ANOVA); ***$P < 0.0004$; $F(2,54) = 9.109$). Tukey's multiple comparison P values (Monomer (A), NH_4Cl+ tau (B), tau (C)): (A-B) not significant NS = 0.3515; (B-C) **$P = 0.0040$; (A-C) **$P = 0.0029$. Experiments were performed from $n = 3$ animals. All data points from the repeats with mean values and standard deviation are plotted. Bottom: The reduced aggregation of tau protein can be visualised in the fluorescence lifetime images (right). The control (right, top) shows tau aggregation (as evidenced by a reduction in lifetime, with more yellow pixels) whereas the addition of NH_4Cl (right, bottom) reduces tau aggregation (with an increase in lifetime shown by more blue pixels). Fluorescence intensity images (left) show punctate staining suggesting tau is localised to vesicular structures. Bottom figure adapted from Colin Hockings, all data collected by the author.

3.2.1 Discussion

The neutralisation of endolysosomal compartments using the weak base NH_4Cl drastically reduced the aggregation of monomeric tau protein. Interestingly, the absence of NH_4Cl during trypsin, FBS wash steps, or medium replacement that allowed the reacidification of these compartments resulted in some tau aggregation even following 4 hr incubation in NH_4Cl. Therefore, the initiation of tau aggregation must occur rapidly in the presence of low pH. To better understand the effect of NH_4Cl, a pH sensor was calibrated and images were analysed using 'pixel-wise' versus 'image-wise' analysis to explore vesicular pH in more detail.

Oregon Green™ 514 dextran (dextran-OG514) was selected for use as a fluorescence lifetime pH sensor due to higher resolution compared with previously characterised Oregon Green™ 488 dextran (calibrated by Chetan Poudel, Dr. Michelle Teplensky, Figure 43). As a first step, it was necessary to make a calibration curve for dextran-OG514 by clamping lysosomes at a series of known pH using extracellular buffers. This curve could then be used to measure the pH of vesicular compartments. This would be useful to determine the pH in endolysosomal compartments following the addition of 10 mM NH_4Cl. Although NH_4Cl is commonly used as a weak base to neutralise pH in cells, the exact pH change that occurred inside of neuronal compartments by this concentration is unknown. This pH change on the addition of 10 mM NH_4Cl is important to know as it is sufficient to prevent aggregation inside of neurons. As a second step dextran-OG514 could be optimised for two-colour FLIM using two channels to correlate pH (using dextran-OG514 lifetime) with tau aggregation status (using AlexaFluor®-594 lifetime) for each pixel. In

progression towards two-colour FLIM, the calibration of dextran-OG514 was carried out such that endosomal and lysosomal compartments could be distinguished by pH using pixel-wise, versus image-wise, image analysis.

3.3 Measuring the pH at which tau forms aggregates inside of neuronal compartments

3.3.1 Calibrating Oregon Green™ 514 dextran as a pH lifetime sensor

Fluorescence lifetime imaging and calibration curve for dextran-OG514 in HEK-293 cells was performed by Chetan Poudel. Cell preparation, treatment, imaging and analysis in primary neurons was performed by the author.

A calibration curve was made for measuring pH using fluorescence lifetime imaging. Lysosomes containing Oregon Green™ 514 dextran (dextran-OG514) were clamped to the pH of extracellular medium through using Na+/H+ ionophore monensin and the K^+/H^+ ionophore nigericin. Figure 39 (A) shows the calibration curve for the fluorescence lifetime of dextran-OG514 measured for a range from pH 4-pH 6.5. The fluorescence lifetime of dextran-OG514 decreases with decreased buffer pH through the range that was measured (pH4-6.5). Figure 39 (B) shows the fluorescence lifetime images of dextran-OG514 that has been taken into lysosomes of live cells that are buffered at a specific pH. In the cells with lysosomes that have been equilibrated to low pH, the fluorescence lifetime of the dextran-OG514 is correspondingly lower as compared to those in higher pH buffer showing higher lifetimes of lysosomal dextran-OG514. The results of the calibration curve for dextran-OG show a 3x greater dynamic range than pH sensor Oregon Green™ 488 dextran (calibrated by Chetan Poudel, Dr. Michelle Teplensky, Figure 43).

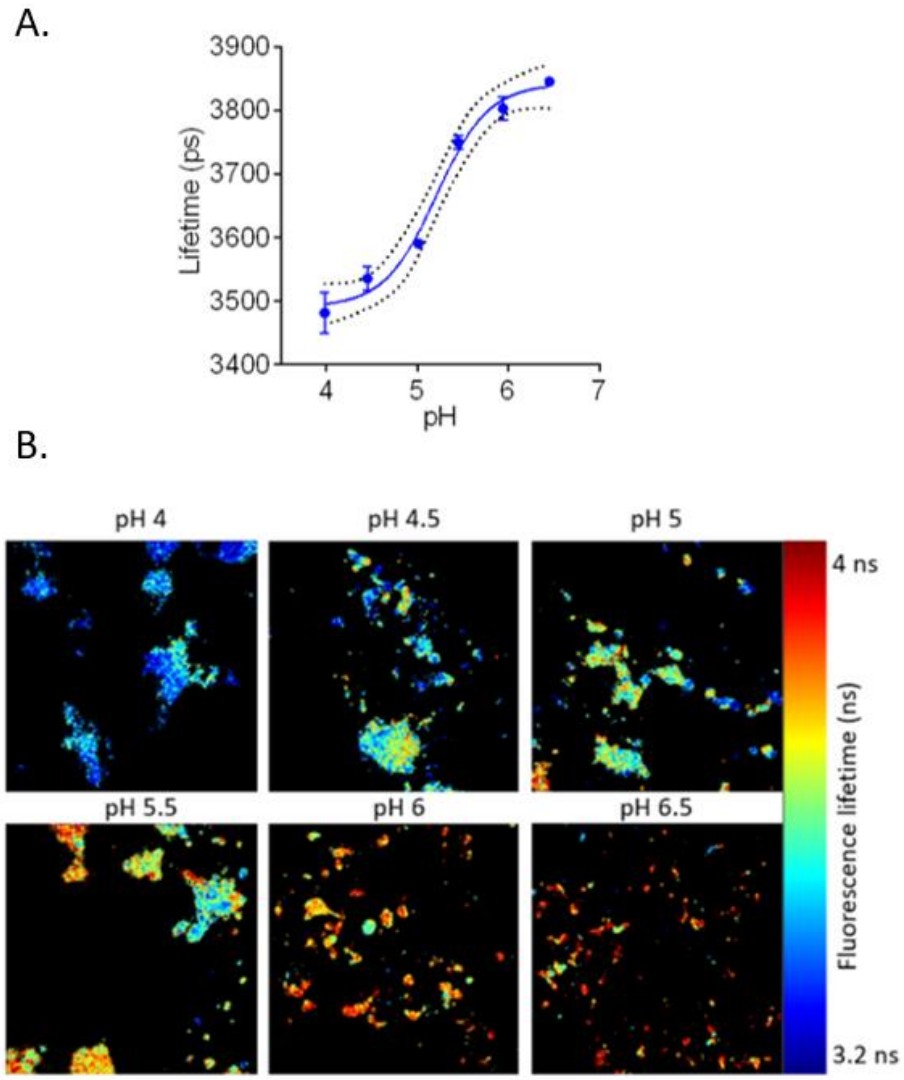

Figure 39. Calibration of dextran-OG514. The calibration curve (A) shows the fluorescence lifetime of pH sensitive dye dextran-OG514 at ranges measured from pH 4 – pH 6.5. The fluorescence lifetime images (B) of dextran-OG514 taken into lysosomes in live cells that have been buffered to a specific pH. The experiment included *n* = 3 independent repeats with n > 3 technical repeats. Mean values with standard error of the mean (SEM) are plotted. Figure prepared by Chetan Poudel.

3.3.2 Optimising Oregon Green™ 514 dextran as a pH lifetime sensor in neuronal compartments

Using this calibration curve, dextran-OG514 can be used to measure the pH inside of neuronal compartments. Although we have shown that NH_4Cl significantly decreases the aggregation of tau, it has not been shown to what extent 10mM NH_4Cl neutralises low pH compartments. To test

whether dextran-OG514 showed the same properties when added to primary hippocampal neurons as when used in HEK-293T cells, fluorescence lifetime measurements were made of dextran-OG514 inside of primary hippocampal neurons (Figure 40). The method was adapted compared to previous dextran treatment in HEK-239T cells; the dextran-OG514 concentration, incubation time and washes were reduced as they appeared toxic to cells and/or diminished dextran-OG514 fluorescence in punctate lysosomal-like appearance.

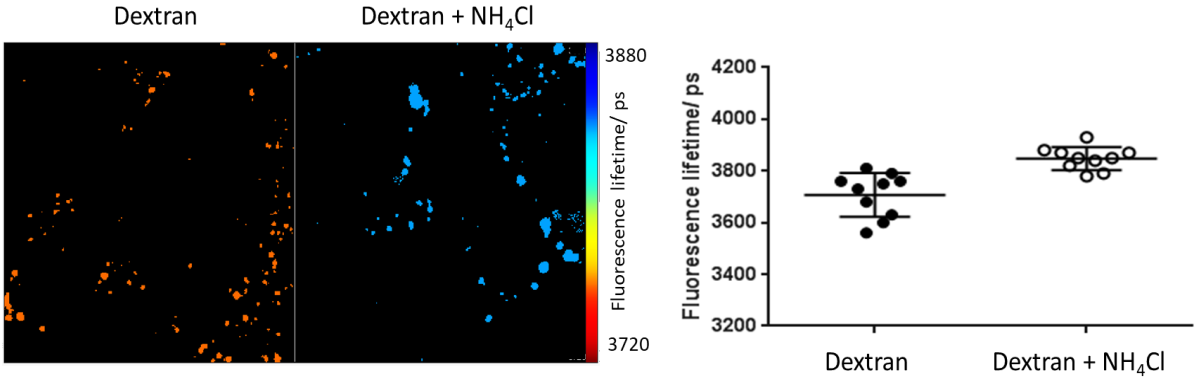

Figure 40. The pH of endolysosomal compartments inside of hippocampal neurons was measured using the fluorescence lifetime of dextran-OG514. The experiment included *n* = 3 independent repeats with n > 3 technical repeats. Mean values with standard deviation are plotted. Statistics were not carried out between groups as only the mean value was required to determine the pH using the calibration curve.

The fluorescence lifetime of dextran-OG514 taken up by neurons in the presence or absence of NH_4Cl was measured using FLIM. Figure 40 (right) shows that the fluorescence lifetime for dextran treated cells was 3707 ± 85.12 ps (mean ± standard deviation) which increased to 3848 ± 44.17 ps in the presence of NH_4Cl. Using the calibration curve previously collected (Figure 39, top), these fluorescence lifetimes correspond to pH 5.3 and 6.5 respectively. Although the pH of lysosomes is 4.0-5.0, due to the analysis method that averages pixels across the image ('image-wise') the pH may be higher from less acidic endosomal compartments that would be included in these measurements. The measurements are likely to be an average of all fluid-phase endocytosis mechanisms, as dextran can colocalise with macropinosomes, phagosomes, early endosomes and late endosomes, ranging from an initial pH 7.2 of extracellular fluid that acidify to pH 5.5 (Tsang *et al.*, 2000). Previous work in the group (Michel *et al.*, 2014) has shown that tau is not only localised to lysosomes but also in endosomes, and therefore it could be expected that the pH of all

of the vesicles in which punctate tau fluorescence is seen could be directly measured using dextran-OG514.

The pH measured in cell compartments treated with NH_4Cl was ~pH 6.5. This value is similar to values reported in the literature (~pH 6.3, Poole & Ohkuma, 1981) using a similar, but ratiometric imaging method and treatment in macrophages instead of neurons on addition of 10 mM NH_4Cl to lysosomes. As pH 6.5 is at the maximum of the curve that was calibrated for dextran-OG514, it is also possible that the pH is above this measurement. As the fluorescence lifetime of dextran was at the upper end of the curve limit it is safest to state that on 10 mM NH_4Cl addition, the pH of intracellular vesicles is > 6.5.

3.3.3 The use of Oregon Green™ 514 dextran with labelled tau protein for two-colour FLIM

Two-colour FLIM can be used to correlate the pH (using dextran-OG514 lifetime) to the aggregation state of tau protein (using AlexaFluor®-594 lifetime) that is added to cells. Exogenous monomeric tau has been shown to aggregate at low pH in endolysosomal compartments (Michel et al., 2014), and neutralisation of these compartments by NH_4Cl to > pH 6.5 reduces this aggregation.

Previous analysis of fluorescence lifetime images used an image-wise analysis method for averaging the lifetime of each pixel across each image, the resolution of specific lifetimes per pixel were lost. In an attempt to correlate fluorescence lifetime and pH between specific cellular compartments, a pixel-wise method was selected which measured lifetimes on a pixel-per-pixel basis (or for selected binning of pixels). Figure 41 (bottom) illustrates the different representation of fluorescence lifetime measurements by using pixel-wise versus image-wise analysis. Both methods of analysis showed no significant differences for the aggregation of tau in the presence or absence of NH_4Cl for this set of data (Appendix A.2). The use of pixel-wise analysis resulted in highly variable fluorescence lifetime measurements even following binning of multiple pixels. This resulted in puncta with a broad spectrum of fluorescence lifetimes. Figure 41 (red arrows) shows that in some cases puncta with fluorescence lifetimes corresponding to low pH or high pH appeared to correlate to pixels suggesting aggregated/unaggregated tau states respectively. This

was as predicted from previous studies whereby tau aggregation occurs at low pH but not at pH > 6.5. Conversely Figure 41 (white arrows) also shows that the opposite of this predicted effect is true and there is not a clear relationship that can be drawn between compartmental pH and tau aggregation state from this study. Alongside this, fluorescence lifetime measurements of dextran-OG514 showed a trend of higher lifetimes than previous measurements without tau treatment (dextran-OG514: 3835 ± 106.30 ps versus 3707 ± 85.12 ps. Dextran-OG514 + NH_4Cl: 3947 ± 64.15 ps versus 3848 ±44.17 ps). However, by using pixel-wise analysis the lifetimes 'per-pixel' could be correlated between corresponding tau and dextran images. It was therefore possible that by using pixel-wise analysis that relationships between tau aggregation state within particular pH compartments could be established, which may show differences in tau aggregation.

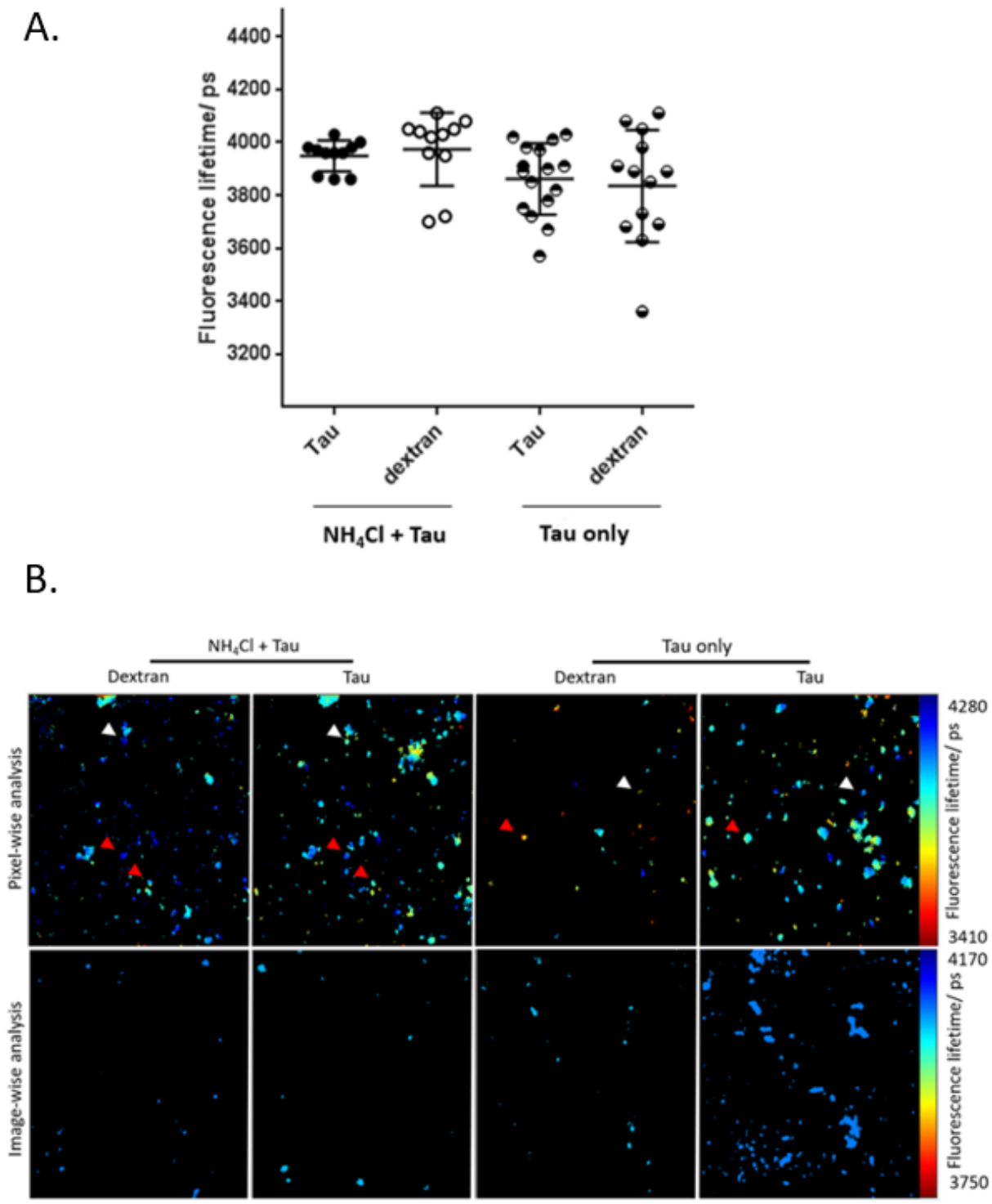

Figure 41. Two-colour FLIM for relating tau aggregation to vesicular pH in hippocampal neurons. A. No differences are seen in the aggregation of tau + NH_4Cl versus tau alone ($P = 0.0554$; $t = 2.010$; d.f. = 2; two-tailed unpaired *t*-test, image-wise analysis, for pixel-wise analysis see Appendix A.2) Experiments were performed from $n = 3$ animals, with n > 3 images per repeat. All data points from the repeats and mean values with standard

deviation are plotted. Statistics were not performed on dextran data as only the mean value was required for use with the calibration curve). B. (top) Pixel-wise versus B. (bottom) image-wise analysis of two-colour FLIM dextran-514 and tau protein images. Bottom panel demonstrate the spatial information lost by averaging across all pixels, whereas the spatial resolution of lifetimes remains using pixel-wise analysis, but large variation of lifetimes within puncta occurs. Arrowheads (red) show examples of puncta with the expected relationship between low pH and tau aggregation or high pH (NH_4Cl) and high lifetime between dextran-OG514 and tau images. However, arrowheads (white) show the converse relationship also occurs.

Figure 42. (a,b,c) shows the pairing together of the fluorescence lifetime of Tau-Alexa Fluor®594 and the fluorescence lifetime of dextran-OG514 for each pixel in the image set. Pixels where both lifetime values were not present were discarded from the correlation analysis. The paired pixels for each image set (eg. NH_4Cl + tau, tau only) were pooled and plotted as an xy plot with the lifetime of dextran-OG514 in x-axis and tau in the y-axis. Figure 42 (a) shows the majority of pixels with a high tau lifetime correspond to high dextran fluorescence lifetime (> ~3750 ps, ~pH > 5.5). This would be as expected from previous data and our hypothesis that monomeric tau remains unaggregated until exposure to low pH compartments. Some pixels display decreased lifetime with corresponding high dextran fluorescence lifetime suggesting that some aggregated tau may exist in these compartments and that NH_4Cl alone may not be sufficient to prevent tau aggregation in all cases. However, the mean lifetime of tau in the presence of NH_4Cl is significantly higher than in the absence of NH_4Cl (3790 ± 238.8 ps (mean ± standard deviation) versus 3973 ps ± 171.6 ps respectively; Figure 42, (d)). Figure 42 (b) shows the corresponding fluorescence lifetimes of tau and dextran in control cells that were not treated with NH_4Cl. A distribution of lifetimes are seen showing all combinations including aggregated tau at high pH (dextran lifetime > ~3750 ps, ~pH > 5.5), unaggregated tau at high pH, aggregated tau at low pH (dextran lifetime < ~3750 ps, ~pH < 5.5), unaggregated tau at low pH. A continuous gradient between low and high pH can be seen with average dextran fluorescence lifetime of 3821 ± 221.3 ps (mean ± standard deviation, ~pH 5.85) which increased to 4011 ± 137.4 ps (~pH > 6.5) in the presence of NH_4Cl. Unaggregated and aggregated forms of tau occurring throughout this gradient. Although it was predicted that a linear relationship may exist showing a continuous increase in aggregation state with decreasing pH, interestingly, only two discrete tau lifetimes appear to be detected. These two discrete lifetimes may correspond to conformational states in the presence versus absence of beta-sheet formation to induce self-quenching of fluorophores. Whether there

are different populations within these two discrete sets has not been determined. The finding that aggregated forms of tau occur in high pH conditions may be expected by our model due to re-uptake of aggregates into early, high pH, endosomes over the incubation time prior to imaging.

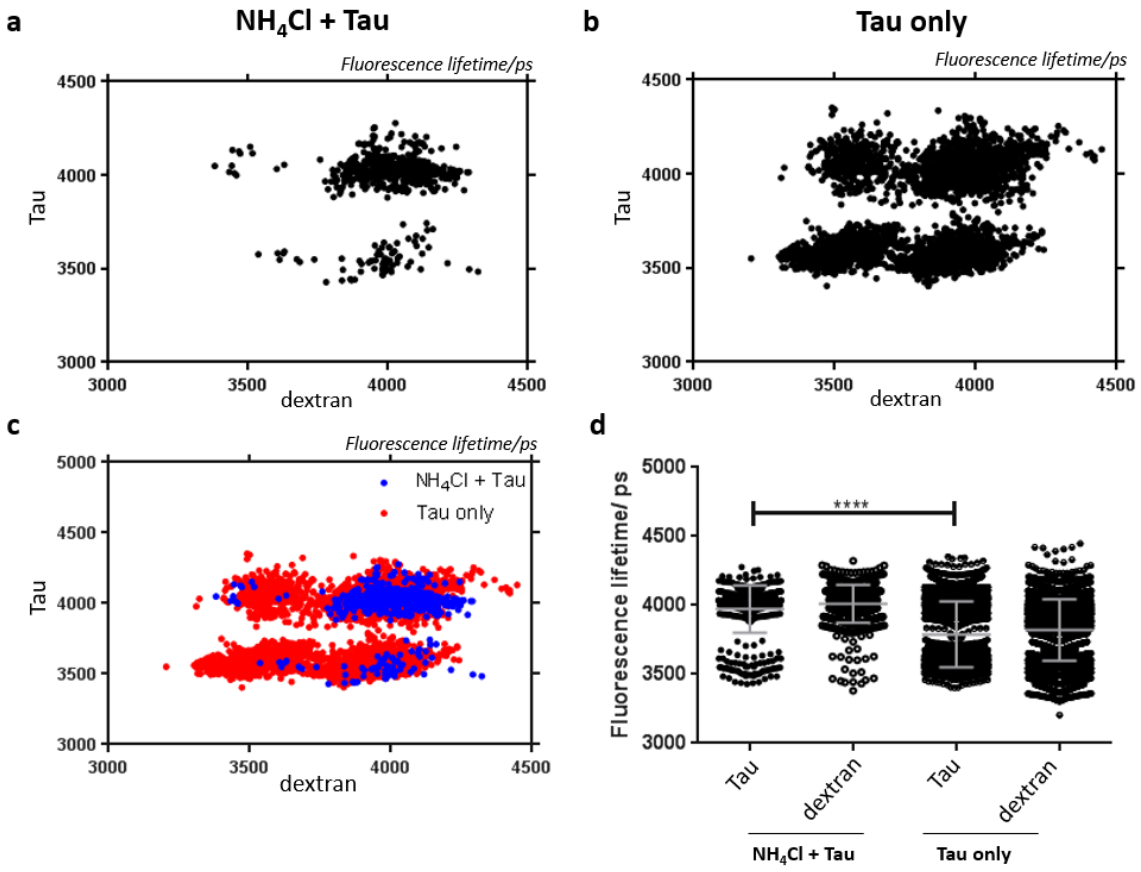

Figure 42. The fluorescence lifetime of tau and the fluorescence lifetime of dextran-OG514 paired together for each pixel in the image set. An xy plot with the lifetime of dextran-OG514 in x-axis and Tau-Alexa Fluor®594 in the y-axis pixel in the image set, plotted for NH_4Cl + tau (a), tau only (b) or combined (c) data. The fluorescence lifetime of these pixels shows a significant increase in tau aggregation as measured following exclusion of pixels without corresponding fluorescence in each channel (**$P < 0.0001$; $t = 18.11$; d.f. = 2; two-tailed unpaired *t*-test). The experiment included $n = 3$ animal repeats with n > 3 technical repeats that were pooled for analysis. All data (a,b,c,d) with mean values and standard deviation (d) are plotted.**

This method has therefore been successful in identifying two discrete tau populations across a continuous pH range. Although fewer data points are shown for the NH_4Cl + tau condition, these points are greatly enriched for both higher tau and dextran lifetimes, corresponding to unaggregated tau at high (> ~6.5) pH. The benefit of correlative method of pixel-wise analysis is

that it excludes pixels that do not correspond to fluorescence in both images. This means that only the pH of compartments containing tau protein are included in the analysis.

3.3.4 Discussion

Dextran-OG514 was used to measure the pH of intraneuronal vesicles, which was measured as pH 5.3 when averaged across compartments. The dynamic range of OG-514 is 3x that of previously calibrated Oregon Green™ 488 dextran (Chetan Poudel, Dr. Michelle Teplensky, Figure 43).

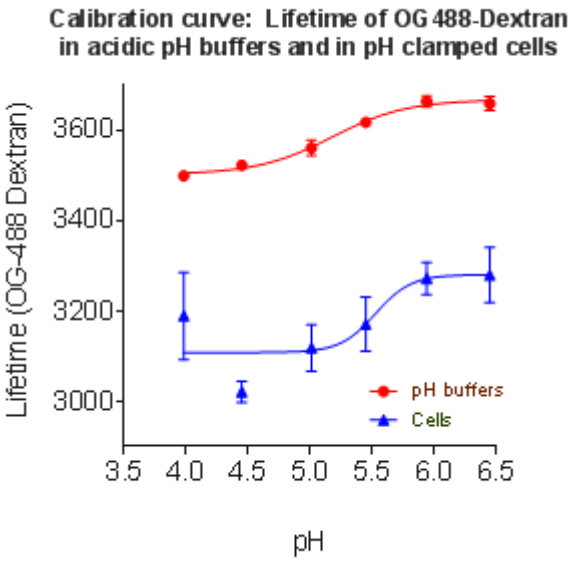

Figure 43. The calibration curve of Dextran OG-488 shows lower resolution as a pH sensor compared to dextran-OG514. Figure: Chetan Poudel.

The pH of intraneuronal vesicles were then measured following the addition of 10 mM NH_4Cl to the extracellular medium and were measured as > pH 6.5. Following the addition of monomeric tau to cell medium in the presence or absence of NH_4Cl, to prevent tau aggregation, the pH of intraneuronal compartments were again measured. The measurements of dextran-OG514 showed a trend of higher lifetimes than in previous measurements without tau. It is possible that this is an effect of tau protein but more likely due to difficulties with a reproducible preparation and imaging method. Dextran-OG514 fluorescence appeared to remain <1 hr after media replacement and

therefore offered a short timescale for imaging, which required 3min / image/ colour. Alongside this fluorescence for tau would often not correspond to fluorescence from dextran-OG514 in the same field-of-view, and therefore between each image multiple fields of view were tested to find fluorescence corresponding to the same population of cells. These difficulties with the imaging method may explain the variability between the lifetime measured in the two-colour imaging as compared to dextran alone. To ensure fluorescent pixels in the tau images corresponded to pixels in the dextran images, correlative analysis was carried out. This also allowed the pH of vesicles to be directly related to the aggregation state of tau. The variability of puncta seen with pixel-wise analysis even following binning of many pixels (Figure 41, bottom panel) is similar to that seen in Figure 39 for the calibration of dextran-OG514 in HEK-293T cells. This variation within puncta may explain the variation between data sets from different experimental days seen for correlation analysis. Complete binning of all data sets for each condition was therefore used for correlative analysis (Figure 42 (a,b)). Following binning, a clearer relationship between pH and aggregation was shown to reveal two discrete aggregation states that occur across a continuous pH range. In the NH_4Cl + tau condition, pixels are enriched at high fluorescence lifetimes for tau and dextran, corresponding to unaggregated state and high (> 6.5) pH. It appears that some pixels corresponding to aggregated tau at low pH are also seen in this condition. Whether these arise from the small number of pixels corresponding to tau aggregation at low pH, or represent a pH-independent mechanism of aggregation is unknown. It would be of interest to repeat this study with measurements at different timepoints to understand the progression of pixels between aggregation state and high/low pH.

What remains unclear is whether other endolysomal ions such as Ca^{2+} may contribute to this aggregation. NH_4Cl causes a dose dependent increase in $[Ca^{2+}]_i$, and lysosomes contain $4\text{-}6\times10^{-4}$ M $[Ca^{2+}]$, which though approximately half that of extracellular medium, is higher than cytosolic $[Ca^{2+}]$. It was therefore hypothesised that Ca^{2+} may directly influence tau aggregation, which could explain the dependence of aggregation rate on neuronal activity in hippocampal neurons (Section 1.5.2.).

3.4 Intracellular calcium concentrations have no effect on tau aggregation

To determine whether calcium concentrations inside of cells had a direct effect on tau aggregation, cells were incubated in conditions of low (EGTA + ionomycin), high (ionomycin) and high with stimulation (ionomycin + KCl) calcium conditions. Ionomycin causes release of Ca^{2+} from intracellular stores whilst EGTA chelates Ca^{2+} in the extracellular medium taken into endocytic vesicles with tau. For initial experiments, cells were incubated in these conditions for 3 hr prior to imaging and imaged for ~ 1hr. No significant differences are measured for the aggregation state of tau, as measured by fluorescence lifetime, between different Ca^{2+} treatments. This result suggesting that Ca^{2+} flux inside of cells does not directly affect the concentration of tau that is aggregated over 3 hr (Figure 44).

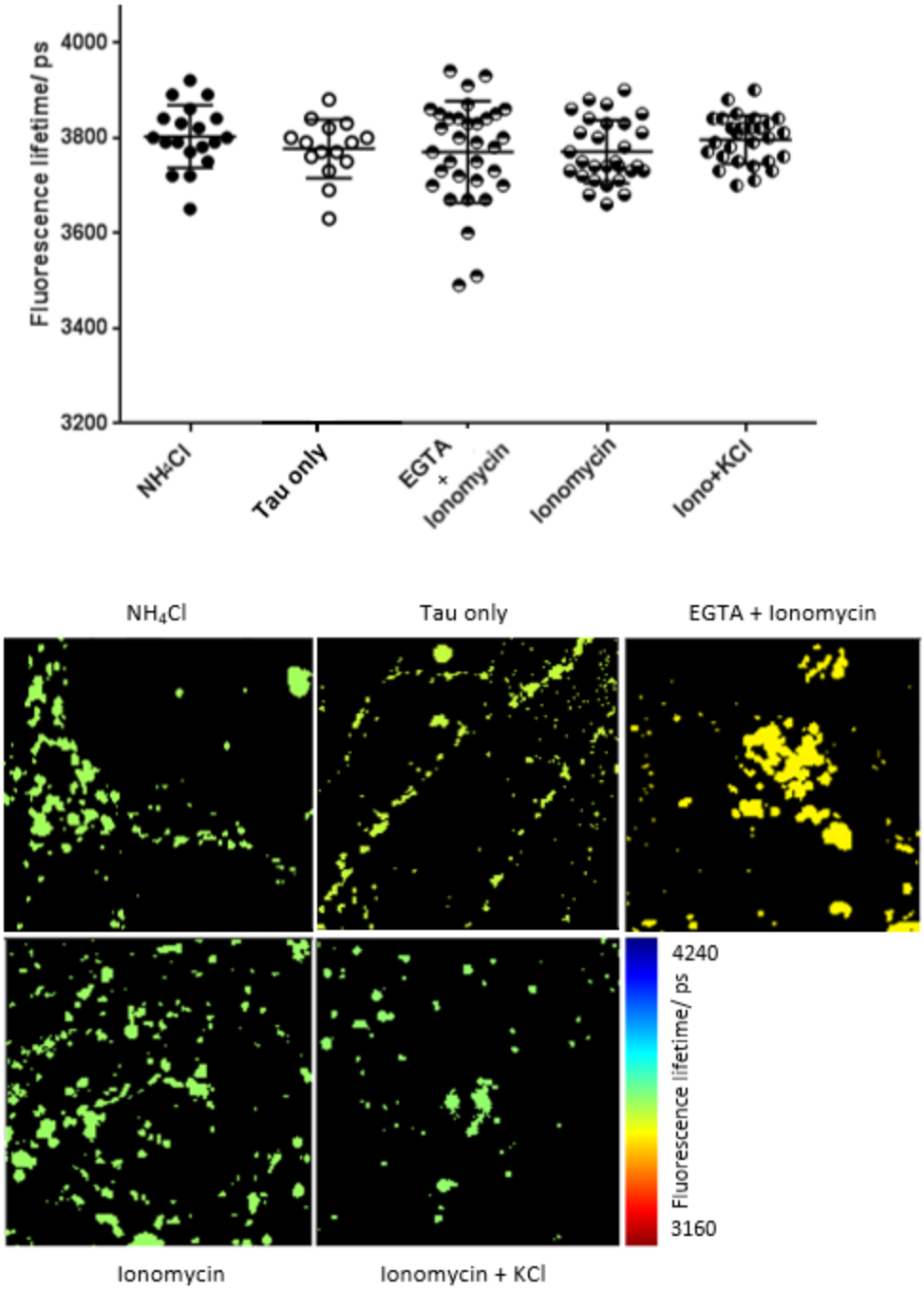

Figure 44. No significant differences were observed for the fluorescence lifetime of tau-594 following 3 hr treatment of primary hippocampal neurons with drugs that alter intracellular Ca^{2+} concentration (one-way analysis of variance (ANOVA); NS, *P* = 0.4247; F (4, 119) = 0.9736). Tukey's multiple comparison *P* values (NH4Cl + tau (A), tau only (B), EGTA + ionomycin (C), ionomycin (D), ionomycin + KCl (E)): (A-B) not significant (NS) = 0.8594; (A-C) NS = 0.5696; (A-D) NS = 0.6029; (A-E) NS = 0.9981; (B-C) NS = 0.9986; (B-D) NS = 0.9990; (B-E) NS = 0.9348; (C-D) NS > 0.9999; (C-E) NS = 0.6807; (D-E) NS = 0.7155.

Experiments were performed from *n* = 3 animals. All data points from the repeats and mean values with standard deviation are plotted).

It was considered possible that 3 hr incubation of cells in treatments that disrupted homeostasis may result in depletion of ATP and knock-on effects due to depletion of ATP stores that were not directly related to [Ca^{2+}]. It was also considered that Ca^{2+} may not itself be buffered as expected over this long time period due to loss of ATP-dependent pump mechanisms or the induction of cell death pathways. To prevent unexpected side-effects and cytotoxicity from long-term disruption of Ca^{2+} it was decided that cells could be treated to a shorter, 30 min, incubation in these drug conditions before imaging the fluorescence lifetime. Previous studies in the group have investigated the aggregation of exogenous monomeric tau protein that is taken into endolysosomal compartments of cells. Much of this work used SH-SY5Y cells and tau incubated over 8 hr before imaging the fluorescence lifetime. It was therefore unknown how long tau protein would take to aggregate inside of primary hippocampal neurons and experiments were initially carried out over 4 hr. However, due to the need to add ammonium chloride during each step of the trypsin wash to prevent initiating aggregation (in conversation with Dr. Claire Michel and Na Yu) it was hypothesised that the aggregation of tau may occur quickly. If aggregation occurred quickly, the effect of cellular Ca^{2+} may be masked by imaging at 4 hr if aggregation of tau were saturated at this timepoint. To determine whether tau sufficiently aggregated in this timespan such that it was detectable by FLIM, cells were treated for 30 min in the presence or absence of NH_4Cl before imaging (Figure 45).

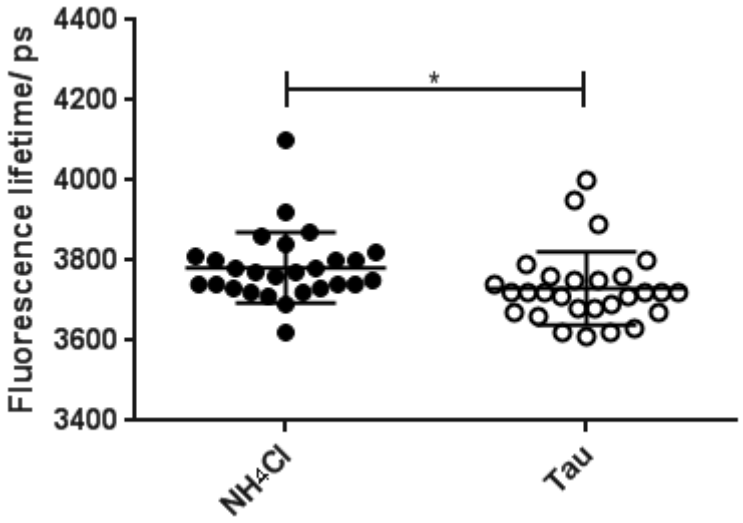

Figure 45. Tau protein aggregates to a detectable concentration for measurement by fluorescence lifetime imaging within 30-50 min incubation (**P* **= 0.0399;** ***t*** **= 2.107; d.f. = 2; two-tailed unpaired** ***t*****-test). Experiments were performed from** ***n*** **= 3 animals, with** ***n*** **> 3 images per repeat, yielding similar results).**

A significant difference was observed between tau only versus tau + NH_4Cl treated cells. Sufficient tau protein aggregated between 30-60 min of imaging that the lifetime change was detectable using FLIM. This was a much faster timescale than previously expected. To ascertain whether treatment of cells with drugs that alter intracellular or vesicular Ca^{2+} concentration would affect the concentration of tau that aggregated at an earlier timepoint, cells were incubated for 30 min and imaged between 30-60 min using FLIM.

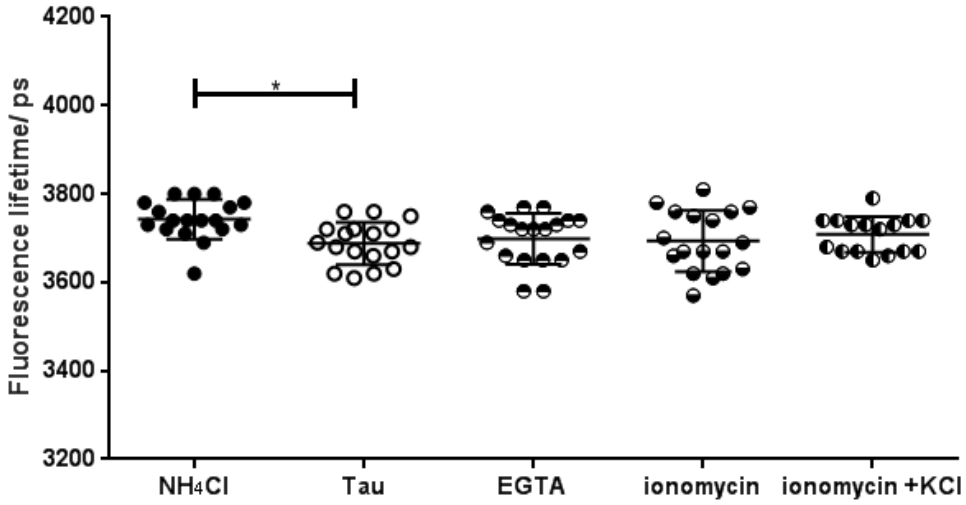

Figure 46. No significant differences were observed following a shorter, 30 min, treatment of cells with drugs that alter intracellular or vesicular Ca^{2+} concentration (one-way analysis of variance (ANOVA); ****P* **= 0.0216; F (4, 84) = 3.031). Tukey's multiple comparison *P* values (NH4Cl + tau (A), tau (B), EGTA + ionomycin (C), ionomycin (D), ionomycin + KCl (E)): (A-B) ****P* **= 0.0216; (A-C) not significant (NS) = 0.0931; (A-D) NS = 0.0503; (A-E) NS = 0.3285; (B-C) NS = 0.9735; (B-D) NS = 0.9832; (B-E) NS = 0.9273; (C-D) NS = 0.9984; (C-E) NS = 0.9832; (D-E) NS = 0.7155. Experiments were performed from *n* = 3 animals. All data points from the repeats and mean values with standard deviation are plotted).

Neurons incubated for 30 min in drugs that alter cytosolic or vesicular [Ca^{2+}] did not affect the concentration of tau aggregation over 30-70 min (Figure 46). Together with 3-4 hr incubation data, it appears that cellular calcium concentrations do not directly affect tau aggregation within the < 4 hr timescale where we begin to see tau aggregation. Therefore, it seems apparent that alteration to calcium in cells has no direct effect on aggregation. These findings were shown using conditions affecting [Ca^{2+}] in cells. Changes to $[Ca^{2+}]_i$ were hypothesised to affect tau aggregation via one of two main mechanisms. Either a) changes in synaptic vesicle cycling rate was expected to determine the incubation time of tau in low pH compartments and its aggregation rate; b) alternatively it was thought Ca^{2+} might have a direct role in tau conformation and aggregation. From this study, we have shown a) does not contribute to tau aggregation in a way that we were able to measure through the use of Ca^{2+} treatments. For b) this was hard to conclude as there is strict buffering of Ca^{2+} in the cytosol and cell compartments by numerous Ca^{2+} buffering proteins or channels. It is possible that our treatment would mostly alter cytosolic [Ca^{2+}] and introduce very little variation in Ca^{2+} conditions inside the vesicles. Vesicular tau in endolysosomal compartments may be relatively immune to cytosolic Ca^{2+} changes, and less affected by lower doses of ionomycin treatment which

particularly target ER membrane (Foyouzi-Youssefi *et al.*, 2000) as compared to higher concentrations effecting other membrane, including lysosomes (Shang *et al.*, 2016). The most direct treatment is therefore EGTA chelation of Ca^{2+} in the extracellular medium taken into endocytic vesicles with tau. For this reason, to further understand the direct relationship tau may have on vesicles it was tested whether aggregation could be measured by incubating tau in different calcium and pH conditions in the absence of uptake into cells where the concentrations could be strictly regulated. Alongside this, it was aimed to better understand why tau was seen to aggregate in such a short time period (30-50 min) following uptake into neurons, though not in studies without cellular uptake. Although specific molecules such as heparin, and other polyanionic cofactors, have been found to induce aggregation of tau (Goedert *et al.*, 1996; Friedhoff *et al.*, 1998), it was of interest which physiological factors may induce aggregation in the experiments adding exogenous tau to cells without any additional cofactors.

3.5 Calcium ion concentrations, pH, and synaptic vesicles on tau aggregation in the absence of cellular uptake

An interesting paradox is the longer timescale that it takes for tau to aggregate at low pH without cellular uptake, as compared with its ability to aggregate within 30-50 min following uptake into low pH compartments inside of cells. For tau aggregates to become detectable without cellular uptake, as measured by ThT assays or AFM studies, tau incubation takes on the order of weeks (unpublished data, Dr. Amberley Stephens, see also Section 3.5.1). This suggests that there is another mechanism required to catalyse the seeding of tau aggregation. Initial mechanisms considered for tau seeding included [Ca^{2+}], cell membrane - which strongly attracts tau protein due to negative charge, or synaptic vesicle protein synaptogyrin-3, which tau has been shown to bind to during immobilisation of vesicles at actin (McInnes *et al.*, 2018). Synthetic membrane vesicles have also previously been shown to catalyse the formation of toxic tau species (Ait-Bouziad *et al.*, 2017). However, it is possible that ThT assays and AFM are not sensitive enough to detect the initial aggregate structures, such as those that form inside of cells, as compared with TCSPC-FLIM. Therefore, it was of interest whether tau formed aggregates detectable by TCSPC-FLIM over 4 hr without cellular uptake when incubated at low pH. It has previously been shown that tau

does not form aggregates over 4 hr at pH 7.2 detectable by TCSPC-FLIM (Michel *et al.*, 2014, see also Section 3.2), and full length tau is known not to readily aggregate without induction (Goedert *et al.*, 1996; Pérez *et al.*, 2002; Mirbaha *et al.*, 2018). The combination of pH, [Ca^{2+}], and synaptic vesicles were used in the absence of cells to understand whether these components contributed to initiating the aggregation of tau protein. Increasing concentrations of Ca^{2+} were added to low pH (5.3) or physiological pH (7.2) solution in the presence of synaptic vesicles. The samples were incubated for 4 hr as previously used for measurements of tau aggregation inside of cells. Samples were incubated at physiological temperature, 37°C as has previously been shown to increase the rate of aggregation (Friedhoff *et al.*, 1998). Samples were compared to the 'monomer' solution composed of tau protein in pH 7.2 HBSS.

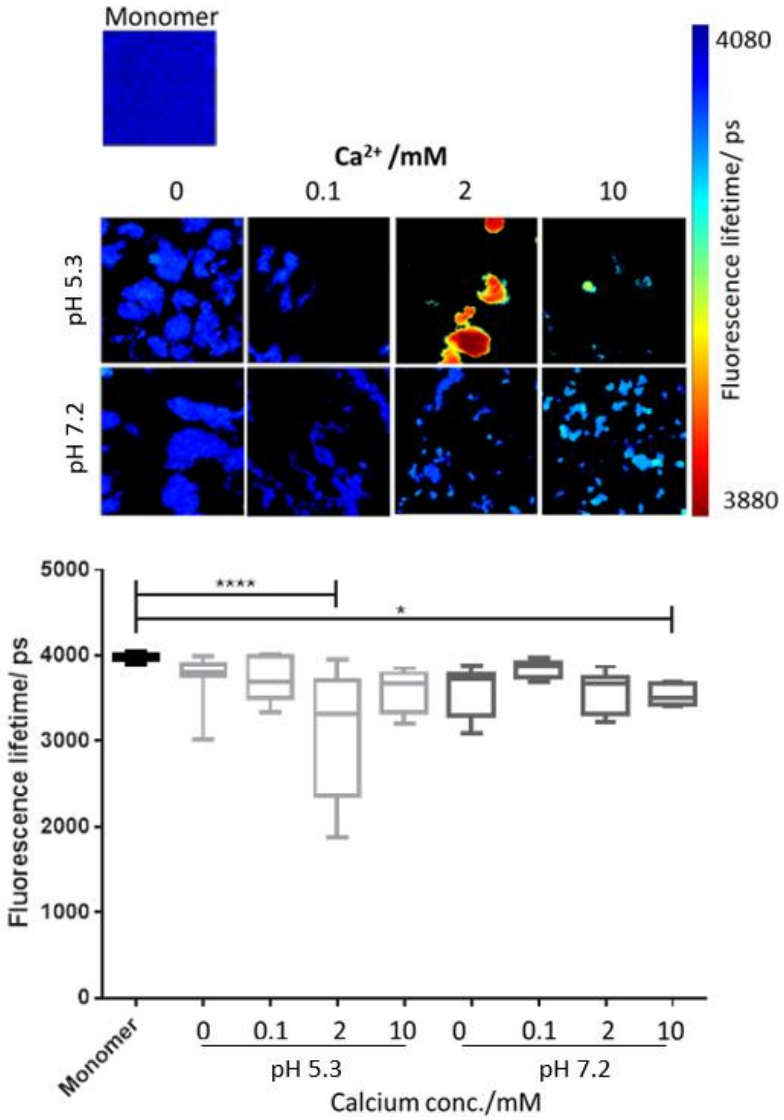

Figure 47. Fluorescence lifetime of 1µM tau monomer incubated with 1.2 µg/µL synaptic vesicles, concentrations of calcium ions, at low or physiological pH (one-way analysis of variance (ANOVA); ****P < 0.0001; F (8,70) = 5.245). Dunnett's multiple comparison P values (left to right): not significant (NS) = 0.5110; NS = 0.4778; ****P < 0.0001; NS = 0.0654; NS = 0.0539; NS = 0.9295; NS = 0.0688; NS = 0.0289. The experiment included 3 independent repeats with n > 3 technical repeats. Mean values with standard deviation are plotted).

Data show that 2 mM Ca^{2+} in pH 5.3 solution with synaptic vesicles resulted in the most significant decrease in the fluorescence lifetime measured for tau protein (Figure 47). It was possible that the 2 mM Ca^{2+} concentration that tau experienced in the extracellular space, combined with low pH 5.3 inside of vesicular membrane were all required to induce tau aggregation inside of cells.

However, due to the large variation of measurements in this data set, arising particularly from the repeat *n* =2 (Figure 48), alongside the large number of groups included in the analysis, it was deemed necessary to repeat the experiment whilst also reducing the number of variables. Screening of 2 mM Ca^{2+}, pH 5.3, and synaptic vesicles was carried out to better identify their contribution to any reduction of tau fluorescence lifetime. The experiment was repeated taking multiple combinations of these variables into consideration as the original experiment did not consider that each variable may have no effect or, opposite effects, on tau aggregation. Solutions were therefore prepared with combinations of low pH or low pH + 2 mM Ca^{2+} in the presence or absence of synaptic vesicles. Samples were incubated for 4 hr and compared to the negative control of pH 7.2 monomer solution.

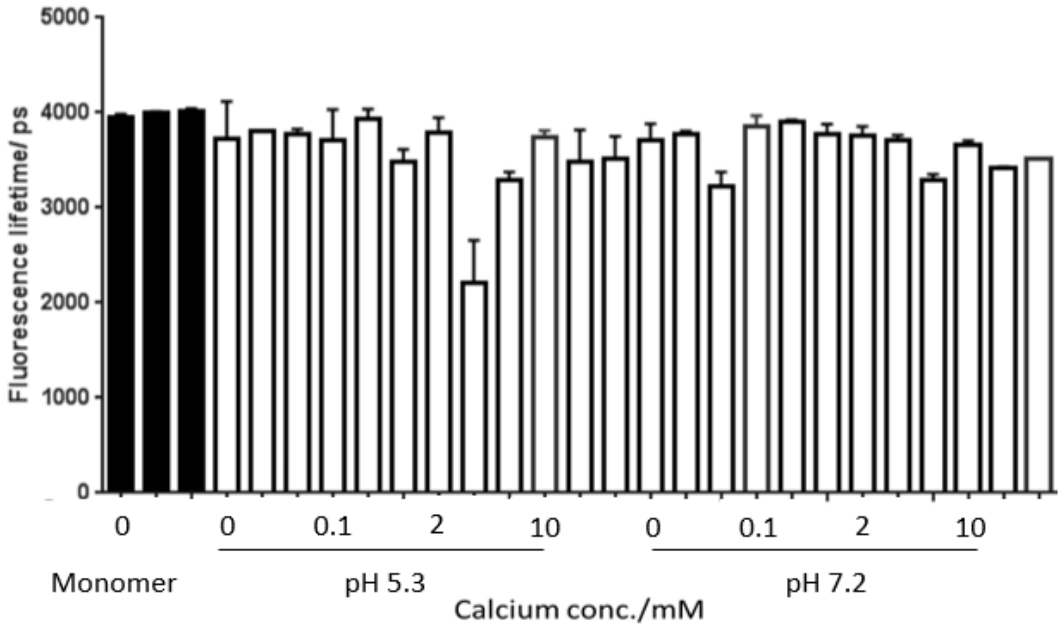

Figure 48. The experimental repeats for each condition are plotted separately to show large variation arising from a single dataset for the condition pH 5.3, 2 mM Ca^{2+}, with synaptic vesicles. Therefore, the experiment was repeated with other pH 5.3 conditions to better understand the contribution of each variable to any reduction in the fluorescence lifetime of tau.

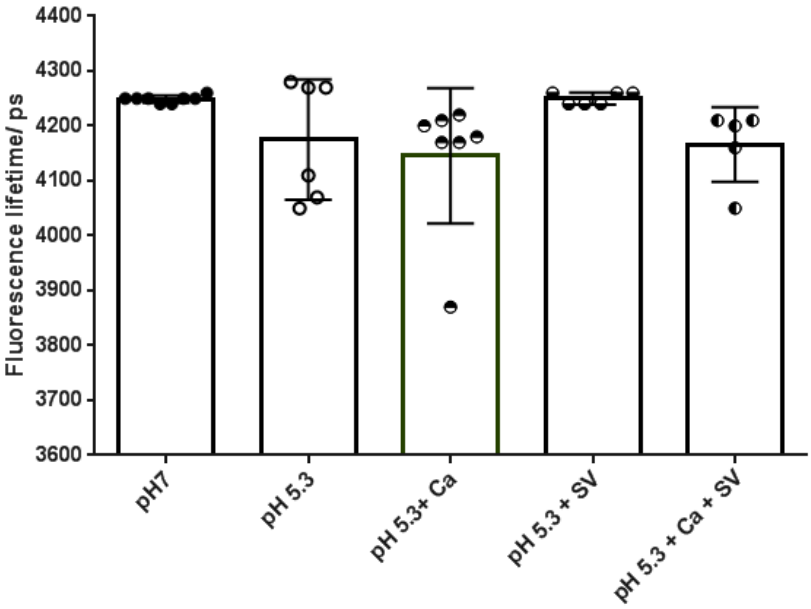

Figure 49. No differences are seen in the fluorescence lifetime of tau when incubated for 4 hr between different pH, calcium ion, and synaptic vesicle conditions (one-way analysis of variance (ANOVA); *P* = 0.0627; F (4, 27) = 2.543). Dunnett's multiple comparison *P* values (left to right): not significant (NS) = 0.2741; NS = 0.0605; NS > 0.9999, NS = 0.2281. The experiment included 3 independent repeats with n > 3 technical repeats. Mean values with standard deviation are plotted).

No differences were found between the pH 5.3 solutions incubated with tau protein for 4 hr as compared with pH 7.2 control (Figure 49). This included the pH 5.3 + 2 mM Ca^{2+} + synaptic vesicle dataset which previously was measured to show decreased fluorescence lifetime compared with pH 7.2 monomer control.

The experiment was repeated using a 24 hr incubation, which was longer than that used for tau incubation studies in neurons but offered a longer period for tau to aggregate to concentrations detectable by TCSPC-FLIM. Samples were incubated for 24 hr and the fluorescence lifetime of tau was measured to determine whether tau protein aggregated in these conditions over this longer timescale.

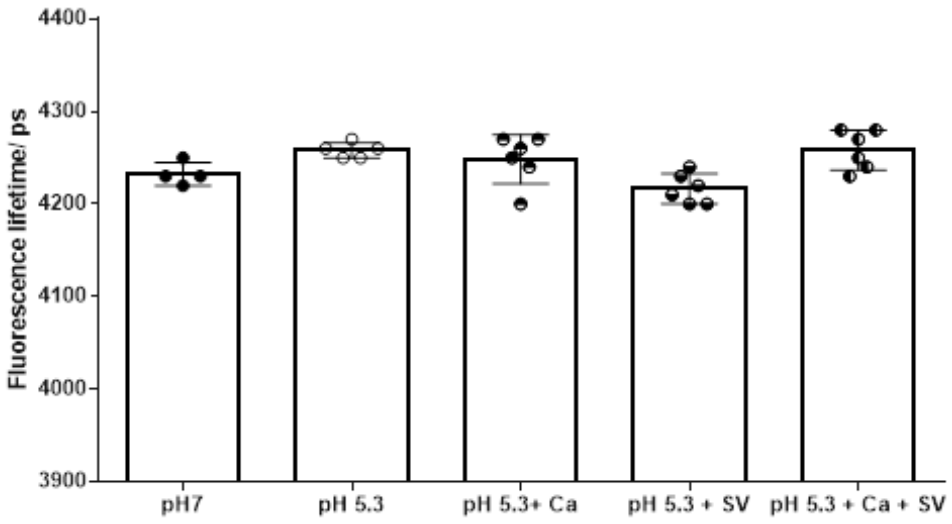

Figure 50. No differences in fluorescence lifetime are seen between pH 5.3 conditions as compared with the pH 7 'monomer' control (one-way analysis of variance (ANOVA); *****P* **= 0.0045; F (4,22) = 5.117). Dunnett's multiple comparison *P* values (left to right): not significant (NS) = 0.1690; NS = 0.5139; NS = 0.5139; NS = 0.1390. The experiment included 3 independent repeats with n > 3 technical repeats. Mean values with standard deviation are plotted).

At 24 hr, no differences were seen between pH 5.3 conditions compared to the negative control of pH 7.2 monomer solution (Figure 50). From these results, it appears that monomeric tau does not form detectable aggregates in solutions at low pH in the presence or absence of synaptic vesicles or Ca^{2+} conditions up to 10 mM.

3.5.1 Discussion

Using fluorescence lifetime imaging, in initial tests, tau was found to aggregate at low pH (5.3) in the presence of 2mM Ca^{2+} and synaptic vesicles. The standard deviation for this group was much larger compared with the other groups however, and therefore this group (pH 5.3 + 2mM Ca^{2+} + synaptic vesicles) was separated into each variable of pH, Ca^{2+}, and synaptic vesicles to better understand what may cause this aggregation. Following repeat, the aggregation state of tau, as measured by its fluorescence lifetime, was not different from the negative control (pH 7.2 'monomer' solution) at either 4 hr or 24 hr incubation. Original data were collected at pH 4, however, this resulted in low fluorescence expected to occur from changes to the fluorophore,

which has only been listed as pH insensitive between pH 4-10 (ThermoFisher). Therefore, data were recollected at pH 5.3, which may be too high of a pH to initiate the aggregation of full-length monomeric tau. Alternatively, pH alone may be insufficient to catalyse the aggregation of tau protein in the short time period measured inside of neuronal compartments.

A complimentary method to verify these results could be useful to reduce variation, such as AFM imaging or Thioflavin T (ThT). A difficulty of verifying the method is that ThT assays rely on the intercalating of ThT with rich β-sheets found in amyloid proteins (Sulatskaya et al., 2011). At 4 hr incubation, it is unlikely that tau will have aggregated to a sufficient extent to provide enough β-sheet fibrils for the assay to detect tau as aggregated. At the oligomer stage, oligomers are found at < 1 % of monomeric protein concentration (Chen *et al.*, 2015). An alternative solution is to use Thioflavin X (ThX) which is capable of binding small oligomeric species that may arise at earlier timepoints than full-scale fibrils. ThX shows 5x increased brightness and 7x increased binding affinity to amyloid proteins as compared with ThT (Needham *et al.*, 2019, pre-print). Results from Dr. Amberley Stephens' experiments (n = 1) using ThT assays to detect whether tau could be aggregated at low pH (4) alone, showed that fibrilisation did occur, but took on the order of 30 days as opposed to 4 hr in cells (Figure 51). This could be due to lack of sensitivity from the ThT assay for oligomeric species and smaller aggregates at 4 hr, or due to the role of cellular uptake on aggregation. Dr. Stephens' results also show a decrease in fibrilisation in the presence of synaptic vesicles, which is different from expected based on previous literature (Ait-Bouziad *et al.*, 2017).

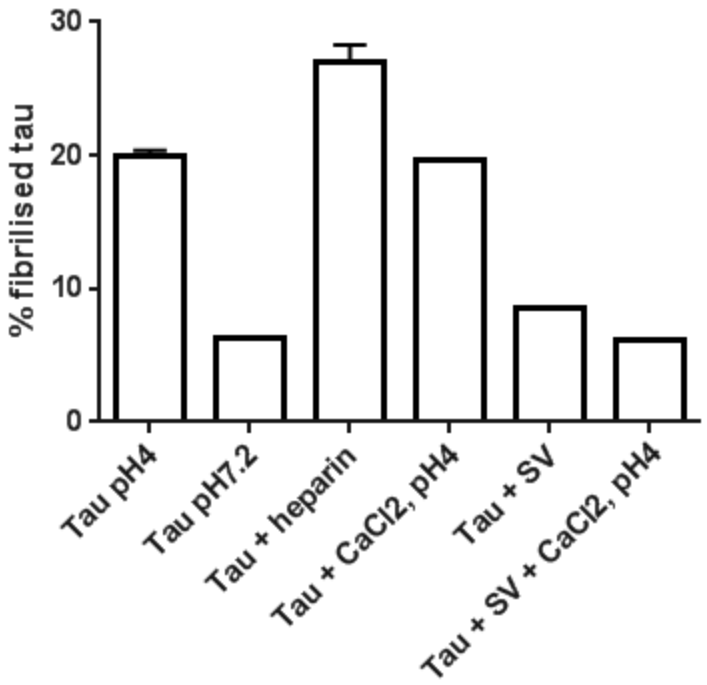

Figure 51. The fibrilisation of monomeric tau protein is increased by heparin or low pH but reduced in the presence of synaptic vesicles as determined by measuring the remaining monomer concentration through absorbance at 280 nm. Data: Dr. Amberley Stephens.

Although this study is only n = 1 and therefore no conclusions can be drawn between the conditions, the results have shown that it is possible for tau to form fibrils at pH 4 over 30 days, 20 rpm rotation and 37 ºC. The structural conformation the fibrils formed at low pH have not yet been analysed to determine whether they are the same paired helical and straight Tau filaments as seen in AD or conformationally different as for heparin-formed fibrils (Fitzpatrick *et al.*, 2017; Zhang *et al.*, 2018).

3.6 Chapter 3 Summary

In this chapter, the novel finding was made that tau aggregation is significantly reduced inside of neurons by neutralising low pH, endolysosomal vesicles, by using the weak base ammonium chloride (NH_4Cl). This 10 mM concentration is sufficient to prevent the aggregation of tau over at

least 4 hr incubation. Through the calibration of Oregon Green™ 514 dextran the average pH of endocytic compartments was measured to be pH 5.3. This pH increased to at least pH 6.5 following the addition of 10 mM NH_4Cl, which was sufficient to prevent significant aggregation of tau protein. Following calibration of Oregon Green™ 514 it was possible to directly correlate two channels of fluorescence to understand the aggregation state of tau and pH of endocytic compartments on a per pixel basis. Two discrete populations of tau were detected using two-colour FLIM that were present throughout the pH gradients measured with dextran-OG514. Whether the aggregated tau measured at high (> 6.5) pH were initially formed from low (< 6.5) pH vesicles or through a pH independent method is not clear from the 4 hr timepoint. Without cellular uptake, incubation of tau at pH 5.3, the average pH measured for endocytic compartments inside of cells, did not cause detectable aggregation of tau at 4 hr or 24 hr incubation. Therefore, based on TCSPC-FLIM with ThT and AFM studies, a process inside of cells appears necessary to catalyse the aggregation of tau, though this mechanism is not directly linked to Ca^{2+} or synaptic vesicles at pH5.3.

Altering the intracellular concentrations of calcium ions (Ca^{2+}) does not affect the amount of aggregated tau measured at 30 min or 4 hr. As monomeric tau has previously been shown to increase intracellular Ca^{2+} (Gómez-Ramos *et al.*, 2006, 2008), our finding suggests that this does not directly feed back to the aggregation of tau protein. Ca^{2+} did not result in a change in the measured fluorescent lifetime of tau protein *in vitro* without cells when mimicking intracellular (100 µM) or extracellular (2 mM) Ca^{2+} concentrations. A decrease in fluorescence lifetime was measured at pH 5.3 with synaptic vesicles and 10 mM Ca^{2+} (Figure 47), though due to the variability of the results this would be worth repeating with reduced variables. This also suggests that neuronal activity may not affect the rate of tau aggregation by increasing intracellular Ca^{2+} alone, and therefore an alternative mechanism must be considered.

The rate of tau aggregation is known to be greatly enhanced by polyanions including RNA, heparin, and polyglutamate which resembles the acidic tail of tubulin. This aggregation is enhanced at pH ~6 and low ionic strengths (< 50 mM), and temperatures above 30 °C (Friedhoff *et al.*, 1998). The mechanism through which low pH induces tau aggregation is not known, particularly as the structure of tau has been shown to remain relatively unchanged by pH (Jeganathan *et al.*, 2008). Although it has been shown that incubation for 30 days at pH 4 is

sufficient to cause fibrilisation of tau that is detectable using ThT assay, the structure of these fibrils is yet to be determined as to whether they are similar to aggregates inside of cells, or found in AD patients brain. Therefore, the question still remains as to whether pH alone is sufficient to cause the aggregation seen inside of cells, or whether there is a catalytic mechanism that results in measurable aggregation within 30 – 50 min. It has been shown that the aggregated exogenous tau in endolysosomal vesicles can associate with endogenous tau (Michel *et al.*, 2014), as known to occur in AD. The mechanism through which aggregated tau is able to escape endolysosomal vesicles in this case is unknown, but has been shown to occur from lysosomes (Calafate *et al.*, 2016), and phosphorylated tau at membranes has also been shown to be directly released through membrane (Merezhko *et al.*, 2018). Another question in this model of uptake and aggregation of exogenous monomeric tau is at what stage in the pathway hyperphosphorylation occurs as is seen in AD neurofibrillary tangles. The hTau40 that is added does not have any phosphorylation, and therefore whether it is phosphorylated on entry to the cell, once released from vesicles, or associates with phosphorylated endogenous tau remains unknown but will be of interest. Alongside phosphorylation, the uptake of monomeric tau from our, and other studies (Evans *et al.*, 2018) is yet to show any direct link between uptake, aggregation and cell death. It is possible that neurodegeneration occurs over a much larger timescale than the initial neuronal dysfunction, as is shown to occur in AD where pathology and symptoms occur over years and decades (Sperling *et al.*, 2011; Hunsberger *et al.*, 2014; Jackson *et al.*, 2017). Therefore, the next question in better understanding the internalisation and aggregation of exogenous tau inside of neurons, is whether it causes any pathophysiological hallmarks related to synaptic dysfunction that may explain early symptoms of memory impairment.

CHAPTER 4

4.1 A pathological phenotype arising from exogenous monomeric tau: Nanomechanical studies using Atomic force microscopy for measuring cell stiffness

It was considered that exogenous monomeric tau may affect cell stiffness through recruiting endogenous tau following its aggregation. Atomic force microscopy (AFM) was used for live-cell topographical imaging that simultaneously allowed quantitative nanomechanical measurements of primary neurons in solution. Cells were treated with monomeric tau protein, nocodazole to depolymerise microtubules, or toxic levels of DMSO to induce cell death. Three areas across each hippocampal neuron were averaged to gain a stiffness measurement for each cell (Figure 52). The stiffness of hippocampal neurons treated with exogenous tau was compared to controls.

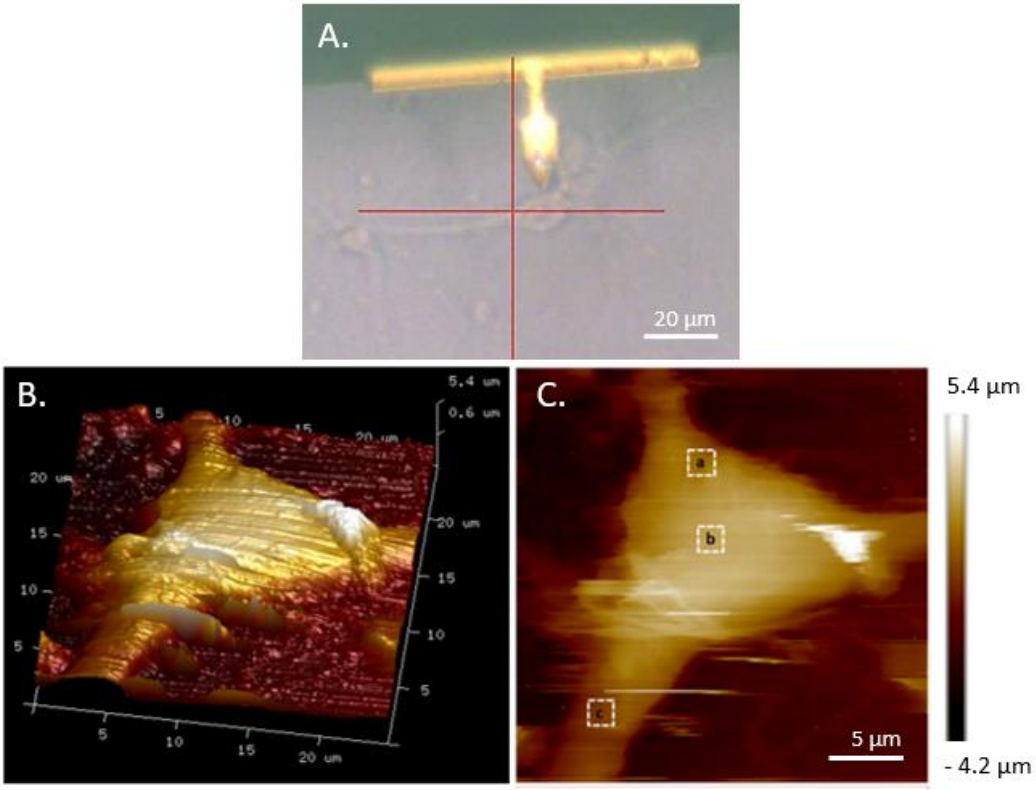

Figure 52. Topographical imaging of a hippocampal neuron to gain stiffness measurements. A. The AFM probe tip in contact with a hippocampal neuron. B. 3D representation of a 25 µm^2 topographical image of a hippocampal neuron with C. Three selected areas to be averaged for a stiffness measurement for the cell.

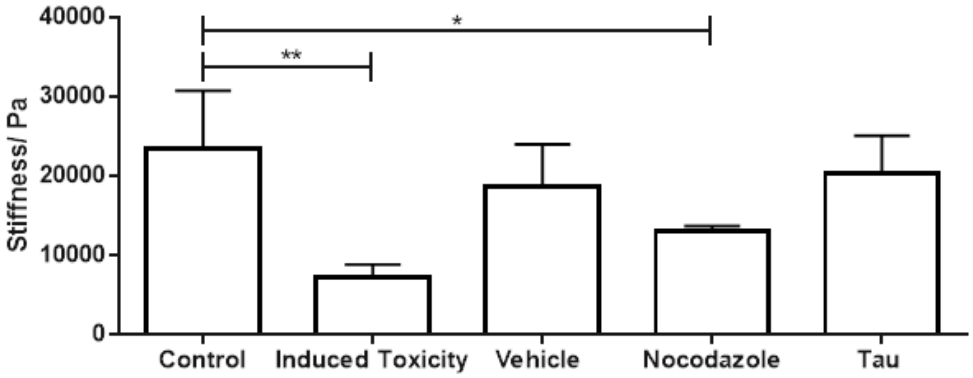

Figure 53. The stiffness of neurons treated with exogenous tau protein was compared with controls. Induced toxicity was used as a positive control to test the method was sensitive enough to detect stiffness changes. Nocodazole was used to depolymerise microtubules to determine whether this would produce a measurable stiffness change. No changes to stiffness were detected for cell incubated with tau for 4 hr (one-way analysis of variance

(ANOVA); *****P* **= 0.0072; F (4, 13) = 5.688). Dunnett's multiple comparison *P* values (left to right): *****P* **= 0.0027; not significant (NS) = 0.6378; ****P* **= 0.0500; NS = 0.7214. Experiments were performed from *n* = 3 animals with n >= 1 cells per animal. Mean values with standard deviation are plotted.

No differences in stiffness were measured between control and tau-treated cells (Figure 53). The cells treated with high concentration of DMSO to induce cell death showed decreased stiffness compared to control cells. This shows that a) the method is capable of detecting cell stiffness arising from acute cytotoxicity b) treatment of cells with exogenous tau does not induce acute toxicity resulting in stiffness loss. Cells treated with the microtubule depolymerising drug, nocodazole, also showed decreased stiffness as compared with control cells. This suggests that the method is capable of detecting stiffness changes from microtubule depolymerisation independently from the effects of vehicle (low concentration DMSO) or cell toxicity (high concentration DMSO). As no differences are seen between tau treated cells and controls it appears that exogenous tau does not cause dramatic changes to cell stiffness over 4 hr.

Further studies to measure stiffness of neuronal synapses using this AFM method were attempted. The aim was to determine whether a decrease in synaptic stiffness preceded synaptic loss occurring in AD. However, imaging of dendrites resulted in dragging of the membrane by the probe tip even using decreased speeds and forces. Although topographical images could be taken (Figure 54 (left)), when the modulus images were analysed, there appeared to be increased low modulus areas as compared with true cell regions seen from topographical images (Figure 54 (right)). The membrane dragging therefore made it too ambiguous to select true cellular regions from the modulus images, and to discern regions that may be synaptic compartments. For this reason, attempts to use synaptosomes as synaptic models were made (Figure 55).

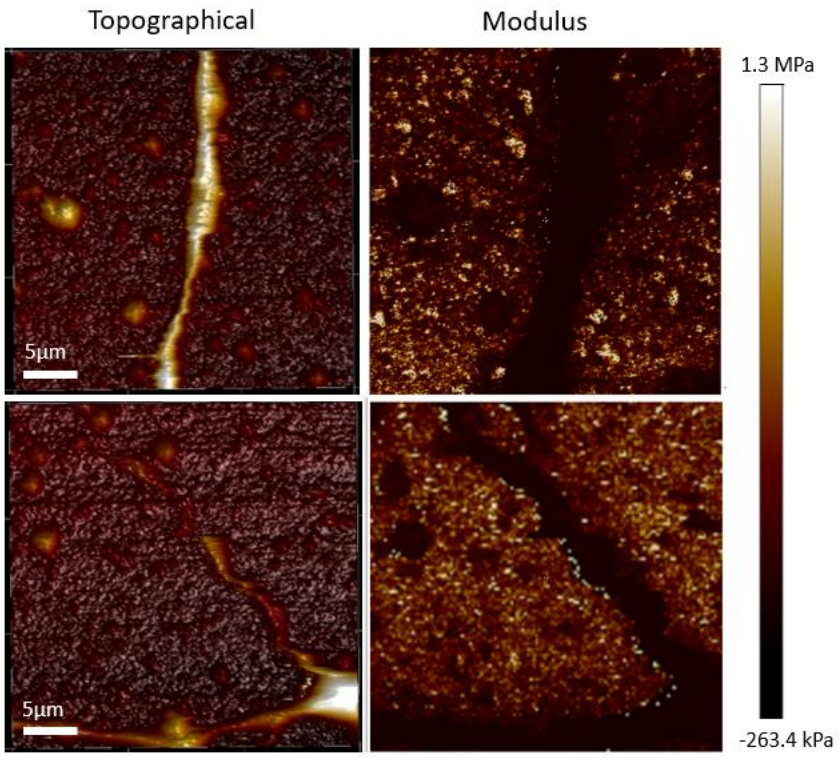

Figure 54. AFM was used in attempt to measure the stiffness of synaptic compartments. From topographical images (left) it was difficult to identify compartments due to dragging of membrane, even at slow scan speeds. Modulus images (right) also demonstrate the dragging of membrane as seen by the increased area showing low stiffness compared to the topographical images.

Stiffness measurements of isolated synaptic compartments, synaptosomes, were made. It was possible to measure the stiffness of synaptosomes in different conditions. However, it was decided that the absence of intact microtubules in synaptosomes made them an unsuitable model to understand how exogenous tau may cause unbinding and aggregation of endogenous tau.

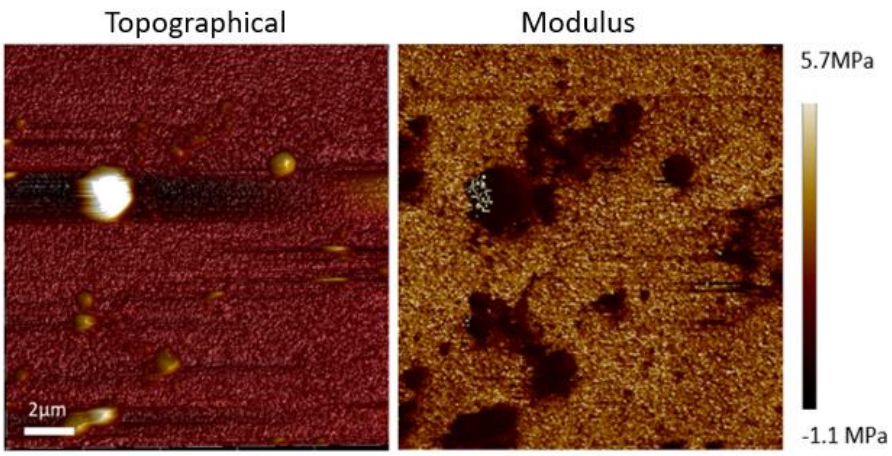

Figure 55. AFM was used to measure the stiffness of synaptosomes. Although the method was capable of topographical and stiffness measurements, there was limited physiological relevance using this model.

4.2 Chapter 4 Discussion

Exogenous monomeric tau does not cause changes in cell stiffness following 4 hr incubation. This suggests that if endogenous tau is recruited to internalised, aggregated exogenous tau, that it is either not recruited from microtubules resulting in depolymerisation, or that substantial recruitment occurs later than 4 hr time-period. As most tau (>95%) is bound to microtubules (Reynolds et al., 2005), it is not clear where tau would alternatively be recruited from unless it were temporarily unbound following MT dynamics or newly synthesised. It is also possible that the method is not sensitive enough to detect small scale changes of microtubule-dependent stiffness, or changes to localised areas of neurons that were not selected during analysis.

Another possibility is that the major contribution to the measured cell stiffness was not the microtubules. Although microtubules have been shown as the main contributing factor to cell stiffness from AFM measurements under certain conditions (Curry et al., 2017; Lee et al., 2015; (Ouyang, Nauman and Shi, 2013), it has also been shown that at low strain, actin networks, and not microtubules are deformed during stiffness measurements (Kubitschke *et al.*, 2017). For small cellular deformations, only the actin cortex that forms networks at the cell surface is effectively probed, at large deformation, the microtubule network also contributes. The ~200 pN force used

for the scanning probe method was selected so as not to damage the intricate axonal and dendritic networks of the neurons; however, it is possible that this force only superficially probed the cells without interacting with the microtubule network. As nocodazole treatment showed a decrease to cell stiffness it seems that this method can detect the depolymerisation of microtubules, as at least an indirect impact of other cellular processes following microtubule depolymerisation. The time that nocodazole causes microtubule depolymerisation has been shown as dose-dependent (Jang *et al.*, 2016). It is possible that depolymerisation occurs at a longer, concentration-dependent, timescale following tau aggregation. In this project, a low dose of nocodazole (70 nM) was used to prevent toxicity to the hippocampal neurons; however it has been shown that primary neurons treated with a low dose of 0.1–100 nM can be incubated in nocodazole for 3 d before measurements (Verstraelen *et al.*, 2017). Therefore, although tau does not affect the stiffness of neurons following 4 hr incubation, it is possible that endogenous tau is recruited from microtubules at a later stage. Measurements on cells treated with tau could be taken after a longer timepoint such as post-24 hr incubation to see whether the process occurs at a later stage of pathology. We can therefore conclude that although exogenous monomeric tau may have effects on cell stiffness following incubation >4 hr, this is not an early pathological phenotype occurring within 4 hr of tau uptake and aggregation as detected through FLIM.

The attempt to measure the stiffness of synapses in living cells proved unsuccessful due to membrane dragging. This method has not been previously published and therefore may require further technical advancements for these measurements to be possible. Stiffness measurements on synaptosomes were possible. Although these measurements can be useful for other studies, synaptosomes were deemed unsuitable for understanding processes involving possible recruitment of endogenous tau, thought of predominantly as an axonal protein.

CHAPTER 5

5.1 A pathological phenotype arising from exogenous monomeric tau: electrophysiological studies

The aim of this chapter is to determine whether there are any electrophysiological deficits arising from the internalisation of exogenous monomeric tau by neurons, and how this relates to tau aggregation. Following from Chapter 3, cellular internalisation of exogenous monomeric tau results in its aggregation due to low pH but not due to changes to intracellular calcium ions. Other than the finding that monomeric tau can result in increased concentrations of intracellular calcium ions (Gómez-Ramos et al., 2008; Gómez-Ramos et al., 2006), no clear pathological phenotype has been detected following the uptake and aggregation of exogenous monomeric tau. Chapter 4. has shown that during the initial aggregation stages of tau inside of neurons, no stiffness changes are measured from neurons. Therefore, initial pathology may not directly occur from large-scale depolymerisation of microtubules following tau unbinding and sequestration in aggregates. Due to the finding that the rate of tau pathology *in vivo* in an rTg4510 tau mouse model is activity dependent (Wu *et al.*, 2016), it was considered that activity may increase the aggregation of tau measured to aggregate between 30 min to 4 hr time periods. Although previous studies have only shown oligomeric and soluble aggregated forms of tau having an effect on the initiation of long-term plasticity (Polydoro *et al.*, 2014; Fá *et al.*, 2016; Puzzo *et al.*, 2017), no studies have found relationships between uptake and aggregation of exogenous monomeric tau on long-term plasticity.

As a first step, a method was devised to optogenetically stimulate neurons between multiple experimental set-ups to determine whether any activity-dependent electrophysiological deficits arise from the internalisation of exogenous monomeric tau by neurons, and how this relates to tau aggregation.

5.2 The stimulation of neurons with a custom developed optogenetic device, OptoGenie

Device design was in collaboration with Omid Siddiqui. Dr. Tanja Fuchsberger gained measurements from cells.

An optogenetic stimulation device was designed for the optical excitation of cells between multiple experimental set-ups. In this study the set-ups included: an incubator for long-term stimulation during the time neurons were incubated with tau; on a patch-clamp rig or microelectrode array device for cellular recordings and confirmation that the device is capable of stimulating cells; and on an optical microscope for simultaneous stimulation and imaging, particularly using fluorescence lifetime as a measure of tau aggregation.

To achieve these three keys aims of accessibility, portability, and adaptability, a simple and modular design is used (Figure 56). The OptoGenie device has two main components, the central component based on an Arduino to set the frequency and power of the laser diode; and the laser component made up of the laser diode, lens, and aperture. The Arduino Uno is ideal as an accessible electronic prototyping platform due to low cost, commercial availability, and the Arduino IDE providing an open source, easily downloadable and shareable resource for collaborators. The Arduino IDE is used to control the pulse width and stimulation rate of the laser diode, allowing the stimulation protocol to be easily varied for each experiment. The Arduino powers the laser diode either via mains power supply or a 9V battery adaptor. The diode can be powered by a battery for use in the cell culture incubator, whereby cables that reach between the device and mains power supply could be inconvenient or interfere with incubator sterility. A variable resistor allows control of the power, such that the output intensity can be measured and adjusted per experiment, depending on the requirements. For the laser component, a single plano convex lens is used to collimate the laser light. In conjunction with a variable aperture, this allows for adjustment of the laser spot size onto the sample to select the population of cells to excite. The central component and laser component are held in place by proprietary adaptor posts and clamps, that can be purchased (Thorlabs Inc.) or replaced with any standard size posts and clamps that may already be available to the researcher. These adaptor posts add to the flexibility and portability of the system as the mounting of the posts can be used to alter the distance and angle of the laser

component to the cells, or remove the laser component entirely to reassemble on an alternative experimental set-up.

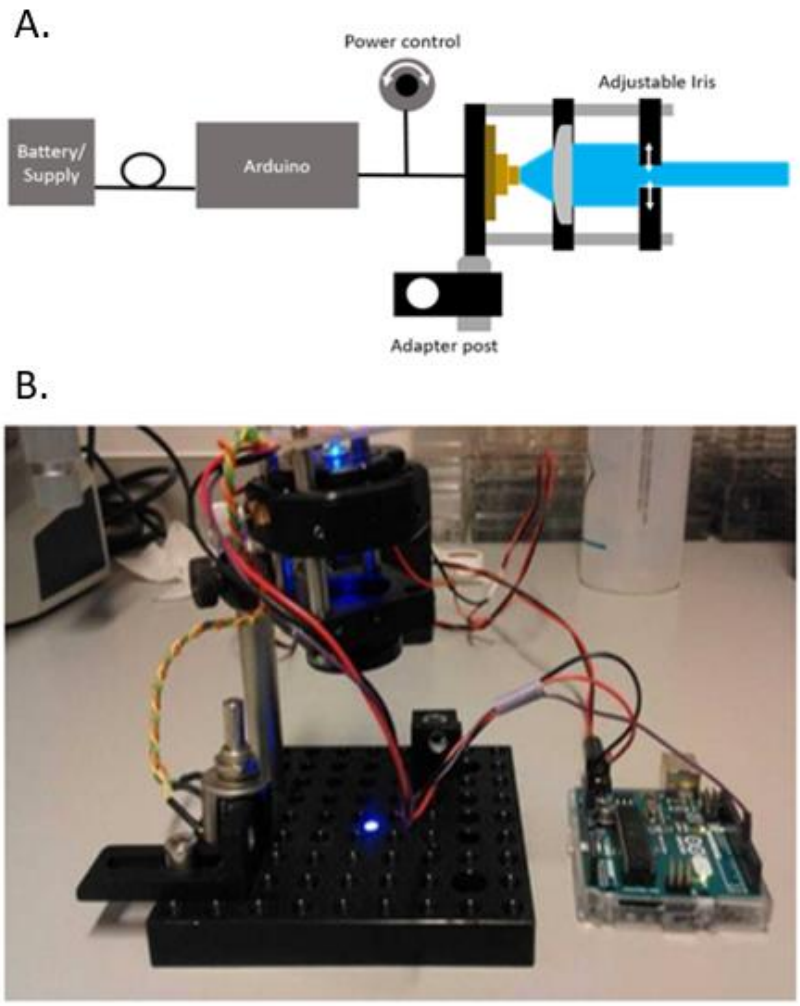

Figure 56. Designing an optogenetic stimulation device for multiple experimental set-ups. A. The schematic of the Optogenie device including the laser diode controlled by a variable resistor and Arduino Uno for setting intensity and stimulation frequencies. The system is highly portable due to its compact and simple design. Figure: Omid Siddiqui. B. The assembled OptoGenie device. The device can be used for placement in a cell incubator, optical microscope or patch-clamp rig thanks to its small size and removeable LED head.

To test the functionality of the device, primary CA3 hippocampal neurons that selectively expressed channelrhodopsin-2 (ChR2) from the Grik4 promoter were chosen for whole-cell patch

recordings as detected by co-expression of YFP to ChR2 (Figure 57 (top, left)). The device frequency was set to 1 ms stimulation pulses and the intensity of the pulse was adjusted until an action potential was evoked (Figure 57 (top, right)). The power required for stimulating an action potential was found to be between 5-9 mW, for a 6 mm pulse area used (83.3-150 mW/cm^2) depending on the expression level of ChR2 the cell. This intensity range was reliable in all cells that were patched (n = 7).

As a second step, voltage traces of YFP-negative cells were recorded to detect excitatory postsynaptic potentials (EPSPs) following a single 1 ms optogenetic stimulation of neighbouring YFP-positive cells (Figure 57 (bottom, left)) or following 50 Hz stimulation (Figure (57 bottom, right)) of YFP-positive cells with optogenetic stimulation.

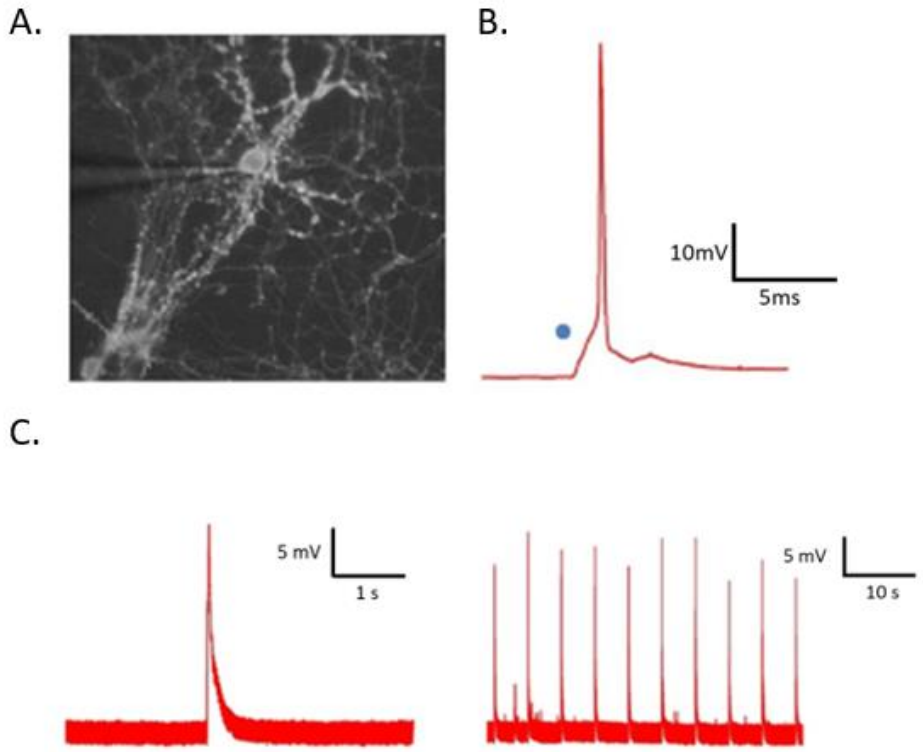

Figure 57. Whole-cell patch clamp recording from a cultured hippocampal CA3 neuron. A. Neurons selected for patch-clamp recordings co-expressed YFP as a marker of ChR2 expression. B. 1 ms blue light from the laser diode (represented by blue dot) resulted in a recorded action potential. C. Excitatory postsynaptic potentials (EPSPs) recorded from

cells synaptically connected to neurons excited by optogenetic stimulation. Figure: Dr. Tanja Fuchsberger.

After showing that OptoGenie was capable of the optogenetic stimulation of neurons expressing ChR2 using mains power, the device components such as the laser diode and Arduino were powered by a 9 V battery. Measurements were made to test whether the light intensity that the cells received would remain constant over the experimental time-length of 2.5 hr for use inside a cell incubator. For comparison, 2.5 hr recordings of 600 ms light pulses were made using mains power at the stimulation power required (~9 mW, 6 mm) and using the laser diode on full power as an upper bound of the power drop that could be expected in this time. Due to the power meter not having the temporal sensitivity to detect the stimulation frequency used in actual tests, an approximate equivalent stimulation pattern was used.

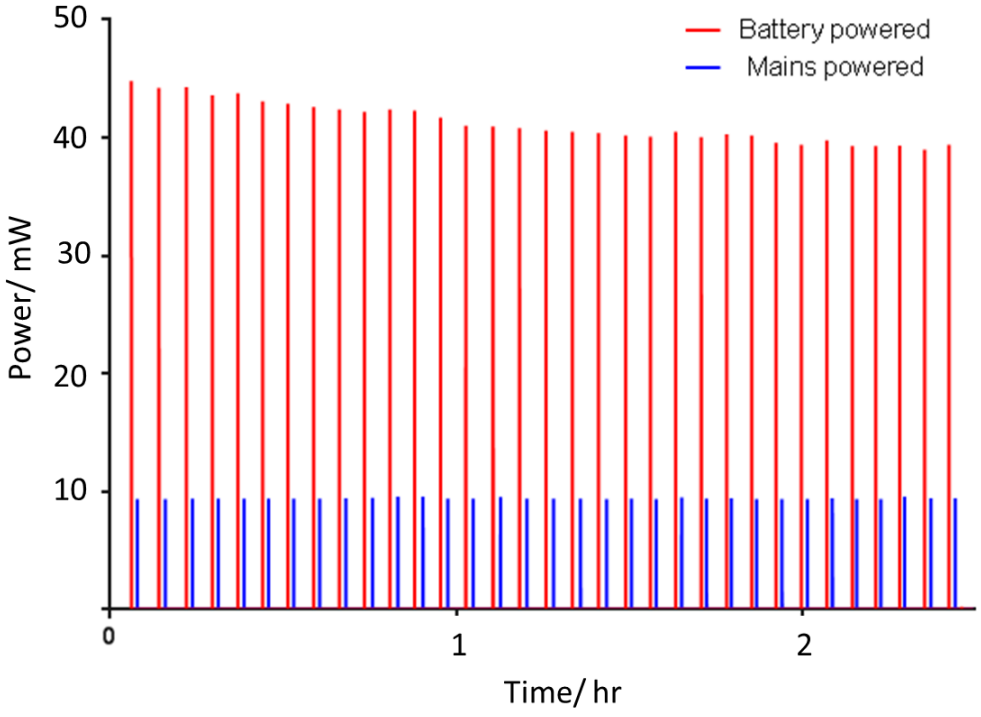

Figure 58. 600 ms light pulses emitted from laser diode pulses when powered by mains (blue) or battery (red) to measure the power loss over 2.5 hr.

When powered by a 9 V battery, the measured power of the laser diode set to 44.8 mW starting power dropped by 12.9 % (to 39.0 mW) over 2 .5 hr (Figure 58). When using mains power, the measured power of the laser diode set to 9.38 mW starting power did not show an overall decrease in power but had small fluctuations (±0.08 mW) throughout the recording. Although it may be expected for the power drop to be less for lower starting powers, in this project the starting power of the device has been set to between 9-10 mW (6 mm spot) for each experiment used to stimulate neurons expressing ChR2. This is an important consideration for any experimenter intending on using Optogenie with battery power, especially if a new battery is not used for each experiment or the experiment exceeds 2.5 hr.

5.3 Whole-Cell Patch Clamping recordings of optogentically stimulated cells treated with exogenous monomeric tau

This section was performed by Dr. Tanja Fuchsberger

Cells were incubated for 2.5 hr in 1 µM exogenous monomeric tau protein in the presence or absence of optogentic stimulation of 33 Hz every 10 s. Following 2.5 hr incubation, the response of neurons to a single stimulation from an external electrode was recorded using the whole-cell patch-clamp method. Figure 59 shows control cells, without exogenous tau treatment or optogenetic stimulation, showed a response following a single stimulation from an external electrode. Cells stimulated with optogenetic excitation for 2.5 hr in the absence of exogenous tau show increased potentiation following a single stimulation. Cells treated with exogenous tau in the absence of optogenetic stimulation show a response equal to that of untreated control cells. Cells treated with exogenous tau and optogenetic stimulation show complete depression of activity following a single stimulation.

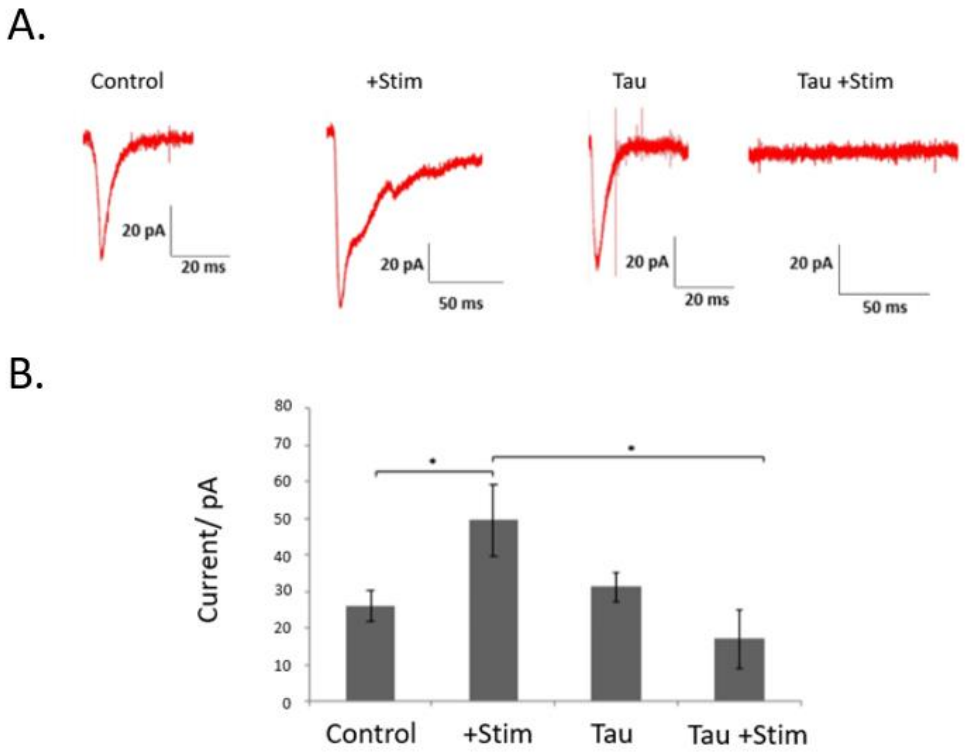

Figure 59. A. EPSPs were recorded from neurons by using an intracellular patch-clamp electrode following a single stimulation with an external electrode. B. An activity-dependent depression of synaptic transmission is seen in tau-treated neurons (N=9, n=3). Figure: Dr. Tanja Fuchsberger.

Even though cells that received 2.5 hr tau incubation and optogenetic stimulation showed no, or greatly reduced, response to a single stimulation from an external electrode, the membrane resistances of these cells were similar to control cells during the patch-clamp insertion (on the order of 200-400 mOhm). This membrane resistance shows that the cells were viable, but unable to generate a response.

From the finding that neuronal stimulation is required to induce the deficits in synaptic activity seen following incubation of cells with exogenous monomeric tau, two mechanisms of pathology were hypothesised. 1) Deficits in synaptic responses were induced by an increased rate of tau aggregation dependent upon neuronal stimulation. These increased number of aggregates may thereby interfere with synaptic function by an unknown mechanism. 2) Deficits in synaptic responses were induced by increased tau aggregation in synapses themselves, or translocation of

aggregated tau into synapses. To determine 1), fluorescence lifetime microscopy with simultaneous optogenetic stimulation of cells was used to measure tau aggregation. To determine 2), immunofluorescence for quantifying the colocalisation of synaptic markers with tau protein were used to compare unstimulated versus stimulated cells.

5.4 Fluorescence lifetime imaging of optogentically stimulated cells treated with exogenous monomeric tau

It was hypothesised that stimulation of cells would increase the rate of tau aggregation. This was based on previous findings *in vivo* (Wu *et al.*, 2016) and the hypothesis that the optogenetic stimulation of cells treated with exogenous tau caused depression of synaptic activity (Figure 59) through an increased rate of tau aggregation. To determine whether optogenetic stimulation increased the rate of tau aggregation, the OptoGenie device was fixed onto the inverted TCSPC-FLIM microscope (Figure 60). This allowed simultaneous optogenetic stimulation and fluorescence lifetime imaging. Cells were incubated with tau for 20 min followed by optogenetic stimulation for 30 min before the fluorescence lifetime of tau protein was measured from 50 min – 2.5 hr. The aggregation of tau over this time period was compared between unstimulated cells versus optogenetically stimulated cells. Figure 60 shows that the optogenetic stimulation of neurons significantly increases the aggregation of tau over the 2.5 hr time-course measured as a decrease in the fluorescence lifetime of tau protein.

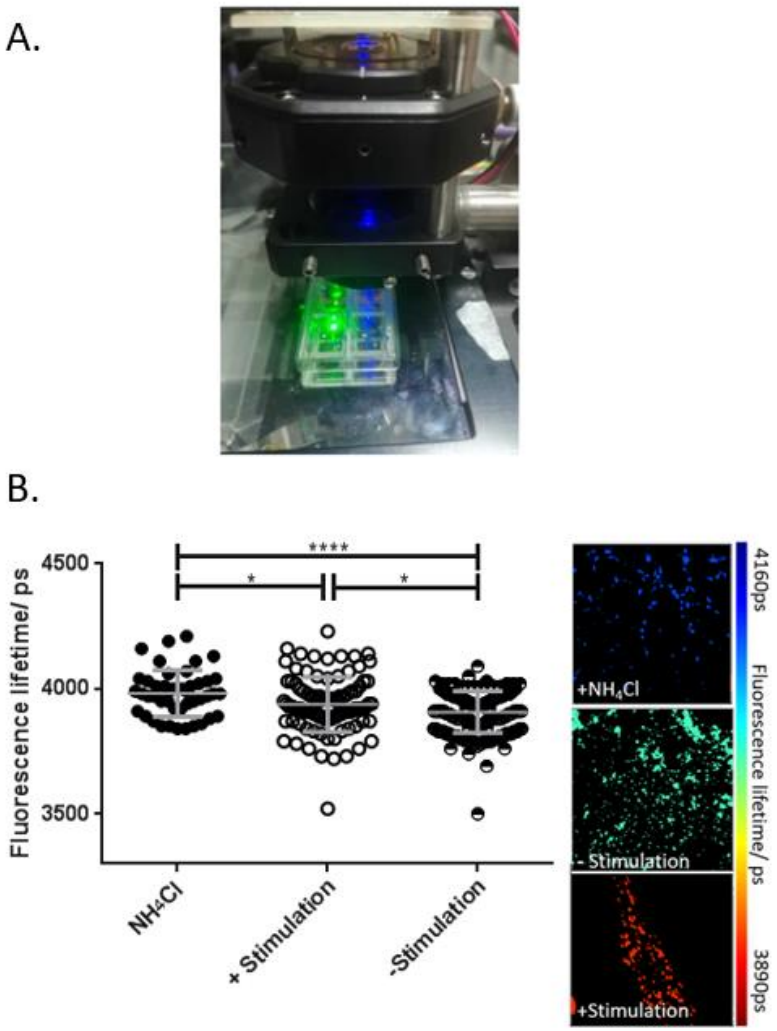

Figure 60. Optogenetic stimulation increases the aggregation of tau protein. A. simultaneous optogenetic stimulation and fluorescence lifetime imaging was achieved by fixing the Optogenie device onto the inverted FLIM microscope. B. Optogenetic stimulation of cells increases the aggregation of tau protein compared to unstimulated cells over 2.5 hr as measured by a decreased fluorescence lifetime of tau protein (one-way analysis of variance (ANOVA); ****$P < 0.0001$; F (2,328) = 12.59). Tukey's multiple comparison P values (NH_4Cl+ tau (A), + stimulation (B), - stimulation (C)): (A-B) *$P = 0.0248$; (B-C) ****$P < 0.0001$; (A-C) **$P = 0.0232$. Experiments were performed from $n = 3$ animals with n > 8 technical repeats per animal. All data points from the repeats with mean values and standard deviation are plotted.

The study was repeated using several methods of chemical stimulation including bicuculline, KCl, and glutamate as a second approach to stimulate cells versus optogenetic stimulation. Chemical stimulation can target specific ion channels to depolarise cells as compared with optogenetic ChR2 stimulation which are non-specifically permeable ion channels that are not inherently found inside of hippocampal neurons.

Initial studies were carried out to replicate the timescale of the experiments using optogenetic stimulation. In these studies, neurons were incubated with tau for 20 min prior to stimulation. Once stimulants were added, cells were incubated for a further 30 min before imaging over 1 hr. No differences were measured between the fluorescence lifetime of tau protein in unstimulated conditions versus conditions using chemical stimulation of neurons (Figure 61).

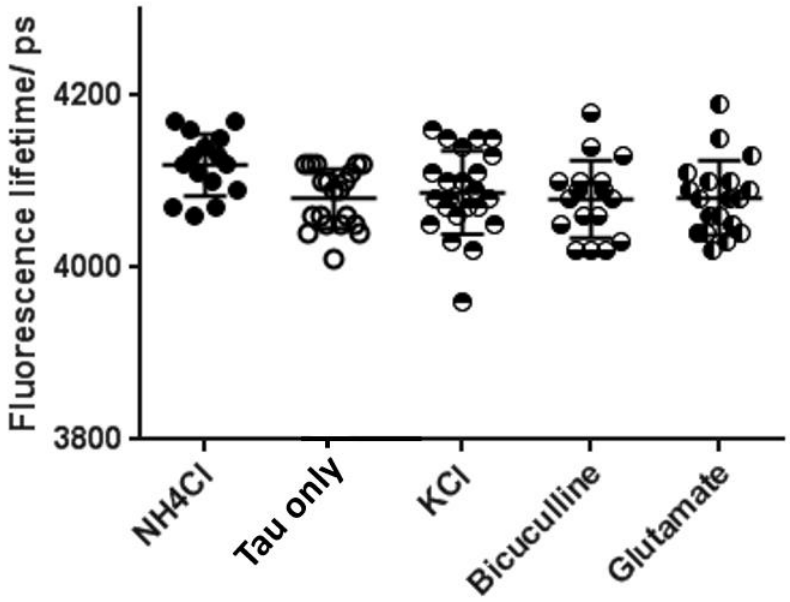

Figure 61. No differences are seen in the fluorescence lifetime of tau protein at 50-110 min between chemical stimulation conditions versus unstimulated or ammonium chloride treated controls (one-way analysis of variance (ANOVA); *P = 0.460; F (4, 89) = 2.530). Tukey's multiple comparison P values (NH_4Cl (A), tau (B), KCl (C), Bicuculline (D), Glutamate (E)): (A-B) not significant (NS) = 0.0628; (A-C) NS = 0.1609; (A-D) NS = 0.666; (A-E) NS = 0.0743; (B-C) NS = 0.9836; (B-D) NS > 0.9999; (B-E) NS > 0.9999; (C-D) NS = 0.9761; (C-E) NS = 0.9886; (D-E) NS > 0.9999. Experiments were performed from n = 3 animals with n > 4 technical repeats per animal. All data points from the repeats with mean values and standard deviation are plotted.

As no differences at the early timepoint were measured between unstimulated cells and stimulation conditions, it was considered that imaging over a longer timescale may be required to detect differences between these conditions. However, a concern was that long incubation with the chemical stimulants may result in ATP depletion and cell death. Therefore, cells were incubated with tau for 3 hr before 30 min incubation with chemical stimulants prior to imaging for 1 hr. Again, no differences were measured between the fluorescence lifetime of tau protein between unstimulated cells and those incubated with chemical stimulants (Figure 62).

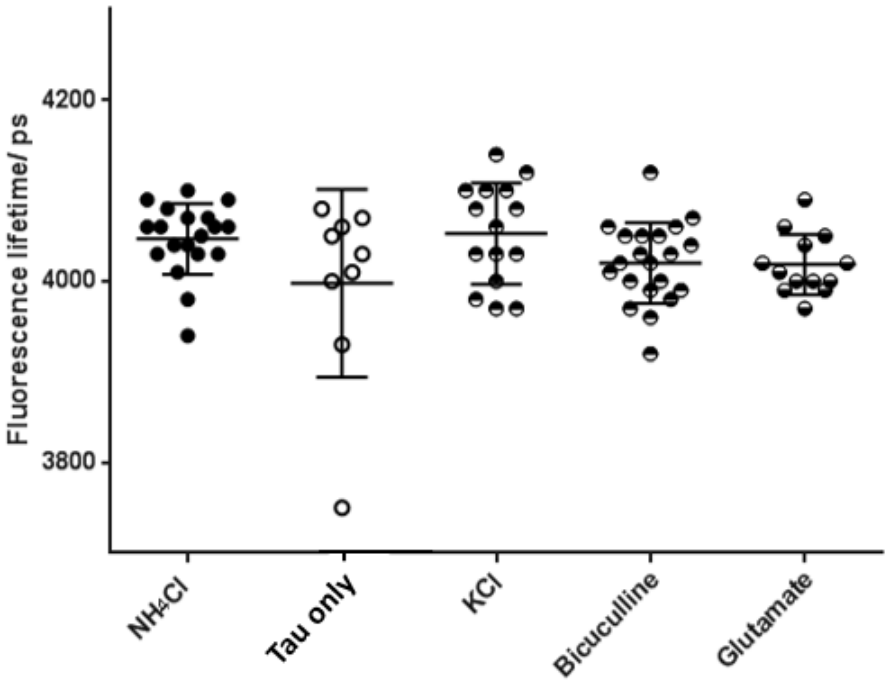

Figure 62. No differences were measured for the fluorescence lifetime of tau protein between stimulation conditions after 3 hr tau incubation and 30-90 min incubation with a chemical stimulant (one-way analysis of variance (ANOVA); NS = 0.717; F (4, 72) = 2.254). Tukey's multiple comparison *P* values (NH_4Cl (A), tau (B), KCl (C), Bicuculline (D), Glutamate (E)): (A-B) not significant (NS) = 0.1749; (A-C) NS = 0.9979; (A-D) NS = 0.5210; (A-E) NS = 0.5911; (B-C) NS = 0.1240; (B-D) NS = 8391; (B-E) NS = 0.9021; (C-D) NS = 0.3873; (C-E) NS = 0.4575; (D-E) NS = > 0.9999. Experiments were performed from *n* = 3 animals with n > 4 technical repeats per animal. All data points from the repeats with mean values and standard deviation are plotted.

Chemical stimulation did not result in any difference to the fluorescence lifetime measurements of tau at 50-110 min or 3.5-4.5 hr. This is different to optogenetic stimulation where the fluorescence lifetime of tau is seen to decrease following stimulation over 2.5 hr. An initial consideration was that at the fluorescence lifetime of tau would become saturated at a certain aggregation state or timepoint. If saturated by aggregation state, if tau further aggregated beyond a specific size the lifetime would not show further decrease. If saturated by timepoint, the majority of monomeric tau would form aggregates by the timepoint measured and no further decrease in lifetime would be seen beyond this. It was considered that this was not likely to be the case, as the lifetime of aggregated tau has been shown to vary by both structure and time. K18 forms of tau versus hTau40 aggregated from low pH or heparin induction all have different fluorescence lifetimes. Over time the lifetime has also been shown to reduce from 8 hr in SH-SY5Y cells measured to be less than aggregated tau inside of neurons (3154 ± 56 ps for hTau40-488), and was shown to further decrease over 64 hr (2779 ± 132 ps for hTau40-488) (Michel *et al.*, 2014). The experiments were repeated at earlier timepoints to prevent an effect of saturation alongside repeating the timescale of the optogenetic stimulation studies. The ability to detect differences in aggregation between optogenetically stimulated versus unstimulated neurons also suggests that the saturation of aggregation was not an explanation for negative results from chemical stimulation studies.

There are several reasons why chemical stimulation may not result in any measured differences of tau aggregation, as determined by its fluorescence lifetime. It is possible that the 30 min chemical treatment before imaging is not long enough to cause substantial effects on aggregation and that an effect may be detected by later measurements. However, it is also possible that neurons are unable to sustain high levels of activity during the full incubation period and therefore the measurements do not accurately portray stimulation conditions. 30 min incubation before imaging was considered a suitable period to allow any effects of stimulation to occur whilst limiting ATP depletion and cell death. Ideally drugs would be washed on and off for ~30 s- 2 min before wash-off and allowing cells recovery time. However, other than the requirement to supply tau in all of the medium steps, it was considered that multiple media replacements may be damaging to primary neuronal cultures, which are sensitive to media changes. This highlights another key difference between optogenetic versus chemical treatment experiments, as it was not possible to temporally control the stimulation of cells when using chemicals or provide specific low- or high- frequency signalling. Although the chemical stimulation of neurons has previously been shown to increase

the rate of tau pathology (Wu *et al.*, 2016), there are several key differences that may explain the negative results from using chemical treatment in this project. Wu et al., (2016) use *in vivo* stimulation via Designer Receptor Exclusively Activated by Designer Drug (DREADDs), which are activated systemically 2 times per day 6-7 hr apart; this allows stimulation over a specific time period before systemic clearance and metabolic recovery of cells before the next stimulation treatment. The timescale of the treatments also greatly varies, as DREADD stimulation was used over 2-6 weeks as compared with 1 treatment over 1.5 hr. However, the timescale of the optogenetic stimulation is also much longer (three times per day, five times per week for four weeks, compared to over 2.5 hr) yet we see an increase in tau aggregation as measured using FLIM (Figure 60). To better understand how neuronal activity of cells correlates with tau aggregation, particularly when using the chemical stimulants over time periods over which their effect on cells is unpredictable, it would be useful to repeat these experiments with cells plated on MEA devices. MEAs could allow simultaneous measurements of fluorescence lifetime with recordings of neuronal activity (Chapter 7).

The stimulation of neurons caused a measurable increase in the concentration of aggregated tau protein during the measured timepoints of 50 min- 2.5 hr (Figure 60). Increased aggregation may arise through one, or both mechanisms of A) Propagation of aggregates between cell networks: As discussed in Wu et al., (2016) increased neuronal activity results in increased propagation and thereby seeding of pathology between neighbouring cells. Our group has shown that as tau aggregates are trafficked from the soma into axons the fluorescence lifetime of the aggregates decreases (Na Yu, Dr. Colin Hockings, Unpublished data). Therefore, it is possible that the increased aggregation measured from optogenetically stimulated cells arises from increased trafficking of aggregates from the soma as opposed (or in combination with) increased tau internalised into the soma or synapses. Experimental or computational measurements have not yet been carried out to calculate how the fluorescence lifetime may relate the decrease in lifetime from many small aggregates versus fewer large aggregates composed of the same overall tau concentration. B) cell intrinsic aggregation: tau internalisation, aggregation and toxicity with the same cell. Increased stimulation would cause an increased rate of bulk endocytosis for recovery of synaptic vesicles. Increased endocytic uptake of tau would result in an increased rate of aggregation from entering low pH environments during synaptic vesicle cycling or lysosomal pathways. Although B) may offer a faster mechanism as compared with A) for forming aggregated

tau, activity-dependent increases in endocytosis are mostly associated with synapses and this may contribute to only a small proportion of tau internalised by cells, though we are yet to provide direct evidence showing that tau endocytosed at synapses forms aggregates.

However, whichever mechanism is responsible for the increased aggregation of tau, it was hypothesised that increased aggregation alone may not result in the dramatic activity-dependent deficits in synaptic activity measured in tau-treated cells (Figure 59). As a significant increase in tau aggregation was measured between unstimulated cells versus ammonium chloride treated cells, an explanation is required for the mechanism through which an even further increase in aggregation is required to cause synaptic dysfunction. It is possible that a threshold concentration is required to cause this pathology, potentially through signalling apoptosis though no obvious signs from morphology or changes to membrane resistance suggest this (though further measures would be required to verify). Alternatively, an increase in aggregate size or species conformation, potentially from increased axonal trafficking in this time period, may be sufficient to produce more toxic species that result in pathology.

Therefore, our first hypothesis was that activity-dependent depression of synaptic transmission of tau-treated cells occurred via a mechanism in which exogenous tau entered into synaptic compartments, and not increased aggregation alone. To determine whether there was an increase of exogenous tau inside of synaptic compartments from neurons that had received optogenetic stimulation, immunofluorescence to quantify the colocalisation of exogenous tau with synaptic markers was carried out.

5.5 Immunofluorescence to determine synaptic colocalisation of exogenous tau in optogentically stimulated cells

[Due to poor breeding of Grik4-Ai32 mice and departmental flooding the following data consists of N=2 data for PSD95 results and N=1 for bassoon results. Any claims mentioned in these sections are therefore trends that cannot be confirmed until further experimental repeats.]

Following fluorescence lifetime measurements over 2.5 hr either in unstimulated or optogenetically stimulated conditions, cells were washed with trypsin to remove fluorescently-

labelled tau protein bound to cell membrane. Cells were immediately fixed for immunofluorescence to detect pre-synaptic compartments (bassoon) or post-synaptic compartments (PSD95). Following optimisation of immunofluorescence (IF), quantitative analysis was carried out to determine the extent of colocalisation between synaptic compartments with fluorescently labelled tau protein taken into cells. As a first step, comparisons were made between different software packages and measures of colocalisation such as Mander's coefficient, Mander's coefficient with thresholding, and object-based distance colocalisation. Two-colour fluorescent beads were used as a calibration sample to measure random, chromatically aberrated, or chromatically corrected samples; this was repeated for a tau sample image as a measure of variation that may arise from a real IF sample (for full results see Appendix A.4). The most accurate and reproducible measures of colocalisation using the calibration and tau sample were gained by JACoP (Just Another Colocalization Plugin ; Bolte & Cordlières, 2006) with distance based (object overlap) colocalisation. Values used from calibration measurements to determine 'no colocalisation' with 'perfect colocalisation' for statistical analysis of the real datasets can be seen in Appendix A.5

Figure 63 shows immunofluorescence images of neurons treated with fluorescently-labelled exogenous monomeric tau protein (cyan) in the presence or absence of optogenetic stimulation. Antibodies against bassoon or PSD95 were used for the detection of pre- or post-synaptic compartments, respectively (magenta). Although the results require more experimental repeats before analysis can be performed, preliminary data show a trend towards increased colocalisation of synaptic markers PSD95 and bassoon with tau protein (white arrowheads). Once all datasets have been gained, each condition can be analysed as compared with 'no colocalisation' and 'perfect colocalisation' calibration sets to determine the significance of the overlap between synaptic markers with tau protein.

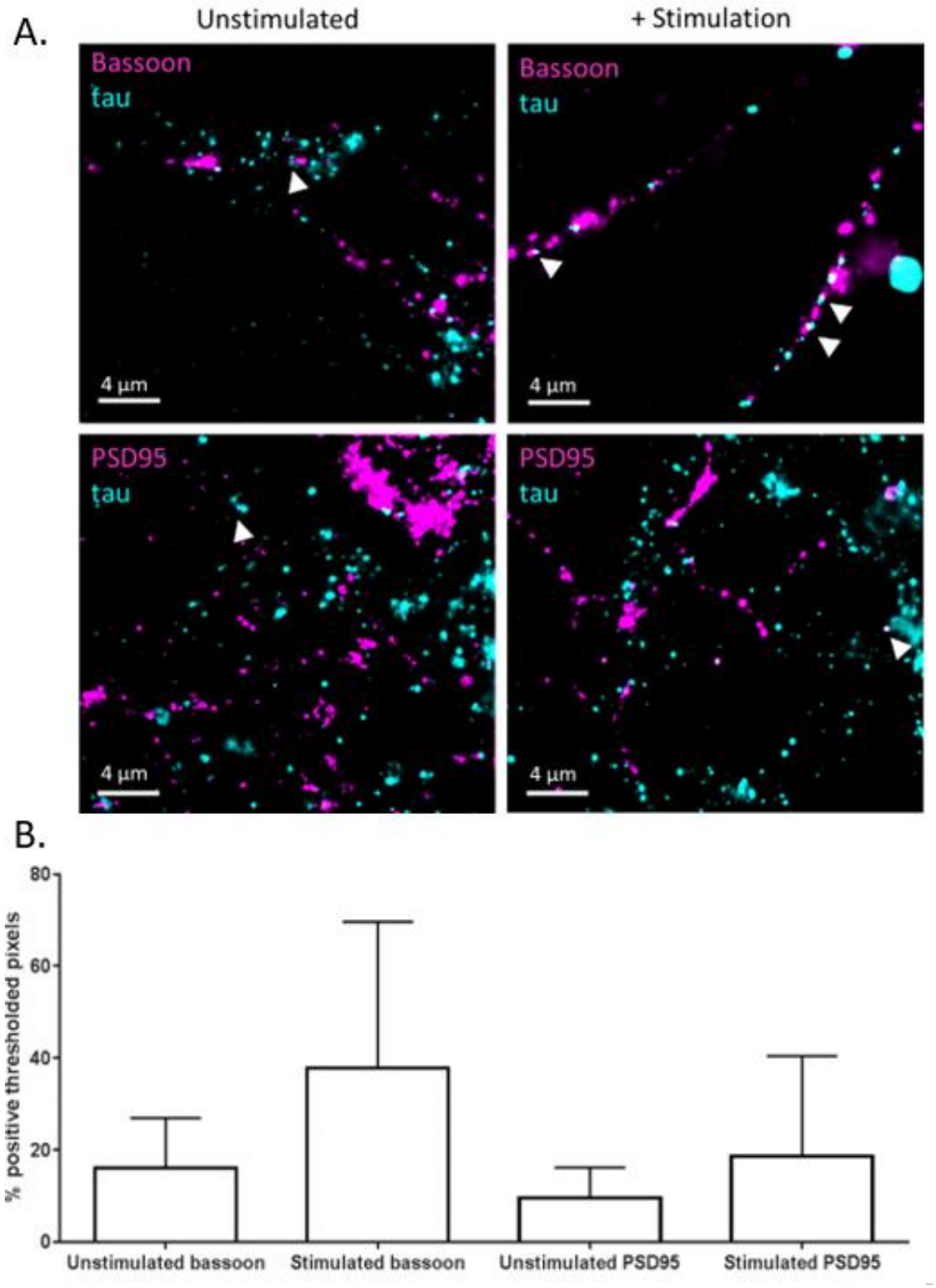

Figure 63. Colocalisation of exogenous tau with synaptic markers. A. Immunofluorescence showing pre-synaptic (bassoon) or post-synaptic (PSD95) compartments with internalised tau protein (white arrowheads). B. Quantification of the colocalisation between synaptic compartments with internalised monomeric tau protein. Data are preliminary (N=1 bassoon, N=2 PSD95) and therefore statistical analysis has not been carried out. Data show mean values with standard deviation.

5.6 Chapter 5 Discussion

A novel optogenetic stimulation device has been designed and implemented. The device consists of a laser diode with a variable resistor to adjust the intensity, and an Arduino Uno to control the stimulation frequency. The development of OptoGenie was based on the 3 aims for an effective optogenetic stimulation device. Aims included (1) Accessible: inexpensive and easy to assemble by researchers across all disciplines to build from commercially available components, including many that are common to laser laboratories. This target was successfully achieved by using low-cost commercial components combined with many structural parts that would be readily available in an optics lab. The most expensive component consists of the posts and base used for structurally supporting the laser diode head. These components can alternatively be replaced by similar parts that are more accessible to researchers as they are not directly necessary for the function of optogenetic stimulation. (2) Portable: flexible to use between incubators, electrophysiology rigs and optical microscopes, and allowing the device can be passed between collaborators at multiple departments. We achieved portability by combining small and robust electronic components including an Arduino and variable resistor. No optical fibre coupling, or fragile components were used and the most expensive items were metal posts or clamps which are unlikely to be easily damaged during everyday use and transport. Alongside this, the battery adaptor cable allows the device to be powered in any location required without the need for power sockets. (3) Adaptable: accommodating to researchers' needs so that alternative laser diode wavelengths, stimulation area or stimulation frequency can be used. The adaptability of the device is thanks to the simple design. Components such as the laser diode can be easily switched depending on the wavelength requirements. Other features can also be added including lenses to make a smaller focal spot area with the required intensity for excitation of a smaller population of cells beyond the minimum size of the adjustable iris. In the future, additions such as a Raspberry Pi can be combined with OptoGenie for the ability to monitor and control the device from afar. A USB power bank can also be combined with the device to offer a rechargeable power source to decrease long term costs and environmental impact.

These three aspects of the OptoGenie have allowed the integration of projects investigating the activity-dependence of tau pathology through stimulating cells in a cell incubator for longer studies requiring incubation of tau or long-term stimulation; on optogenetic rigs to gain cell recordings

and test the stimulation intensity is suitable for the ChR2 expression between cultures or animal lines; or on optical microscopes for simultaneous imaging, in this project for the simultaneous stimulation and measurement of the fluorescence lifetime of tau protein on an inverted FLIM microscope. In attempt to make the device low-cost and portable, a 450 nm laser was selected for use as finding a laser diode capable of achieving the power necessary, small enough to be portable and inexpensive enough to be accessible to all researcher was not possible for 470 nm based on commercial options available. The results have shown that the 450 nm laser diode is capable of stimulating channelrhodopsin-2. The datasheet suggests the maximum wavelength of the laser diode is 460 nm, however at the temperature used for our experiments, the wavelength was measured to be 458 nm. Figure 64 shows that although peak response of channelrhodopsin-2 occurs at ~470 nm, a smaller yet sufficient current is still measured between the 450-460 nm range possible from our laser diode (Lin et al., 2009). Therefore, although future devices could be developed using a laser diode with 470 nm light, which may require different intensity of optogenetic stimulation, we have shown that this is not necessary, and stimulation is possible using the laser diode in our study.

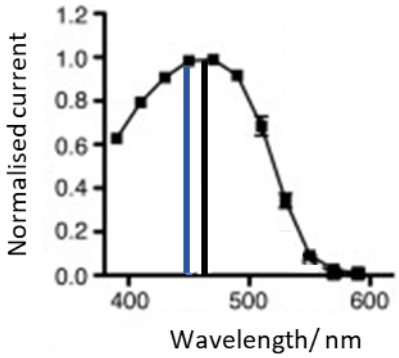

Figure 64. A curve showing the current produced by ChR2 between activated with light between 400-600 nm. The peak current is produced by blue light of ~470 nm (black bar) however channel activation with 450nm light (blue line) also produces a relatively large current. Adapted from: Lin et al., 2009.

A consideration when using the device is that following repeated use of the 9 V battery, the power that is measured from the laser diode decreases at different rates. For the first measurement, a recording was taken over 2.5 hr using the laser diode at maximum power of ~ 45 mW to show the maximum percentage drop that would occur for the specific stimulation pulse used. As a second

measurement, a recording was made using the laser diode at 8.7 mW power as is used for cell stimulation, to test whether the power decreased at a different rate on continual battery use. This time a 33 %, as compared with 12.9 %, decrease in power occurred over the 2.5 hr (Figure 65). It is therefore an important consideration when using a battery to power OptoGenie that the starting power must be set high enough to stimulate cells by the end of the experiment. This power clearly depends on the charge of the battery at the start of the experiment, which can be determined using a multimeter if a new battery is not used. Additionally, future iterations may include a USB power bank to supply a more steady source of power since most power banks have electronic regulators, which help protect the device from surges as they are charging.

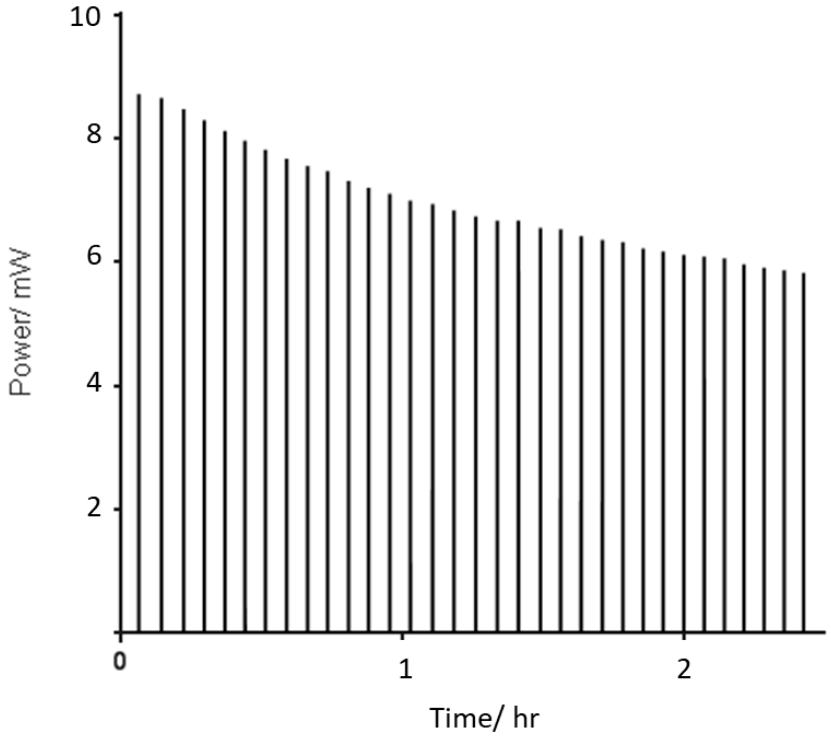

Figure 65. A 2.5 hr power measurement from the laser diode using a 9 V battery with a starting power of 8.7 mW. Reusing a battery that previously powered a 2.5 hr recording resulted in a 33 % drop in power for the 2nd recording. This is > 2x the power decrease as compared to the 1st recording that started at 45 mW and decreased by 12.9 % over 2.5 hr.

Using Optogenie for optogenetic stimulation in an incubator, followed by whole-cell patch-clamp recordings, it was found that cells treated with exogenous monomeric tau and optogenetic

stimulation for 2.5 hr showed a depression of synaptic transmission following stimulation with an external electrode (Figure 59). The combination of tau protein and stimulation therefore greatly diminishes the amplitude of an evoked response from these neurons. It was predicted that optogenetic stimulation would increase the rate of tau aggregation based on a previous study showing that stimulation increases the propagation of tau pathology between neurons (Wu *et al.*, 2016). Similarly, using simultaneous optogenetic stimulation and fluorescence lifetime imaging of tau as a sensor for its aggregation state, we were able to show an increase in aggregation between unstimulated and stimulated neurons treated with exogenous monomeric tau protein.

It is worth noting the key differences between previously published work investigating the role of neuronal activity in tau pathology by Wu et al., (2016) with this study. Previous work used the rTg4510 mice (Ramsden *et al.*, 2005; SantaCruz *et al.*, 2005) that express 13-fold higher level than endogenous mouse tau and in mutant P301L form; this study uses Grik4-Ai32 mice expressing wildtype tau only. The timescales of the work are also very different, in part because Wu et al., (2016) use an *in vivo* model that displays mild pathology at 6 weeks but over 18 months to become apparent. Their studies investigating optogenetic stimulation on tau pathology are over a 20 day period, and chemogenetic studies with DREADDs over 2-6 weeks. This work is based *in vitro* using hippocampal cell cultures, where tau aggregation from 30-50 min has been shown. This early detection may be due to the method of TCSPC-FLIM as opposed to assays such as X-34 (or ThT*)* that bind more aggregated beta-sheet structures than oligomers and smaller fibrils. Although they state that they do not experience an accumulation of exogenous monomeric tau inside of cells, they also suggest that it is possible, especially for neurons from the rTg4510 line, that low molecular weight misfolded tau oligomers were formed in the cultures but were not detectable by morphology, dyes used such as X-34. The rTg4510 model shows tau multimers (140 and 170 kDa), suggestive of oligomeric aggregates, accumulating early in this mouse model and correlate better with memory deficits as compared with neurofibrillary tangles (Berger *et al.*, 2007). A benefit of the *in vivo* system and longer timescale is the ability to show the propagation of pathology through synaptically connected networks. In our culture model, without using microfluidic devices, we are unable to show directional propagation of uptake of tau between cells or a specific starting location that seeds this pathology. The later stage pathology is also able to show atrophy of brain areas whereas in our early timepoint model we do not see evident signs of cell death though only morphology and membrane resistance of cells are used as measures as opposed to thorough

live/dead assays. Although atrophy in the brain regions of rTg4510 overexpressing mutant tau mice is shown, no behavioural studies were carried out to link this to cognitive deficits seen in Alzheimer's disease. Wu et al., (2016) show that the activity-dependent propagation of tau pathology was neurotoxic, as the increased pathology correlated with enhanced hippocampal cell layer atrophy. The sole measure of pathology is beta-sheet-positive tau aggregates inside of cells and crude damage to the hippocampal formation. No further investigation is carried out to show whether this activity-dependent propagation of tau causes physiological impairment or behavioural deficits, even though studies have previously shown this model displays cognitive deficits correlating with early tau aggregates (Berger *et al.*, 2007). It would therefore be of interest to determine whether in rTg4510 mice given opto- or chemo-genetic stimulation, memory deficits occur earlier, preceding hippocampal cell layer atrophy. As previously discussed, experimental or computational measurements have not yet been carried out to calculate how the fluorescence lifetime may relate the decrease in lifetime from many small aggregates versus fewer large aggregates when composed of the same overall tau concentration. This is an interesting question however, due to the thought that larger, insoluble forms of tau may be neuroprotective as compared with soluble structures shown to exert toxicity. Whether stimulation favours the formation of more, soluble structures and/or their conversion into larger structures, potentially through trafficking may explain some of the activity-dependent pathogenesis of tau. Based on the Wu et al., (2016) an increase in higher order aggregates that accumulate in recipients more readily are seen, however a proportional increase in lower order aggregates may also occur. From our studies, it was not possible to specify whether there is an overall increase in aggregation or of a specific form that leads to the synaptic deficits shown. Although working at an *in vitro* level, our project is the first study to clearly show a pathway between the formation of aggregated tau and a physiological correlate for memory impairment that may link tau pathology with the symptoms seen in Alzheimer's disease.

Several mechanisms are considered for the activity-dependent synaptic deficits that we have shown to occur in tau treated neurons following 2.5 hr of optogenetic stimulation. It is difficult to justify how an increase in aggregation alone may result in the differences of evoked responses measured for the tau treated versus stimulated and tau treated conditions. As the tau treated cells show significantly more aggregated tau as compared with ammonium chloride treated cells, an explanation is required as to why these cells are able to generate an evoked response as compared

with the stimulated tau-treated condition. As discussed, it is possible that there is a threshold of tau aggregation that elicits this pathological response, and below this, cells are able to maintain their physiological function. It is possible that some increased aggregation occurs from activity-dependent uptake and aggregation inside of synaptic compartments arising from bulk endocytosis and synaptic vesicle regeneration at low pH. Alternatively, the decreased fluorescence lifetime may measure an increase in larger, or more toxic conformations of tau aggregates generated from stimulation; for example, the fluorescence lifetime of tau has been shown to further decrease following transport from the soma along microtubules and into neighbouring cells (Na Yu, Dr. Colin Hockings, Unpublished data). An activity-dependent transportation and propagation of tau may therefore be sufficient to cause the pathological synaptic deficits from stimulated tau-treated cells. It was also hypothesised that this pathway would result in translocation of tau aggregated into synaptic compartments. Therefore, whether tau protein entered synapses directly from the extracellular medium via an activity-dependent increase of endocytosis, or was translocated to synapses following stimulation, it would be expected that tau would colocalise with synaptic compartments. Due to the anterograde pre- to post- synaptic directionality in networks of neurons, it could be predicted that stimulation may affect the uptake and transport of cell aggregates from the pre-synaptic to the post-synaptic cell. This would make sense for the trend of increased tau in pre-synaptic versus post-synaptic compartments and explain an activity-dependent increase in pathology if aggregated are transferred synaptically. If the majority of aggregates are transferred in an anterograde fashion this would also follow the directionality of pathology seen during Braak stage tau pathology (Braak and Braak, 1991).

We have yet to show evidence that tau protein is directly taken into synaptic compartments from the extracellular medium either in the presence or absence of stimulation. Alongside this, although this study shows a trend towards colocalisation of synaptic compartments with tau protein following stimulation, no study has yet determined whether this tau is in monomeric or aggregated form. Previous work has shown that monomeric mutant or phosphorylated tau inside of the pre-synaptic compartment is sufficient to cause dysfunction but predicts similar could be true of small tau multimers (Zhou *et al.*, 2017; McInnes *et al.*, 2018). To determine whether aggregated tau is responsible for the pathological phenotype we have shown, the experiments could be repeated in the presence of ammonium chloride solution to significantly decrease the aggregation of tau. This could also determine whether neuronal activity is sufficient to cause pathology or whether low pH

endolysosomal compartments are required, as we would predict. Further studies to understand tau aggregation at pre-synaptic compartments will be carried out using the microfluidic devices designed in Chapter 6. Inside of these devices, cells can be plated inside of a single compartment with their axons growing into the 2nd fluidically isolated compartment. Fluidic isolation between the cell bodies and dendrites, versus the pre-synaptic terminals will allow only their pre-synaptic compartments to be treated with tau protein to measure uptake and aggregation status in unstimulated versus stimulated neurons. These studies will help determine whether pre-synaptic compartments are sufficient for the uptake of tau, and the aggregation state of any internalised tau can be measured using FLIM. Alongside this by optogenetic stimulation of the compartment containing cell bodies, we can determine whether internalisation and aggregation of tau can activity-dependent from an increased rate of endocytosis or solely by trafficking from other cell regions (Figure 66, a). If tau is taken up directly by synapses as opposed to translocation from the soma, these studies inside of microfluidic devices will be useful to determine whether monomeric tau can be aggregated inside of synaptic compartments (Figure 66, b_1), or is taken up as aggregates released from other cell regions (Figure 66, c_1).

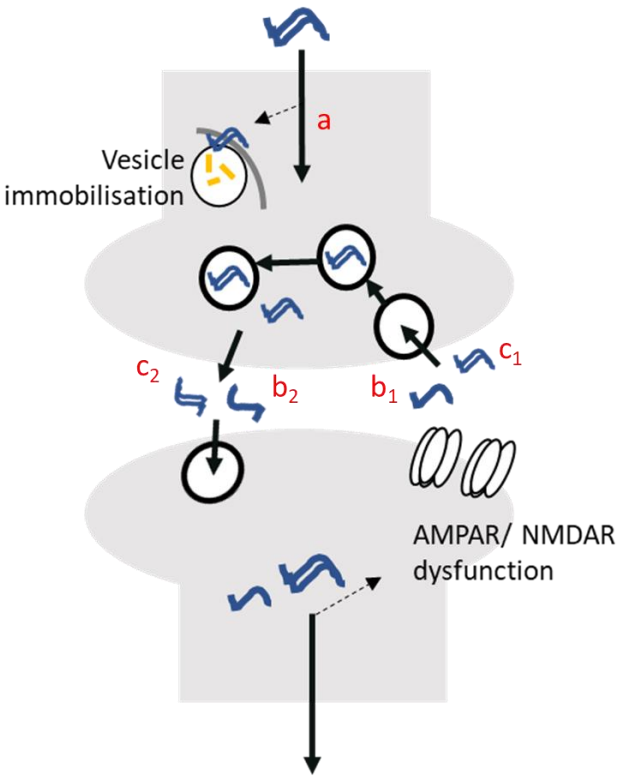

Figure 66. A schematic displaying the possible ways that exogenous tau could enter the synaptic compartments. (a) Tau could be translocated from distal regions in aggregated form. (b_1, b_2) tau could enter synaptic compartments in monomeric form and aggregate inside of compartments at low pH, or alternatively be initially transported in monomeric form. (c_1,c_2) aggregates could be internalised directly by endocytosis at the synaptic compartments. Possible synaptic mechanisms that could either experience direct or indirect tau-pathology, such as vesicle immobilisation or receptor dysfunction, to result in a depression of synaptic transmission are also shown.

Understanding the localisation of tau aggregates inside of neurons may clarify the pathological mechanism of the activity-dependent depression of synaptic transmission of tau treated cells. Tau aggregates appear mostly in the soma, at least in the earlier stages of formation (Michel *et al.*, 2014), though can be trafficked along mircotubules to distal regions. During stages of aggregation and trafficking it is possible that these aggregates cause disruption without directly entering synapses such as block microtubule transport and prevent exchange between synapses and somatic organelles. The inhibition of transport will also inhibit the complex pathway of AMPARs from the cell body along cytoskeletal structures for regulating excitatory transmission (van der Sluijs, 2011). Due to tau aggregates following the progression of the endolysosomal pathway, alongside physically blocking transport, aggregates that cannot be degraded may change the dynamics of

available endosomes. This will affect the membrane availability for other processes including endocytosis-exocytosis balance, and pathways requiring endosomal transport such as vesicle trafficking from the ER and protein maturation/modification/degradation. One suggestion has been that tau aggregates may result in a retraction of the endoplasmic reticulum thereby starving synapses of proteins required for protein turnover and plasticity (in conversation, Dr. Gabi Kaminki).

Though only a trend has been established between colocalisation of synaptic compartments with tau protein from preliminary studies (n = 1, bassoon, n = 2 PSD95), if increased tau entry into synaptic compartments results in synaptic deficits, this could occur through several mechanisms. The mechanism may be induced from the pre- or post-synaptic side, or alternatively both. A pre-synaptic mechanism would prevent the propagation of a response through failure to signal the release of synaptic vesicles, or regenerate their population. These could arise from the inability to accumulate Ca^{2+} in the axonal terminal, a reduction in the vesicles pool, or possibly, alterations in presynaptic mGluR receptors or an imbalance of inhibition (Polydoro *et al.*, 2014). A post-synaptic mechanism would, as compared with stimulated controls showing increased potentiation, prevent the generation of a response with increased conductance through either impaired channel function by failure of channel or subunit trafficking insertion and stabilisation, or specific phosphorylation of subunits.

Previous studies have investigated pathological roles of tau at the pre- or postsynaptic compartments. Tau has previously been found in pre- and post- synaptic compartments of human controls, however occurs in increased ubiquitinated and phosphorylated forms in AD patients (Tai *et al.*, 2012). Our results showing an activity-dependent depression in synaptic transmission in tau treated neurons correspond more similarly to effects showing a decrease in release probability of synaptic vesicles (Polydoro et al., 2009; Zhou et al., 2017), compared with the converse which has also been suggested (Polydoro *et al.*, 2014). In the pre-synaptic compartment, mutant (R406W, V337M or P301L) or phosphorylated tau is capable of immobilising synaptic vesicles by preventing their release from F-actin. Tau is capable of this immobilisation through directly binding synaptic vesicle protein synaptogyrin-3, acting like a vesicle clustering molecule similar to synapsins. It has also been proposed that tau binding to synaptogyrin-3 may also have an unknown physiological role (Zhou *et al.*, 2017; McInnes *et al.*, 2018). Deficits from this

dysfunction are not seen from low frequency (0.2 Hz) stimulation that employ the recycling pool of vesicles for release but following high frequency (10 Hz) stimulation requiring the reserve population of vesicles. Under high frequency stimulation, normal levels of release cannot be maintained (Zhou *et al.*, 2017). This work showed that this pathology only occurred with mutant FTD-17 or hyperphosphorylated tau as opposed to wildtype tau, which showed less synaptic colocalisation. However, it was also suggested that the formation of dimers and multimers could also add to the ability of tau to immobilise vesicles. This was in part based on a comparison with α-synuclein, which has been shown to have a similar pathogenic method of immobilising synaptic vesicles by aggregation (Diao *et al.*, 2013; Wang *et al.*, 2014; Zhou *et al.*, 2017). Pre-synaptic oligomeric amyloid-beta$_{1-42}$ is capable of inhibiting CK2 activation and the rapid clathrin-independent endocytosis pathway, resulting in reduction of synaptic vesicle pools and transmitter release. Put together, it is possible that the toxic combination of amyloid-beta with tau is through the inability to compensate for this disruption to rapid endocytosis to replenish this synaptic vesicle pool (Moreno *et al.*, 2009; Ittner *et al.*, 2010). The ability for tau's suppression on neuronal activity to dominate amyloid-beta's hyperexcitability has been previously shown (Busche *et al.*, 2019). During our experiments, depression of synaptic transmission is seen following repeated high frequency stimulation (33 Hz). If this pathology is acting through a pre-synaptic mechanism it may be through a stage of the signaling and release of synaptic vesicles. Speculatively, it is therefore possible that activity-dependent synaptic deficits we see from tau-treated neurons occur from entry of aggregated tau into synapses resulting in the immobilisation of SVs. This could be tested by paired-pulse ratio measurements and super-resolution microscopy to determine the colocalisation of exogenous tau with SV markers such as synaptogyrin-3.

Postsynaptic roles in tau pathophysiology have also been shown. Often this appears in pathways related to AMPAR or NMDAR localisation, trafficking or functioning (Hoover *et al.*, 2010; Ittner *et al.*, 2010; Warmus *et al.*, 2014; Decker *et al.*, 2016; Miyamoto *et al.*, 2017; Suzuki and Kimura, 2017). In their study using rTgP301L mice, Hoover et al., (2010) suggested that their electrophysiological and immunocytochemical results showed that tau mutation or hyperphosphorylation impaired trafficking or anchoring of AMPARs and NMDARs. Multiple indirect mechanisms of NMDAR or AMPAR-dependent impairment have been shown through changes to import of Fyn kinase, PSD95, and KIdney/BRAin (KIBRA) proteins into the post-synaptic compartment (Ittner *et al.*, 2010; Warmus *et al.*, 2014; Tracy *et al.*, 2016). KIBRA has

been associated with late onset Alzheimer's disease (Corneveaux *et al.*, 2010). KIBRA knockdown results in an increase of AMPAR recycling following NMMDAR internalisation, and is thought to regulate trafficking of GluR2-containing AMPARs (Makuch *et al.*, 2011). Acetylated forms of tau seen in AD brain (K274 and K281) are able to prevent the recruitment of KIBRA into post-synaptic compartments to promote memory loss (Tracy *et al.*, 2016). Loss of tau also prevented postsynaptic targeting of Fyn kinase, which is capable of phosphorylating NMDARs to stabilise them to PSD95 (Nakazawa *et al.*, 2001). In hT-337M mice (express human tau V-337M FTD genetic mutation; McMillan et al., 2008) show impaired synaptic localisation of glutamate receptors themselves with increased somatic location but reduced import into synaptosomal fractions. These mice also showed NMDAR hypofunction, which upon rescue was able to restore behavioural abnormalities (Warmus *et al.*, 2014). Reduced post-synaptic glutamate receptor localisation was assumed to a depletion of PSD95 in the post-synaptic compartment, resulting in smaller postsynaptic densities following a reduction or mutation of tau (Nakazawa *et al.*, 2001; Warmus *et al.*, 2014). Due to coordinating structures such as Fyn-PSD95 interaction and forming dendritic nanoclusters of Fyn kinase, direct roles for tau as a postsynaptic scaffold protein have been suggested (Ittner & Götz, 2011; Padmanabhan et al., 2019). It is therefore possible that the prevention of wildtype tau functioning due to pathogenic tau states may cause impairment of postsynaptic activity. Further studies are required to understand the role of post-synaptic dysfunction to our findings. To understand the contribution of NMDARs to our findings, inhibitor AP5 will be used to block these channels during optogenetic stimulation. NMDA/AMPA ratios will also be measured in stimulated and unstimulated cells to determine whether these are affected.

Putting these studies together, tau may mediate activity-dependent pathology at both the pre- and post-synaptic compartment. If tau has similar structural or vesicle tethering roles at the pre- and post- synaptic compartments, potentially mediated for import, stabilisation, or cycling via actin-mediated endosomal receptor sorting (van der Sluijs and Hoogenraad, 2011; Tracy *et al.*, 2016; McInnes *et al.*, 2018), these could both see disruption in both synaptic compartments as pathology progresses. Many of the pathways that may be targeted by tau pathology are activity-dependent and occur pre-synaptically to specify the release machinery or post-synaptically to specify the receptor machinery to maintain learning and memory mechanisms throughout lifetime (Südhof, 2018). Due to the anterograde transport of tau between cells, it would be logical that pre-synaptic compartments would receive and transfer pathological species and likely express pathological

phenotypes in the first instance. Post-synaptic impairment may alternatively feedforward from loss of functional input arising from tau-dependent pre-synaptic dysfunction. Using our *in vitro* model, without the use of microfluidic devices to define unidirectionality, this transfer of pathology would be difficult to prove as aggregates may be taken up post-synaptically from the cell medium without direct transfer from the pre-synaptic compartment of a connecting neuron.

Understanding the activity-dependence of tau pathology may also elucidate physiological roles that tau could facilitate in synaptic compartments. As shown in Figure 9 (Section 1.5.3.) tau has been found capable of binding to a number of proteins with roles associated with clathrin-mediated endocytosis. It is feasible that tau acts as either a tethering protein between vesicles (similarly to a synapsin as shown to occur, at least in pathological conditions (McInnes *et al.*, 2018)) with microtubules, or actin-mediated mechanisms for either supplying, stabilising, or transporting components required for plasticity.

As next steps, experiments were designed to better understand the mechanism through which activity-dependent synaptic impairment may occur to tau-treated neurons, specifically whether there is a pre- or post- synaptic deficit in the first instance. One approach would be glutamate uncaging to stimulate specific cells from which intracellular recording could measure the post-synaptic response. However due to the limited availability of the resources to perform uncaging experiments, an alternative experiment was designed. Microfluidic culture chips that allow paired recordings of cells whilst maintaining fluidic isolation of tau could be used to distinguish between pre- and post- synaptic impairment. Alongside these recordings, microfluidic devices can help isolate pre-synaptic protrusions to understand tau uptake and aggregation mechanisms and its activity-dependent role in the depression of synaptic transmission.

CHAPTER 6

6.1 The design of microfluidic devices for patch-clamp electrophysiology

Several prototypes were made in the attempt to develop a microfluidic chip that could be used for patch-clamp electrophysiology. Design requirements included: access to cell bodies for patch-clamp insertion; geometry capable of allowing by patch-pipettes entry into cells at the angle determined by the manipulator whilst remaining small enough to fit within the patch-clamp stage; thin enough to fit within working distance of the objective; capable of maintaining fluidic isolation; limited evaporation; repeatable length of microchannels.

Initial designs included the use of one-layer master mould with 4 µm high x 10 µm width axonal microchannels. Cell compartments to allow access to cell bodies could be cut or punched out from PDMS at designs locations (Figure 67 (1a, b)) or at preferred distances (Figure 67 (2a)).

One-layer master-mould designs were found to be unfunctional due to hydrophobic, air-blocked microchannels. Both one-layer designs resulted in compartments that were unable to exchange medium as the hydrophobic microchannels were unable to fill with solution (Figure 68).

A two-layer master mould design was tested in an attempt to fabricate culture chips with microchannels that were not blocked by air, such that they allowed cell medium to enter and axonal growth. Commercial Xona (Xona Microfluidics) devices are a two-layer design that have different microchannel and cell compartment heights. These devices readily fill with cell medium following plasma bonding to glass coverslips; it was hypothesised that a two-layer design may reduce air blocking of the channels by preventing channel collapse during punching or aiding capillary action.

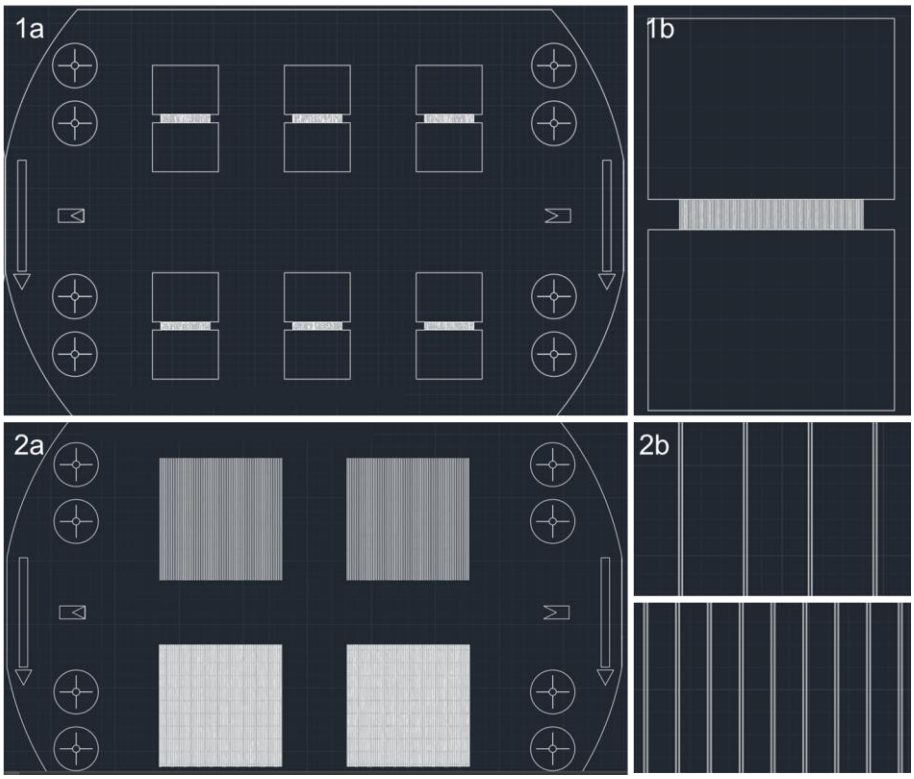

Figure 67. Initial prototypes of microfluidic chips for patch-clamp electrophysiology were 1-layer master-mould designs. (1a) A mask design for the 1-layer device featuring 900 µm length x 4 µm height x 10 µm width microchannels alongside 2 compartments to be punched out to access cell bodies. (2a) one-layer 4 µm height x 10 µm width microchannels spaced (2b, top) 200 µm or (2b, bottom) 100 µm apart. Compartments could be cut or punched out from channels at desired locations accordingly.

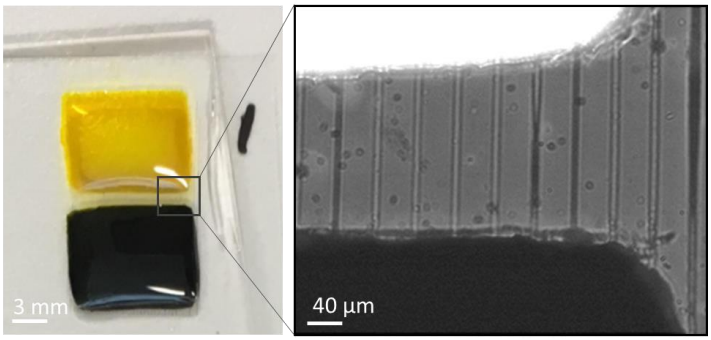

Figure 68. The initial prototype for the microfluidic cell culture chip using a one-layer master-mould. The device resulted in microchannels that were blocked by air either through collapse of the microchannel junctions at the cutting points, or unoptimised plasma treating preventing the channels from becoming hydrophilic. This method

therefore prevented the flow of solution between compartments. (Left) compartments filled with equal volumes of dye did not mix following 24 hr.

Devices were therefore designed as two-layer master-moulds (Figure 69 (a)) that allowed for two different feature heights, resulting in microchannels of 4 µm height but with cell compartments of 100 µm height. The two-layer devices did not block with air, allowing cell medium to enter such that axons could grow between compartments (Figure 69 (c,d)). The chip geometry ensured that it was small enough to fit onto the patch-clamp rig stage and that the PDMS did not block the angle of access to cells by the patch-clamp electrodes (Figure 69 (b)). The microchannels length was designed to be 450 µm, which remained consistent between devices due to the two-layer design and punch method to remove PDMS at the cell compartments.

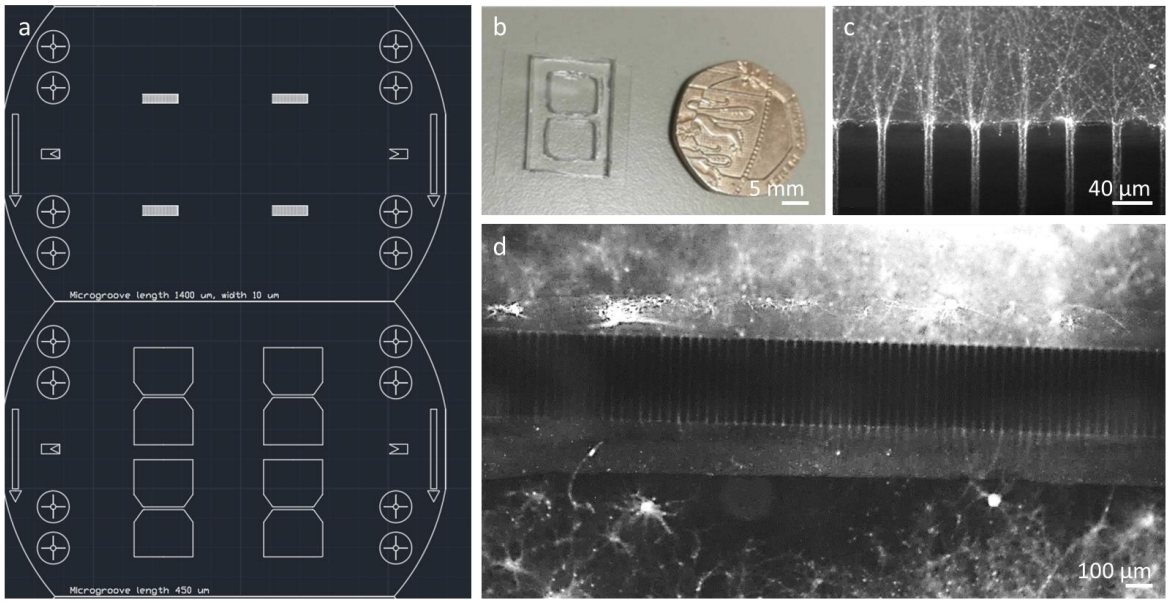

Figure 69. The final two-layer chip design for patch-clamp electrophysiology. (a) The mask design with the 2nd layer compartment resulting in microchannels of 450 µm. (b) The final chip design, roughly the size of a 20 pence coin, fits on the patch-clamp rig stage and allows an angle for patch pipette to access the cell compartment. (c and d) axons grow through microchannels to connect cell bodies in each compartment, as shown by actin innumofluorescence.

A punch was designed to remove the PDMS from cell compartments so that neurons could be plated and accessed by the patch-pipette. The punch featured two (8 mm x 6 mm) rectangular compartments spaced 900 µm apart (Figure 70). The 900 µm spacing meant aligning of the compartments on either side of the microchannels could be done by eye without cutting into the microchannels. The 900 µm spacing resulted in a small overhang of the PDMS at each side of the microchannels of ~175 µm which prevented direct access to cells under this layer, but kept the length of the channels reproducible.

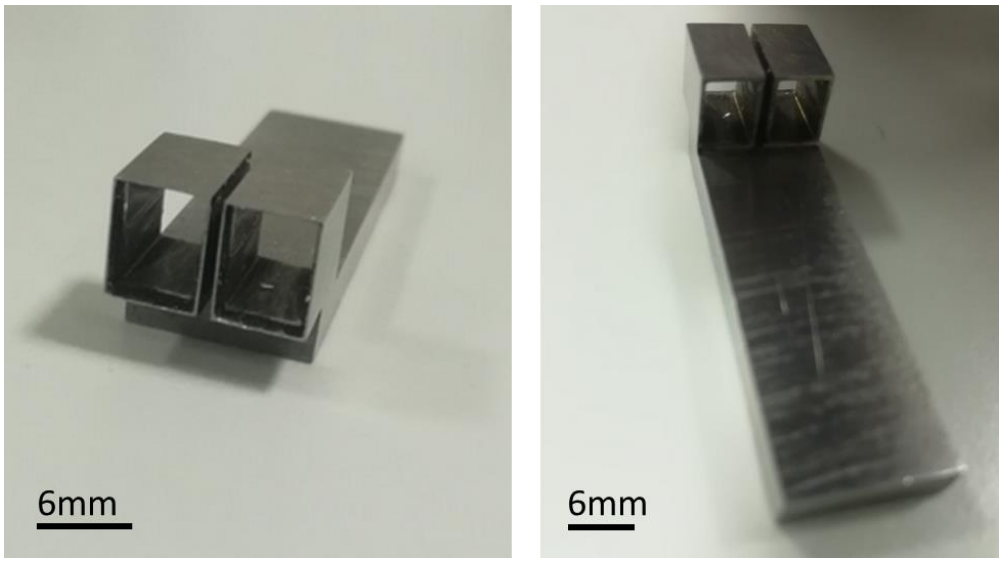

Figure 70. A metal punch that can cut PDMS compartments on either side of the 900 µm channel spacing. A novel punch method based on a biopsy punch allows reproducible cutting as compared with cutting by scalpel. Punch fabrication by Alistair Ross at the Department of Engineering.

Tests were carried out to ensure the cell compartments maintained fluidic isolation for the duration of the experiments for which they would be used, which was considered to be a maximum of 4 hr (Figure 71). Fluorogenic dye was added to a cell compartment to test its fluidic isolation from the 2nd compartment that had 3x extra volume to induce fluidic isolation due to pressure differences. Imaging of both compartments to test for the presence of dye showed that isolation was maintained at 30 min and 4 hr as dye was seen in only the 1st compartment. Tests at 24 hr showed dye on both side due to equilibria between the two compartments from flow through the microchannels. These tests show that fluidic isolation using 3x volume difference is capable of maintaining fluidic

isolation in the devices for at least 4 hr. If volume differences were maintained accordingly it would be possible to extend the length of experiment if required.

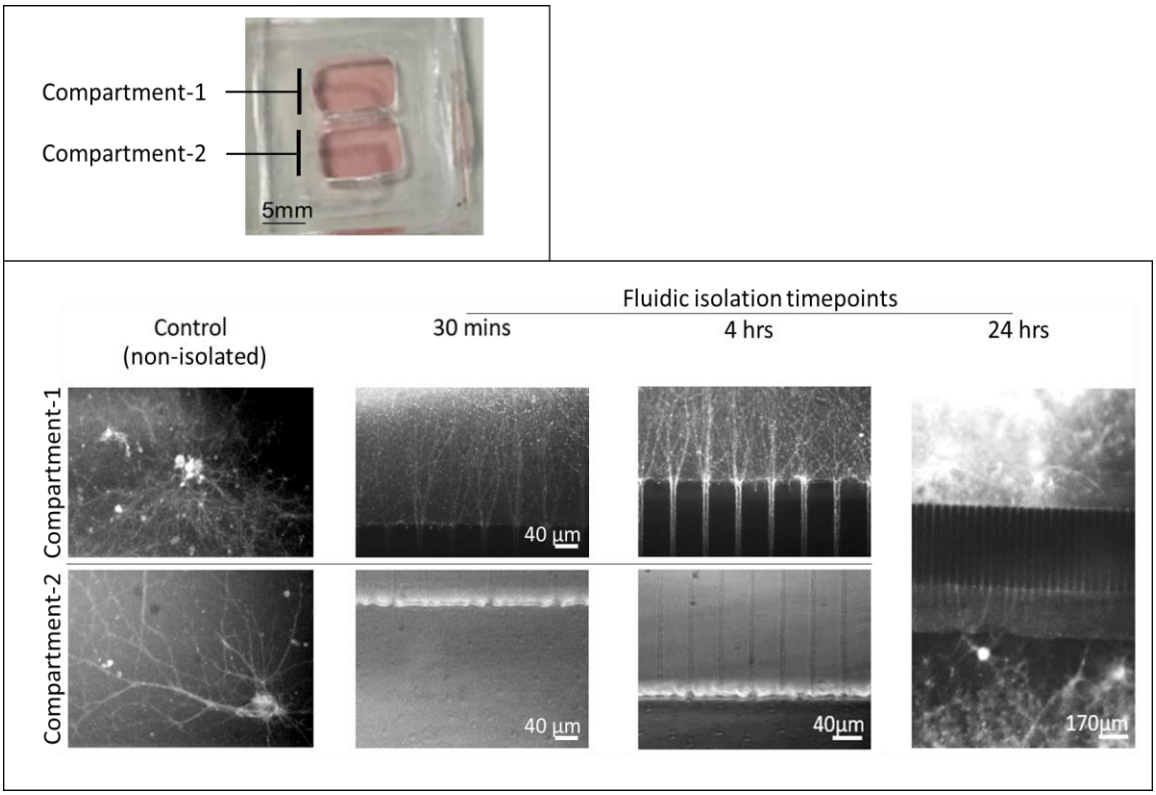

Figure 71. Fluidic isolation tests, using a fluorogenic dye binding to actin, show isolation is maintained for at least 4 hr. Control condition shows dye added to each compartment. In compartments where dye was only added to compartment-1 and isolated by a 3x volume difference in the compartment-2, no dye is seen at 30 min or 4 hr. Once volumes equilibrate by 24 hr fluidic isolation is no longer maintained and dye can be seen in both compartments.

6.2 Chapter 6 Discussion

Microfluidic devices that can be used for patch-clamp electrophysiology have been designed, and successfully showed fluidic isolation for at least 4 hr. The neuronal culture chips allow cell growth between channels and have limited evaporation of medium. The design of the device allows it to fit in the geometry of the patch-clamp rig such that cell compartments can be accessed by patch-pipettes. The unique method to punch out cell compartments offers a highly reproducible way to preserve the microchannels with a length of 450 µm.

Following the functional design and implementation of microfluidic culture chips for patch clamp electrophysiology, a previously published method was found (Jokinen *et al.*, 2013). This method is very similar to the independently developed method described above. Both methods utilise a 2-layer master mould suggesting the requirement for two-layers as opposed to a single height across the device achieved using a one-layer master mould. Though these methods are incredibly similar, there are a couple of differences in fabrication steps. Both methods remove the PDMS above the cell plating compartments, though through different mechanisms, the punch mechanism developed in this project has several advantages. Jokinen et al., (2013) use a scalpel to cut away PDMS over the cell compartment by eye, which can introduce variation between devices and is a more time-consuming method. The method of cutting the PDMS layer above the cell compartments is done by narrowly covering the height of the 700 µm cell compartment features on the master mould with PDMS, so that it is thin enough to carefully cut away. This produces very thin (700 µm) PDMS chips. The thin height of the chips requires additional PDMS wells to be layered over the cell compartment wells to increase the volume of cell medium that can be added, to prevent evaporation and maintain fluidic isolation. The additional wells add an extra fabrication step and potential complication when using the devices for fluidic isolation studies or experiments where evaporation of medium may need to be considered such as during imaging. Although the method developed for this project is limited to ~2 mm device height for access of patch-pipettes and the field-of-view of the objective, the punch method allows this full 2 mm height whilst preserving the microchannels. Evaporation of cell medium in the 2 mm devices was found to be dependent upon the cell incubator used, but was capable of maintaining sufficient volume in 95 % humidity. The other main difference between the designs is the channel length. Jokinen et al., (2013) use 2 mm × 7.5 µm × 3 µm microchannel dimensions. It takes cells 10 DIV for neuronal axons to grow

through 2 mm microchannels, whereas channels are only required to be ~260 μm to prevent crossing by dendrites; this project selected 450 μm channels to maintain fluidic isolation through hydrostatic pressure whilst reducing the distance of axonal growth.

As next steps, the device will be used for 1) plating cells in only one compartment such that the axons grow through and form 'pre-synaptic' structures in the 2nd compartment. Tau can then be added to this 2nd compartment to see whether it is taken up by pre-synaptic compartments and capable of aggregation without entering at the soma and transport through axons. 2) Understanding the pre- versus post-synaptic contribution of depression of an evoked response following treatment with exogenous tau in the presence of optogenetic stimulation.

CHAPTER 7

7.1 The characterisation of custom developed optically transparent multielectrode array devices for improved simultaneous neuronal recordings and FLIM

Optically transparent multielectrode arrays (MEAs) were developed using graphene (Philippa Hooper) or PEDOT:PSS (Sagnik Middya) electrode materials, for simultaneously imaging and recording electrical activity of neurons. The devices were designed to have improved function as compared to current commercial devices with transparent indium tin oxide (ITO) electrodes, which oxidises to show reduced transparency and increased impedance with repeated stimulation (Gross et al., 1993). Applications of the MEAs included correlating spontaneous neuronal activity with calcium dynamics and tau aggregation or using the MEAs to repeat the optogenetic method of stimulating neurons in the presence of tau to detect depression of neuronal activity. Before the MEAs could be used for biological experiments it was important to 1) determine suitable, biocompatible materials for the insulating layer and confirm that the electrode layer was equally biocompatible and 2) to characterise the materials used to ensure that they did not affect the fluorescence lifetime of fluorophores. 3) determine whether laser light results in cross-talk with voltage measurements by the electrodes.

All device fabrication was carried out by Philippa Hooper or Sagnik Middya. All cell culture, FLIM microscopy, and voltage measurements using MEAs were performed by the author.

7.2 Characterising substrates for the viability of neurons and fluorescence lifetime

Primary neurons were grown on substrates that were considered for use as the insulating (PMMA, Al2O3, SU-8, Si3N4, and AZ5214E) or conducting layers (graphene, ITO, gold) for custom designed microelectrode arrays (MEAs). Images were taken at DIV 14-17 for basic viability checks of neurons. The basic criteria of neuronal viability were that neurons had attached on the substrate and survived to this age with the ability to grow axonal and dendritic protrusions without clustering in discrete areas on the coverslip or rounding up and dying. Figure 72 shows the materials that were initially considered for use as materials in the graphene or PEDOT:PSS MEAs.

Materials including, graphene-coated coverslip, ITO, Au, PMMA, Al_2O_3, Si_3N_4, borosilicate coverslip (control) were found to be biocompatible. SU-8 and AZ5214E were deemed not biocompatible due to rounding of cells and lack of dendritic and axonal protrusions showing poor health and/or cell death. Substrates showing neuronal viability were further tested to confirm that they did not change the fluorescence lifetime of reference dyes (with known fluorescence lifetimes) when imaged on borosilicate glass coverslips as standard.

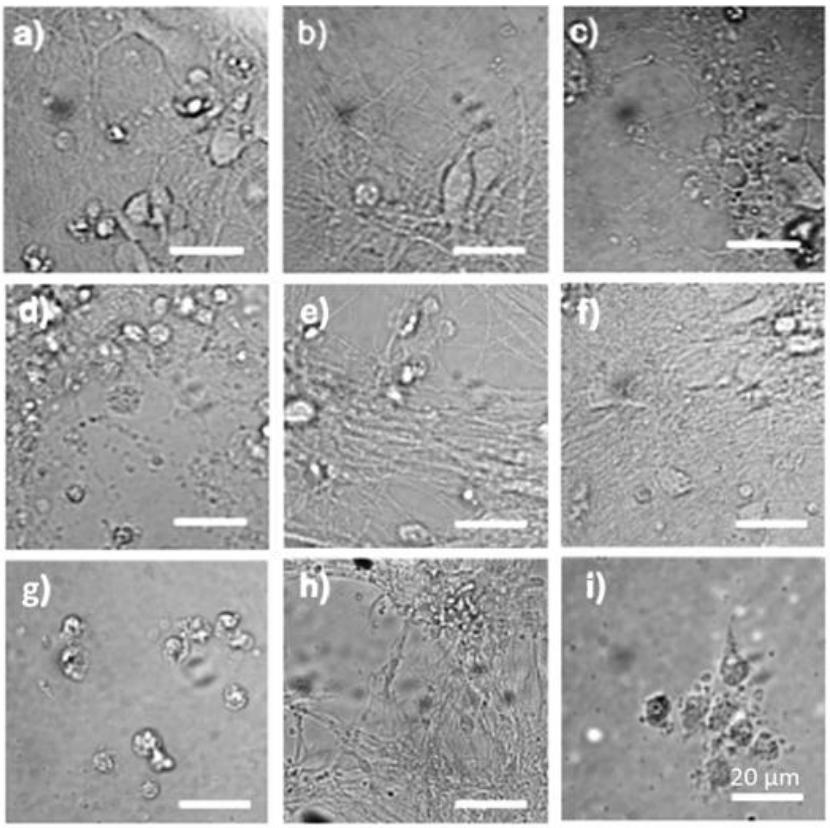

Figure 72. Neurons were grown on substrates of interest to DIV 14-17 to test whether they were biocompatible. Substrates included: a) borosilicate coverslip, b) graphene coated coverslip, c) ITO, d) Au, e) PMMA, f) Al_2O_3, g) SU-8, h) Si_3N_4, and i) AZ5214E. Materials were deemed biocompatible due to attachment and growth of neurons and cell protrusions. Of substrates tested AZ5214E and SU-8 were not biocompatible as cells were unable to form protrusions and survive to the experimental timepoint. Substrates fabricated by Philippa Hooper.

The fluorescence lifetime of reference dye Oregon Green 488 BAPTA-1 was measured on substrates considered for use as insulating layer alternative to parylene C for custom designed graphene MEAs. Insulating substrates that were biocompatible included PMMA, Al_2O_3, and

Si3N4; Si_3N_4 was removed from further study due to a relatively low impedance. ITO and graphene were also compared as the conductive electrode material; Au was tested for the connecting leads (Figure 73).

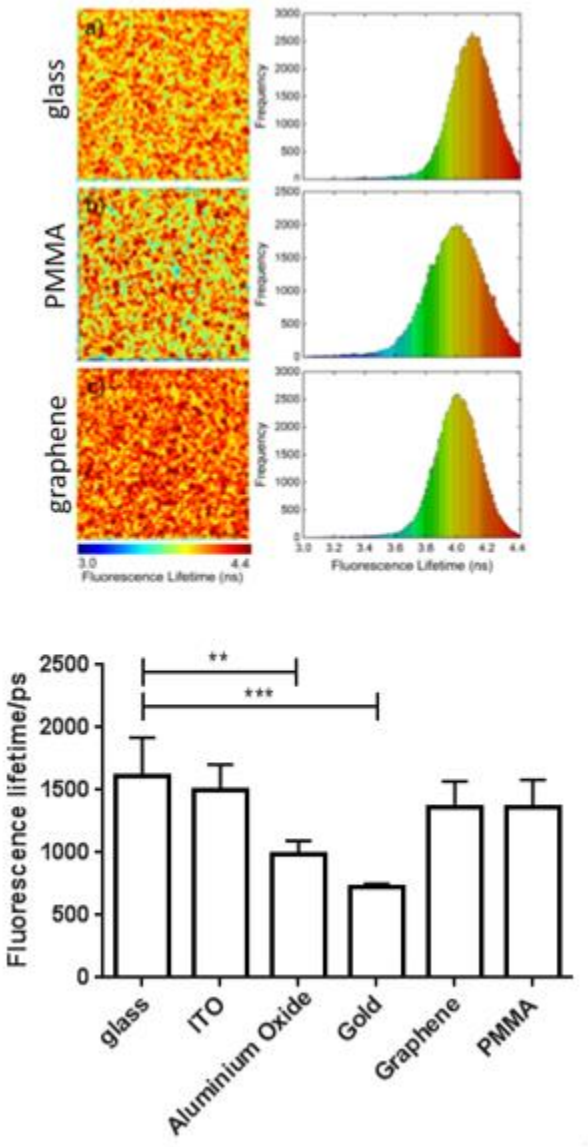

Figure 73. Testing whether common substrates affect the measured fluorescence lifetime of a standard dye. Top: The fluorescence lifetime of reference dye Oregon Green 488 BAPTA-1 on materials considered for use as conductive (graphene) or insulating (PMMA) materials in the MEA (top figure prepared by Chetan Poudel based on data from the author). Bottom: The pixel-wise lifetime measurements of the materials selected for the final version of the graphene MEA showing their similar lifetimes as plotted in the

cumulative histograms. Aluminium oxide and gold resulted in a decreased fluorescence lifetime of the reference dye as compared with glass (one-way analysis of variance (ANOVA); *****P* = 0.0011; F (5, 20) = 6.391). Dunnett's multiple comparison *P* values (left to right): not significant (NS) = 0.8960; *****P* = 0.0042; ******P* = 0.0006; NS = 0.4143; NS = 0.2100. Results display data from *n* = 3 experimental repeats with n >= 1 technical repeat. Mean values with standard deviation are plotted).

PMMA was selected (by Philippa Hooper) as a biocompatible material suitable for the insulating layer for the graphene MEA. All final materials for the graphene MEA (graphene, conducting layer; PMMA, insulating layer) and PEDOT:PSS MEA (PEDOT:PSS, conducting layer; parylene C, insulating layer; development carried out previously in the Malliaras group) were measured for final confirmation that they did not affect accurate fluorescence lifetime measurements of a reference dye. Borosilicate glass coverslips were used as a control to measure the fluorescence lifetime of rhodamine 6G in water, with known lifetime of 4.04 ns (Waharte et al., 2006). Figure 74 shows that all materials selected for use in the custom developed MEAs resulted in a measured lifetime of rhodamine 6G comparable to measurement on glass.

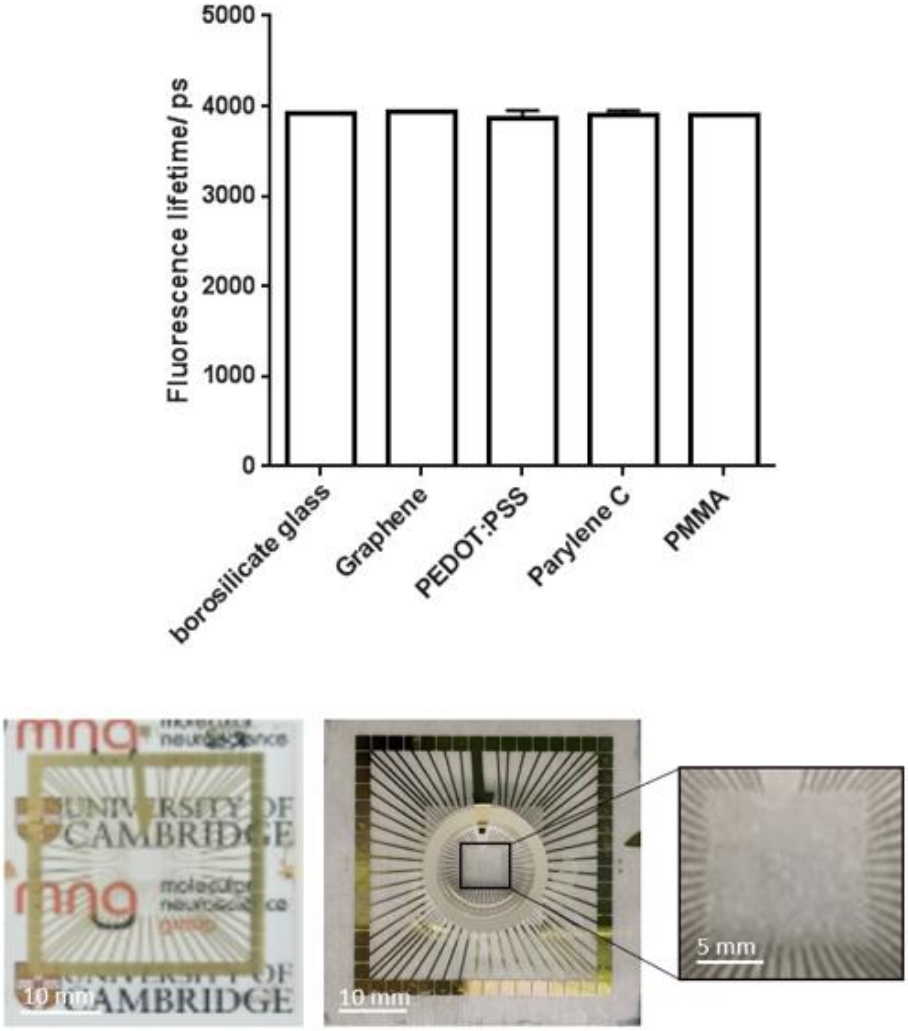

Figure 74. Confirming that the substrates selected for use do not affect the measured fluorescence lifetime of a standard dye. (Top) Fluorescence lifetimes of microelectrode array substrates using rhodamine 6G as a reference dye show that all produce accurate measurements as compared to borosilicate glass (control). (Bottom, left, Philippa Hooper) The final graphene MEA device (Bottom, right, Sagnik Middya) and the final PEDOT:PSS device resulting in optically transparent electrodes that do not impair biocompatibility of neuronal culture growth or fluorescence lifetime measurements (one-way analysis of variance (ANOVA); Not significant (NS) = 0.3702; F (4, 18) = 1.138). Dunnett's multiple comparison *P* values (left to right): NS = 0.9977; NS = 0.3692; NS = 0.9977; NS = 0.9863. Results display data from *n* = 3 experimental repeats with n >= 1 technical repeat. Mean values with standard deviation are plotted).

As an additional test to detect cross-talk between the laser and the electrode, a PEDOT:PSS device was placed in the MEA head-stage to record the voltage whilst receiving illumination from the confocal laser. Figure 75 shows the 1 s voltage trace from the MEA whilst the laser is on (blue) and whilst the laser is off (red). A significant difference (**, $p < 0.0019$) in voltage is seen between the laser being on or off resulting in a large increase in the baseline voltage measured.

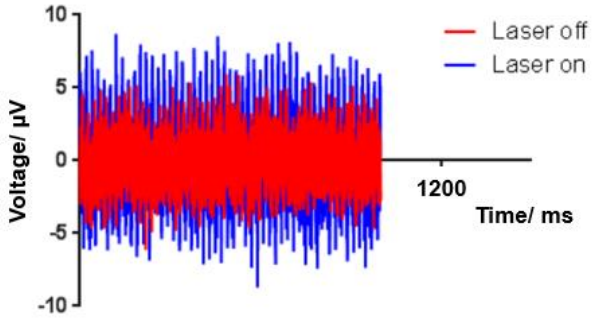

Figure 75. Overlaid 1 s voltage traces measured by the PEDOT:PSS electrode when the laser light is on or off. Laser light results in an increase in the measured baseline voltage.

Neurons were grown on graphene MEA devices to DIV14-17 and imaged with a calcium indicator using the inverted FLIM microscope. Figure 76 shows the placement of the optically transparent graphene electrode (red circle) that is imaged through to detect the calcium concentration in cells as a measure of fluorescence lifetime. This study shows that cells are able to grow on the MEAs whilst high resolution optical imaging can be performed through the graphene electrode. As a next step, voltage measurements can be simultaneously recorded from the cells.

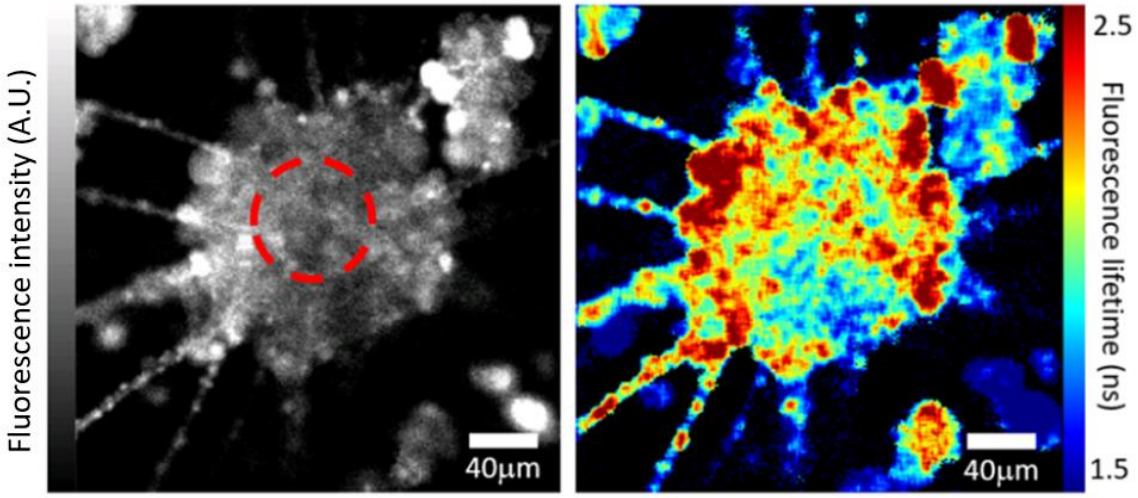

Figure 76. Neurons grown on graphene MEAs were imaged using fluorescence lifetime imaging and calcium indicator. Circle indicates the graphene electrode which is optically transparent and can be imaged through. Image prepared by: Chetan Poudel. Cell culture and treatment by the author.

7.3 Discussion

This project has contributed towards the development of improved optically-transparent MEAs by helping to characterise alternative materials as compared with the commercial available ITO MEAs. The biocompatibility, fluorescence lifetime, and cross-talk between voltage recordings and laser light, of MEA materials have been investigated.

In the decision of which insulating layer material to use a number of considerations needed to be taken into account. The PEDOT:PSS device used parylene C as a standard insulating layer. Parylene C is removed by reactive ion etching in locations required to expose the electrode to make contact with cells; extreme care allows reactive ion etching not to damage the PEDOT:PSS layer. As reactive ion etching would destroy the single atomic graphene layer, alternative materials that use etching by photolithorgraphy (SU-8, AZ5214E), phosphoric acid (Si_3N_4), tetra-methyl ammonium hydroxide (TMAH; Al_2O_3), or electron beam lithography (PMMA) were selected (by Philippa Hooper) for testing. Following tests for biocompatibility, only Si_3N_4, PMMA and Al_2O_3 remained feasible for use. Due to the lower impedance of Si_3N_4 resulting in a 'parasitic shunting effect' (Dauwe *et al.*, 2002), only PMMA and Al_2O_3 were tested to ensure they did not alter the

fluorescence lifetime of a reference dye. PMMA was selected (by Philippa Hooper) as it was shown not to alter the fluorescence lifetime and was simpler to deposit and pattern than Al_2O_3 by deposition by spin coating and patterning using electron beam lithography. Al_2O_3 required atomic layer deposition (ALD) and patterning using a PMMA mask, electron beam lithography and TMAH wet etching. During fluorescence lifetime characterisation using Oregon Green 488 BAPTA-1 it was found that Al_2O_3 resulted in a lower lifetime than glass coverslips alone. The reason for this is not known, but should be taken into consideration when Al_2O_3 is used as a substrate for methods dependent upon measuring an accurate fluorescence lifetime. It is possible that this reduced lifetime is due to metal-induced energy transfer as aluminium has plasmon resonance which vanishes when the oxide fraction reaches 50 % (Gérard and Gray, 2015). The decreased fluorescence lifetime measured with Al_2O_3 was an interesting and unexpected finding, and if due to plasmon resonance could be used for metal-induced energy transfer applications in future experiments, alongside gold and graphene.

Metal-induced energy transfer (MIET) is an important consideration of graphene and gold. MIET can enhance the measured intensity of an excited fluorophore but subsequently accelerates its return to ground state, resulting in a decreased fluorescence lifetime. This is heavily dependent upon distance between the metal and fluorophore as the energy transfer rate is directly proportional to the distance (Enderlein, 2000; Chizhik *et al.*, 2012). Graphene is known to affect the fluorescence lifetime of fluorophores within ~30 nm of its surface resulting in a reduced lifetime due to single-molecule energy transfer to graphene (Kaminka *et al.*, 2019). In this project, fluorescence measurements were taken > 30 nm above the surface, as is likely to occur when using biological samples or tissue. If using a sample thinner than 30 nm an optically transparent spacing substance such as PDMS or agarose may be considered for use to ensure the imaging of the sample is > 30 nm from the graphene surface. A spacer may greatly reduce the electrical signal measured if graphene is simultaneously used as an electrode. Au was also found to cause a reduced measured fluorescence lifetime for rhodamine 6G. Although Au is also capable of MIET, it is more likely that this effect was due to decreased transmittance of light due to the thickness of the Au coverslip as compared to energy transfer, though both factors could occur in combination (Chizhik *et al.*, 2014).

MEAs using PEDOT:PSS as an electrode, and parylene C as an insulating layer, were shown not to have an effect on the fluorescence lifetime measurements of a reference dye, rhodamine 6G. The electrodes were shown to have an increased baseline voltage when measurements were taken in the presence of a 488 nm laser. This increased voltage is likely due to the photovoltaic effect as PEDOT:PSS is commonly used in optoelectronic devices and its conductivity has previously been shown to be increased by laser radiation (Yun *et al.*, 2019). The increased amplitude of the baseline voltage from the laser on the electrode results in noise that may mask an increased amplitude of extracellular, local field potential (LFP) recordings proportional to increased neuronal activity; alternatively, the increased amplitude of the high frequency noise may be detected as multi-unit activity (MUA) during signal processing. Further measurements with an active sample will therefore be required to determine whether in practice the increased baseline voltage results in noise that causes false negative LFP, or false positive MUA measurements, of voltage traces from neurons.

A consideration for both devices is the vibrations arising from the microscope objective lens when in contact with the devices, resulting in a low frequency noise in the voltage recordings. This noise is irregular and therefore unlikely to be easily filtered out, however it is possible to use an air objective that does not require direct contact with the device. Alternatively, sequential MEA measurements and imaging can be taken, however in combination with a fast imaging method this may be less suitable. The long timescale (~3 min) of TCSPC imaging makes it unlikely that much information will be lost during sequential measurements, and therefore this may be a better solution if the photovoltaic noise seen from the PEDOT:PSS results in greatly decreased signal-to-noise.

Future directions for improved optically transparent MEAs include two main applications using correlative fluorescence lifetime imaging and recording of neuronal activity. Applications of the MEAs include 1) correlating calcium dynamics and tau aggregation with spontaneous neuronal activity to see the relationship between neuronal activity and the aggregation rate of tau. This project will use fluorescence lifetime sensors for calcium (Oregon green BAPTA) and tau aggregation (hTau40-Alexa®-594) to determine how these variables relate to any measured changes in spontaneous neuronal activity. Previous studies have shown that monomeric exogenous tau results in an increased concentration of intracellular calcium, this project has shown that

neuronal activity results in synaptic depression. With MEAs it will be possible to better understand the timescale of neuronal activity and tau aggregation. 2) using the MEAs to repeat the optogenetic method used to stimulate neurons in the presence of tau to detect any changes to evoked neuronal activity as a second method to confirm these results. Using MEAs to stimulate and record from populations of neurons, it will also be possible to understand tau-dependent changes to activity at the network level, particularly if hippocampal slice cultures – with clear directional connectivity - are used.

CHAPTER 8

8.1 Metal-organic frameworks for tau immunotherapy

Continuing from previous findings that extracellular monomeric tau is endocytosed by cells and aggregates in low pH compartments, an immunotherapy method was developed to prevent initial uptake of tau protein and therefore prevent aggregation and seeding of tau into aggregates. The novel method for immunotherapy would use antibodies grafted to metal-organic frameworks (MOF-Ab). The size of the MOF would be designed to prevent the uptake of exogenous monomeric tau protein into cells by capturing and clearing the protein in the extracellular space. A key initial question before the continuation of the project is a) whether the antibody is taken up by neurons in full-sized IgG or antigen-binding fragment (Fab) form once bound to tau; b) whether antibody is taken up by neurons in its unbound state; c) whether the antibodies affected the endocytosis of exogenous tau protein into neurons before being grafted to the MOF. This chapter therefore answers these initial questions to show that the attachment of antibody to a MOF is fundamental for preventing any uptake of tau protein into cells and therefore eliminate the possibility that tau protein can seed further aggregation.

For determining a) whether antibody was internalised by neurons following binding to the C-terminus of tau, antibody and tau protein were incubated for 30 min before addition to primary hippocampal neurons. Figure 77 (A) shows the contrast-adjusted fluorescence intensity images of neuronal cultures following a trypsin wash to remove extracellular fluorescently-labelled antibody, alongside the background only control where no antibody was added. Figure 77 (B) shows that the average intensity of both the IgG and Fab were significantly higher as compared to background-only control. As a trypsin wash and media replacement were used to remove membrane-bound and extracellular protein, it is considered that the intensity measurement (above background intensity) was due to antibody taken into cells. Although the antibody intensity is higher as compared to background-only control, it is not possible to make direct comparisons between fab or IgG uptake due to 4x concentration of IgG used to compensate for its low labelling efficiency, and 2x fluorophores per IgG as compared to 1x per fab. No differences were seen between anti-tau antibodies as compared with antibody (IgG) control. This is likely due to insufficient removal of control antibody during washing steps as can be seen in Figure 77 by high intensity clumps of

antibody remaining in the media. In the future pHrodo® -conjugated antibody may be used to reduce background such that only internalised antibody that enters low pH compartments produces fluorescence intensity.

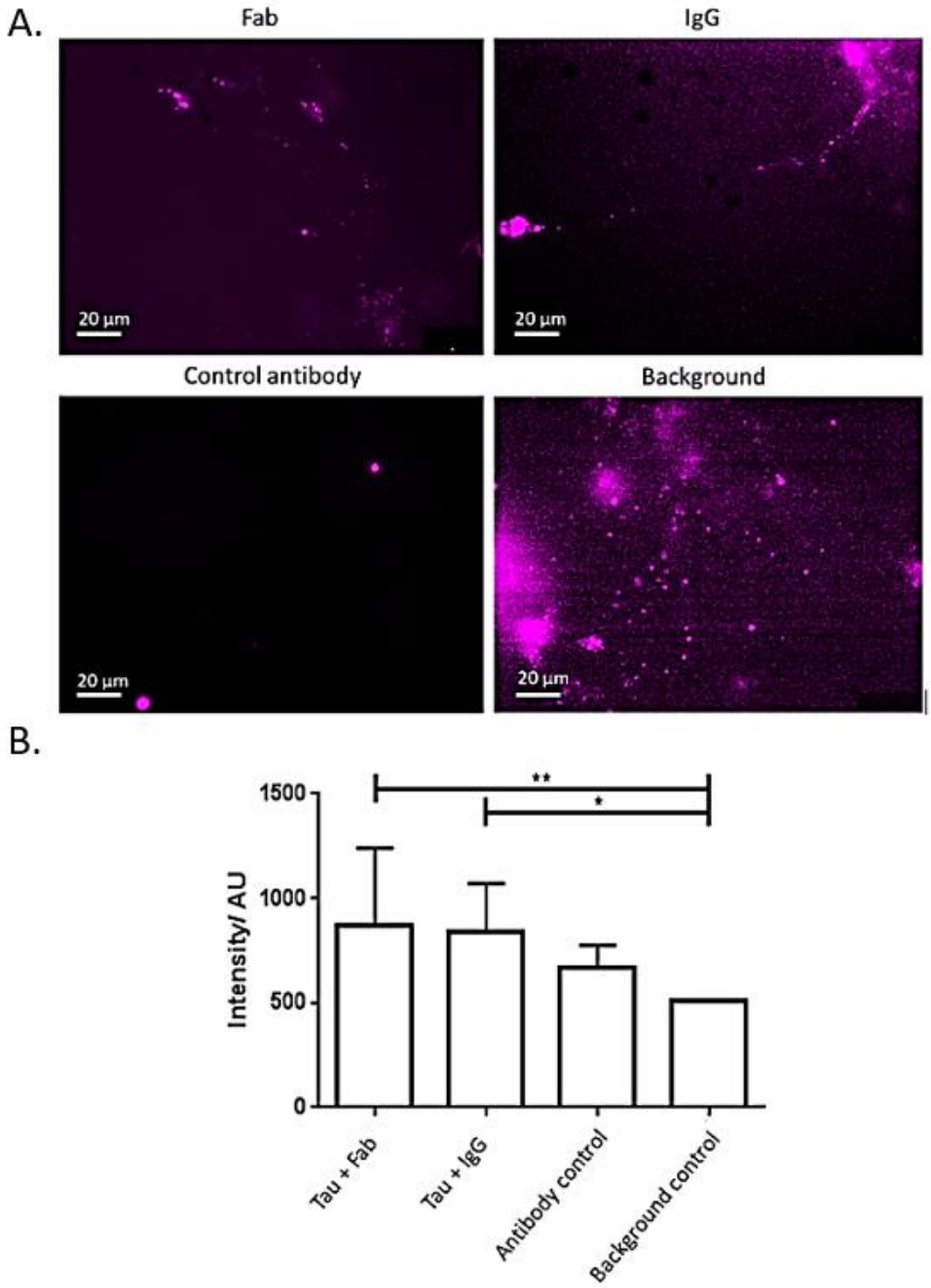

Figure 77. The addition of tau-incubated antibody to cells results in an increase in the fluorescence intensity. (A) Contrast-adjusted fluorescence intensity images of neurons treated with fluorescently-labelled antibody. (B) The increase in fluorescence intensity of neurons treated with antibody suggests that some antibody is taken into cells, preventing

its removal in the trypsin and medium wash before imaging, as expected to occur for control antibody-AF647 (one-way analysis of variance (ANOVA); *****P* **= 0.0022; F (3, 44) = 5.716). Tukey's multiple comparison *P* values (Tau + Fab (A), Tau + IgG (B), Antibody control (C), Background control (D)): (A-B) Not significant (NS) = 0.9817; (A-C) NS = 0.1400; (A-D) *****P* **= 0.0030; (B-C) NS = 0.3085; (B-D) ****P* **= 0.0114; (C-D) NS = 0.4005. Experiments were performed from *n* = 3 animals with n >= 2 technical repeats per animal. Mean values with standard deviation are plotted).

Next, the colocalisation between the antibody with tau was investigated. Unlike average intensity measurements, colocalisation analysis would not take into account high intensity spots of antibody remaining in the medium and may therefore be more robust method to detect antibody internalisation with tau protein. Figure 78 shows that both forms of anti-tau antibody resulted in greater colocalisation with tau as compared to non-specific antibody control. It is not possible to quantify the difference in colocalisation between the fab versus IgG due to 4x concentration of IgG used to account for low labelling efficiency. However, it can be seen (Figure 78 A, white arrows) that both forms of anti-tau antibody colocalise with tau inside of neurons.

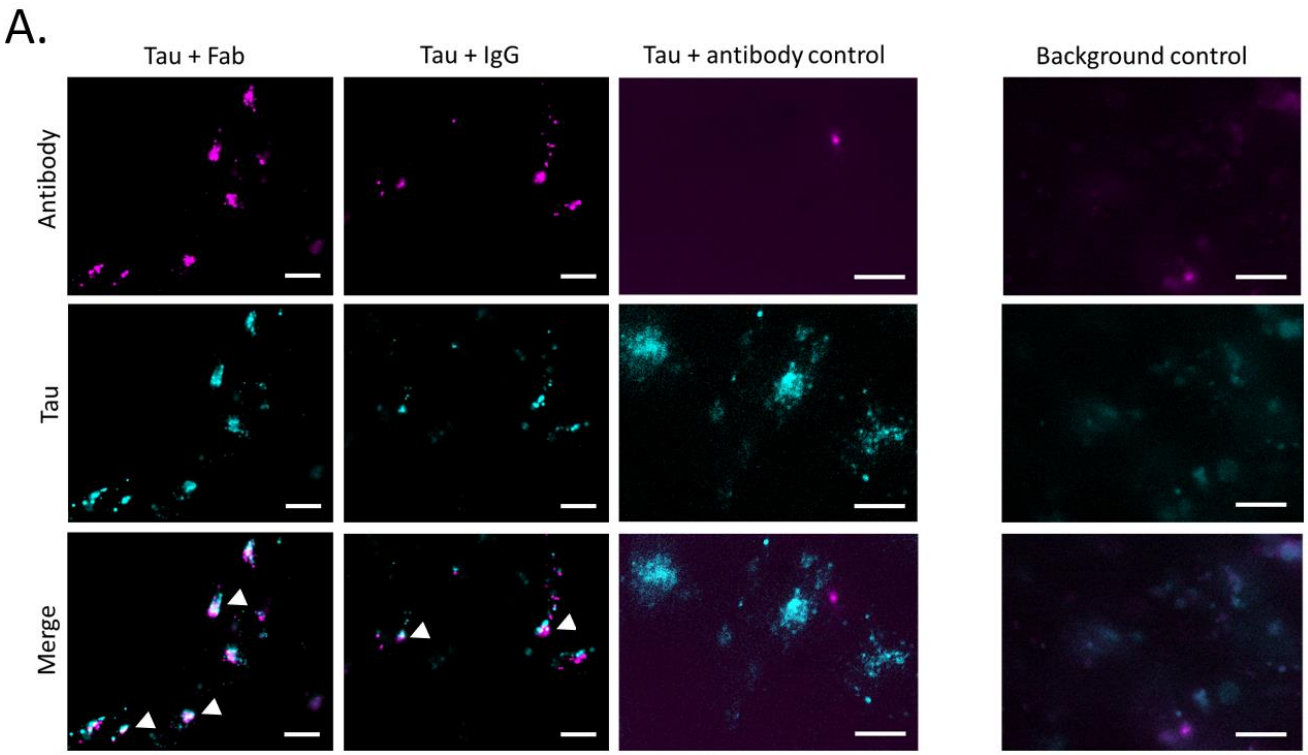

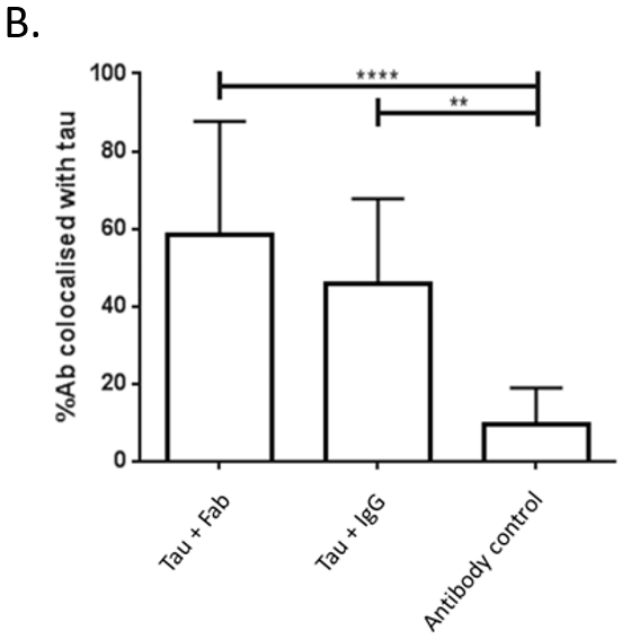

Figure 78. (A.) The colocalisation (white arrowheads) of antibody (magenta) with tau protein (cyan). (B) Both fab and IgG forms of antibody are shown to colocalise with tau as compared to a non-specific antibody negative control (Scale bar = 12 µm) (one-way analysis of variance (ANOVA); *******P* < 0.0001; F (2,32) = 12.59). Tukey's multiple comparison *P* values (Tau + Fab (A), Tau + IgG (B), Antibody control (C)): (A-B) NS = 0.3431; (A-C) *******P* < 0.0001; (B-C) *****P* = 0.0027. Experiments were performed from *n* = 3 animals with n >= 2 technical repeats per animal. Mean values with standard deviation are plotted).

The intensity of tau protein following incubation with antibody was measured to determine whether antibody binding decreased the total concentration of tau that entered cells. Decreased tau internalisation has been previously shown for a similar polyclonal C-terminal anti-tau IgG antibody (Evans *et al.*, 2018) though not for anti-tau Fab forms. It was hypothesised that through binding the antibody, the molecular size of the tau complex would be increased and may delay or inhibit entry into the cell. This was not expected to occur for the non-specific antibody control which did not have a paratope for the C-terminal of tau. Due to a trypsin wash prior to imaging it was assumed that measured intensity was due to tau that had been taken into cells and thereby protected from digestion with trypsin and removal in the medium change. Figure 79 shows that both anti-tau antibodies result in significantly less entry of tau protein into cells as compared with non-specific antibody control, but no difference compared with background autofluorescence. Data therefore show that antibody binding decreases the entry of tau into cells. No differences are

seen between the anti-tau IgG or fab form of antibody when used at equal concentration suggesting both have a similar mechanism to greatly reduce uptake of tau over the 4 hr experiment.

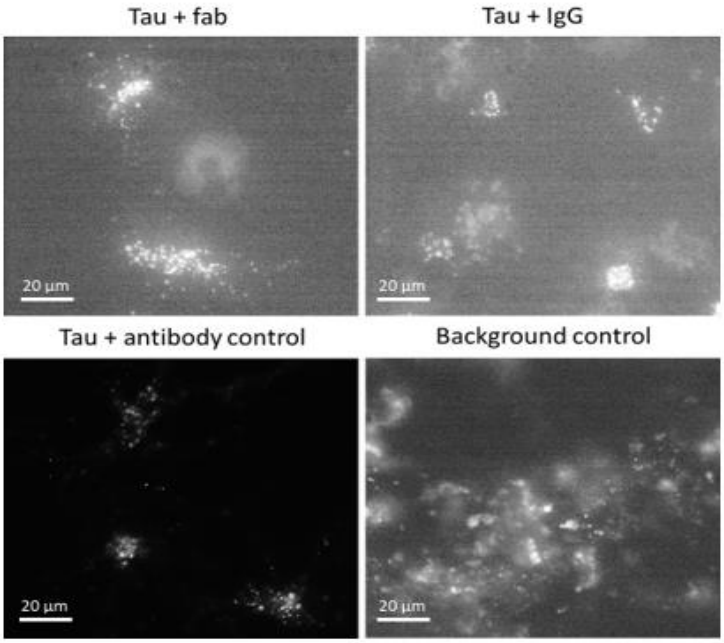

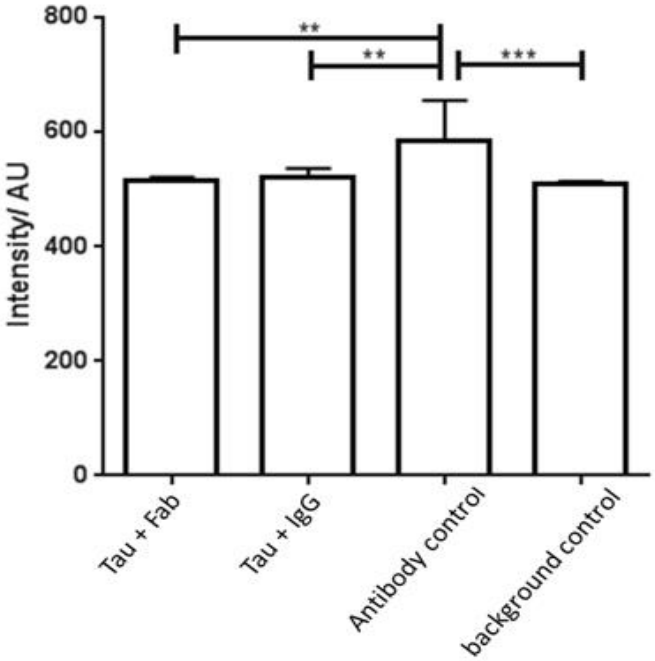

Figure 79. Intensity measurements for the uptake of fluorescently-labelled exogenous tau protein into neurons when treated with unlabeled anti-tau antibody versus control. Both

forms of anti-tau antibody (IgG and fab) are shown to reduce tau uptake into neurons as compared with anti-Fc antibody control, which does not reduce tau uptake (one-way analysis of variance (ANOVA); ******P* = 0.0002; F (3, 34) = 8.927). Tukey's multiple comparison *P* values (Tau + Fab (A), Tau + IgG (B), Antibody control (C), background control (D)): (A-B) NS = 0.9857; (A-C) *****P* = 0.0028; (A-D) NS = 0.9935; (B-C) *****P* = 0.0027; (B-D) NS = 0.9079; (C-D) ******P* = 0.0004. Experiments were performed from *n* = 3 animals with n >= 2 technical repeats per animal. Mean values with standard deviation are plotted).

As a final test, to determine whether either form of antibody was internalised without binding to tau protein, cells were washed with fresh medium prior to the addition of antibody to remove tau from death or free release by cells in the culture medium. Following a shorter 1.5 hr incubation to reduce tau entry into medium, cells were washed and imaged to measure average intensity. Figure 80 shows no observable differences between anti-tau antibody, antibody control, and background control suggesting that removal of basal tau from medium and shorter incubation greatly reduces anti-tau antibody uptake by neurons. It therefore seems that binding of antibody to tau greatly increases the uptake of anti-tau antibody as previously demonstrated for IgG but not fab protein (Lewis D. Evans *et al.*, 2018). The trend towards increased intensity of the anti-tau IgG and fab, as compared to antibody control, suggest it could be possible that tau is released into the medium during this time. During the 1.5 hr incubation, tau released from cell death or free release, as has been suggested to be a physiological mechanism (Pooler *et al.*, 2013), could result in a complex allowing antibody entry. Due to a trend of lower intensity of control antibody as compared with anti-tau antibody forms, it is more likely that gradual tau accumulation in the medium allows entry as compared with a slower uptake mechanism for all antibodies that cannot be detected at the 1.5 hr timepoint. Though it is also possible that the shorter 1.5 hr incubation period masks the uptake of antibody. This method may not be sensitive enough to distinguish between antibody conditions if only low concentrations of antibody are internalised before the 4 hr measurement, which detected differences between anti-tau antibody and background control.

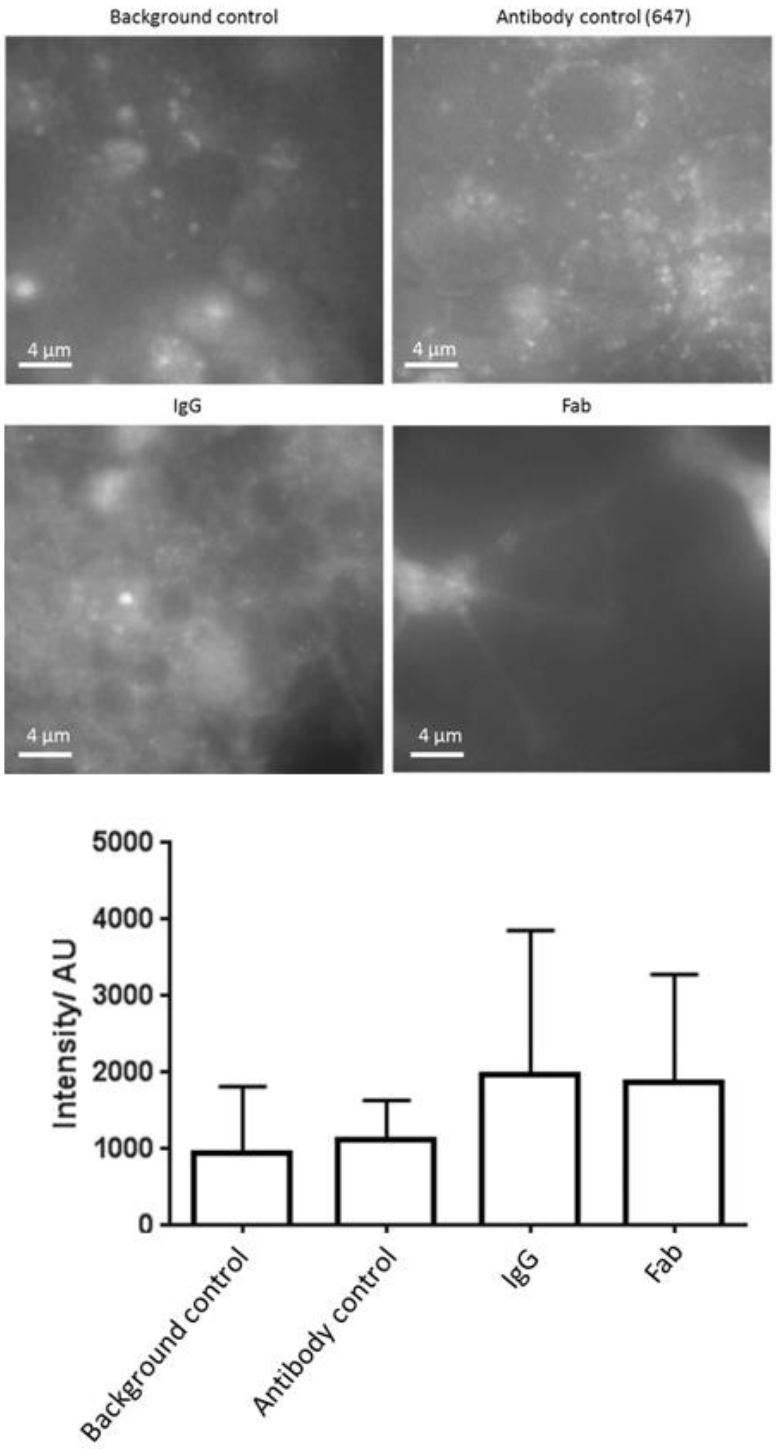

Figure 80. No differences are seen between the intensity of cells treated with fluorescently-labelled anti-tau antibodies, antibody control, or background-only control following a 1.5 hr incubation (one-way analysis of variance (ANOVA); not significant (NS) = 0.01778; F (3, 39) = 1.725). Tukey's multiple comparison *P* values (Background control (A), Antibody control (B), IgG (C), Fab (D)): (A-B) NS = 0.9906; (A-C) ***P* = 0.3707; (A-D) NS = 0.33905; (B-C) NS = 0.4506; (B-D) NS = 0.4090; (C-D) NS = 0.9982. Experiments were performed

from *n* = 3 animals with n >= 2 technical repeats per animal. Mean values with standard deviation are plotted).

For this reason, it is difficult to conclude whether a lower intensity of anti-tau antibody is measured at 1.5 hr due to the smaller concentration of tau in the cell medium or due to limited detection capability in this shorter time period.

8.2 Discussion

Immunotherapy targeting tau protein is a current avenue for the treatment of Alzheimer's disease. A number of ongoing studies are using anti-tau antibody to bind various species of tau protein to neutralise their toxicity. We have designed a novel approach through preventing the internalisation of tau protein before aggregation can occur in low pH intracellular vesicles and thereby preventing the formation of toxic tau species. As it has previously been shown that C-terminal anti-tau IgG is able to enter cells by forming a complex with monomeric tau (Lewis D. Evans *et al.*, 2018), we have repeated these experiments with slight variations including a monoclonal IgG and fab antibodies, primary rat neurons, and wildtype tau as compared to P301S mutant tau. Results show that anti-tau IgG and anti-tau fab both colocalise with tau when added to neuronal cultures, suggesting that both forms of antibody are capable of entering cells on binding tau. We have also shown that both forms of anti-tau antibody can effectively reduce the amount of tau that is measured in neurons. Although this has previously been shown to be the case for C-terminal targeting anti-tau IgG, we show a similar effect with anti-tau fab in decreasing tau internalisation by cells. Following on from these findings, the grafting of antibody to the metal organic framework (MOF) will be necessary to prevent any internalisation of tau protein, as shown to occur in complex with the antibody itself. Although the anti-tau antibodies have shown to greatly reduce the amount of tau taken into cells, at least some entry of tau occurs following antibody binding. To eliminate the possibility of tau entry into low pH cellular compartments we will investigate the use of several forms of MOF. The size and the surface chemistry of MOFs can greatly influence the cellular uptake of the nanoparticle. For drug delivery, MOFs are usually synthesised in a range between 80-200 nm as MOFs of these sizes are known to easily enter cells. By synthesising MOFs with increasing diameters, it was shown that MOFs larger than 600 nm are unable to enter into cells

(Orellana-Tavra *et al.*, 2017). Therefore, for this project three different sized MOFs will be tested for proof of concept. The largest MOF will have >600 nm diameter, a medium MOF of 100-200 nm and small MOD of ~ 50 nm will be grafted with anti-tau antibodies (Fab or full size IgG). The MOF-Abs will be incubated with extracellular tau, and measurements of Ab and tau uptake and aggregation will be measured.

Once the IgG and fab have been grafted to the MOF it will be important to confirm that they are no longer capable of entering cells both in the absence of tau or once antibodies have bound to tau protein and may be capable of hijacking tau uptake pathways as seen for ungrafted anti-tau antibodies. Next stages in the project include the addition of full-IgG, Fab fragment, and antibody-grated MOF (MOF-Ab) to neurons treated with exogenous monomeric tau to determine which concentration is necessary to prevent uptake and intracellular aggregation of tau. Although the ungrafted anti-tau antibody reduces the concentration of tau that is measured inside of cells, it is not known whether this prevents aggregation of the tau that enters in free or antibody-complex form. Due to the binding epitope of the antibodies being located at the far C-terminal of tau, it is possible that the antibody does not prevent the microtubule-binding-region from initiating aggregated structures as the C-terminal composes a fuzzy region outside of this core (Fitzpatrick *et al.*, 2017). This study did not measure the fluorescence lifetime of tau that was colocalised with antibody to determine its aggregation state, but this would be a useful next step to determine how effective the ungrafted antibody is before comparing to the MOF-Ab as an alternative therapeutic. If the antibody does not prevent aggregation of tau, it may inhibit further trafficking of tau species to synaptically connected neurons by altering its transported destination (McEwan *et al.*, 2017).

It has also been suggested that low concentration of extracellular tau has a physiological purpose, and by removing tau this may result in some physiological deficit, though this deficit has yet to be shown (Pooler *et al.*, 2013; Lewis D. Evans *et al.*, 2018). Conversely it is known that increased intracellular concentration of tau promotes its aggregation as has been shown in overexpression models, and H1 haplotype as increased risk for AD (Kwok *et al.*, 2004; Guo and Lee, 2011; d'Orange *et al.*, 2018). The group has also shown that relatively high concentrations of extracellular tau (1 µM) result in significant aggregation inside of cells (Michel *et al.*, 2014). For this reason, targeting high concentrations of tau protein may be the key benefit of the MOF-Ab therapy such as in cases where high concentrations of extracellular tau occur, such as cell death

from traumatic brain injury, which is a risk factor for AD. Acute treatment may be sufficient to remove excess tau protein from the extracellular medium from the site of impact to prevent uptake and aggregation by neighbouring neurons. Alternatively the treatment may be suited as an early stage preventative treatment for AD particularly in people with increased risk of AD such as H1 haplotype in attempt to stop seeding and spreading between neuronal networks at the earliest Braak stages (Braak and Braak, 1991). It is less clear whether the treatment may be as effective to reduce symptoms at later stages of disease progression when much pathology has already arisen, particularly once neuronal death occurs. However, immunotherapy against beta-amyloid has shown that by altering the equilibrium of beta-amyloid structures, an antibody was able to reduce plaque load through shifting beta-amyloid from the brain to the periphery, without needing to bind to aggregates in the brain (DeMattos *et al.*, 2001). This suggests that it is possible for immunotherapy to have an effect at later stages of disease to potentially reverse some of the protein pathology. Before use in human patients, the uptake and clearance mechanisms of the ungrafted antibodies and MOF-Ab will need to be thoroughly elucidated. Different IgG antibodies show different penetration of the blood-brain barrier, as some immunotherapies have been shown capable of systemically entering the brain, with one study showing ~0.1 % penetration efficiency (Games *et al.*, 1995; Bard *et al.*, 2000). The larger size MOF may inhibit entry via the blood-brain barrier and therefore smaller sizes or other delivery methods may need to be considered, which may be possible such as in extreme TBI cases. For conventional immunotherapy, antibody-bound tau may promote degradation by microglial phagocytosis, be taken into cells whereby it will promote its clearance by lysosomal degradation, or via systemic removal by the lymphatic system or blood-brain barrier (Nobuhara *et al.*, 2017). For the larger MOF-Ab structures it is important to test in 3D cultures and *in vivo* models how they are able to clear the extracellular space once saturated with tau molecules and that they do not accumulate in brain tissue.

This chapter has therefore validated anti-tau antibody for use with MOF-Ab to prevent the internalisation and aggregation of exogenous monomeric tau. The novel finding through which this is based on include:

- Monocloncal anti-tau fab (alongside IgG) pre-incubated with tau colocalises with exogenous tau inside of neurons.

- Monoclonal anti-tau fab (alongside IgG) reduce the overall uptake of tau into neurons, though some tau is still able to enter in the presence of 10x Ab, potentially in a tau-Ab complex.
- MOFs grafted with anti-tau antibodies may be an effective novel approach to remove high concentrations of extracellular tau either at pre-clinical stages of pathology in high-risk AD cases, or in acute traumatic brain injury patients.

CHAPTER 9

9.1 Developing an improved biopatterning method for the selective differentiation of neural stem cells

Neural stem cell therapy has already shown promise in AD particularly through the neurotrophic release of BDNF (Blurton-Jones *et al.*, 2009; Jiao *et al.*, 2016) and GDNF (Hampton *et al.*, 2010; Wang *et al.*, 2011). A biopatterning technique was used to improve long-term survival of stem cells by covalently binding protein growth factors onto the novel implantation scaffold, bacterial cellulose. The aim was to improve survival and maturation of stem cells into neurons as compared with cells grown on cellulose in the absence of growth factors, mimicking the diseased human brain.

9.2 Optimisation of a novel biofunctionalisation method

Multiple biofunctionalisation methods were attempted in the development of a simple and reliable option. These included poly-L-lysine (PLL), plasma adherence, ELISA carbonate/bicarbonate method and (3-Aminopropyl)triethoxysilane (APTES). None of these methods showed reliable functionalisation of the unmodified protein (Figure 81) and therefore epoxysilanisation was explored, which would be capable of reacting with exposed amine groups on the antibody

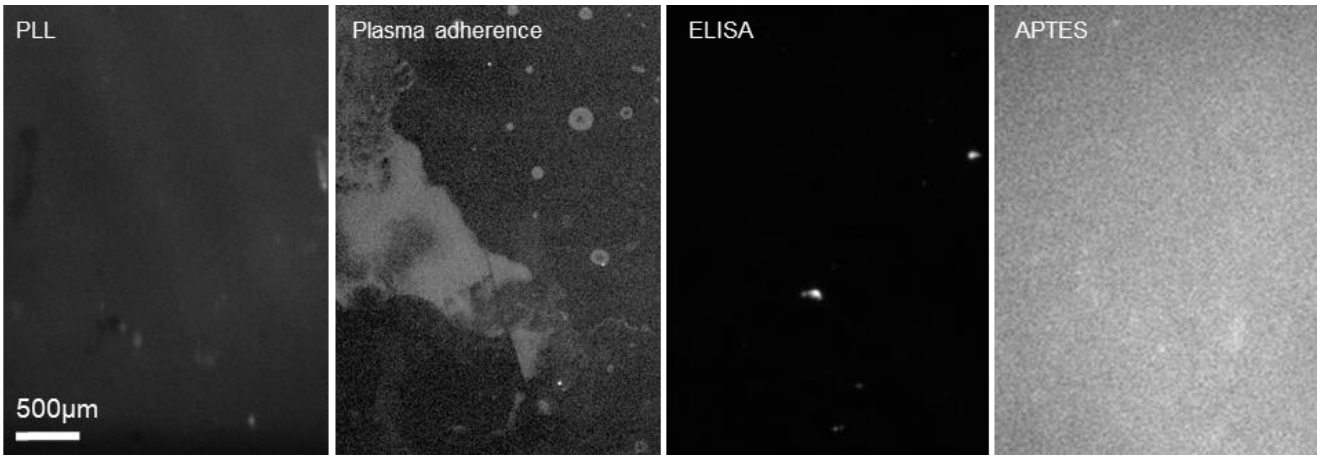

Figure 81. Initial attempts to functionalise unmodified, AlexaFluor®-647-labelled antibody onto coverglass based on previously published methods. Both covalent and non-covalent

methods resulted in uneven and low-efficiency coating of silicon borohydride glass coverslips.

The epoxysilane, (3-glycidoxypropyl)trimethoxysilane (GPTMS), was used and showed reproducible, highly-efficient, covalent modification of silicon borohydride glass with protein (Figure 82). As a first attempt, the conventional method of GPTMS modification was used to show that this could be successfully implemented.

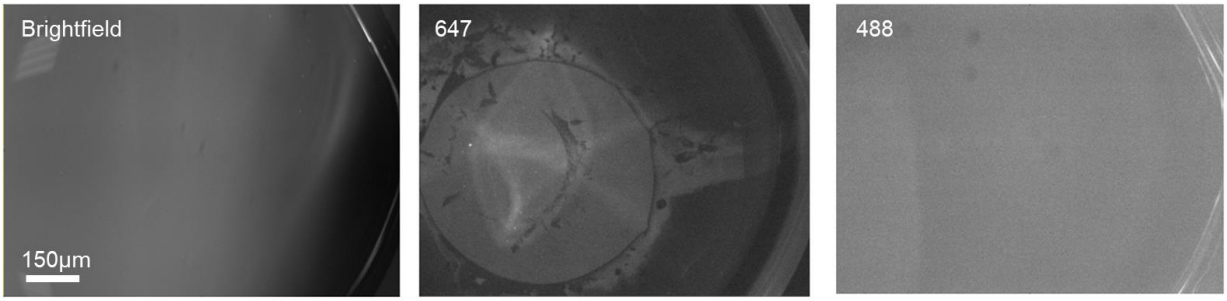

Figure 82. The use of epoxysilane (3-glycidoxypropyl)trimethoxysilane for functionalising coverglass with unmodified, AlexaFluor®-647-labelled antibody showed high efficiency and reproducibility. The figure shows the pipetted spot of functionalised antibody on the coverglass. The same area is also shown by brightfield and 488nm excitation to demonstrate that the patterning is not from autofluorescence of GPTMS but specific to the functionalised AlexaFluor®-647-labelled antibody.

Following the conventional method of biofunctionalisation using GPTMS, further simplifications of this method were developed to make it faster and easier. The novel method used one reagent, could be done on a lab bench, and was completed within 5 hr. In addition to this, the use of PDMS stamps could result in the printing of GPTMS in grid shapes for biopatterning protein, and not non-specific GPTMS deposition across the coverglass as would occur by using the conventional method. For biopatterning, PDMS stamps of 200 x 200 µm grids previously designed by Jane Fojas and larger 700 x 500 µm grids by Amanda Haack were used. Initial optimisation of PDMS stamps to make grid patterns involved patterning of PLL to coverglass for the growth of neurons (Figure 83).

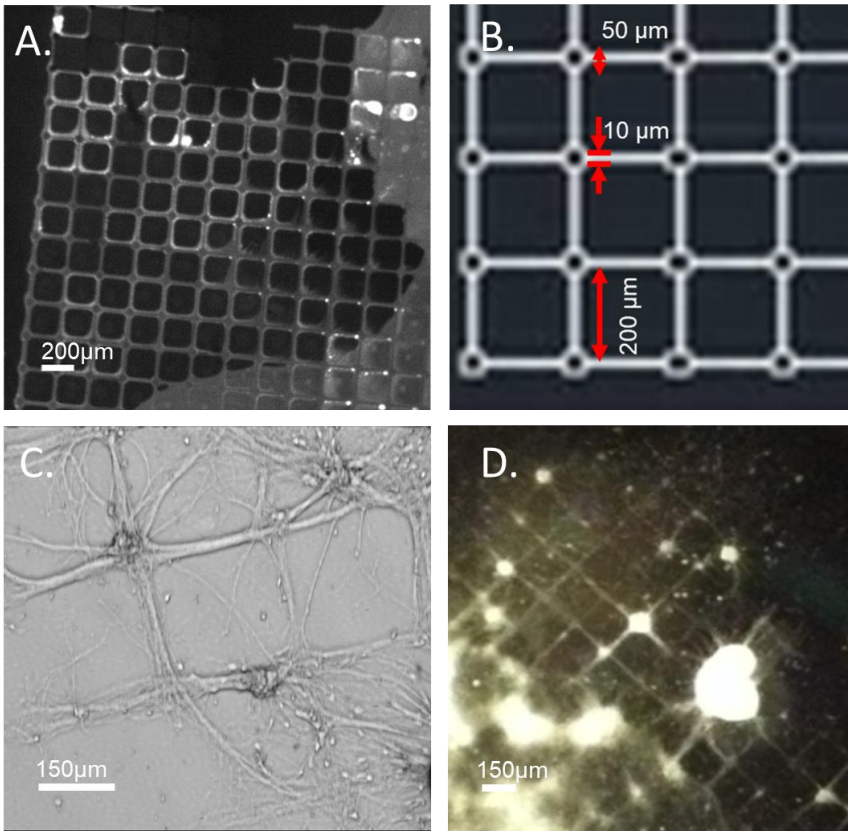

Figure 83. The optimisation of grid patterning using PDMS stamps(A) Patterning of a FITC-PLL grid using a PDMS stamp. (B) Design of the PDMS stamps used for patterning grid shapes, showing a basic unit that was repeated over an area of 1 cm^2 as designed by Jane Fojas. (C, D) Neurons plated onto FITC-PLL grids grow preferentially following the PLL grid lines.

Following successful optimisation of the PDMS patterning using PLL, the patterning of GPTMS for covalent modification of glass with protein was developed. A novel method of GPTMS treatment was used that directly applied GPTMS to the stamp with no other reagents, and due to direct contact with the substrate, could be completed in 5 hr. Multiple proteins were biofunctionalised to show the non-specificity of GPTMS for proteins, due to its reactivity with amine or hydroxyl groups (Figure 84).

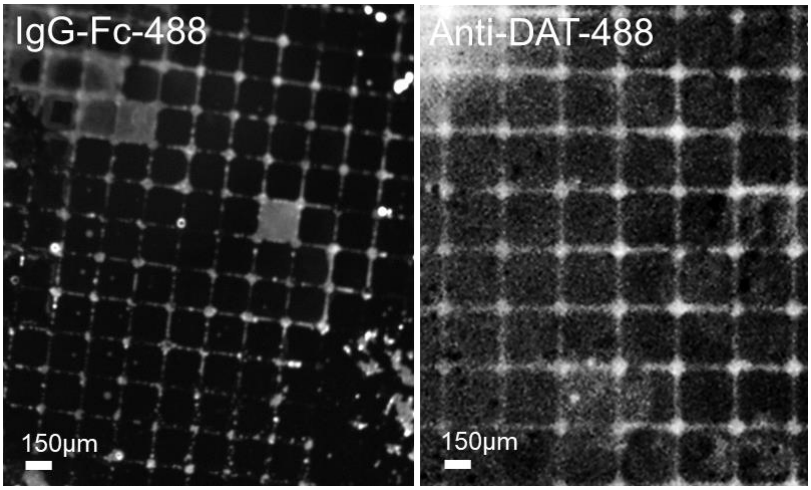

Figure 84. Covalent functionalisation of protein to coverglass. Functionalisation of IgG-Fc and anti-DAT-ECD, both 488-labelled, to a glass coverslip. The grid pattern was achieved through applying epoxysilane with a PDMS stamp, to which the protein was covalently functionalised.

To ensure the method was specific to the exicitation/emission of the fluorophore and not autofluorescence of the GPTMS, a control of GPTMS only without labelled-protein was imaged. Figure 85 shows the fluorescence is specific to functionalised protein as it does not appear in the GPTMS-only image.

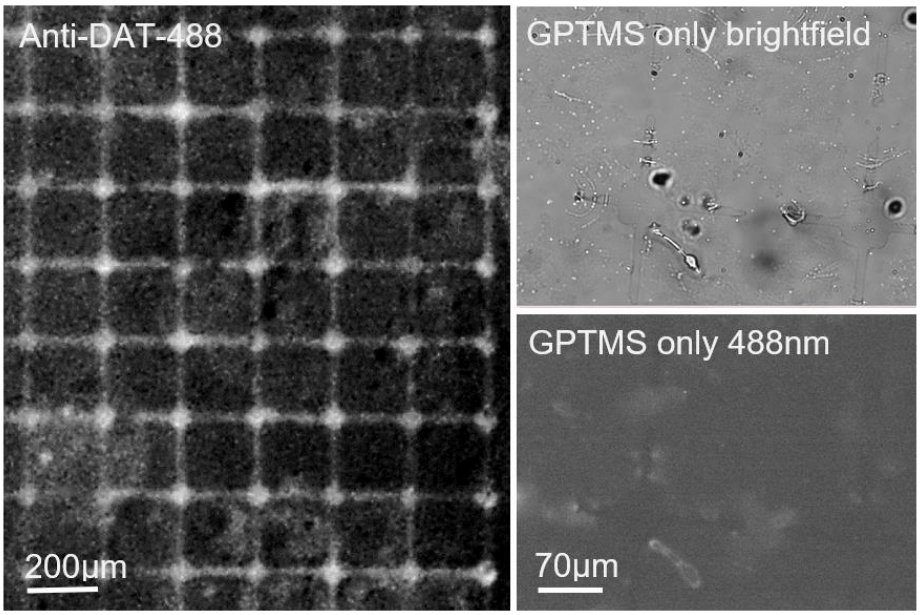

Figure 85. Functionalisation of anti-DAT-488 to a glass coverslip. A selected region of a GPTMS grid without antibody is shown by brightfield and 488nm excitation to show that the patterning is not from autofluorescence of GPTMS but specific to the functionalised 488 conjugated protein.

This novel biopatterning technique is inexpensive, requiring no specialist bioprinting methods or commercial coverslips unlike many other biopatterning methods (Czöndör *et al.*, 2013), and offers a one-reagent solution to functionalising glass coverslips with protein. In comparison to other methods it also offers a fast, reproducible covalent technique only requiring a reusable PDMS stamp, GPTMS and any protein of interest without the need for modification with a specific functional group.

The ability to pattern proteins that signal to cells, either as adhesion proteins or growth factors, offers a large number of applications for this versatile method. Previous examples of biofunctionalisation include binding adhesion proteins to coverglass to promote the adherence of specific cell regions such as pre- or post-synaptic compartments, so they are in the range of imaging by total internal reflection (TIRF) microscopy (Czöndör *et al.*, 2013). The localisation of signalling proteins to regions of a coverslip can provide a highly controlled microenvironment for cells. It was therefore considered whether functionalising substrates with specific growth factors

could be used to guide the differentiation of neural stem cells in a highly controlled manner, and to provide trophic support and favourable microenvironments for use in neural prosthetics.

9.3 The novel biofunctionalisation of grafts for neural prosthetics

Based upon literature findings, the two main challenges with stem cell therapies include 1) replicable and efficient differentiation of stem cells into the required lineage, 2) long-term survival of cells following implantation due to unfavourable host microenvironments. Previous studies used BDNF to increase differentiation of neural stem cells towards neuronal lineages; this differentiation was improved with functionalised BDNF as compared with BDNF free in the media (Ahmed, Reynolds and Weiss, 1995; Horne *et al.*, 2010a). Although BDNF increased cells with neuronal fate, it had no improvement of their long-term survival. Another study showed pre-treatment of cells with GDNF resulted in increased cell survival following implantation (Wang *et al.*, 2011). For this reason, BDNF and GDNF were functionalised to offer continual trophic support to stem cells, both to encourage replicable and highly efficient differentiation to mature neurons, and for long-term health and survival. Preliminary tests used plastic coverslips as an intermediate stiffness between glass and cellulose to determine whether BDNF and GDNF may have beneficial properties before adding a further variable of BC as a substrate.

BDNF and GDNF were patterned in 700 µm x 500 µm grids onto plastic coverslips as proof-of-concept that cell proliferation would occur specifically within biofunctionalised regions during early timepoints. As controls, IgG AlexaFluor®-647 alone was patterned, coverslips that had not been stamped with GPTMS were treated with BDNF and GDNF for an equal time to test for any effects of residual protein. Coverslips were also patterned in the presence or absence of laminin to allow cell adhesion, either with BDNF and GDNF functionalisation, with BDNF and GDNF in the cell medium, or without BDNF or GDNF.

Human neural stem cells were plated and imaged by Dr. Roberta Azzarelli. The cells were grown in the absence of EGF and FGF2 and fixed at DIV7. Cells were immunostained for MAP2 as a mature neuronal marker as well as Tuj1 as a postmitotic neuronal marker of differentiation.

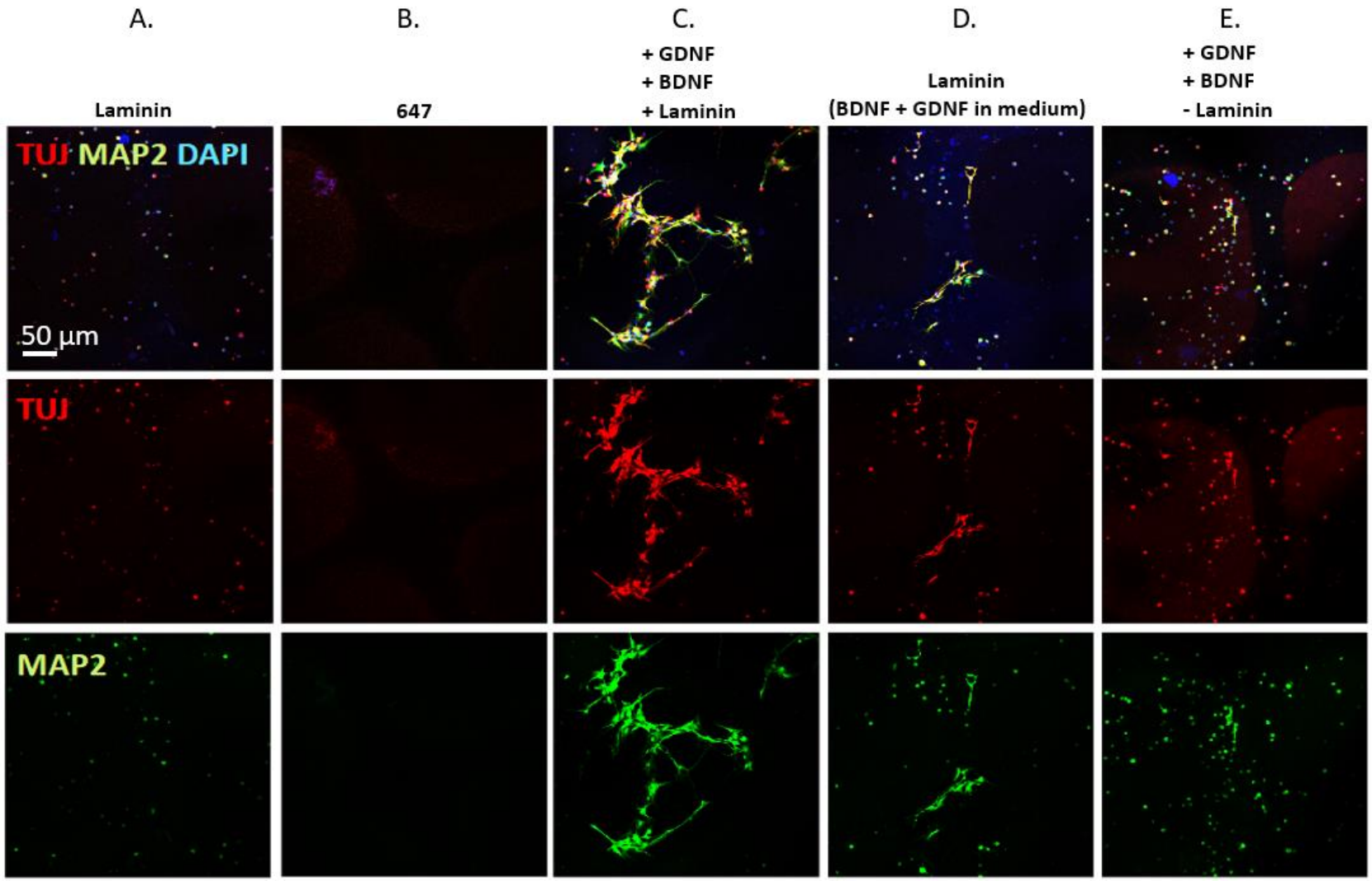

Figure 86. Human neural stem cells were grown to DIV7. A,B, E. Cells are unable to adhere and survive in the absence of BDNF + GDNF +laminin. C,D. BDNF, GDNF and laminin allow adhesion and survival of cells. C. The functionalisation of GDNF and BDNF improves neuronal fate and survival as determined by area of neuronal markers TUJ and MAP2. Image: Roberta Azzarelli.

As Figure 86 shows, when cells are grown in the absence of EGF and FGF2 in cell culture medium, BDNF, GDNF and laminin are required for the adhesion, differentiation and survival of cells to mature neurons. Although cells plated on coverslips functionalised with laminin initially adhere, they are unable to survive in the unconditioned medium, and detach or retract by DIV7, as shown by punctate staining. Cells plated on the functionalised AlexaFluor®-647-conjugated antibody grids are unable to adhere to the plastic coverslips, as shown by lack of staining. Cells plated on grids containing BDNF, GDNF and laminin are able to adhere to the coverslips, proliferate and form mature neurons by DIV7, as shown by the presence of MAP2 and Tuj1 positive cells with extended dendritic and axonal protrusions. Cells plated on grids containing only laminin, but with BDNF and GDNF added to the cell medium show that the cells are capable of adhering to the plastic coverslips; although the cells show increased protrusions and survival as compared with the laminin only condition, they show decreased survival as compared with functionalised BDNF and GDNF with laminin. The cells plated on coverslips functionalised with BDNF and GDNF but without laminin show that cells may be capable of attachment to the grid but are unable to grow protrusions of survive to DIV7 as shown by punctate staining. In this case, as compared to the negative control, AlexaFluor®-647-conjugated antibody condition, it appears cells are able to bind BDNF and GDNF for attachment, but unable to grow further in the absence of matrix proteins.

Due to the functionalisation of BDNF and GDNF (with laminin) improving the growth of neural protrusions, as compared with free BDNF and GDNF in the medium in our studies (n = 3) and previously shown (Horne *et al.*, 2010a), it was predicted that the cells would grow preferentially in the grid as compared with bare coverslip gaps in the grid. Additionally, the necessity of laminin for the growth and maturation of stem cells into differentiated neurons has been previously shown (Memanishvili *et al.*, 2016). This was further shown with brightfield imaging showing grid outlines, whereby protrusions of cells grew preferentially within grid boundaries, although adhesion of cell bodies did not necessarily occur in these locations (Figure 87).

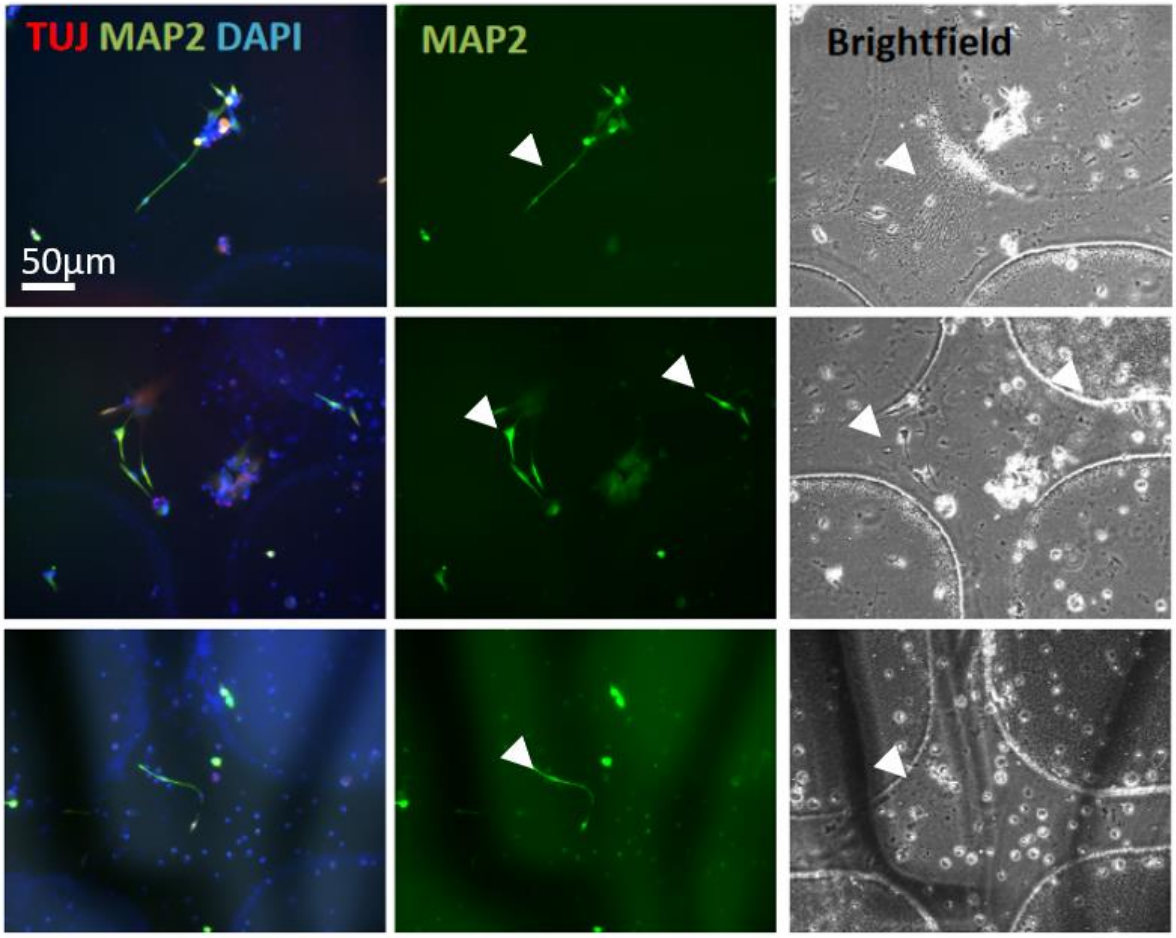

Figure 87. Preferential growth and maturation of neural stem cells on protein-patterned grids. Human neural stem cells plated on grids of functionalised BDNF, GDNF and laminin. Although the initial adherence of the cells occurred across the coverslip, the growth of MAP2 and Tuj1 protrusions remained within grid boundaries (white arrowheads). Image: Roberta Azzarelli.

Reproduceable trials between three coverslips (within one experimental repeat) showed the growth, differentiation and survival of human neural stem cells on functionalised BDNF, GDNF and laminin grids. Although no measurements were made to quantify differences in between precursor versus differentiation of cells between conditions, the main benefit from the biofunctionalisation of BDNF, GDNF and laminin was the ability of cells to survive and differentiate without any exogenous growth factors in the medium (analysis Appendix A.6). The method was therefore combined with BC biofunctionalisation as an improved technique for neural prosthetics to aid the survival of cells in diseased brain with limited trophic support. As the growth

of the cells was most successful within locations of functionalised protein, the BC was functionalised across the entire surface, and not in biopatterned locations, to improve neuronal outcome.

9.4 Functionalisation of bacterial cellulose for neural prosthetics

Bacterial cellulose (BC) was cultured by Sam Nehme and provided freeze-dried in PBS. The methods for functionalisation of BC were based upon previous literature that used never-dried cellulose fibres and nanocellulose and therefore needed to be adapted and shown as reproducible for use on large sheets of freeze-dried BC (Beaumont et al., 2018; Abdelmouleh et al., 2002).

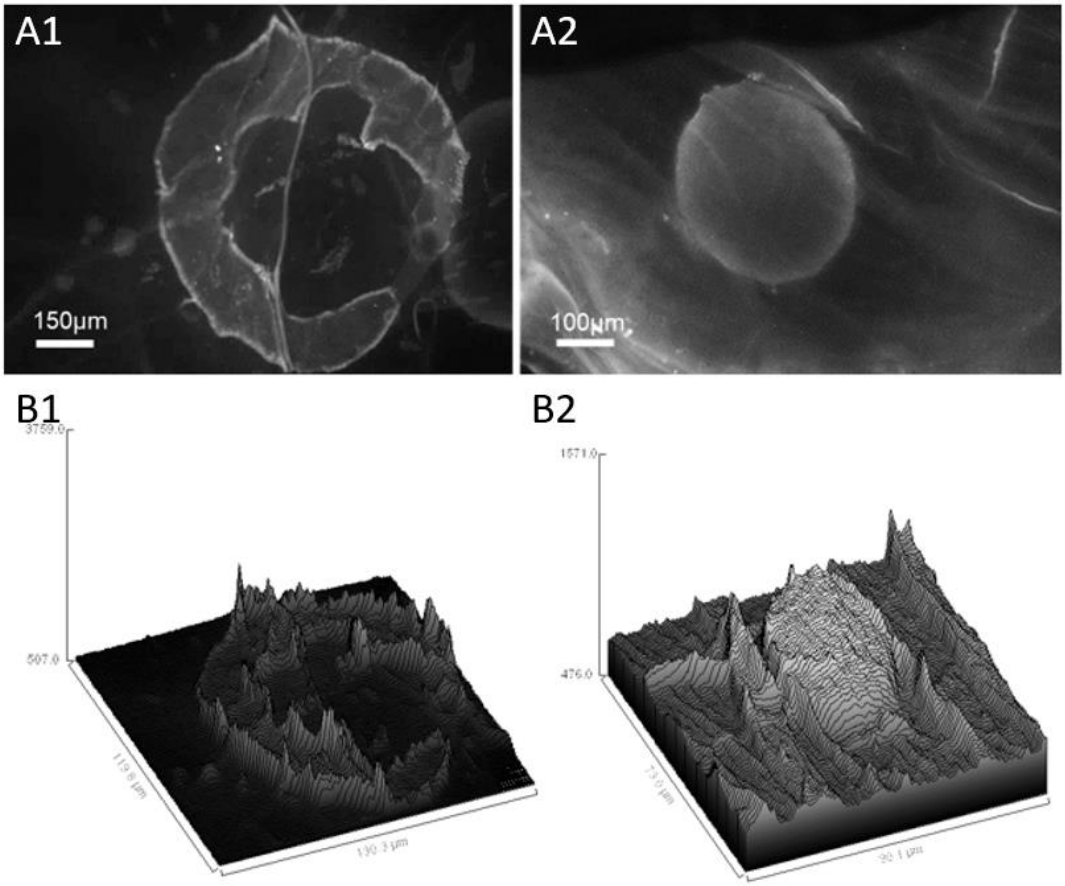

Figure 88. Functionalisation of cellulose with AlexaFluor®-488. Cellulose was modified by a pipette spot of antibody using two methods. A1: the conventional method, which involves curing of bacterial cellulose and rehydration resulted in cracking and breakage of the protein spot. A2: the 'one-pot' method did not require heating or full drying of cellulose before the

addition of protein and therefore maintained cellulose in its expanded structure, thereby preventing protein cracking. B1,B2: Surface fluorescence intensity profiles show an increase in intensity in regions where AlexaFluor®-488 has covalently bonded to cellulose.

Two methods for biofunctionalisation of cellulose were tested and both methods worked successfully. The conventional 'curing' method was a faster method, however resulted in hornification, temporary shrinkage of cellulose, and crosslinking reactions by the trivalent silanol; this resulted in cracking of the functionalised protein layer during rehydration in PBS (Beaumont *et al.*, 2018; Abdelmouleh *et al.*, 2002). Figure 88 shows a comparative sample from each method using AlexaFluor®-488-labelled antibody as an example protein where the spots illustrate the location that the protein was pipetted before 3x wash and imaging in PBS. The conventional method (Figure 88 (left)) shows cracking and breakage of the functionalised protein that is likely to occur following rehydration due to the expansion of cellulose. The conventional method is therefore invasive compared with the 'aqueous one-pot silanisation' method (Beaumont *et al.*, 2018) whereby the cellulose maintains some level of moisture due to incomplete drying prior to the addition of protein. The 'one-pot' method therefore does not show fractures in the protein following full rehydration in PBS (Figure 88 (right)). Due to the wet environment of the brain, where the prosthetic would be inserted in patients, it is important that the method is compatible with rehydration following modification without damage to the desired structure, or patterning. Although specific patterning may not be necessary depending on the use of the biofunctionalisation of cellulose, it is still important that there is not risk of protein breakage once the implant is inserted, which could result in large protein clumps in the brain. For this reason, the 'one-pot' method was selected for further neural prosthetic applications.

9.5 Functionalisation of bacterial cellulose with growth factors for neural stem cell differentiation and survival

This section is based on $n = 1$ data for growing stem cells on bacterial cellulose. Analysis therefore uses data pooled from technical repeats.

Following the successful functionalisation of bacterial cellulose (BC) with protein, it was determined whether BC sheets were biocompatible for the growth of stem cells. Alongside biocompatibility, it was of interest whether functionalisation of BC with BDNF, GDNF and laminin would enhance the differentiation of stem cells into mature neurons in the absence of any other exogenous growth factors. As controls, stem cells were plated onto a laminin coated plastic dish or laminin coated BC in the presence of growth factors EGF and FGF2 to show that there was no effect of BC on stem cell proliferation (Figure 89 (A, B)). For analysis see (Appendix A.7). Alternatively, cells were plated onto BC that had been biofunctionalised with BDNF, GDNF and laminin, or laminin-only, in the absence of exogenous growth factors in the medium (Figure 89 (C, D)). Only a small number of cells survived on the laminin-only coated BC in the absence of BDNF as compared to laminin-only with exogenous growth factors (Figure 89 (B, D)). The number of cells that survived and differentiated into postmitotic neurons by DIV7, as measured by the area of Tuj1 immunofluorscence, in the absence of growth factors was significantly increased on BC biofunctionalisation with BDNF, GDNF and laminin as compared with laminin-only (Figure 89 (C, D)).

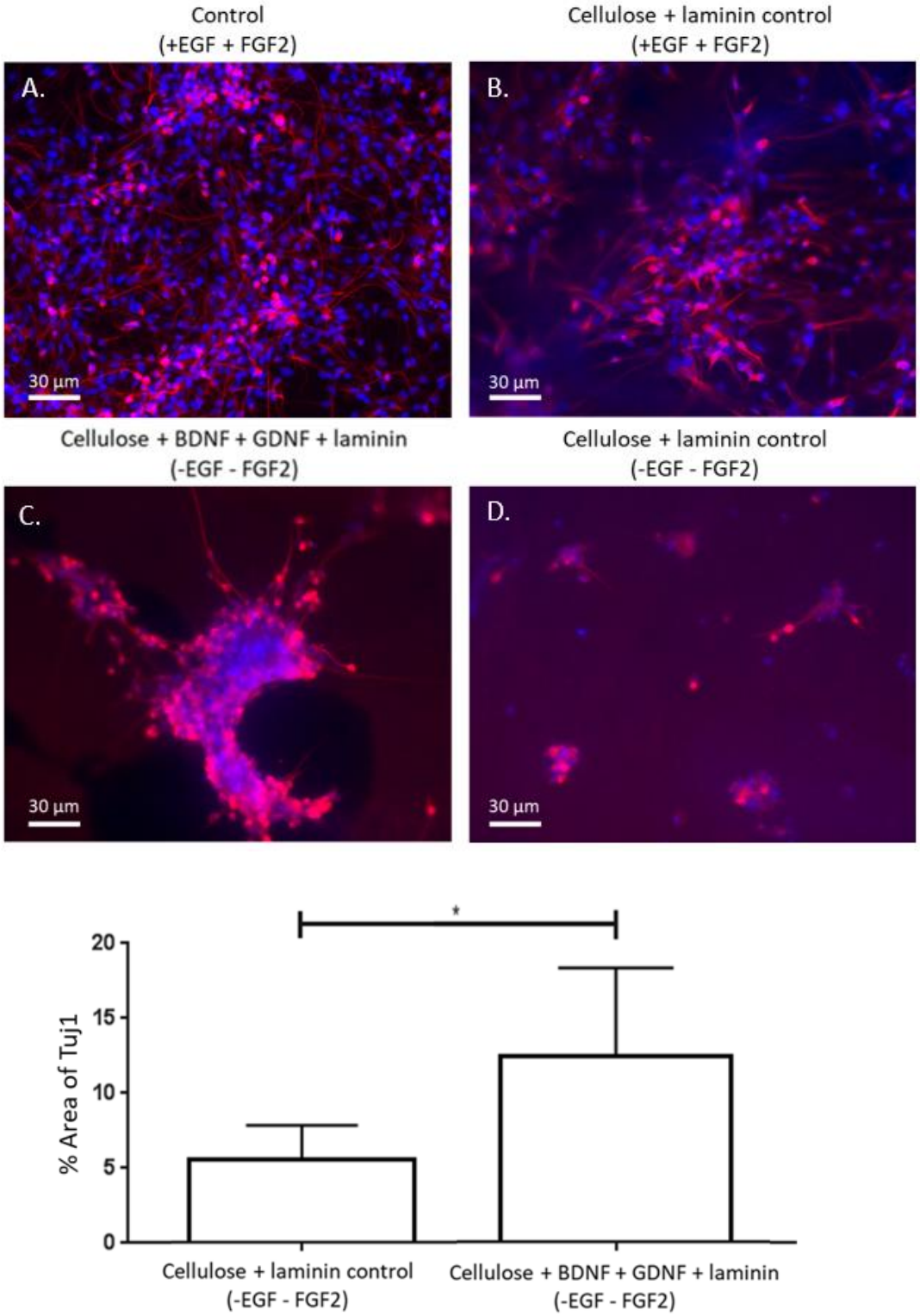

Figure 89. Cells plated onto BC were able to grow axonal and dendritic protrusions and develop into mature neurons as shown by Tuj1 immunofluorescence (red). (A, B) BC did not affect the area of Tuj1 as compared to plastic dishes in the presence of exogenous growth factors, EGF and FGF2. (C, D) In the absence of EGF and FGF2, BC biofunctionalisation

with BDNF, GDNF and laminin significantly increase the area of Tuj1 as a measure of neuronal growth and differentiation into postmitotic neurons (*$P = 0.0455$; $t = 2.168$; d.f. = 16; two-tailed unpaired *t*-test). Experiments were performed from $n = 1$ experimental repeat, with $n >= 4$ images per repeat, yielding similar results. Mean values with standard deviation are plotted). Images captured by Roberta Azzarelli, figure and analysis by author.

Due to high background from excitation of cellulose with the 488 nm laser due to autofluorescence, it was not possible to analyse the mature neuronal marker MAP2 from cells grown on BC due to the secondary antibody emission corresponding to this spectra (Appendix A.8). This prevents the ability to make direct comparisons into cells that form mature neurons for each condition. For this reason, the percentage area of Tuj1 intensity across each image was used as a measure of neuronal growth and differentiation into postmitotic neurons. Cells that were unable to adhere and grow resulted in no, or small rounded spots of Tuj1 intensity and therefore a small intensity area compared with cells that adhered and grew protrusions. This was interpreted as a suitable method following significantly different percentage area measurements of negative controls (the presence of only laminin or exogenous growth factors) as compared with positive controls (the presence of laminin and exogenous growth factors; for analysis see Appendix A.10).

Although cells were able to survive to DIV7 in conditions without growth factors in the medium, it resulted in more clustering of cells compared with conditions with growth factors. Clustering of cells may attempt to limit the diffusion of trophic support from paracrine signaling by decreasing the distance the factors need to diffuse to reach neighbouring cells following secretion to compensate for lack of exogenous growth factors in the cell medium. Clustering may therefore be reduced in future experiments by applying smaller volumes of culture medium to cells to increase the concentration of secreted factors in the medium. However, in comparison to laminin-only BC without growth factors, the BDNF, GDNF and laminin BC had greater cell growth and protrusions connecting clusters of cells. Although cells formed large clusters, on the BDNF, GDNF and laminin BC, these populations had long protrusions extending between them. The main interpretation of these results is therefore that biopatterning of BDNF and GDNF with laminin significantly increases the survival and differentiation of neurons as measured by percentage area of Tuj1 (Figure 89, see Appendix A.11 for pooled $n = 2$ data between plastic coverslips and cellulose). From these measurements alone we cannot claim that when growth factors are available in the medium, in the presence of laminin coating, patterning of GDNF and BDNF has any

significant advantages. However, using EGF and FGF in the cell medium encourages self-renewal and can result in differentiation of stem cells at high confluency, therefore this is not a direct comparison to use as a positive control for biofunctionalised cellulose in the absence of EGF and FGF. Experiments therefore need to be repeated using BDNF and GDNF in the medium to show whether survival and maturation is comparable to when these factors are biofunctionalised. Based on previous results we would expect maturation and Tuj1 positive cells when BDNF is free in the medium versus functionalised (Horne et al., 2010). As next steps, it would be of interest to compare the growth, maturation and survival of these cells over longer (~30 days) time periods and whether cells remained in clusters during these periods or formed more homogenous networks. Alternatively, a specific survival assay such as MTS could be used as a direct measure of proliferation. Previous work has shown that although BDNF can result in a twofold increase in neuronal number at DIV10, this is significantly reduced after DIV21 as the one-off BDNF treatment did not improve cell survival (Ahmed, Reynolds and Weiss, 1995). It would therefore be of interest to determine whether the combined functionalisation of GDNF improves survival of neurons at DIV21. The biofunctionalisation of BC with BDNF and laminin alone resulted in a significantly smaller percentage area of Tuj1 staining at DIV7 as compared with combined functionalisation of GDNF, BDNF and laminin. However due to lack of experimental repeats the contribution on GDNF to differentiation and survival at DIV7 to DIV21 will need verification and is therefore provided as preliminary data in Appendix A.9. Alongside this, we have not determined the maturity of these neurons by electrophysiology measurements. Stimulating and recording from these cells would be important to show that following differentiation, mature neurons are capable of firing and responding to action potentials and therefore capable of integrating into the brain of patients with neurodegenerative conditions.

9.6 Chapter 9 Summary

From this project, a biopatterning technique has been developed through the combination of microcontact printing using PDMS stamps with the functionalisation of protein using epoxysilane. The finding that this method can be used to pattern growth factors has resulted in a novel application of functionalising bacterial cellulose (BC) for enhanced neural stem cell prosthetics. The functionalisation of cellulose is not limited to the proteins, BDNF and GDNF, used in this study but can be substituted for any protein of interest with an exposed amine or hydroxyl group. There are multiple applications arising from this project that will be valuable directions for future research. However, several hurdles still exist with stem cell implantation treatment including the implantation method into the brain, and survival in diseased environment. Although the growth factor-functionalised scaffolds aim to improve the local environment of the cells that may have poor neurotrophic support, the protection of the cells against amyloid pathology must also be considered. Neural stem cell treatment has already shown promise in AD particularly through the neurotrophic release of BDNF (Blurton-Jones *et al.*, 2009; Jiao *et al.*, 2016). However, stem cells do not reduce or reverse tau pathology or prevent further spreading of toxic species of tau capable of seeding pathology inside of healthy cells or the stem cells themselves. Stem cell graft used in Parkinson's studies have shown mixed amounts of Lewy body pathology. It appears that evident Lewy body pathology can take ~10 years to begin in grafted cells (Li *et al.*, 2016). However, it is unknown whether cell death masks the true infection of these cells. Estimates suggest stem cell implantation provides ~15 – 18 years of clinical benefits post-graft, which in some cases may be sufficient (Kefalopoulou *et al.*, 2014). Studies have used genetically-engineered stem cells to prevent infection of stem cells with amyloid seeding through using knock-out of the endogenous amyloid, such as *SCNA* for alpha-synuclein (Chen *et al.*, 2019). This is based upon findings that exogenous seeds combine with endogenous protein to cause pathology. Due to the relatively long timescale through which graft pathology occurs, this may not be an immediate concern for the development of neural prosthetics technology. In addition to this, stem cell implantation is currently an invasive treatment, as cells must be able to access the lesion area inside of the CNS.

Stem cell implantation is therefore a relatively late treatment used once final stages of pathology have occurred including mass cell death. Although invasive, stem cell treatment could provide a long-term source of neurotrophic factors in the brain; many studies have looked at BDNF as a treatment for neurological disorders but a difficultly is that only limited amounts of BDNF can cross the blood–brain barrier. AAV-BDNF treatment has also been suggested but viral treatments are currently restricted in human use. Functionalisation of scaffolds to promote stem cell health following implantation may therefore be a viable treatment for late stage therapy (Nagahara and Tuszynski, 2011; Jiao *et al.*, 2016). Treatment that can help prevent the progression of AD at mild cognitive impairment (MCI) and initial Braak stage I, before significant symptoms occur may therefore be the optimal way to prevent later stages of AD or provide a cure. Immunotherapy therefore offers an alternative, early stage treatment to prevent progression of pathology through synaptic connection to distal brain regions and stop further symptoms rather than alleviate behavior at late stages.

Alongside improvements on these hurdles, multiple other applications and advancements on this work can be continued in future research. Although this project looks to develop a prosthetic that can reproducibly differentiate stem cells into neurons for implantation by offering an enriched survival-promoting environment, other applications are also possible. Functionalisation of immunosuppressants to the scaffolds for slow local release in the brain has also been suggested. This would offer the key benefit of protecting the xenograph from causing an immune response during initial transplantation into the brain. Biopatterning proteins can also be an effective method to study the differentiation of stem cells into populations of neuronal subtypes. Specifically patterning adhesion proteins into locations of interest it could be possible to grown networks of cell subtypes in a single culture dish as factors do not need to be added to the cell medium and therefore do not produce a homogenous population. This could be interesting for organoid growth of modelling layers of the cortex. This biofunctionalisation method could also be combined with the PhD thesis of Sam Nehme, which looks to insert conductive nanoparticles into cellulose. The conductive nanoparticles embedded in cellulose will be used to understand how the maturity of neural stem cells is related to electrical stimulation. Biopatterning proteins including adhesion proteins or growth factors, in combination with signals through electrical conduction may help us to better understand how these factors interact during the development of cell networks. This knowledge may help us to understand the optimal environment that is required for differentiating

neural stem cells for transplantation into the human brain to provide trophic and stimulation as support.

A collaboration with Dr. Venkat Pisupati and the group of Professor Roger Barker will continue to investigate the use of bacterial cellulose as a matrix for stem cell implantation. The long-term aim of the work is to find suitable methods of dopaminergic stem cell therapies for Parkinson's disease through translational studies from cell culture to rodent models to human patients. Although this project has investigated the biocompatibility of BC by using it as a substrate to plate and differentiate neurons on, the immunogenic properties still need to be confirmed. As the cellulose is produced by bacteria which incase themselves inside of the macrosheets as a method to float near the surface of water for aerobic respiration, it is important that the bacteria are thoroughly stripped from the cellulose before patient use. Some bacterial components including carbohydrates such as the cell wall and lipopolysaccharide, which *Gluconacetobacter hansenii* (G. *hansenii*) produce as they are a Gram negative bacterium. Therefore, as well as confirming there are no immunogenic components of the bacterium remaining as a biproduct of the cellulose macrosheets, it is important to confirm the pure BC structure is also safe for human use. Once BC has been confirmed as safe to use, comparisons on plain versus biofuncitonalised cellulose to improve cell survival can be explored.

The aim of this project was to make an enhanced stem cell scaffold for use in neurodegenerative disorders such as Alzheimer's disease and Parkinson's disease. Biofunctionalisation of the biocompatible scaffold material, bacterial cellulose, was used to reproducibly differentiate neural progenitor cells into mature neurons and offer an enriched survival-promoting environment following implantation into diseased tissue. The biofunctionalisation of BDNF, GDNF and laminin have shown that immediately after the derivation stage it is possible to differentiate progenitor cells into postmitotic neurons within 7 days as opposed to 2-4 weeks as in the method this study was based on (Sun *et al.*, 2008). Results are being repeated with BDNF and GDNF only in the medium to compare the effect of free versus functionalised factors. Improved cell survival and differentiation of neural stem cells was shown in medium lacking growth factors. Expression of mature neuronal marker (Tuj1+) was over a significantly higher substrate area within 7 days of plating onto the biofunctionalised scaffold as compared with cells on scaffold alone. This biofuncitonalisation method can therefore also be used to reduce costs as it requires less expensive

growth factors to be added to the culture medium for a differentiation protocol. It also shows proof-of-concept for improving stem cell survival and differentiation in a diseased environment where available trophic support cannot be sustained by local tissue and would instead be supplied by the scaffold or implanted cells themselves. Novel contributions from this chapter therefore include:

- Biopatterning coverslips with a 4 hr epoxysilane method using microcontact printing (though the epoxysilane method itself has been published)
- Functionalising freeze-dried and sheet cellulose, as opposed to fresh nanoparticles (though the acid-base silanisation method itself has been published).
- Functionalising sheet cellulose for stem cell scaffolds
- Functionalised BDNF and GDNF causing increased stem cell differentiation in the absence of growth factors in the medium.

CHAPTER 10

10.1 Conclusion and future directions

Section 1 focussed on better understanding the causes and cellular pathways involved in the aggregation of exogenous monomeric tau protein that is internalised by neurons. The section aimed to unite the finding from the group that pH causes tau aggregation (Michel *et al.*, 2014), with work from literature showing that neuronal activity increases the rate of tau pathology (Wu *et al.*, 2016). The results from Section 1, taken together with aggregation data from Section 2, based on the hypothesis discussed in Section 1.2, are shown in Table 1.

Table 15. Amended from Table 1 (Section 1.2). Summarises the experimental results aimed at understanding the relationship between pH and neuronal activity in the aggregation of monomeric exogenous tau.

Variable	pH	$[Ca^{2+}]$	Neuronal stimulation
Hypothesis	Tau aggregation is dependent upon low pH	Increased calcium concentration increases tau aggregation	Neuronal stimulation increases tau aggregation
Method	Fluorescence lifetime microscopy Ammonium chloride A calibrated dextran-OG514 lifetime sensor	Fluorescence lifetime microscopy Chemical treatment	Fluorescence lifetime microscopy Chemical treatment Optogenetics
Results	**Tau aggregation is pH dependent and neutralising the pH of endo/lysosomes reduces tau aggregation. Low pH**	Calcium ion concentration does not affect the aggregation of internalised monomeric tau.	Chemically induced neuronal stimulation does not affect the aggregation of up-taken monomeric tau.

	without cellular uptake may cause tau to aggregate, but at a slower rate.		**However, optogenetic stimulation of neurons increases the measured aggregation of tau.**

As discussed in Section 1.5.1., a key question about the activity-dependence of tau pathology was whether the initial aggregation of tau is a passive or an active mechanism. A passive mechanism would result from monomeric tau forming aggregates based upon the various environments that it is exposed. During extracellular uptake into endolysosomal vesicles this would include concentration changes in H^+ and Ca^{2+} ions. An active mechanism would mean that exogenous Tau is able to seed aggregation of endogenous Tau which may occur during cytoskeletal rearrangement of vesicle trafficking. As part of my work, I show that Ca^{2+} ions alone are not enough to drive the initial aggregation of exogenous monomeric tau protein. Cellular uptake into low pH vesicles is the responsible component for formation of tau aggregates, as aggregation is significantly decreased following neutralisation of endolysosomes. However, some cellular component appears to catalyse this aggregation at faster rates than measured *in vitro* without cellular uptake. It remains to be determined whether this is due to cellular or vesicular confinements. In line with the above, neuronal activity increases the measured aggregation, likely through an active mechanism involving increased endocytic entry of tau into low pH compartments or trafficking seeding-capable aggregates along axons and between acceptor cells to enhance aggregation (Na Yu, Dr. Colin Hockings, unpublished data), if not both to different extents. Although it is possible that stimulation increases the rate of endocytic uptake of tau, though this would mostly occur through synaptic clathrin-mediated or bulk endocytosis and may not be the predominant aggregation effect measured (Cheung et al., 2010). We have not yet been able to separate the contribution of any activity-dependent increased uptake and thereby aggregation of tau, versus trafficking and propagation. The model we suggest is that exogenous monomeric tau requires cellular uptake into low pH compartments to catalyse aggregation followed by an activity-dependent increased rate of formation, or size of aggregate following translocation. Without combining ammonium chloride treatment with optogenetic stimulation, we cannot rule out that neuronal activity cannot directly initiate aggregation of monomeric tau.

Future work in this section could further optimise the use of the pH sensor dextran-OG514 in neurons for understanding the pH and aggregation of tau on a per-vesicle level. This could be particularly useful to show whether pH ~5.3 inside of cellular endosomal compartments is sufficient to induce aggregation, which was not the case without cellular uptake over 24 hr (Chapter 3). Alongside this, more tests to better understand the time-course of tau aggregation at low pH, including incubation of tau from 4 hr-24 hr to determine how long it takes to aggregate at pH 4.5 without cellular uptake. To show that the increased aggregation of tau following neuronal stimulation is pH-dependent, these experiments could be repeated with the addition of 10 mM ammonium chloride to the cell medium.

Section 2 continues to discover a pathological phenotype that can link the aggregation of tau at low pH, and its activity-dependent increase, to early synaptic dysfunction correlating to memory impairment seen in mild cognitive impairment and Alzheimer's disease. Hallmarks of pathology are explored from 2 diverse angles by using measurements of mechanical and electrophysiological cell properties as discussed in Table 16.

Table 16. Amended from Table 2 (Section 1.2). Shows the results from the experiments hypothesised to reveal pathological phenotypes following neuronal internalisation and aggregation of monomeric exogenous tau.

Phenotype	Mechanical	Electrophysiological
Hypothesis	Stiffness of neurons is decreased by tau aggregation following microtubule destabilisation	Tau aggregation is activity-dependent Activity-dependent impairment to synaptic function
Method	Atomic force microscopy (AFM)	Fluorescence lifetime microscopy Whole-cell patch-clamp recordings Optogenetics Microelectrode arrays

Novel technology developed	N/A	Microfluidic culture chips Optogenetic stimulation device Microelectrode arrays (contributed)
Results	Exogenous monomeric tau has no effect on cell stiffness	**Exogenous monomeric tau causes activity-dependent depression of synaptic activity**

This section has shown that exogenous monomeric tau does not alter mechanical properties of neurons as measured using atomic force microscopy following 4 hr incubation, whereas exogenous monomeric tau causes depression of synaptic activity within 2.5 hr of repeated neuronal stimulation. How this activity-dependent impairment to synaptic transmission occurs is still being tested. We predict that the mechanism does not arise through increased aggregation alone, but more likely activity-dependent translocation or disruption to a synaptic mechanism. The question remains whether neuronal activity causes translocation of tau into synaptic compartments. If transportation to synapses occurs, this could be through the escape of tau from vesicles in monomeric or aggregated form, or via activity-dependent transport of lysosomes into post-synaptic compartments (Goo *et al.*, 2017; Padamsey *et al.*, 2017). Lysosomal dysfunction alone has been shown to cause pre-synaptic impairment and attenuation of the synaptic vesicle cycle without the need for transportation of lysosomes into synapses (Sambri *et al.*, 2017).

Therefore, to follow from the previously mentioned model, exogenous monomeric tau requires cellular uptake into low pH compartments to catalyse aggregation followed by an activity-dependent increased rate of formation, or size of aggregate following translocation. In the case of increased rate of formation, this would be direct uptake and aggregation in synapses by clathrin-mediated and bulk endocytosis, resulting in synaptic impairment. If translocation, this could allow a further aggregation of tau during trafficking into synaptic compartments to result in impairment. If dysfunction is purely pre-synaptic this could be through lysosomal dysfunction causing synaptic impairment.

Future work could include determining whether all pathological effects of internalised exogenous monomeric tau are activity-dependent. Exogenous monomeric tau does not affect the stiffness of neurons, a next step could be to determine whether stiffness is affected when neurons are treated with tau in the presence of neuronal stimulation. It is possible that there is an unbinding of tau from microtubules that is also an activity-dependent process leading to impaired transport and structural integrity. Alternatively, it is possible that the structural role of tau as a microtubule binding protein is not directly responsible for deficits seen, at least during early stages of pathology.

As a future step to understanding the pathological mechanism leading to depression of synaptic transmission, it is important to determine which pathways are affected following neuronal activity in the presence of exogenous monomeric tau. An initial question is whether tau species that cause this pathophysiology are in aggregated form. To determine this, tau-treated neurons should be to stimulated in the presence of ammonium chloride to limit the aggregation of tau during the 2.5 hr protocol. Additionally, the involvement of NMDARs is an important aspect of this pathophysiology and should be tested by using an NMDAR antagonist such as AP5 during stimulation. This is relevant for understanding whether the stimulation protocol induces LTP in stimulated control cells, and whether tau-treated and stimulated cells show an opposite NMDAR-dependent depression. If these results show that tau can mediate impairment to LTP, it will be in agreement with previous models in the literature that do not use FTD missense mutant forms of tau (Polydoro *et al.*, 2009; Fá *et al.*, 2016; Koch *et al.*, 2016). An impairment in LTP and imbalance of LTP towards LTD would be the *in vitro* equivalent to *in vivo* research by Koch et al., (2016) in human AD patients to understand memory impairment using theta burst stimulation with transcranial magnetic stimulation. Whether this pathology is expressed pre- or post-synaptically (or both) will also be determined to further clarify the mechanisms that may be involved. From previous literature it appears likely that either the synaptic trafficking, scaffolding or cycling of proteins or vesicles required for plasticity are impaired during early stages of tau pathology. This could either be through direct entrance of tau into synaptic compartments or through lysosomal dysfunction (Ittner *et al.*, 2010; Warmus *et al.*, 2014; Tracy *et al.*, 2016; Miyamoto *et al.*, 2017; Sambri *et al.*, 2017; Suzuki and Kimura, 2017; Zhou *et al.*, 2017; McInnes *et al.*, 2018; Shrivastava *et al.*, 2019). Although this may not be the only pathophysiology that exogenous monomeric tau causes, it may be the first phenotype to express itself so evidently following neuronal activity.

Section 3 aims to use the knowledge gained from section 1 and 2 to provide new and effective treatments for Alzheimer's disease (AD). Again, this is approached from 2 diverse angles as discussed in Table 17 that may work well as complimentary treatments to target different aspects of the disease progression.

Table 17. 2 Novel therapies were developed for the treatment of Alzheimer's disease based on immunotherapy and neural prosthetics.

Treatment	**Metal-organic frameworks for anti-tau immunotherapies**	**Biofunctionalisation of bacterial cellulose for neural stem cell prosthetics**
Treatment method	Bind and remove exogenous monomeric tau protein	Cell replacement therapy with an enhanced BDNF and GDNF local environment
Novel aspect	Therapeutic antibody grafted to a metal-organic framework (MOF-Ab)	Biofunctionalisation and use of bacterial cellulose to enhance differentiation and survival for stem cell scaffolding.
Results	**Both forms of antibody, IgG and Fab are internalised into neurons on binding tau protein.**	**Freeze-dried sheets of bacterial cellulose can be functionalised with growth factors. This promotes the survival and maturation of neural stem cells into neurons.**

There is much discussion in the field about the need for multiple treatments at different stages of AD progression to target contributing factors of pathology. This section has shown the proof-of-concept for 2 novel therapeutic strategies for the treatment of AD at pre-symptomatic and early stage, or late clinical stages.

In pre-symptomatic or mild cognitive impairment cases during the earliest stages of pathology, and for high risk genetic cases or following traumatic brain injury, we recommend tau immunotherapy as a preventative medicine to inhibit further pathology. Our metal organic framework tethered with antibodies (MOF-Ab) aim to prevent initial monomeric tau uptake before the stage of aggregation and the formation of tau species capable of seeding further pathology.

This treatment is therefore a preventative measure and its ability to work at later stages to inhibit the spread of small aggregates is unknown due to its C-terminal of tau paratope. Therefore, if sufficient tau enters cells and begins to form toxic species capable of seeding pathology, which spread to distal brain regions and cause late stage neurodegeneration and cell death, stem cell therapy may be a suitable means. Neural stem cell therapy has already shown promise in AD particularly through the neurotrophic release of BDNF (Blurton-Jones *et al.*, 2009; Jiao *et al.*, 2016). To improve long-term survival of stem cells, scaffolds containing protein growth factors have been developed. These cells show improved survival and maturation into neurons as compared with cells grown on cellulose in the absence of growth factors. However, stem cells are unable to reverse tau pathology or prevent further spreading of pre-existing species of tau seeding pathology in neighbouring brain areas. Therefore, anti-tau immunotherapy may be a combinative method to prevent further tau pathology inside of stem cells that form synaptic connections with diseased cells, and distal networks that do not receive paracrine signalling directly from implanted cells.

As future work on this project we are repeating the results at DIV 7 showing that the area of Tuj1 is greater when stem cells are grown on biofunctionalised scaffolds as compared to cellulose alone. An additional control condition will be added with BDNF and GDNF in the medium instead of EGF and FGF2 for an unfunctionalised cellulose scaffold. This will offer a more suitable control as compared with EGF and FGF2 in the medium, which causes self-renewal and eventually differentiation of cells at high confluency and therefore is not an accurate representation of these measures compared to conditions without EGF and FGF2. We will also repeat specific cell survival assays at DIV 7 and DIV 30 to quantify this more specifically. Alongside this, at DIV 30 we will repeat Tuj1 staining to quantify cells that survived to specifically differentiate into mature neurons between conditions. In these studies, although we provide proof of concept for the benefits of biofunctionalised cellulose scaffolds, the long-term survival in diseased brain with low trophic support, high cell death, and amyloid pathology, has not been thoroughly explored. Once immunogenicity results and long-term survival are shown in vitro, translational studies will be further explored, including functionalisation of other important factors or immunosuppressants.

10.1.1 Novel technology development and characterisation

Alongside these original findings, technology was developed or characterised as part of this project for future continuation on this work. Novel technologies were developed in Section 1 & 2 to help progress our understanding of tau pathology in AD including microfluidic chips for patch-clamp electrophysiology and an optogenetic stimulation device, OptoGenie; in section 3, novel technologies were developed to contributing this knowledge gained from section 1 & 2 towards an effective treatment. These include the concept of MOF-grafted therapeutic antibodies, a novel microcontact printing biofunctionalisation technique, and an enhanced stem cell scaffold.

10.2 Summary of key findings

Section 1: Understanding pH and neuronal activity for the aggregation of monomeric tau

- Exogenous monomeric tau has no effect on the stiffness of neurons
- The aggregation of exogenous monomeric tau is dependent upon low pH and neuronal activity but not calcium concentration directly

Section 2: a pathological phenotype for exogenous monomeric tau

- The pathiophysiology of exogenous monomeric tau is dependent upon neuronal stimulation
- It is still unknown how exogenous monomeric tau exerts its pathological effects following stimulation, though may be related to an activity-dependent increase in aggregation or synaptic localisation, though further studies are required.

Section 3:

- Therapeutic antibody (full-sized IgG and antigen-binding fragment (Fab)) is internalised by neurons in complex with tau protein. Grafting antibody to metal-organic frameworks

(MOF-Ab) may prevent pathology by clearing monomeric tau before it is taken into cells where it aggregates at low pH.

- Bacterial cellulose can be used as a cell scaffold for neural prosthetics whereby biopatterning with growth factors enhances the survival and differentiation of neural stem cells to neuronal lineage at early stages. This may provide a beneficial local environment directly following transplantation into diseased tissue.

Put together these original findings suggest that pH is responsible for the aggregation of monomeric tau taken up by neurons. However, the pathophysiology of exogenous tau is dependent upon neuronal stimulation which results in depression of neuronal response. The method through which the stimulation of tau-treated neurons results in pathology is still unknown. It is exciting that this finding may explain why neurons of the entorhinal cortex and hippocampus are particularly vulnerable to tau pathology. If neuronal stimulation frequencies that increase the Ca^{2+} conduction in synapses commonly occurs in these anatomical regions as processes in learning and memory it is possible that these same mechanisms are susceptible to tau pathology and result in the synaptic impairment that we see in patients.

From these findings, two avenues of therapeutic treatments are suggested. One method is for early-stage treatment to prevent the uptake of the protein tau in the extracellular space before it is taken up by cells and aggregates at low pH. The second method uses neural stem cells to provide the neurotrophic factors, such as BDNF, and signalling that is lost following neurodegeneration in the diseased AD brain. A scaffold method provides growth factors to support the local environment of implanted cells. A combination of immunotherapy and stem cell implantation is suggested as a long-term effective treatment to protect implanted cells from protein pathology. This project therefore found a novel pathological phenotype for exogenous monomeric tau protein, and suggests interventions suitable for the prevention or treatment of progressing clinical stages of AD.

APPENDIX

A.1 The experimental repeats for measurements of the fluorescent lifetime of tau in the presence or absence of the weak base ammonium chloride. *n*=3 show lower measurements for each group due to developments to the FLIM system in this time period.

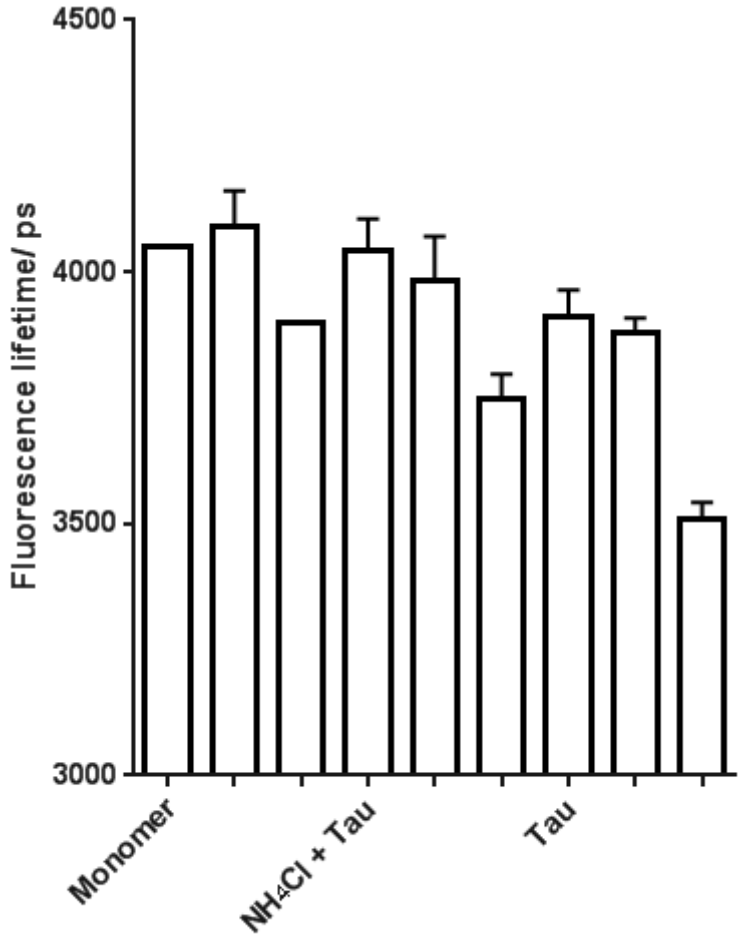

A.2 Pixel-wise analysis of the fluorescence lifetime of tau across the whole image (not correlated by pixels for dextran-OG514).

$P = 0.0645$; $t = 1.925$; d.f. = 2; two-tailed unpaired t-test). Experiments were performed from $n = 3$ experimental repeat, with $n > = 2$ images per repeat, yielding similar results.

A.3 Code loaded onto the Arduino Uno for the optogenetic stimulation of neurons

This example code is in the public domain.

```
  */
int blue_laser = 9;

// the setup routine runs once when you press reset:
void setup() {
   // declare pin 9 to be an output:
   pinMode(blue_laser, OUTPUT);
}

// the loop routine runs over and over again forever:
void loop() {
   digitalWrite(blue_laser, HIGH);
   delay(10);
   digitalWrite(blue_laser, LOW);
   delay(33);
   digitalWrite(blue_laser, HIGH);
   delay(10);
    digitalWrite(blue_laser, LOW);
   delay(33);
    digitalWrite(blue_laser, HIGH);
   delay(10);
   digitalWrite(blue_laser, LOW);
   delay(10000);
   }
```

A.6 The biofunctionalisation of coverslips with BDNF, GDNF and laminin increases the survival and differentiation of neurons in the absence of exogenous growth factors, as measured by the percentage area of Tuj1 intensity (one-way analysis of variance (ANOVA); ****$P < 0.0001$; F (4,8) = 28.64). Tukey's multiple comparison P values (+lam -GF (A), -lam -GF (B), -lam +GF (C), lambdnfgdnf-GF (D), +lam+GF (E): (A-B) not significant (NS) > 0.9999; (A-C) NS = 0.9968; (A-D) *P = 0.0163; (A-E) ****$P < 0.0001$; (B-C) NS = 0.9997; (B-D) *$P = 0.0384$; (B-E) ***P = 0.0002; (C-D) NS = 0.0512; (C-E) ***P = 0.0002; (D-E) **P = 0.0020. Experiments were performed from $n = 1$ experimental repeat with n >= 2 technical repeats per experiment. Mean values with standard deviation are plotted).

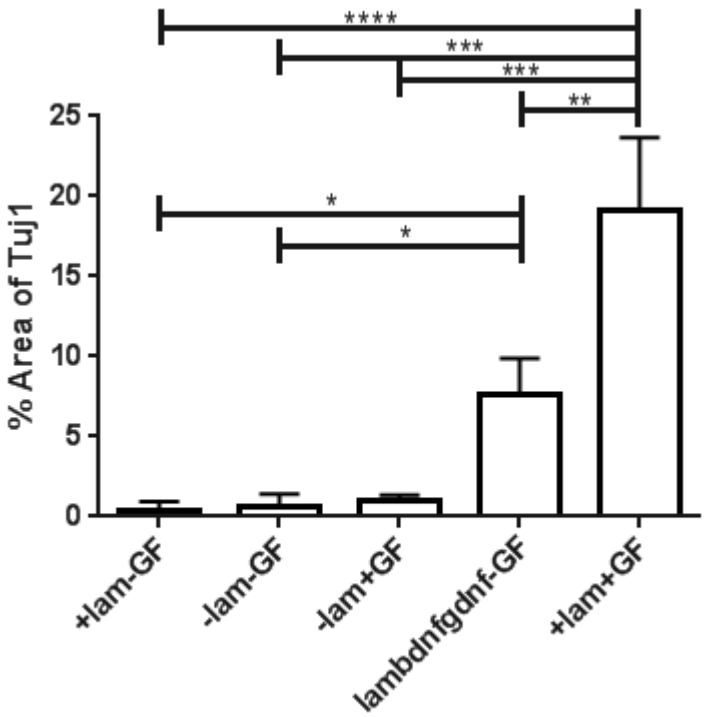

A.7 No significant differences were seen between MAP2 area for plastic wells versus bacterial cellulose coated with laminin and treated with the growth factors EGF and FGF2. MAP2 (red) area was used as a measure for neural cell marker due to autofluorescence preventing use of mature neuronal marker Tuj1. ($P = 0.0554$; $t = 2.010$; two-tailed unpaired t-test). Experiments were performed from $n = 1$ experimental repeat, with $n >= 2$ images per repeat, yielding similar results.

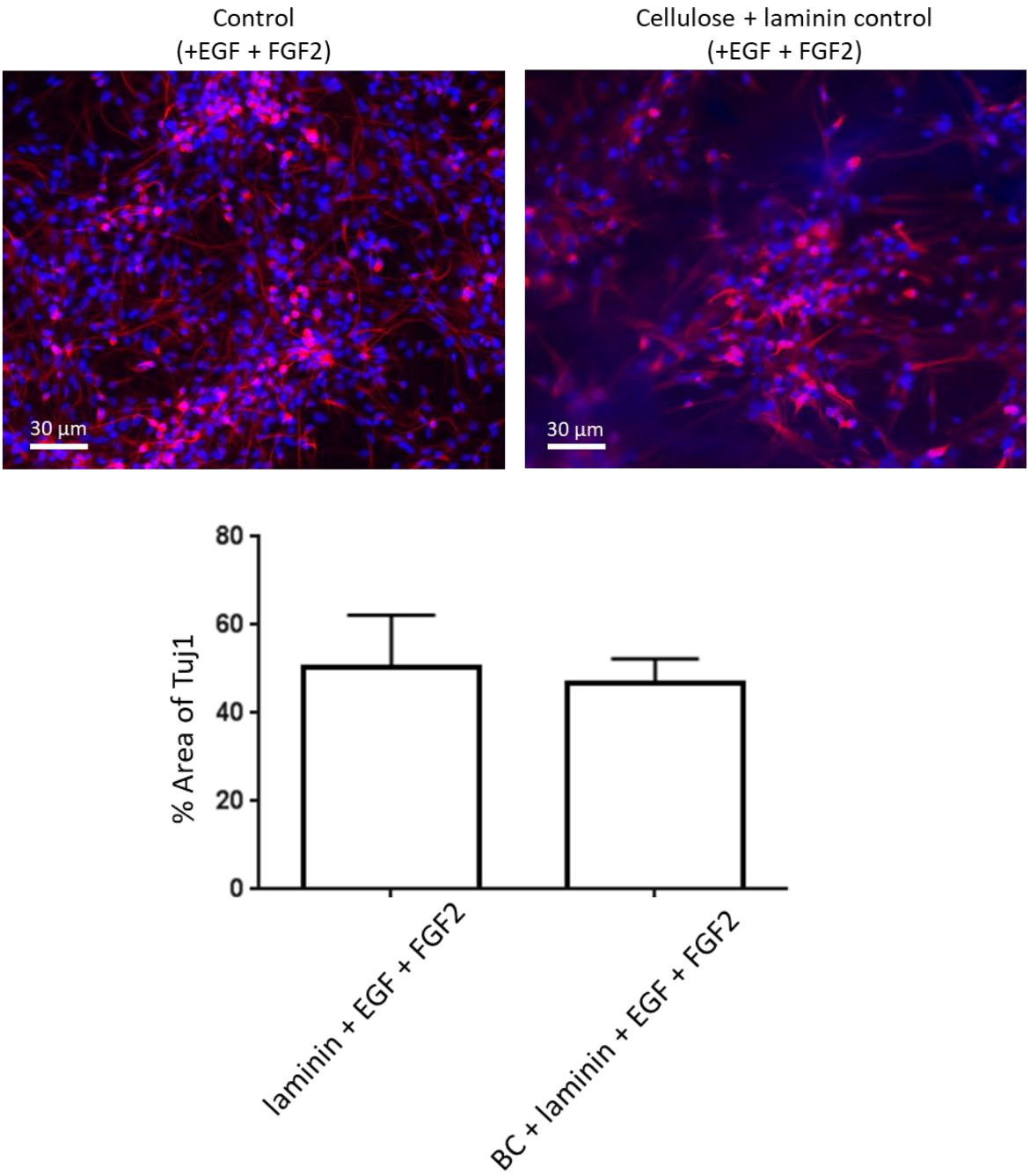

A.8 Autofluorescence of bacterial cellulose from excitation with the 488 nm laser resulted in high background preventing the ability to image Tuj1 immunofluorescence. Analysis was therefore based on MAP2 immunofluorescence using 647 nm excitation, which did not result in high background autofluorescence.

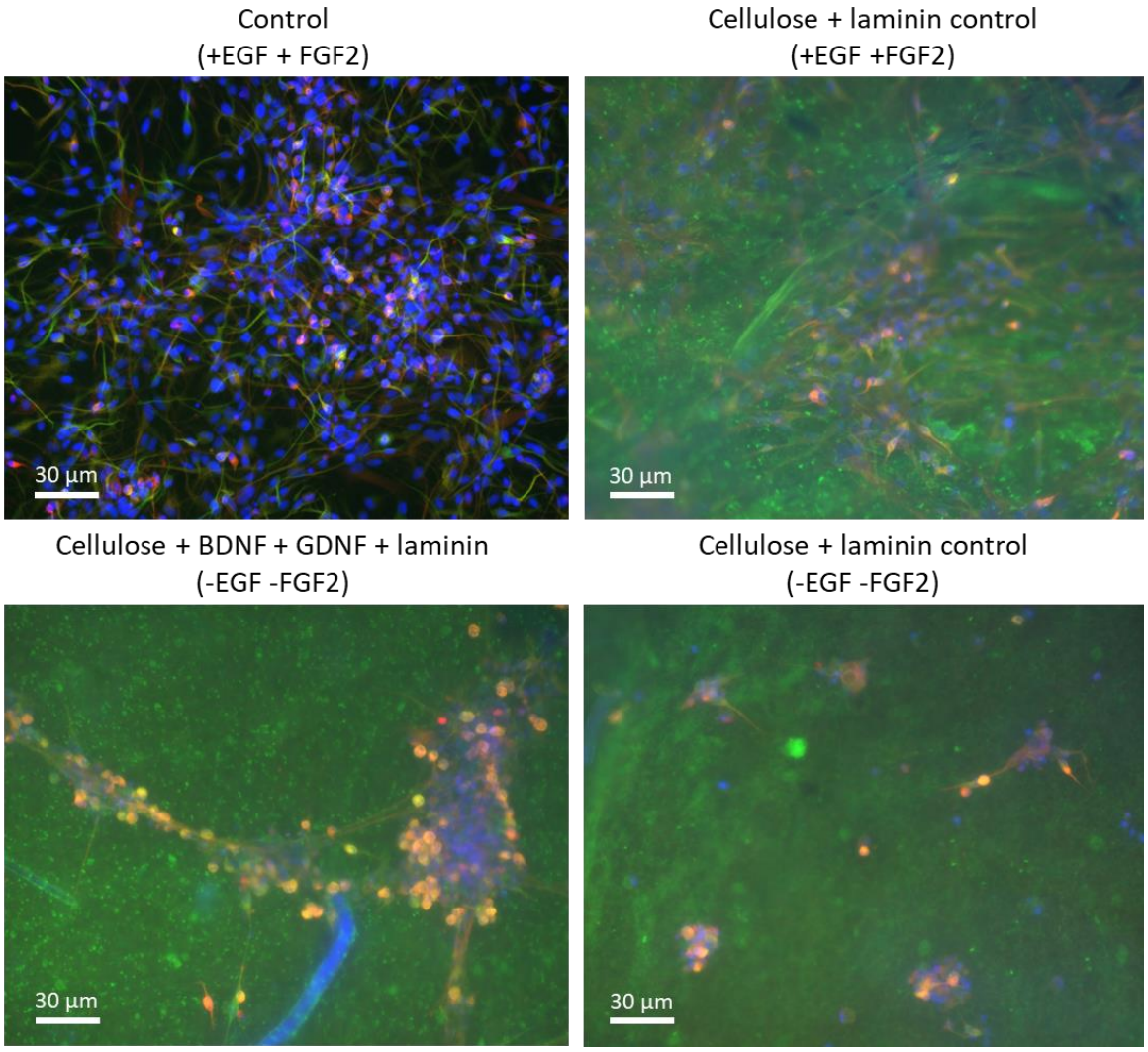

A.9 Increased Tuj1 area is seen for Bacterial cellulose biofunctionalised with BDNF, GDNF and laminin as compared with BDNF and laminin alone. Due to lack of experimental repeats, these results are omitted from the Chapter X. ($^{**}P = 0.0073$; $t = 3.046$; d.f. = 17; two-tailed unpaired t-test). Experiments were performed from $n = 1$ experimental repeat, with $n > = 5$ images per repeat, yielding similar results. All data points from the repeats and mean values with standard deviation are plotted).

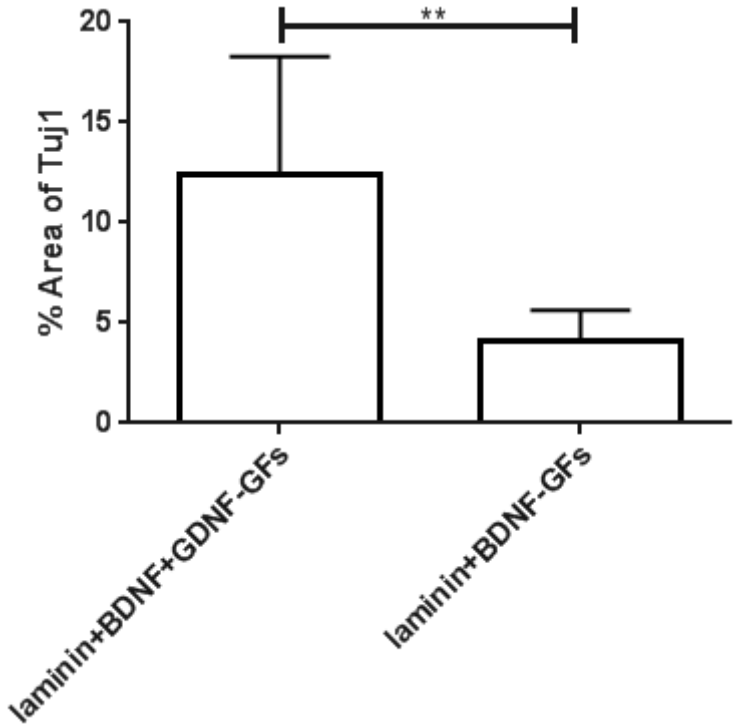

A.10 Percentage area of Tuj1 intensity was considered a suitable measure due to the ability to detect significant differences between negative (laminin or exogenous growth factors) versus positive (laminin and exogenous growth factors) controls (one-way analysis of variance (ANOVA); ****$P < 0.0001$; F (3, 16) = 19.73). Tukey's multiple comparison P values (+lam -GF (A), -lam -GF (B), -lam +GF (C), +lam +GF (D): (A-B) not significant (NS) = 0.9826; (A-C) NS = 0.9890; (A-D) ****$P < 0.0001$; (B-C) NS = > 0.9999; (B-D) **$P = 0.0013$; (C-D) **$P = 0.0015$. Experiments – laminin were performed from $n = 1$ experimental repeat with n = 2 technical repeats per experiment. Experiments +laminin were performed from BC and coverslip pooled data $n = 2$ experimental repeats with n >= 7 technical repeats. Mean values with standard deviation are plotted).

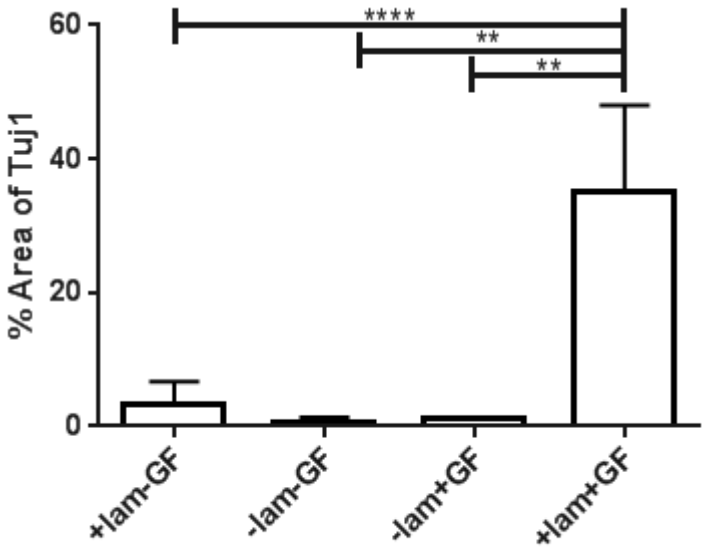

A.11 Biopatterning with BDNF, GDNF and laminin increases the survival and differentiation of neurons in the absence of exogenous growth factors. Data between cellulose and plastic coverslips were pooled (**$P = 0.0075$; $t = 3.164$; d.f. = 1; two-tailed unpaired t-test). Experiments were performed from $n = 2$ experimental repeats, with $n > = 3$ images per repeat, yielding similar results. All data points from the repeats and mean values with standard deviation are plotted).

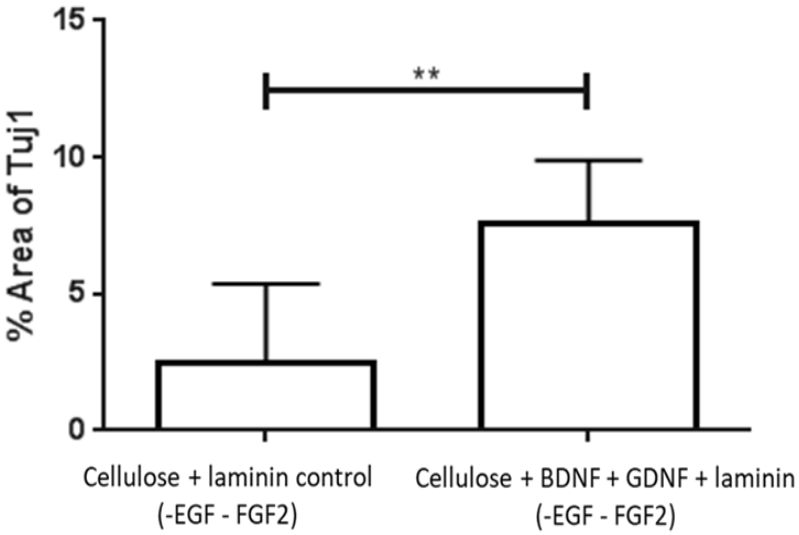

A.5 The distance based (object overlap) colocalisation method using ImageJ plug-in JACoP was selected as the most accurate and reproduceable method between samples (Just Another Colocalization Plugin ; Bolte & Cordlières, 2006). The percentage of positive thresholded pixels between the 2 channels were plotted to determine values corresponding to 'no colocalisation' and 'perfect correlation' for statistical evaluation of the real sample datasets.

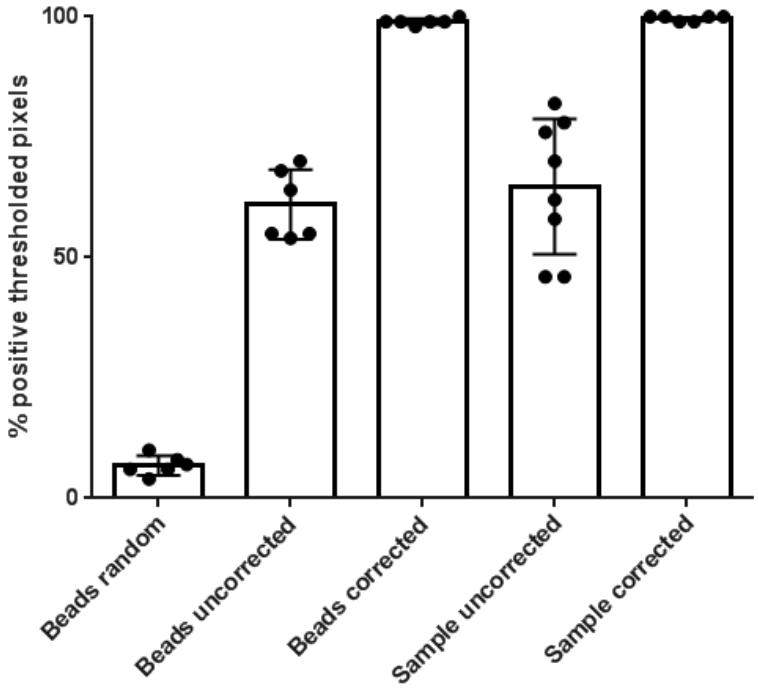

A.4 Determining a suitable method for colocalisation analysis. The comparison of measures for colocalisation of channel A with channel B as based on a 2-colour bead calibration sample or tau immunofluorescence sample.

		Sample				
Analysis software	**Colocalisation descriptor**	**Random transform bead sample**	**Original uncorrected bead sample**	**Aberration corrected bead sample**	**Corrected image sample with aberrated image sample (average n=4)**	**Corrected image sample wi corrected image sample (avera n=4)**
ImageJ plug-in	Mander's coefficient (thresholded): tM1, tM2	0.104, 0.000	0.479, 0.498	0.488, 0.447	0.062, 0.156	1, 1
	Distance based colocalization: % of positive A thresholded pixels % of positive B thresholded pixels	N/A	N/A	N/A	N/A	N/A

ImageJ plug-in JACoP (Just Another Colocalization Plugin ; Bolte & Cordlières, 2006)	Mander's coefficient (thresholded): tM1, tM2	0.033, 0.027	0.088, 0.066	0.209, 0.178	0.554, 0.306	0.105, 0.305
	Distance based colocalization: % of positive A thresholded pixels, % of positive B thresholded pixels	10, 8	64, 55	99, 99	67, 63	100, 100

REFERENCES

Ahmed, S. et al. (2013) 'Small-scale isolation of synaptic vesicles from mammalian brain', Nature Protocols. 8(5), p. 998.

Ahmed, S., Reynolds, B. A. and Weiss, S. (1995) 'BDNF enhances the differentiation but not the survival of CNS stem cell-derived neuronal precursors.', The Journal of neuroscience : the official journal of the Society for Neuroscience. 15(8), pp. 5765–78.

Ahmed, T. et al. (2014) 'Cognition and hippocampal synaptic plasticity in mice with a homozygous tau deletion', Neurobiology of Aging. 35(11), pp. 2474–2478.

Ait-Bouziad, N. et al. (2017) 'Discovery and characterization of stable and toxic Tau/phospholipid oligomeric complexes', Nature Communications. 8(1), p. 1678.

Allyson, J. et al. (2010) 'Blockade of NR2A-Containing NMDA Receptors Induces Tau Phosphorylation in Rat Hippocampal Slices', Neural Plasticity. 2010(340168) pp. 1–10.

Alonso, A. C. et al. (1994) 'Role of abnormally phosphorylated tau in the breakdown of microtubules in Alzheimer disease.', Proceedings of the National Academy of Sciences of the United States of America. National Academy of Sciences, 91(12), pp. 5562–6.

Alonso, A. C., Grundke-Iqbal, I. and Iqbal, K. (1996) 'Alzheimer's disease hyperphosphorylated tau sequesters normal tau into tangles of filaments and disassembles microtubules.', Nature Medicine, 2(7), pp. 783–7.

Altman, J. and Das, G. D. (1965) 'Autoradiographic and histological evidence of postnatal hippocampal neurogenesis in rats', The Journal of Comparative Neurology. 124(3), pp. 319–335.

Andreadis, A., Brown, W. M. and Kosik, K. S. (1992) 'Structure and novel exons of the human .tau. gene', Biochemistry. 31(43), pp. 10626–10633.

Aniksztejn, L. and Ben-Ari, Y. (1991) 'Novel form of long-term potentiation produced by a K^+channel blocker in the hippocampus', Nature, 349(6304), pp. 67–69.

Arendash, G. W. et al. (2004) ‘Multi-metric behavioral comparison of APPsw and P301L models for Alzheimer’s Disease: linkage of poorer cognitive performance to tau pathology in forebrain’, Brain Research, 1012(1–2), pp. 29–41.

Arlt, J. et al. (2013) ‘A study of pile-up in integrated time-correlated single photon counting systems’, Review of Scientific Instruments. American Institute of Physics, 84(10), p. 103105.

Arriagada, P. V, Marzloff, K. and Hyman, B. T. (1992a) ‘Distribution of Alzheimer-type pathologic changes in nondemented elderly individuals matches the pattern in Alzheimer’s disease.’, Neurology, 42(9), pp. 1681–8.

Askari, H. et al. (2014) ‘Electrical and optical properties of ITO thin films prepared by DC magnetron sputtering for low-emitting coatings’. arXiv:1409.5293.

Augustinack, J. C. et al. (2002) ‘Specific tau phosphorylation sites correlate with severity of neuronal cytopathology in Alzheimer’s disease’, Acta Neuropathologica, 103(1), pp. 26–35.

Bading, H., Ginty, D. and Greenberg, M. (1993) ‘Regulation of gene expression in hippocampal neurons by distinct calcium signaling pathways’, Science, 260(5105), pp. 181–186.

Bali, P. et al. (2017) ‘Potential for Stem Cells Therapy in Alzheimer’s Disease: Do Neurotrophic Factors Play Critical Role?’, Current Alzheimer research. 14(2), p. 208.

Ballatore, C., Lee, V. M.-Y. and Trojanowski, J. Q. (2007) ‘Tau-mediated neurodegeneration in Alzheimer's disease and related disorders’, Nature Reviews Neuroscience. Nature Publishing Group, 8(9), p. 663.

Bamann, C. et al. (2008) ‘Spectral Characteristics of the Photocycle of Channelrhodopsin-2 and Its Implication for Channel Function’, Journal of Molecular Biology, 375(3), pp. 686–694.

Bard, F. et al. (2000) ‘Peripherally administered antibodies against amyloid β-peptide enter the central nervous system and reduce pathology in a mouse model of Alzheimer disease’, Nature Medicine. 6(8), pp. 916–919.

Bareket-Keren, L. and Hanein, Y. (2012) ‘Carbon nanotube-based multi electrode arrays for

neuronal interfacing: progress and prospects.', Frontiers in neural circuits. 6(122), p. 122.

Barghorn, S. and Mandelkow, E. (2002) 'Toward a Unified Scheme for the Aggregation of Tau into Alzheimer Paired Helical Filaments', Biochemistry. 41(50), pp. 14885–14896.

Barnes, S. J. et al. (2010) 'Stable Mossy Fiber Long-Term Potentiation Requires Calcium Influx at the Granule Cell Soma, Protein Synthesis, and Microtubule-Dependent Axonal Transport', Journal of Neuroscience. 30(39), pp. 12996–13004.

Barton, A. J. et al. (1996) 'Alteration in brain presenilin 1 mRNA expression in early onset familial Alzheimer's disease.', Neurodegeneration. 5(3), pp. 213–8.

Bartus, R. T. (1997) 'The Calpain Hypothesis of Neurodegeneration: Evidence for a Common Cytotoxic Pathway', The Neuroscientist. 3(5), pp. 314–327. doi: 10.1177/107385849700300513.

Beaumont, M. et al. (2018) 'molecules A General Aqueous Silanization Protocol to Introduce Vinyl, Mercapto or Azido Functionalities onto Cellulose Fibers and Nanocelluloses', Molecules, 23(1427). doi: 10.3390/molecules23061427.

Becker, W. (2012) 'Fluorescence lifetime imaging - techniques and applications', Journal of Microscopy. (10.1111), 247(2), pp. 119–136.

Berger, Z. et al. (2007) 'Accumulation of Pathological Tau Species and Memory Loss in a Conditional Model of Tauopathy', 27(14), pp. 3650–3662.

Berridge, M. J. (2010) 'Calcium hypothesis of Alzheimer's disease', Pflügers Archiv. 459(3), pp. 441–449.

Berridge, M. J., Lipp, P. and Bootman, M. D. (2000) 'The versatility and universality of calcium signalling', Nature Reviews Molecular Cell Biology. 1(1), pp. 11–21.

Berriman, J. et al. (2003) 'Tau filaments from human brain and from in vitro assembly of recombinant protein show cross-beta structure.', Proceedings of the National Academy of Sciences of the United States of America. 100(15), pp. 9034–8.

Bezprozvanny, I. and Mattson, M. P. (2008) 'Neuronal calcium mishandling and the pathogenesis

of Alzheimer's disease', Trends in Neurosciences, 31(9), pp. 454–463.

Bizon, J. L. and Gallagher, M. (2005) 'More is less: neurogenesis and age-related cognitive decline in Long-Evans rats.', Science of aging knowledge environment . 2005(7), p. re2.

Bizon, J. L., Lee, H. J. and Gallagher, M. (2004) 'Neurogenesis in a rat model of age-related cognitive decline', Aging Cell. (10.1111), 3(4), pp. 227–234.

Blennow, K. et al. (2016) 'Traumatic brain injuries', Nature Reviews Disease Primers, 2(1), p. 16084.

Bliss, T. V. and Collingridge, G. L. (2013) 'Expression of NMDA receptor-dependent LTP in the hippocampus: bridging the divide', Molecular Brain. 6(1), p. 5.

Bliss, T. V. P. et al. (2018) 'Long-term potentiation in the hippocampus: discovery, mechanisms and function', Neuroforum. 24(3), pp. A103–A120.

Bliss, T. V. P. and Gardner-Medwin, A. R. (1973) 'Long-lasting potentiation of synaptic transmission in the dentate area of the unanaesthetized rabbit following stimulation of the perforant path', The Journal of Physiology. 232(2), pp. 357–374.

Bliss, T. V. P. and Lømo, T. (1973) 'Long-lasting potentiation of synaptic transmission in the dentate area of the anaesthetized rabbit following stimulation of the perforant path', The Journal of Physiology, 232(2), pp. 331–356.

Blurton-Jones, M. et al. (2009) 'Neural stem cells improve cognition via BDNF in a transgenic model of Alzheimer disease.', Proceedings of the National Academy of Sciences of the United States of America. 106(32), pp. 13594–9.

Boche, D. et al. (2010) 'Neuropathology after active Aβ42 immunotherapy: implications for Alzheimer's disease pathogenesis', Acta Neuropathologica. 120(3), pp. 369–384.

Boekhoorn, K. et al. (2006) 'Improved Long-Term Potentiation and Memory in Young Tau-P301L Transgenic Mice before Onset of Hyperphosphorylation and Tauopathy', Journal of Neuroscience, 26(13), pp. 3514–3523.

Bolte, S. and Cordelières, F. P. (2006) ‘A guided tour into subcellular colocalization analysis in light microscopy’, Journal of Microscopy, 224(3), pp. 213–232.

Bonafina, A. et al. (2018) ‘GDNF/GFRα1 Complex Abrogates Self-Renewing Activity of Cortical Neural Precursors Inducing Their Differentiation’, Stem Cell Reports, 10(3), pp. 1000–1015.

Boron, W. F. and De Weer, P. (1976) ‘Intracellular pH transients in squid giant axons caused by CO2, NH3, and metabolic inhibitors’, The Journal of General Physiology, 67(1), pp. 91–112.

Boyden, E. S. et al. (2005) ‘Millisecond-timescale, genetically targeted optical control of neural activity’, Nature Neuroscience, 8(9), pp. 1263–1268.

Boyden, E. S. (2011) ‘A history of optogenetics: the development of tools for controlling brain circuits with light.’, F1000 biology reports. 3, p. 11.

Braak, H. and Braak, E. (1991) ‘Neuropathological stageing of Alzheimer-related changes’, Acta Neuropathologica, 82(4), pp. 239–259.

Bramham, C. R. and Messaoudi, E. (2005) ‘BDNF function in adult synaptic plasticity: The synaptic consolidation hypothesis’, Progress in Neurobiology, 76(2), pp. 99–125.

Brette, R. and Destexhe, A. (2012) ‘Intracellular recording’, in Brette, R. and Destexhe, A. (eds) Handbook of Neural Activity Measurement. Cambridge: Cambridge University Press, pp. 44–91.

Brion, J.-P. et al. (1993) ‘Developmental Changes in τ Phosphorylation: Fetal τ Is Transiently Phosphorylated in a Manner Similar to Paired Helical Filament-τ Characteristic of Alzheimer’s Disease’, Journal of Neurochemistry. 61(6), pp. 2071–2080.

Brown, M. R., Geddes, J. W. and Sullivan, P. G. (2004) ‘Brain Region-Specific, Age-Related, Alterations in Mitochondrial Responses to Elevated Calcium’, Journal of Bioenergetics and Biomembranes, 36(4), pp. 401–406.

Bunch, J. S. et al. (2007) ‘Electromechanical resonators from graphene sheets.’, Science (New York, N.Y.). American Association for the Advancement of Science, 315(5811), pp. 490–3.

Busche, M. A. et al. (2019) ‘Tau impairs neural circuits, dominating amyloid-β effects, in

Alzheimer models in vivo', Nature Neuroscience, 22(1), pp. 57–64.

Cai, Z. et al. (2019) 'Precise Construction of Cell-Instructive 3D Microenvironments by Photopatterning a Biodegradable Hydrogel', Chemistry of Materials. American Chemical Society, 31(13), pp. 4710–4719. doi: 10.1021/acs.chemmater.9b00706.

Calafate, S. et al. (2016) 'Loss of Bin1 Promotes the Propagation of Tau Pathology', Cell Reports, 17(4), pp. 931–940.

Calcraft, P. J. et al. (2009) 'NAADP mobilizes calcium from acidic organelles through two-pore channels', Nature. 459(7246), pp. 596–600.

Casteels, R. and Kuriyama, H. (1966) 'Membrane potential and ion content in the smooth muscle of the guinea-pig's taenia coli at different external potassium concentrations', The Journal of Physiology. 184(1), pp. 120–130.

Chai, X., Dage, J. L. and Citron, M. (2012) 'Constitutive secretion of tau protein by an unconventional mechanism', Neurobiology of Disease. 48(3), pp. 356–366.

Charafeddine, R. A. et al. (2019) 'Tau repeat regions contain conserved histidine residues that modulate microtubule-binding in response to changes in pH.', The Journal of biological chemistry. 294(22), pp. 8779–8790.

Chen, Q. et al. (2012) 'Tau protein is involved in morphological plasticity in hippocampal neurons in response to BDNF', Neurochemistry International. 60(3), pp. 233–242.

Chen, S. W. et al. (2015) 'Structural characterization of toxic oligomers that are kinetically trapped during α-synuclein fibril formation', Proceedings of the National Academy of Sciences, 112(16), pp. E1994–E2003.

Chen, Y. et al. (2019) 'Engineering synucleinopathy-resistant human dopaminergic neurons by CRISPR-mediated deletion of the SNCA gene', European Journal of Neuroscience. 49(4), pp. 510–524.

Chen, Z. et al. (2019) 'Learnings about the complexity of extracellular tau aid development of a

blood-based screen for Alzheimer's disease.', Alzheimer's & dementia : the journal of the Alzheimer's Association. 15(3), pp. 487–496.

Chizhik, A. I. et al. (2012) 'Electrodynamic Coupling of Electric Dipole Emitters to a Fluctuating Mode Density within a Nanocavity', Physical Review Letters. 108(16), p. 163002.

Chizhik, A. I. et al. (2014) 'Metal-induced energy transfer for live cell nanoscopy', Nature Photonics, 8(2), pp. 124–127.

Chornenkyy, Y., Fardo, D. W. and Nelson, P. T. (2019) 'Tau and TDP-43 proteinopathies: kindred pathologic cascades and genetic pleiotropy', Laboratory Investigation. 99(7), pp. 993–1007.

Christensen, K. A., Myers, J. T. and Swanson, J. A. (2002) 'pH-dependent regulation of lysosomal calcium in macrophages', Journal of Cell Science, 115(3).

Coen, K. et al. (2012) 'Lysosomal calcium homeostasis defects, not proton pump defects, cause endo-lysosomal dysfunction in PSEN-deficient cells.', The Journal of cell biology. R 198(1), pp. 23–35.

Cohen, N. J. and Squire, L. R. (1980) 'Preserved learning and retention of pattern-analyzing skill in amnesia: dissociation of knowing how and knowing that.', Science (New York, N.Y.). American Association for the Advancement of Science, 210(4466), pp. 207–10.

Collingridge, G. L., Kehl, S. J. and McLennan, H. (1983) 'Excitatory amino acids in synaptic transmission in the Schaffer collateral-commissural pathway of the rat hippocampus.', The Journal of Physiology, 334(1), pp. 33–46.

Conejero-Goldberg, C. et al. (2014) 'APOE2 enhances neuroprotection against Alzheimer's disease through multiple molecular mechanisms', Molecular Psychiatry. 19(11), pp. 1243–1250.

Congdon, E. E. et al. (2013) 'Antibody Uptake into Neurons Occurs Primarily via Clathrin-dependent Fcγ Receptor Endocytosis and Is a Prerequisite for Acute Tau Protein Clearance', Journal of Biological Chemistry, 288(49), pp. 35452–35465.

Corder, E. et al. (1993) 'Gene dose of apolipoprotein E type 4 allele and the risk of Alzheimer's

disease in late onset families', Science, 261(5123), pp. 921–923.

Coria, F. et al. (1993) 'Prevalence of age-associated memory impairment and dementia in a rural community.', Journal of Neurology, 56(9), pp. 973–976.

Corneveaux, J. J. et al. (2010) 'Evidence for an association between KIBRA and late-onset Alzheimer's disease', Neurobiology of Aging, 31(6), pp. 901–909.

Curry, N. et al. (2017) 'Correlative STED and Atomic Force Microscopy on Live Astrocytes Reveals Plasticity of Cytoskeletal Structure and Membrane Physical Properties during Polarized Migration ', Frontiers in Cellular Neuroscience 19(11), p. 104.

Czaja, W. K. et al. (2007) 'The Future Prospects of Microbial Cellulose in Biomedical Applications', Biomacromolecules, 8(1), pp. 1–12.

Czöndör, K. et al. (2013) 'Micropatterned substrates coated with neuronal adhesion molecules for high-content study of synapse formation', Nature Communications. Nature Publishing Group, a division of Macmillan Publishers Limited. All Rights Reserved., 4, p. 2252.

d'Orange, M. et al. (2018) 'Potentiating tangle formation reduces acute toxicity of soluble tau species in the rat', Brain. Narnia, 141(2), pp. 535–549.

Dauwe, S. et al. (2002) 'Experimental evidence of parasitic shunting in silicon nitride rear surface passivated solar cells', Progress in Photovoltaics: Research and Applications. 10(4), pp. 271–278.

Dayanandan, R. et al. (1999) 'Mutations in tau reduce its microtubule binding properties in intact cells and affect its phosphorylation.', FEBS letters, 446(2–3), pp. 228–32.

de Calignon, A. et al. (2012) 'Propagation of Tau Pathology in a Model of Early Alzheimer's Disease', Neuron, 73(4), pp. 685–697.

Decker, J. M. et al. (2016) 'The Tau/A152T mutation, a risk factor for frontotemporal-spectrum disorders, leads to NR 2B receptor-mediated excitotoxicity', EMBO reports, 17(4), pp. 552–569.

Dehmelt, L. and Halpain, S. (2005) 'The MAP2/Tau family of microtubule-associated proteins', Genome Biology. 6(1), p. 204.

DeMattos, R. B. et al. (2001) ‘Peripheral anti-A beta antibody alters CNS and plasma A beta clearance and decreases brain A beta burden in a mouse model of Alzheimer’s disease.’, Proceedings of the National Academy of Sciences of the United States of America. 98(15), pp. 8850–5.

Deng, W., Aimone, J. B. and Gage, F. H. (2010) ‘New neurons and new memories: how does adult hippocampal neurogenesis affect learning and memory?’, Nature Reviews Neuroscience. 11(5), pp. 339–350.

Deng, Y.-B. et al. (2006) ‘Implantation of BM mesenchymal stem cells into injured spinal cord elicits de novo neurogenesis and functional recovery: evidence from a study in rhesus monkeys’, Cytotherapy, 8(3), pp. 210–214.

Dermaut, B. et al. (2005) ‘Tau is central in the genetic Alzheimer-frontotemporal dementia spectrum.’, Trends in genetics. 21(12), pp. 664–72.

DeVos, Sarah L. et al. (2013) ‘Antisense Reduction of Tau in Adult Mice Protects against Seizures’, Journal of Neuroscience, 33(31).

DeVos, S. L. et al. (2013) ‘Antisense Reduction of Tau in Adult Mice Protects against Seizures’, Journal of Neuroscience, 33(31), pp. 12887–12897.

Diao, J. et al. (2013) ‘Native α-synuclein induces clustering of synaptic-vesicle mimics via binding to phospholipids and synaptobrevin-2/VAMP2’, eLife, 2, p. e00592.

Dickson, E. J. et al. (2012) ‘Orai-STIM-mediated Ca2+ release from secretory granules revealed by a targeted Ca2+ and pH probe.’, Proceedings of the National Academy of Sciences of the United States of America. 109(51), pp. E3539-48.

Dickstein, D. L. et al. (2010) ‘Changes in dendritic complexity and spine morphology in transgenic mice expressing human wild-type tau’, Brain Structure and Function, 214(2–3), pp. 161–179.

Dieni, S. et al. (2012) ‘BDNF and its pro-peptide are stored in presynaptic dense core vesicles in brain neurons’, The Journal of Cell Biology. 196(6), pp. 775–788.

Diering, G. H. et al. (2013) ‘Endosomal acidification by Na+/H+ exchanger NHE5 regulates TrkA cell-surface targeting and NGF-induced PI3K signaling.’, Molecular biology of the cell, 24(21), pp. 3435–48.

Diniz, B. S. and Teixeira, A. L. (2011) ‘Brain-Derived Neurotrophic Factor and Alzheimer’s Disease: Physiopathology and Beyond’, NeuroMolecular Medicine, 13(4), pp. 217–222.

Doran, M. et al. (2007) ‘Familial early-onset dementia with tau intron 10 + 16 mutation with clinical features similar to those of alzheimer disease’, Archives of Neurology, 64(10), pp. 1535–1539.

Doyle, A. D. et al. (2009) ‘One-dimensional topography underlies three-dimensional fibrillar cell migration.’, The Journal of cell biology. 184(4), pp. 481–90.

Duan, Y. et al. (2012) ‘Advances in the Pathogenesis of Alzheimer’s Disease: Focusing on Tau-Mediated Neurodegeneration’, Translational Neurodegeneration. 1(1), p. 24.

Dunn, K. W., Kamocka, M. M. and McDonald, J. H. (2011) ‘A practical guide to evaluating colocalization in biological microscopy.’, American journal of physiology. 300(4), pp. C723-42.

Egashira, Y. et al. (2016) ‘Unique pH dynamics in GABAergic synaptic vesicles illuminates the mechanism and kinetics of GABA loading.’, Proceedings of the National Academy of Sciences of the United States of America. 113(38), pp. 10702–7.

Ehlers, M. D. (2003) ‘Activity level controls postsynaptic composition and signaling via the ubiquitin-proteasome system’, Nature Neuroscience. 6(3), p. 231.

Emilsson, L., Saetre, P. and Jazin, E. (2006) ‘Alzheimer’s disease: mRNA expression profiles of multiple patients show alterations of genes involved with calcium signaling’, Neurobiology of Disease, 21(3), pp. 618–625.

Enderlein, J. (2000) ‘A Theoretical Investigation of Single-Molecule Fluorescence Detection on Thin Metallic Layers’, Biophysical Journal. 78(4), pp. 2151–2158.

Evans, D. A. et al. (1989) ‘Prevalence of Alzheimer’s disease in a community population of older

persons. Higher than previously reported.', JAMA, 262(18), pp. 2551–6.

Evans, L. D. et al. (2018) 'Extracellular Monomeric and Aggregated Tau Efficiently Enter Human Neurons through Overlapping but Distinct Pathways', Cell Reports. 22(13), pp. 3612–3624.

Fá, M. et al. (2016) 'Extracellular Tau Oligomers Produce An Immediate Impairment of LTP and Memory', Scientific Reports. 20(6), p. 19393.

Fein, J. A. et al. (2008) 'Co-Localization of Amyloid Beta and Tau Pathology in Alzheimer's Disease Synaptosomes', The American Journal of Pathology. 172(6), pp. 1683–1692.

Fitzpatrick, A. W. P. et al. (2017) 'Cryo-EM structures of tau filaments from Alzheimer's disease', Nature. 547(7662), p. 185.

Florenzano, F. et al. (2017) 'Extracellular truncated tau causes early presynaptic dysfunction associated with Alzheimer's disease and other tauopathies.', Oncotarget. 8(39), pp. 64745–64778.

Fontaine, S. N. et al. (2016) 'DnaJ/Hsc70 chaperone complexes control the extracellular release of neurodegenerative-associated proteins', The EMBO journal. 35(14), pp. 1537–1549.

Foyouzi-Youssefi, R. et al. (2000) 'Bcl-2 decreases the free Ca2+ concentration within the endoplasmic reticulum', Proceedings of the National Academy of Sciences, 97(11), pp. 5723–5728.

Frandemiche, M. L. et al. (2014) 'Activity-Dependent Tau Protein Translocation to Excitatory Synapse Is Disrupted by Exposure to Amyloid-Beta Oligomers', Journal of Neuroscience, 34(17).

Frank, J. H. et al. (2007) 'A white light confocal microscope for spectrally resolved multidimensional imaging', Journal of Microscopy. 227(3), pp. 203–215.

Friedhoff P. et al. (1998) 'Rapid Assembly of Alzheimer-like Paired Helical Filaments from Microtubule-Associated Protein Tau Monitored by Fluorescence in Solution†'. American Chemical Society . 37(28) 10223-30.

Fu, H. J. et al. (2010) 'Amyloid-beta immunotherapy for Alzheimer's disease.', CNS & neurological disorders drug targets. 9(2), pp. 197–206.

Fucile, S. (2004) ‘Ca2+ permeability of nicotinic acetylcholine receptors’, Cell Calcium, 35(1), pp. 1–8.

Fujiwara, N. et al. (2013) ‘Restoration of spatial memory dysfunction of human APP transgenic mice by transplantation of neuronal precursors derived from human iPS cells’, Neuroscience Letters, 17(557), pp. 129–134.

Fulga, T. A. et al. (2006) ‘Abnormal bundling and accumulation of F-actin mediates tau-induced neuronal degeneration in vivo’, Nature Cell Biology. 9(2), p. 139.

Furukawa, K. et al. (2003) ‘Alteration in calcium channel properties is responsible for the neurotoxic action of a familial frontotemporal dementia tau mutation’, Journal of Neurochemistry. 87(2), pp. 427–436.

Games, D. et al. (1995) ‘Alzheimer-type neuropathology in transgenic mice overexpressing V717F β-amyloid precursor protein’, Nature. 373(6514), pp. 523–527.

Ganguly, P. et al. (2015) ‘Tau Assembly: The Dominant Role of PHF6 (VQIVYK) in Microtubule Binding Region Repeat R3’, The Journal of Physical Chemistry B. 119(13), pp. 4582–4593.

Gao, S. et al. (1998) ‘The Relationships Between Age, Sex, and the Incidence of Dementia and Alzheimer Disease’, Archives of General Psychiatry, 55(9), p. 809.

Gasque, G. (2015) ‘A Calcium-Dependent Mechanism of Neuronal Memory’, PLOS Biology. 13(6), p. e1002182.

Gérard, D. and Gray, S. K. (2015) ‘Aluminium plasmonics’, Journal of Physics D: Applied Physics, 48(18), p. 184001.

Gerasimenko, J. V et al. (1998) ‘Calcium uptake via endocytosis with rapid release from acidifying endosomes.’, Current biology. 8(24), pp. 1335–8.

German, D. C. et al. (1989) ‘Midbrain dopaminergic cell loss in parkinson’s disease: Computer visualization’, Annals of Neurology. 26(4), pp. 507–514.

Gerritsen, H. C. et al. (2002) ‘Fluorescence lifetime imaging in scanning microscopes: acquisition

speed, photon economy and lifetime resolution', Journal of Microscopy. 206(3), pp. 218–224.

Gheyara, A. L. et al. (2014) 'Tau reduction prevents disease in a mouse model of Dravet syndrome', Annals of Neurology. 76(3), pp. 443–456.

Giannakopoulos, P. et al. (2003) 'Tangle and neuron numbers, but not amyloid load, predict cognitive status in Alzheimer's disease', Neurology, 60(9), pp. 1495– 1500.

Goedert, M et al. (1989) 'Cloning and sequencing of the cDNA encoding an isoform of microtubule-associated protein tau containing four tandem repeats: differential expression of tau protein mRNAs in human brain.', The EMBO Journal, 8(2), pp. 393–399.

Goedert, M. et al. (1989) 'Multiple isoforms of human microtubule-associated protein tau: sequences and localization in neurofibrillary tangles of Alzheimer's disease', Neuron. 3(4), pp. 519–526.

Goedert, M. et al. (1996) 'Assembly of microtubule-associated protein tau into Alzheimer-like filaments induced by sulphated glycosaminoglycans.', Nature, 383(6600), pp. 550–3.

Goedert, M. and Jakes, R. (1990) 'Expression of separate isoforms of human tau protein: correlation with the tau pattern in brain and effects on tubulin polymerization.', The EMBO Journal, 9(13), pp. 4225–4230.

Goedert, M., Spillantini, M. G. and Crowther, R. A. (1992) 'Cloning of a big tau microtubule-associated protein characteristic of the peripheral nervous system.', Proceedings of the National Academy of Sciences of the United States of America. 89(5), pp. 1983–7.

Gómez-Isla, T. et al. (1996) 'Profound loss of layer II entorhinal cortex neurons occurs in very mild Alzheimer's disease.', The Journal of neuroscience .16(14), pp. 4491–500.

Gómez-Ramos, A. et al. (2006) 'Extracellular tau is toxic to neuronal cells', FEBS Letters. 580(20), pp. 4842–4850.

Gómez-Ramos, A. et al. (2008) 'Extracellular tau promotes intracellular calcium increase through M1 and M3 muscarinic receptors in neuronal cells', Molecular and Cellular Neuroscience.

Academic Press, 37(4), pp. 673–681.

Götz, J. et al. (1995) ‘Somatodendritic localization and hyperphosphorylation of tau protein in transgenic mice expressing the longest human brain tau isoform.’, The EMBO Journal, 14(7), pp. 1304–1313.

Govorunova, E. G. et al. (2015) ‘NEUROSCIENCE. Natural light-gated anion channels: A family of microbial rhodopsins for advanced optogenetics.’, Science. 349(6248), pp. 647–50.

Granqvist, C. G. and Hultåker, A. (2002) ‘Transparent and conducting ITO films: new developments and applications’, Thin Solid Films. 411(1), pp. 1–5.

Grastyán, E. et al. (1959) ‘Hippocampal electrical activity during the development of conditioned reflexes’, Electroencephalography and Clinical Neurophysiology. 11(3), pp. 409–430.

Greenlee, J. et al. (2016) ‘Neuronal Uptake of Paraneoplastic IgG Autoantibodies Reactive with Intracellular Antigens Requires the Fc Portion of the IgG Molecule and Can Be Competitively Inhibited by Normal IgG (P5.295)’, Neurology, 86(16 Supplement).

Grey, K. B. and Burrell, B. D. (2010) ‘Co-Induction of LTP and LTD and Its Regulation by Protein Kinases and Phosphatases’, Journal of Neurophysiology. 103(5), pp. 2737–2746.

Gross, G. W. et al. (1993) ‘Stimulation of monolayer networks in culture through thin-film indium-tin oxide recording electrodes’, Journal of Neuroscience Methods. 50(2), pp. 131–143.

Grundke-Iqbal, I. et al. (1986) ‘Abnormal phosphorylation of the microtubule-associated protein tau (tau) in Alzheimer cytoskeletal pathology.’, Proceedings of the National Academy of Sciences of the United States of America. 83(13), pp. 4913–7.

Grynspan, F. et al. (1997) ‘Active site-directed antibodies identify calpain II as an early-appearing and pervasive component of neurofibrillary pathology in Alzheimer’s disease.’, Brain research, 763(2), pp. 145–58.

Gunaydin, L. A. et al. (2010) ‘Ultrafast optogenetic control’, Nature Neuroscience. 13(3), pp. 387–392.

Guo, J. L. and Lee, V. M.-Y. (2011) ‘Seeding of Normal Tau by Pathological Tau Conformers Drives Pathogenesis of Alzheimer-like Tangles’, Journal of Biological Chemistry, 286(17), pp. 15317–15331.

Hajiali, F., Tajbakhsh, S. and Shojaei, A. (2018) ‘Fabrication and Properties of Polycaprolactone Composites Containing Calcium Phosphate-Based Ceramics and Bioactive Glasses in Bone Tissue Engineering: A Review’, Polymer Reviews. 58(1), pp. 164–207.

Hamill, O. P. et al. (1981) ‘Improved patch-clamp techniques for high-resolution current recording from cells and cell-free membrane patches’, Pflügers Archiv. 391(2), pp. 85–100.

Harada, A. et al. (1994) ‘Altered microtubule organization in small-calibre axons of mice lacking tau protein’, Nature. Nature Publishing Group, 369, p. 488.

Harris, J. A. et al. (2012) ‘Human P301L-Mutant Tau Expression in Mouse Entorhinal-Hippocampal Network Causes Tau Aggregation and Presynaptic Pathology but No Cognitive Deficits’, PLOS ONE. 7(9), p. e45881.

Hartigan, J. A. and Johnson, G. V (1999) ‘Transient increases in intracellular calcium result in prolonged site-selective increases in Tau phosphorylation through a glycogen synthase kinase 3beta-dependent pathway.’, The Journal of biological chemistry. 274(30), pp. 21395–401.

Hasegawa, K., Homma, A. and Imai, Y. (1986) ‘An epidemiological study of age-related dementia in the community’, International Journal of Geriatric Psychiatry. 1(1), pp. 45–55.

He, H. J. et al. (2009) ‘The proline-rich domain of tau plays a role in interactions with actin’, BMC Cell Biology, 10(1), p. 81.

Hebb, D. O. (Donald O. (1949) The organization of behavior a neuropsychological theory. L. Erlbaum Associates.

Heldt, S. A. et al. (2007) ‘Hippocampus-specific deletion of BDNF in adult mice impairs spatial memory and extinction of aversive memories’, Molecular Psychiatry, 12(7), pp. 656–670.

Henze, D. A. et al. (2000) ‘Intracellular Features Predicted by Extracellular Recordings in the

Hippocampus In Vivo', Journal of Neurophysiology. 84(1), pp. 390–400.

Hestrin, S. and Schramm, M. (1954) 'Synthesis of cellulose by Acetobacter xylinum. II. Preparation of freeze-dried cells capable of polymerizing glucose to cellulose.', The Biochemical journal. 58(2), pp. 345–52.

Higley, M. J. and Sabatini, B. L. (2008) 'Calcium Signaling in Dendrites and Spines: Practical and Functional Considerations', Neuron, 59(6), pp. 902–913.

Hinrichs, M. H. et al. (2012) 'Tau protein diffuses along the microtubule lattice.', The Journal of biological chemistry. American Society for Biochemistry and Molecular Biology, 287(46), pp. 38559–68.

Hock, C. et al. (2003) 'Antibodies against beta-amyloid slow cognitive decline in Alzheimer's disease.', Neuron, 38(4), pp. 547–54.

Hodgkin, A. L. and Huxley, A. F. (1952) 'A quantitative description of membrane current and its application to conduction and excitation in nerve', The Journal of Physiology. 117(4), pp. 500–544.

Hofer, M. M. and Barde, Y.-A. (1988) 'Brain-derived neurotrophic factor prevents neuronal death in vivo', Nature, 331(6153), pp. 261–262.

Hoffmann, N. A. et al. (2013) 'Impaired plasticity of cortical dendritic spines in P301S tau transgenic mice', Acta Neuropathologica Communications. 1(1), p. 82.

Hofman, A. et al. (1991) 'The Prevalence of Dementia in Europe: A Collaborative Study of 1980–1990 Findings', International Journal of Epidemiology, 20(3), pp. 736–748.

Holman, M. E. (1958) 'Membrane potentials recorded with high-resistance micro-electrodes; and the effects of changes in ionic environment on the electrical and mechanical activity of the smooth muscle of the taenia coli of the guinea-pig', The Journal of Physiology. 141(3), pp. 464–488.

Holth, J. K. et al. (2013) 'Tau Loss Attenuates Neuronal Network Hyperexcitability in Mouse and Drosophila Genetic Models of Epilepsy', The Journal of Neuroscience,

33(4), pp. 1651 LP – 1659.

Hong, M. et al. (1998) ‘Mutation-Specific Functional Impairments in Distinct Tau Isoforms of Hereditary FTDP-17’, Science, 282(5395), pp. 1914 LP – 1917.

Hoover, B. R. et al. (2010) ‘Tau Mislocalization to Dendritic Spines Mediates Synaptic Dysfunction Independently of Neurodegeneration’, Neuron. Cell Press, 68(6), pp. 1067–1081.

Horne, M. K. et al. (2010) ‘Three-Dimensional Nanofibrous Scaffolds Incorporating Immobilized BDNF Promote Proliferation and Differentiation of Cortical Neural Stem Cells’, Stem Cells and Development. 19(6), pp. 843–852.

Hosokawa, T. et al. (1995) ‘Repeated confocal imaging of individual dendritic spines in the living hippocampal slice: evidence for changes in length and orientation associated with chemically induced LTP.’, The Journal of neuroscience . 15(8), pp. 5560–73.

Hunsberger, H. C. et al. (2014) ‘Effect size of memory deficits in mice with adult-onset P301L tau expression.’, Behavioural brain research. 272, pp. 181–95.

Igor Luzinov, † et al. (2000) ‘Epoxy-Terminated Self-Assembled Monolayers: Molecular Glues for Polymer Layers’. American Chemical Society. 16(2), pp.504-516

Iqbal, K., Alonso, A. del C. and Grundke-Iqbal, I. (2008) ‘Cytosolic abnormally hyperphosphorylated tau but not paired helical filaments sequester normal MAPs and inhibit microtubule assembly.’, Journal of Alzheimer’s disease. 14(4), pp. 365–70.

Isaac S. Carrico, † et al. (2007) ‘Lithographic Patterning of Photoreactive Cell-Adhesive Proteins’. American Chemical Society . 129(16), pp.4874-4875.

Israël, M. et al. (1980) ‘ATP-dependent calcium uptake by cholinergic synaptic vesicles isolated from Torpedo electric organ.’, The Journal of membrane biology, 54(2), pp. 115–26.

Ittner, L. M. et al. (2010) ‘Dendritic Function of Tau Mediates Amyloid-β Toxicity in Alzheimer’s Disease Mouse Models’, Cell, 142(3), pp. 387–397.

Ittner, L. M. and Götz, J. (2010) ‘Amyloid-β and tau — a toxic pas de deux in Alzheimer's disease’,

Nature Reviews Neuroscience. 12, p. 67.

J. Irwin, D. and I. Hurtig, H. (2018) 'The Contribution of Tau, Amyloid-Beta and Alpha-Synuclein Pathology to Dementia in Lewy Body Disorders', Journal of Alzheimer's Disease & Parkinsonism, 08(04).

Jain, A., Blum, C. and Subramaniam, V. (2009) 'Fluorescence Lifetime Spectroscopy and Imaging of Visible Fluorescent Proteins', Advances in Biomedical Engineering. pp. 147–176.

Janus, C. et al. (2000) 'Aβ peptide immunization reduces behavioural impairment and plaques in a model of Alzheimer's disease', Nature, 408(6815), pp. 979–982.

Jaworski, J. et al. (2009) 'Dynamic Microtubules Regulate Dendritic Spine Morphology and Synaptic Plasticity', Neuron, 61(1), pp. 85–100.

Van der Jeugd, A. et al. (2012) 'Cognitive defects are reversible in inducible mice expressing pro-aggregant full-length human Tau', Acta Neuropathologica, 123(6), pp. 787–805.

Jackson, J. S. et al. (2017) 'Altered Synapse Stability in the Early Stages of Tauopathy.', Cell reports. 18(13), pp. 3063–3068.

Jang, E.-H. et al. (2016) 'Effects of Microtubule Stabilization by Epothilone B Depend on the Type and Age of Neurons', Neural Plasticity. 2016, pp. 1–12.

Jeganathan, S. et al. (2008) 'The Natively Unfolded Character of Tau and Its Aggregation to Alzheimer-like Paired Helical Filaments †', Biochemistry. 47(40), pp. 10526–10539.

Jiao, S.-S. et al. (2016) 'Brain-derived neurotrophic factor protects against tau-related neurodegeneration of Alzheimer's disease', Translational Psychiatry, 6(10), pp. e907–e907.

Jin, K. et al. (2011) 'Effect of human neural precursor cell transplantation on endogenous neurogenesis after focal cerebral ischemia in the rat', Brain Research, 1374, pp. 56–62.

Jin, N. et al. (2015) 'Truncation and activation of GSK-3β by calpain I: a molecular mechanism links to tau hyperphosphorylation in Alzheimer's disease', Scientific Reports, 5(1), p. 8187.

Johenning, F. W. et al. (2015) ‘Ryanodine Receptor Activation Induces Long-Term Plasticity of Spine Calcium Dynamics’, PLOS Biology. 13(6), p. e1002181.

Jokinen, V. et al. (2013) ‘A microfluidic chip for axonal isolation and electrophysiological measurements’, Journal of Neuroscience Methods. 212(2), pp. 276–282.

Jonas, F., Krafft, W. and Muys, B. (1995) ‘Poly(3, 4-ethylenedioxythiophene): Conductive coatings, technical applications and properties’, Macromolecular Symposia. 100(1), pp. 169–173.

Jonas, R. and Farah, L. F. (1998) ‘Production and application of microbial cellulose’, Polymer Degradation and Stability. 59(1–3), pp. 101–106.

Kaminska, I. et al. (2019) ‘Distance Dependence of Single-Molecule Energy Transfer to Graphene Measured with DNA Origami Nanopositioners’, Nano Letters. 19(7), pp. 4257–4262.

Kanaan, N. M. et al. (2011) ‘Pathogenic Forms of Tau Inhibit Kinesin-Dependent Axonal Transport through a Mechanism Involving Activation of Axonal Phosphotransferases’, The Journal of Neuroscience, 31(27), pp. 9858 LP – 9868.

Kanmert, D. et al. (2015) ‘C-Terminally Truncated Forms of Tau, But Not Full-Length Tau or Its C-Terminal Fragments, Are Released from Neurons Independently of Cell Death.’, The Journal of neuroscience . 35(30), pp. 10851–65.

Karbovnyk, I. et al. (2016) ‘Effect of Radiation on the Electrical Properties of PEDOT-Based Nanocomposites.’, Nanoscale research letters. 11(1), pp. 84.

Karch, C. M., Jeng, A. T. and Goate, A. M. (2012) ‘Extracellular Tau levels are influenced by variability in Tau that is associated with tauopathies.’, The Journal of biological chemistry. 287(51), pp. 42751–62.

Karch, C. M., Jeng, A. T. and Goate, A. M. (2013) ‘Calcium phosphatase calcineurin influences tau metabolism’, Neurobiology of Aging, 34(2), pp. 374–386.

Katz, B. and Miledi, R. (1968) ‘The role of calcium in neuromuscular facilitation’, The Journal of Physiology, 195(2), pp. 481–492.

Kauer, J. A., Malenka, R. C. and Nicoll, R. A. (1988) ‘A persistent postsynaptic modification mediates long-term potentiation in the hippocampus’, Neuron, 1(10), pp. 911–917.

Kefalopoulou, Z. et al. (2014) ‘Long-term Clinical Outcome of Fetal Cell Transplantation for Parkinson Disease’, JAMA Neurology, 71(1), p. 83.

Kessels, H. W. and Malinow, R. (2009) ‘Synaptic AMPA Receptor Plasticity and Behavior’, Neuron. Cell Press, 61(3), pp. 340–350.

Khachaturian, Z. S. (2006) ‘Calcium Hypothesis of Alzheimer’s Disease and Brain Aginga’, Annals of the New York Academy of Sciences, 747(1), pp. 1–11.

Kheyraddini Mousavi, A. et al. (2012) ‘BioPatterning’, in Encyclopedia of Nanotechnology. Dordrecht. pp. 320–328.

Kim, W., Lee, S. and Hall, G. F. (2010) ‘Secretion of human tau fragments resembling CSF-tau in Alzheimer’s disease is modulated by the presence of the exon 2 insert’, FEBS Letters. 584(14), pp. 3085–3088.

Kimura, T. et al. (2014a) ‘Microtubule-associated protein tau is essential for long-term depression in the hippocampus.’, Philosophical transactions of the Royal Society of London. Series B, Biological sciences. 369(1633), p. 20130144.

Kimura, T. et al. (2014b) ‘Microtubule-associated protein tau is essential for long-term depression in the hippocampus’, Philosophical transactions of the Royal Society of London. Series B, Biological sciences. 369(1633), p. 20130144.

King, M. E. et al. (1999) ‘Ligand-Dependent Tau Filament Formation: Implications for Alzheimer’s Disease Progression’, Biochemistry. American Chemical Society, 38(45), pp. 14851–14859.

Kitamura, T. et al. (2009) ‘Adult Neurogenesis Modulates the Hippocampus-Dependent Period of Associative Fear Memory’, Cell, 139(4), pp. 814–827.

Kitiyanant, N. et al. (2012) ‘BDNF-, IGF-1- and GDNF-Secreting Human Neural Progenitor Cells

Rescue Amyloid β-Induced Toxicity in Cultured Rat Septal Neurons', Neurochemical Research, 37(1), pp. 143–152.

Koch, G. et al. (2016) 'Reversal of LTP-Like Cortical Plasticity in Alzheimer's Disease Patients with Tau-Related Faster Clinical Progression', Journal of Alzheimer's Disease. 50(2), pp. 605–616.

Konorski, J. (1950) 'Conditioned reflexes and neuron organization. New York: Cambridge University Press, 1948, pp. 267. $4.00', Journal of Clinical Psychology. 6(1), pp. 107–107.

Kopeikina, K., Hyman, B. and Spires-Jones, T. (2012) 'Soluble forms of tau are toxic in Alzheimer's disease', Translational Neuroscience, 3(3), pp. 223–233.

Koss, D. J. et al. (2016) 'Soluble pre-fibrillar tau and β-amyloid species emerge in early human Alzheimer's disease and track disease progression and cognitive decline', Acta Neuropathologica, 132(6), pp. 875–895.

Kramár, E. A. et al. (2012) 'BDNF upregulation rescues synaptic plasticity in middle-aged ovariectomized rats', Neurobiology of Aging, 33(4), pp. 708–719.

Kubitschke, H. et al. (2017) 'Actin and microtubule networks contribute differently to cell response for small and large strains', New Journal of Physics. 19(9), p. 093003.

Kuchibhotla, K. V. et al. (2008) 'Aβ Plaques Lead to Aberrant Regulation of Calcium Homeostasis In Vivo Resulting in Structural and Functional Disruption of Neuronal Networks', Neuron, 59(2), pp. 214–225.

Kumar, A. and Whitesides, G. M. (1994) 'Patterned Condensation Figures as Optical Diffraction Gratings', Science, 263(5143), pp. 60–62.

Kurbatskaya, K. et al. (2016) 'Upregulation of calpain activity precedes tau phosphorylation and loss of synaptic proteins in Alzheimer's disease brain', Acta Neuropathologica Communications. 4(1), p. 34.

Kuret, J. et al. (2005) 'Evaluating triggers and enhancers of tau fibrillization', Microscopy

Research and Technique, 67(3-4), pp. 141–155.

Kuzum, D. et al. (2014) ‘Transparent and flexible low noise graphene electrodes for simultaneous electrophysiology and neuroimaging’, Nature Communications. 5, p. 5259.

Kwok, J. B. J. et al. (2004) ‘Tau haplotypes regulate transcription and are associated with Parkinson’s disease’, Annals of Neurology. 55(3), pp. 329–334.

Lachmanovich, E. et al. (2003) ‘Co-localization analysis of complex formation among membrane proteins by computerized fluorescence microscopy: application to immunofluorescence co-patching studies’, Journal of Microscopy, 212(2), pp. 122–131.

Lakowicz, J. R. (ed.) (2006) Principles of Fluorescence Spectroscopy. Springer, USA.

Lankiewicz, S. et al. (2000) ‘Activation of Calpain I Converts Excitotoxic Neuron Death into a Caspase-independent Cell Death’, Journal of Biological Chemistry, 275(22), pp. 17064–17071.

Larson, J., Wong, D. and Lynch, G. (1986) ‘Patterned stimulation at the theta frequency is optimal for the induction of hippocampal long-term potentiation’, Brain Research, 368(2), pp. 347–350.

Lasagna-Reeves, C. A. et al. (2010) ‘Preparation and Characterization of Neurotoxic Tau Oligomers’, Biochemistry. American Chemical Society, 49(47), pp. 10039–10041.

Lasagna-Reeves, C. A. et al. (2012) ‘Alzheimer brain-derived tau oligomers propagate pathology from endogenous tau.’, Scientific reports. 2, p. 700.

Lattarulo, C. et al. (2011) ‘Microscopic Imaging of Intracellular Calcium in Live Cells Using Lifetime-Based Ratiometric Measurements of Oregon Green BAPTA-1’, in Methods in molecular biology. pp. 377–389.

Lazarenko, R. M. et al. (2017) ‘Ammonium chloride alters neuronal excitability and synaptic vesicle release’, Scientific Reports. 7(1), p. 5061.

Lee, G. et al. (1998) ‘Tau interacts with src-family non-receptor tyrosine kinases’, Journal of Cell Science, 111(21).

Lee, H. K. et al. (1998) ‘NMDA induces long-term synaptic depression and dephosphorylation of the GluR1 subunit of AMPA receptors in hippocampus.’, Neuron, 21(5), pp. 1151–62.

Lee, S.-M. et al. (2015) ‘Nanomechanical measurement of astrocyte stiffness correlated with cytoskeletal maturation’, Journal of Biomedical Materials Research Part A, 103(1), pp. 365–370.

Lemere, C. A. et al. (1996) ‘The E280A presenilin 1 Alzheimer mutation produces increased A beta 42 deposition and severe cerebellar pathology.’, Nature medicine, 2(10), pp. 1146–50.

Leroy, K. et al. (2012) ‘Lack of Tau Proteins Rescues Neuronal Cell Death and Decreases Amyloidogenic Processing of APP in APP/PS1 Mice’, The American Journal of Pathology, 181(6), pp. 1928–1940.

Li, W. et al. (2016) ‘Extensive graft-derived dopaminergic innervation is maintained 24 years after transplantation in the degenerating parkinsonian brain’, Proceedings of the National Academy of Sciences, 113(23), pp. 6544–6549.

Li, W. and Lee, V. M.-Y. (2006) ‘Characterization of Two VQIXXK Motifs for Tau Fibrillization in Vitro’, Biochemistry. American Chemical Society, 45(51), pp. 15692–15701.

Lin, H.-J., Herman, P. and Lakowicz, J. R. (2003) ‘Fluorescence lifetime-resolved pH imaging of living cells’, Cytometry Part A. 52A(2), pp. 77–89.

Lin, J. Y. et al. (2009) ‘Characterization of engineered channelrhodopsin variants with improved properties and kinetics.’, Biophysical journal. 96(5), pp. 1803–14.

Lindvall, O. and Kokaia, Z. (2010) ‘Stem cells in human neurodegenerative disorders — time for clinical translation?’, Journal of Clinical Investigation, 120(1), pp. 29–40.

Lisman, J. (1989) ‘A mechanism for the Hebb and the anti-Hebb processes underlying learning and memory.’, Proceedings of the National Academy of Sciences, 86(23), pp. 9574–9578.

Liu, C. et al. (2016) ‘Co-immunoprecipitation with Tau Isoform-specific Antibodies Reveals Distinct Protein Interactions and Highlights a Putative Role for 2N Tau in Disease.’, The Journal of biological chemistry. 291(15), pp. 8173–88.

Liu, F. et al. (2014) ‘Combined effect of nerve growth factor and brain-derived neurotrophic factor on neuronal differentiation of neural stem cells and the potential molecular mechanisms.’, Molecular medicine reports. 10(4), pp. 1739–45.

Lloyd, D. P. C. (1949) 'Post-tetanic potentiation of response in monosynaptic reflex pathways of the spinal cord’, The Journal of General Physiology, 33(2), pp. 147–170.

Lømo, T. (1966) ‘Frequency potentiation of excitatory synaptic activity in the dentate area of the hippocampal formation’, Acta Physiologica Scandinavica, 68(128).

Loomis, P. A. et al. (1990) ‘Identification of nuclear tau isoforms in human neuroblastoma cells.’, Proceedings of the National Academy of Sciences of the United States of America. 87(21), pp. 8422–6.

Luna-Muñoz, J. et al. (2007) ‘Earliest Stages of Tau Conformational Changes are Related to the Appearance of a Sequence of Specific Phospho-Dependent Tau Epitopes in Alzheimer’s Disease1’, Journal of Alzheimer’s Disease. 12(4), pp. 365–375.

Lustri, W. R. et al. (2015) ‘Microbial Cellulose — Biosynthesis Mechanisms and Medical Applications’, in Cellulose - Fundamental Aspects and Current Trends. InTech.

Ma, D. et al. (2000) ‘Axonal Transport of Microtubule-Associated Protein 1B (MAP1B) in the Sciatic Nerve of Adult Rat: Distinct Transport Rates of Different Isoforms’, The Journal of Neuroscience, 20(6), pp. 2112 – 2120.

Macías, W. et al. (2001) ‘Potassium chloride depolarization mediates CREB phosphorylation in striatal neurons in an NMDA receptor-dependent manner.’, Brain research. 890(2), pp. 222–32.

Madison, D. V, Malenka, R. C. and Nicoll, R. A. (1991) ‘Mechanisms Underlying Long-Term Potentiation of Synaptic Transmission’, Annual Review of Neuroscience, 14(1), pp. 379–397.

Maeda, S. et al. (2006) ‘Increased levels of granular tau oligomers: An early sign of brain aging and Alzheimer’s disease’, Neuroscience Research. 54(3), pp. 197–201.

Makuch, L. et al. (2011) ‘Regulation of AMPA Receptor Function by the Human Memory-

Associated Gene KIBRA', Neuron. NIH Public Access, 71(6), p. 1022. doi: 10.1016/J.NEURON.2011.08.017.

Mandell, J. W. and Banker, G. A. (1996) 'A spatial gradient of tau protein phosphorylation in nascent axons.', The Journal of neuroscience : the official journal of the Society for Neuroscience, 16(18), pp. 5727–40.

Manders, E. M. et al. (1992) 'Dynamics of three-dimensional replication patterns during the S-phase, analysed by double labelling of DNA and confocal microscopy.', Journal of cell science, 103 (Pt 3), pp. 857–62.

Manders, E. M. M., Verbeek, F. J. and Aten, J. A. (1993) 'Measurement of co-localization of objects in dual-colour confocal images', Journal of Microscopy. 169(3), pp. 375–382.

Mann, D. M. A. et al. (1996) 'Amyloid-beta protein deposition in chromosome 14-linked Alzheimer's disease: Predominance of A-beta42(43)', Annals of Neurology, 40(2), pp. 149–156.

Marinho, B. et al. (2012) 'Electrical conductivity of compacts of graphene, multi-wall carbon nanotubes, carbon black, and graphite powder', Powder Technology. 221, pp. 351–358.

Marty, A. and Neher, E. (1995) 'Tight-Seal Whole-Cell Recording', in Single-Channel Recording. pp. 31–52.

Masliah, E. et al. (2001) 'Altered expression of synaptic proteins occurs early during progression of Alzheimer's disease', Neurology, 56(1), pp. 127 LP – 129.

Massicotte, G. et al. (1991) 'Modulation of DL-alpha-amino-3-hydroxy-5-methyl-4-isoxazolepropionic acid/quisqualate receptors by phospholipase A2: a necessary step in long-term potentiation?', Proceedings of the National Academy of Sciences, 88(5), pp. 1893–1897.

Mattson, M. P. (1990) 'Antigenic changes similar to those seen in neurofibrillary tangles are elicited by glutamate and Ca^{2+} influx in cultured hippocampal neurons', Neuron. Cell Press, 4(1), pp. 105–117.

Mattson, M. P. and Chan, S. L. (2001) 'Dysregulation of Cellular Calcium Homeostasis in

Alzheimer's Disease: Bad Genes and Bad Habits', Journal of Molecular Neuroscience, 17(2), pp. 205–224.

Mayer, M. L., Westbrook, G. L. and Guthrie, P. B. (1984) 'Voltage-dependent block by Mg2+ of NMDA responses in spinal cord neurones', Nature, 309(5965), pp. 261–263.

McEwan, W. A. et al. (2017) 'Cytosolic Fc receptor TRIM21 inhibits seeded tau aggregation', Proceedings of the National Academy of Sciences, 114(3), pp. 574–579.

McMillan, P. et al. (2008) 'Tau isoform regulation is region- and cell-specific in mouse brain', The Journal of Comparative Neurology, 511(6), pp. 788–803.

McInnes, J. et al. (2018) 'Synaptogyrin-3 Mediates Presynaptic Dysfunction Induced by Tau', Neuron, 97(4), pp. 823-835.e8.

McKee, A. C. et al. (1990) 'Hippocampal Neurons Predisposed to Neurofibrillary Tangle Formation Are Enriched in Type II Calcium/Calmodulin-Dependent Protein Kinase', Journal of Neuropathology & Experimental Neurology, 49(1), pp. 49–63.

Mekki Abdelmouleh, † et al. (2002) 'Interaction of Silane Coupling Agents with Cellulose'. American Chemical Society . 18(8), pp. 3203-3208.

Mellman, I. (1996) 'Endocytosis And Molecular Sorting', Annual Review of Cell and Developmental Biology, 12(1), pp. 575–625.

Memanishvili, T. et al. (2016) 'Generation of cortical neurons from human induced-pluripotent stem cells by biodegradable polymeric microspheres loaded with priming factors', Biomedical Materials. 11(2), pp. 025011.

Mendez, M. F. (2017) 'What is the Relationship of Traumatic Brain Injury to Dementia?', Journal of Alzheimer's Disease, 57(3), pp. 667–681.

Meredith Jr., J. E. et al. (2013) 'Characterization of Novel CSF Tau and ptau Biomarkers for Alzheimer's Disease', PLoS ONE. 8(10), p. e76523.

Merezhko, M. et al. (2018) 'Secretion of Tau via an Unconventional Non-vesicular Mechanism',

Cell Reports, 25(8), pp. 2027-2035.e4.

Merriam, E. B. et al. (2013) ‘Synaptic Regulation of Microtubule Dynamics in Dendritic Spines by Calcium, F-Actin, and Drebrin’, Journal of Neuroscience, 33(42),

Michel, C. H. et al. (2014) ‘Extracellular monomeric tau protein is sufficient to initiate the spread of tau protein pathology.’, The Journal of biological chemistry. 289(2),

Millet, L. J. and Gillette, M. U. (2012) ‘New perspectives on neuronal development via microfluidic environments.’, Trends in neurosciences. 35(12), pp. 752–61.

Milner, B., Corkin, S. and Teuber, H.-L. (1968) ‘Further analysis of the hippocampal amnesic syndrome: 14-year follow-up study of H.M.’, Neuropsychologia. 6(3), pp. 215–234.

Mirbaha, H. et al. (2018) ‘Inert and seed-competent tau monomers suggest structural origins of aggregation’, eLife, 7.

Mishkin, M. (1978) ‘Memory in monkeys severely impaired by combined but not by separate removal of amygdala and hippocampus’, Nature, 273(5660), pp. 297–298.

Miyamoto, T. et al. (2017) ‘Phosphorylation of tau at Y18, but not tau-fyn binding, is required for tau to modulate NMDA receptor-dependent excitotoxicity in primary neuronal culture’, Molecular Neurodegeneration. 12(1), p. 41.

Moghadam, F. H. et al. (2009) ‘Transplantation of primed or unprimed mouse embryonic stem cell-derived neural precursor cells improves cognitive function in Alzheimerian rats’, Differentiation. 78(2–3), pp. 59–68.

Mohamed, N.-V. et al. (2015) ‘Starvation and inhibition of lysosomal function increased tau secretion by primary cortical neurons’, Scientific Reports. 4(1), p. 5715.

Mondragón-Rodríguez, S. et al. (2012) ‘Interaction of Endogenous Tau Protein with Synaptic Proteins Is Regulated by N -Methyl-d-aspartate Receptor-dependent Tau Phosphorylation’, Journal of Biological Chemistry, 287(38), pp. 32040–32053.

Moreno, H. et al. (2009) ‘Synaptic transmission block by presynaptic injection of oligomeric

amyloid beta.', Proceedings of the National Academy of Sciences of the United States of America. 106(14), pp. 5901–6.

Mortimer, J. A. et al. (1985) 'Head injury as a risk factor for Alzheimer's disease.', Neurology, 35(2), pp. 264–7.

Moser, B. et al. (2017) 'Fluorescence colocalization microscopy analysis can be improved by combining object-recognition with pixel-intensity-correlation.', Biotechnology journal. 12(1).

Mosiewicz, K. A. et al. (2013) 'In situ cell manipulation through enzymatic hydrogel photopatterning', Nature Materials. 12(11), pp. 1072–1078.

Mrksich, M. et al. (1996) 'Controlling cell attachment on contoured surfaces with self-assembled monolayers of alkanethiolates on gold.', Proceedings of the National Academy of Sciences of the United States of America. 93(20), pp. 10775–8.

Mudher, A. and Lovestone, S. (2002) 'Alzheimer's disease-do tauists and baptists finally shake hands?', Trends in neurosciences, 25(1), pp. 22–6.

Mullard, A. (2019) 'Anti-amyloid failures stack up as Alzheimer antibody flops', Nature Reviews Drug Discovery. 18(327).

Murchison, D. and Griffith, W. H. (2007) 'Calcium buffering systems and calcium signaling in aged rat basal forebrain neurons', Aging Cell, 6(3), pp. 297–305.

Murer, M. G. et al. (1999) 'An immunohistochemical study of the distribution of brain-derived neurotrophic factor in the adult human brain, with particular reference to Alzheimer's disease.', Neuroscience, 88(4), pp. 1015–32.

Musleh, W. et al. (1997) 'Glycine-induced long-term potentiation is associated with structural and functional modifications of -amino-3-hydroxyl-5-methyl-4-isoxazolepropionic acid receptors', Proceedings of the National Academy of Sciences, 94(17), pp. 9451–9456.

Nagahara, A. H. and Tuszynski, M. H. (2011) 'Potential therapeutic uses of BDNF in neurological and psychiatric disorders', Nature Reviews Drug Discovery, 10(3), pp. 209–219.

Nagel, G. et al. (2002) ‘Channelrhodopsin-1: a light-gated proton channel in green algae.’, Science (New York, N.Y.). American Association for the Advancement of Science, 296(5577), pp. 2395–8.

Nagel, G. et al. (2003) ‘Channelrhodopsin-2, a directly light-gated cation-selective membrane channel.’, Proceedings of the National Academy of Sciences of the United States of America. 100(24), pp. 13940–5.

Nakamura, M. et al. (1992) ‘Specific increase in calcium-activated neutral protease with low calcium sensitivity (m-calpain) in proerythroblastic K562 cell line cells induced to differentiation by phorbol 12-myristate 13-acetate.’, Experimental cell research, 200(2), pp. 513–22.

Nakazawa, T. et al. (2001) ‘Characterization of Fyn-mediated Tyrosine Phosphorylation Sites on GluRε2 (NR2B) Subunit of the N -Methyl-d-aspartate Receptor’, Journal of Biological Chemistry, 276(1), pp. 693–699.

Needham, L.-M. et al. (2019) ‘ThX – A next-generation probe for the early detection of amyloid aggregates’, bioRxiv. p. 713594.

Neumar, R. W. et al. (2003) ‘Cross-talk between Calpain and Caspase Proteolytic Systems During Neuronal Apoptosis’, Journal of Biological Chemistry, 278(16), pp. 14162–14167.

Nishiyama, M. et al. (2000) ‘Calcium stores regulate the polarity and input specificity of synaptic modification’, Nature, 408(6812), pp. 584–588.

Nixon, Ralph A (2003) ‘The calpains in aging and aging-related diseases.’, Ageing research reviews, 2(4), pp. 407–18.

Nixon, Ralph A. (2003) ‘The calpains in aging and aging-related diseases’, Ageing Research Reviews. 2(4), pp. 407–418.

Noble, E. E. et al. (2011) ‘The lighter side of BDNF’, American Journal of Physiology-Regulatory, Integrative and Comparative Physiology, 300(5), pp. R1053–R1069.

Noble, W. et al. (2013) ‘The Importance of Tau Phosphorylation for Neurodegenerative Diseases’,

Frontiers in Neurology. Frontiers, 4, p. 83.

Nobuhara, C. K. et al. (2017) 'Tau Antibody Targeting Pathological Species Blocks Neuronal Uptake and Interneuron Propagation of Tau in Vitro', The American Journal of Pathology. Elsevier, 187(6), pp. 1399–1412.

Nowak, L. et al. (1984) 'Magnesium gates glutamate-activated channels in mouse central neurones', Nature. 307(5950), pp. 462–465.

Nyberg, T., Shimada, A. and Torimitsu, K. (2007) 'Ion conducting polymer microelectrodes for interfacing with neural networks', Journal of Neuroscience Methods. 160(1), pp. 16–25.

O'Connor, D. V., Ware, W. R. and Andre, J. C. (1979) 'Deconvolution of fluorescence decay curves. A critical comparison of techniques', The Journal of Physical Chemistry. 83(10), pp. 1333–1343.

O'Keefe, J. (1976) 'Place units in the hippocampus of the freely moving rat', Experimental Neurology, 51(1), pp. 78–109.

Oganesyan, V. et al. (2008) 'Structural characterization of a human Fc fragment engineered for lack of effector functions', Acta Crystallographica Section D: Biological Crystallography. 64(Pt 6), p. 700.

Orellana-Tavra, C. et al. (2017) 'Tuning the Endocytosis Mechanism of Zr-Based Metal–Organic Frameworks through Linker Functionalization', ACS Applied Materials & Interfaces. 9(41), pp. 35516–35525.

Ouyang, H., Nauman, E. and Shi, R. (2013) 'Contribution of cytoskeletal elements to the axonal mechanical properties.', Journal of biological engineering. 7(1), p. 21.

Ouyang, J. (2013) 'Solution-Processed PEDOT:PSS Films with Conductivities as Indium Tin Oxide through a Treatment with Mild and Weak Organic Acids', ACS Applied Materials & Interfaces. 5(24), pp. 13082–13088.

Padmanabhan, P. et al. (2019) 'Frontotemporal dementia mutant Tau promotes aberrant Fyn

nanoclustering in hippocampal dendritic spines.', eLife. Ltd, 8.

Park, D. et al. (2012) 'Human Neural Stem Cells Overexpressing Choline Acetyltransferase Restore Cognitive Function of Kainic Acid-Induced Learning and Memory Deficit Animals', Cell Transplantation, 21(1), pp. 365–371.

Park, H. and Poo, M. (2013) 'Neurotrophin regulation of neural circuit development and function', Nature Reviews Neuroscience. 14(1), pp. 7–23.

Patterson, K. R. et al. (2011) 'Characterization of prefibrillar Tau oligomers in vitro and in Alzheimer disease.', The Journal of biological chemistry. 286(26), pp. 23063–76.

Peineau, S. et al. (2007) 'LTP Inhibits LTD in the Hippocampus via Regulation of GSK3β', Neuron, 53(5), pp. 703–717.

Pérez, M. et al. (2002) 'Polymerization of τ into Filaments in the Presence of Heparin: The Minimal Sequence Required for τ - τ Interaction', Journal of Neurochemistry, 67(3), pp. 1183–1190.

Poirer, J. (2006) 'Apolipoprotein E and Alzheimer's Disease A Role in Amyloid Catabolism', Annals of the New York Academy of Sciences. 924(1), pp. 81–90.

Pollard, S. M. et al. (2006) 'Adherent Neural Stem (NS) Cells from Fetal and Adult Forebrain', Cerebral Cortex. 16(suppl_1), pp. i112–i120.

Polydoro, M. et al. (2009) 'Age-dependent impairment of cognitive and synaptic function in the htau mouse model of tau pathology.', The Journal of neuroscience : the official journal of the Society for Neuroscience. 29(34), pp. 10741–9.

Polydoro, M. et al. (2014) 'Soluble pathological tau in the entorhinal cortex leads to presynaptic deficits in an early Alzheimer's disease model', Acta Neuropathologica, 127(2), pp. 257–270.

Poole, B. and Ohkuma, S. (1981) 'Effect of weak bases on the intralysosomal pH in mouse peritoneal macrophages.', The Journal of cell biology. 90(3), pp. 665–9.

Pooler, A. M. et al. (2012) 'Dynamic association of tau with neuronal membranes is regulated by

phosphorylation', Neurobiology of Aging. Elsevier, 33(2), pp. 431.e27-431.e38.

Pooler, A. M. et al. (2013) 'Physiological release of endogenous tau is stimulated by neuronal activity', EMBO reports. 14(4), pp. 389–394.

Puzzo, D. et al. (2017) 'LTP and memory impairment caused by extracellular Aβ and Tau oligomers is APP-dependent', eLife, 6.

Qu, T. et al. (2001) 'Human neural stem cells improve cognitive function of aged brain.', Neuroreport, 12(6), pp. 1127–32.

Qureshi, H. Y. and Paudel, H. K. (2011) 'Parkinsonian neurotoxin 1-methyl-4-phenyl-1,2,3,6-tetrahydropyridine (MPTP) and alpha-synuclein mutations promote Tau protein phosphorylation at Ser262 and destabilize microtubule cytoskeleton in vitro.', The Journal of biological chemistry. 286(7), pp. 5055–68.

Ramsden, M. et al. (2005) 'Age-Dependent Neurofibrillary Tangle Formation, Neuron Loss, and Memory Impairment in a Mouse Model of Human Tauopathy (P301L)', Journal of Neuroscience, 25(46), pp. 10637–10647.

Regan, P. et al. (2015) 'Tau Phosphorylation at Serine 396 Residue Is Required for Hippocampal LTD', The Journal of Neuroscience, 35(12), pp. 4804 LP – 4812.

Reynolds, M. R., Berry, R. W. and Binder, L. I. (2005) 'Site-Specific Nitration Differentially Influences τ Assembly in Vitro †', Biochemistry, 44(42), pp. 13997–14009.

Rhee, S. W. et al. (2005) 'Patterned cell culture inside microfluidic devices', Lab on a Chip. 5(1), p. 102.

Roberson, E. D. et al. (2007) 'Reducing Endogenous Tau Ameliorates Amyloid -Induced Deficits in an Alzheimer's Disease Mouse Model', Science, 316(5825), pp. 750–754.

Roberson, E. D. et al. (2011) 'Amyloid- /Fyn-Induced Synaptic, Network, and Cognitive Impairments Depend on Tau Levels in Multiple Mouse Models of Alzheimer's Disease', Journal of Neuroscience, 31(2), pp. 700–711.

Roberts, G. W. (1988) ‘Immunocytochemistry of neurofibrillary tangles in dementia pugilistica and Alzheimer’s disease: evidence for common genesis.’, Lancet. 2(8626–8627), pp. 1456–8.

Rocher, A. B. et al. (2010) ‘Structural and functional changes in tau mutant mice neurons are not linked to the presence of NFTs’, Experimental Neurology. Academic Press, 223(2), pp. 385–393.

Rockenstein, E. et al. (2007) ‘Effects of Cerebrolysin™ on neurogenesis in an APP transgenic model of Alzheimer’s disease’, Acta Neuropathologica, 113(3), pp. 265–275.

Rozkiewicz, D. I. et al. (2006) ‘Covalent Microcontact Printing of Proteins for Cell Patterning’, Chemistry - A European Journal. 12(24), pp. 6290–6297.

Rueden, C. T. et al. (2017) ‘ImageJ2: ImageJ for the next generation of scientific image data’, BMC Bioinformatics. 18(1), p. 529.

Ruiz, R. et al. (2008) ‘Cysteine string protein-α is essential for the high calcium sensitivity of exocytosis in a vertebrate synapse’, European Journal of Neuroscience. 27(12), pp. 3118–3131.

Rusmini, F., Zhong, Z. and Feijen, J. (2007) ‘Protein Immobilization Strategies for Protein Biochips’, Biomacromolecules. 8(6), pp. 1775–1789.

Saito, K. et al. (1993) ‘Widespread activation of calcium-activated neutral proteinase (calpain) in the brain in Alzheimer disease: a potential molecular basis for neuronal degeneration.’, Proceedings of the National Academy of Sciences of the United States of America. 90(7), pp. 2628–32.

Salon, M.-C. B. et al. (2007) ‘Studies of interactions between silane coupling agents and cellulose fibers with liquid and solid-state NMR’, Magnetic Resonance in Chemistry. 45(6), pp. 473–483.

Salter, M. W. and Kalia, L. V (2004) ‘Src kinases: a hub for NMDA receptor regulation’, Nature Reviews Neuroscience. 5, p. 317.

Sanjana, N. E. and Fuller, S. B. (2004) ‘A fast flexible ink-jet printing method for patterning dissociated neurons in culture’, Journal of Neuroscience Methods. 136(2), pp. 151–163.

SantaCruz, K et al. (2005) ‘Tau Suppression in a Neurodegenerative Mouse Model Improves

Memory Function', Science, 309(5733), pp. 476 LP – 481.

SantaCruz, K. et al. (2005) 'Tau Suppression in a Neurodegenerative Mouse Model Improves Memory Function', Science, 309(5733), pp. 476–481.

Sapir, T. et al. (2012) 'Tau's role in the developing brain: implications for intellectual disability', Human Molecular Genetics, 21(8), pp. 1681–1692.

Sasi, M. et al. (2017) 'Neurobiology of local and intercellular BDNF signaling.', Pflugers Archiv. 469(5–6), pp. 593–610. doi: 10.1007/s00424-017-1964-4.

Sato, K., Saito, Y. and Kawashima, S. (1995) 'Identification and Characterization of Membrane-Bound Calpains in Clathrin-Coated Vesicles from Bovine Brain', European Journal of Biochemistry. (10.1111), 230(1), pp. 25–31.

Schenk, D. et al. (1999) 'Immunization with amyloid-β attenuates Alzheimer-disease-like pathology in the PDAPP mouse', Nature, 400(6740), pp. 173–177.

Schenk, D. (2002) 'Amyloid-β immunotherapy for Alzheimer's disease: the end of the beginning', Nature Reviews Neuroscience, 3(10), pp. 824–828.

Scheuner, D. et al. (1996) 'Secreted amyloid beta-protein similar to that in the senile plaques of Alzheimer's disease is increased in vivo by the presenilin 1 and 2 and APP mutations linked to familial Alzheimer's disease.', Nature medicine, 2(8), pp. 864–70.

Schindowski, K. et al. (2006) 'Alzheimer's Disease-Like Tau Neuropathology Leads to Memory Deficits and Loss of Functional Synapses in a Novel Mutated Tau Transgenic Mouse without Any Motor Deficits', The American Journal of Pathology. 169(2), pp. 599–616.

Schmechel, D. E. et al. (1993) 'Increased amyloid beta-peptide deposition in cerebral cortex as a consequence of apolipoprotein E genotype in late-onset Alzheimer disease.', Proceedings of the National Academy of Sciences, 90(20), pp. 9649–9653.

Schneider A. et al. (1999) 'Phosphorylation that Detaches Tau Protein from Microtubules (Ser262, Ser214) Also Protects It against Aggregation into Alzheimer Paired Helical Filaments†'.

American Chemical Society . 38(12):3549-58.

Schramm, M. and Hestrin, S. (1954) ‘Factors affecting Production of Cellulose at the Air/ Liquid Interface of a Culture of Acetobacter xylinum’, Journal of General Microbiology, 11(1), pp. 123–129.

Schwaller, B. (2010) ‘Cytosolic Ca2+ Buffers’, Cold Spring Harbor Perspectives in Biology, 2(11), pp. a004051–a004051.

Selkoe, D. J. (2002) ‘Alzheimer’s disease is a synaptic failure.’, Science. 298(5594), pp. 789–791.

Shang, S. et al. (2016) ‘Intracellular TRPA1 mediates Ca2+ release from lysosomes in dorsal root ganglion neurons.’, The Journal of cell biology. 215(3), pp. 369–381.

Sherwood, M. W. et al. (2007) ‘Activation of trypsinogen in large endocytic vacuoles of pancreatic acinar cells’, Proceedings of the National Academy of Sciences, 104(13), pp. 5674–5679.

Siwak-Tapp, C. T. et al. (2007) ‘Neurogenesis decreases with age in the canine hippocampus and correlates with cognitive function’, Neurobiology of Learning and Memory, 88(2), pp. 249–259.

van der Sluijs, P. and Hoogenraad, C. C. (2011) ‘New insights in endosomal dynamics and AMPA receptor trafficking’, Seminars in Cell & Developmental Biology. 22(5), pp. 499–505.

Sokolow, S. et al. (2015) ‘Pre-synaptic C-terminal truncated tau is released from cortical synapses in Alzheimer’s disease’, Journal of Neurochemistry, 133(3), pp. 368–379.

Sondermann, P. et al. (2000) ‘The 3.2-Å crystal structure of the human IgG1 Fc fragment–FcγRIII complex’, Nature, 406(6793), pp. 267–273.

Sorrells, S. F. et al. (2018) ‘Human hippocampal neurogenesis drops sharply in children to undetectable levels in adults’, Nature. 555(7696), pp. 377–381.

Spat, A. et al. (2008) ‘High- and low-calcium-dependent mechanisms of mitochondrial calcium signalling’, Cell Calcium, 44(1), pp. 51–63.

Sperling, R. A. et al. (2011) ‘Toward defining the preclinical stages of Alzheimer’s disease:

recommendations from the National Institute on Aging-Alzheimer's Association workgroups on diagnostic guidelines for Alzheimer's disease.', Alzheimer's & dementia : the journal of the Alzheimer's Association. 7(3), pp. 280–92.

Spruston, N. et al. (1995) 'Activity-dependent action potential invasion and calcium influx into hippocampal CA1 dendrites', Science, 268(5208), pp. 297–300.

Squire, L. R. (2012) Fundamental neuroscience.

Star, E. N., Kwiatkowski, D. J. and Murthy, V. N. (2002) 'Rapid turnover of actin in dendritic spines and its regulation by activity', Nature Neuroscience, 5(3), pp. 239–246.

Staubli, U. and Lynch, G. (1990) 'Stable depression of potentiated synaptic responses in the hippocampus with 1-5 Hz stimulation.', Brain research, 513(1), pp. 113–8.

Steiner, P. et al. (2008) 'Destabilization of the Postsynaptic Density by PSD-95 Serine 73 Phosphorylation Inhibits Spine Growth and Synaptic Plasticity', Neuron. 60(5), pp. 788–802.

Stoothoff, W. H. and Johnson, G. V. W. (2005) 'Tau phosphorylation: physiological and pathological consequences', Biochimica et Biophysica Acta (BBA) - Molecular Basis of Disease. 1739(2–3), pp. 280–297.

Südhof, T. C. (2018) 'Towards an Understanding of Synapse Formation', Neuron, 100(2), pp. 276–293.

Sulatskaya, A. I., Kuznetsova, I. M. and Turoverov, K. K. (2011) 'Interaction of Thioflavin T with Amyloid Fibrils: Stoichiometry and Affinity of Dye Binding, Absorption Spectra of Bound Dye', The Journal of Physical Chemistry B. 115(39), pp. 11519–11524.

Sullivan, T. P. et al. (2004) 'Forced Peptide Synthesis in Nanoscale Confinement under Elastomeric Stamps', Angewandte Chemie International Edition. 43(32), pp. 4190–4193.

Sultan, A. et al. (2011) 'Nuclear Tau, a Key Player in Neuronal DNA Protection', Journal of Biological Chemistry, 286(6), pp. 4566–4575.

Sun, Y. et al. (2008) 'Long-term tripotent differentiation capacity of human neural stem (NS) cells

in adherent culture', Molecular and Cellular Neuroscience, 38(2), pp. 245–258.

Suzuki, M. and Kimura, T. (2017) 'Microtubule-associated tau contributes to intra-dendritic trafficking of AMPA receptors in multiple ways', Neuroscience Letters. 653, pp. 276–282.

Sydow, A. et al. (2011) 'Tau-Induced Defects in Synaptic Plasticity, Learning, and Memory Are Reversible in Transgenic Mice after Switching Off the Toxic Tau Mutant', Journal of Neuroscience, 31(7), pp. 2511–2525.

Syntichaki, P. et al. (2002) 'Specific aspartyl and calpain proteases are required for neurodegeneration in C. elegans', Nature, 419(6910), pp. 939–944.

Tai, H.-C. et al. (2012) 'The Synaptic Accumulation of Hyperphosphorylated Tau Oligomers in Alzheimer Disease Is Associated With Dysfunction of the Ubiquitin-Proteasome System', The American Journal of Pathology, 181(4), pp. 1426–1435.

Takashima, A. (2010) 'The mechanism for tau aggregation and its relation to neuronal dysfunction', Alzheimer's & Dementia: The Journal of the Alzheimer's Association. 6(4), p. S144.

Tashiro, K. et al. (1997) 'NeuroReport : an international journal for the rapid communication of research in neuroscience.', NeuroReport. pp. 2797–2801.

Tatebayashi, Y. et al. (2002) 'Tau filament formation and associative memory deficit in aged mice expressing mutant (R406W) human tau', Proceedings of the National Academy of Sciences, 99(21), pp. 13896–13901.

Thies, E. and Mandelkow, E.-M. (2007) 'Missorting of Tau in Neurons Causes Degeneration of Synapses That Can Be Rescued by the Kinase MARK2/Par-1', Journal of Neuroscience, 27(11).

Thomas, J. A. et al. (1979) 'Intracellular pH measurements in Ehrlich ascites tumor cells utilizing spectroscopic probes generated in situ', Biochemistry. 18(11), pp. 2210–2218.

Tiwari, S. S. et al. (2015) 'Evidence that the presynaptic vesicle protein CSPalpha is a key player in synaptic degeneration and protection in Alzheimer's disease', Molecular Brain, 8(1), p. 6.

Toescu, E. C., Verkhratsky, A. and Landfield, P. W. (2004) 'Ca2+ regulation and gene expression

in normal brain aging', Trends in Neurosciences, 27(10), pp. 614–620.

Tortosa, E. et al. (2011) 'Microtubule-associated Protein 1B (MAP1B) Is Required for Dendritic Spine Development and Synaptic Maturation', Journal of Biological Chemistry , 286(47), pp. 40638–40648.

Tracy, T. E. et al. (2016) 'Acetylated Tau Obstructs KIBRA-Mediated Signaling in Synaptic Plasticity and Promotes Tauopathy-Related Memory Loss', Neuron, 90(2), pp. 245–260.

Tsang, A. W. et al. (2000) 'Altered membrane trafficking in activated bone marrow-derived macrophages.', Journal of leukocyte biology, 68(4), pp. 487–94..

Usenovic, M. et al. (2015) 'Internalized Tau Oligomers Cause Neurodegeneration by Inducing Accumulation of Pathogenic Tau in Human Neurons Derived from Induced Pluripotent Stem Cells', Journal of Neuroscience, 35(42), pp. 14234–14250.

Vanderwolf, C. . (1969) 'Hippocampal electrical activity and voluntary movement in the rat', Electroencephalography and Clinical Neurophysiology. 26(4), pp. 407–418.

Vargas-Caballero, M. et al. (2017) 'Wild-Type, but Not Mutant N296H, Human Tau Restores Aβ-Mediated Inhibition of LTP in Tau-/- mice.', Frontiers in neuroscience. 11, p. 201.

Vazquez, G. et al. (2004) 'The mammalian TRPC cation channels', Biochimica et Biophysica Acta (BBA) - Molecular Cell Research. 1742(1–3), pp. 21–36.

Verstraelen, P. et al. (2017) 'Dysregulation of Microtubule Stability Impairs Morphofunctional Connectivity in Primary Neuronal Networks.', Frontiers in cellular neuroscience. 11, p. 173.

Vladimir V. Tsukruk, *, Igor Luzinov, A. and Julthongpiput, D. (1999) 'Sticky Molecular Surfaces: Epoxysilane Self-Assembled Monolayers'. American Chemical Society. 15(9), pp.3029-3032

Vogelsberg-Ragaglia, V. et al. (2000) 'Distinct FTDP-17 Missense Mutations in Tau Produce Tau Aggregates and Other Pathological Phenotypes in Transfected CHO Cells', Molecular Biology of the Cell. 11(12), pp. 4093–4104.

Waharte, F., Spriet, C. and Héliot, L. (2006) ‘Setup and characterization of a multiphoton FLIM instrument for protein–protein interaction measurements in living cells’, Cytometry Part A, 69A(4), pp. 299–306.

Wakabayashi, T. et al. (2018) ‘pH-Tunable High-Performance PEDOT:PSS Aluminum Solid Electrolytic Capacitors’, ACS Applied Energy Materials. American Chemical Society, 1(5), pp. 2157–2163.

Wang, F. et al. (2011) ‘GDNF-pretreatment enhances the survival of neural stem cells following transplantation in a rat model of Parkinson’s disease’, Neuroscience Research, 71(1), pp. 92–98.

Wang, L. et al. (2014) ‘α-Synuclein Multimers Cluster Synaptic Vesicles and Attenuate Recycling’, Current Biology, 24(19), pp. 2319–2326.

Wang, Y.-J. et al. (2005) ‘The expression of calcium/calmodulin-dependent protein kinase II-α in the hippocampus of patients with Alzheimer’s disease and its links with AD-related pathology’, Brain Research, 1031(1), pp. 101–108.

Wang, Y. and Mandelkow, E. (2015) ‘Tau in physiology and pathology’, Nature Reviews Neuroscience. 17, p. 22.

Warmus, B. A. et al. (2014) ‘Tau-mediated NMDA receptor impairment underlies dysfunction of a selectively vulnerable network in a mouse model of frontotemporal dementia.’, The Journal of neuroscience . 34(49), pp. 16482–95.

Warren, S. C. et al. (2013) ‘Rapid Global Fitting of Large Fluorescence Lifetime Imaging Microscopy Datasets’, PLOS ONE. 8(8), p. e70687.

Washington, P. M., Villapol, S. and Burns, M. P. (2016) ‘Polypathology and dementia after brain trauma: Does brain injury trigger distinct neurodegenerative diseases, or should they be classified together as traumatic encephalopathy?’, Experimental neurology., 275 Pt 3(3), pp. 381–388.

Watanabe, K. et al. (1993) ‘A new bacterial cellulose substrate for mammalian cell culture’, Cytotechnology. 13(2), pp. 107–114.

Waterhouse, E. G. and Xu, B. (2009) ‘New insights into the role of brain-derived neurotrophic factor in synaptic plasticity’, Molecular and Cellular Neuroscience, 42(2), pp. 81–89.

Waters, J., Schaefer, A. and Sakmann, B. (2005) ‘Backpropagating action potentials in neurones: measurement, mechanisms and potential functions’, Progress in Biophysics and Molecular Biology, 87(1), pp. 145–170.

Wati, H. et al. (2006) ‘A decreased survival of proliferated cells in the hippocampus is associated with a decline in spatial memory in aged rats’, Neuroscience Letters. 399(1–2), pp. 171–174.

Weiss G.B. (1975) Stimulation with High Potassium. In: Daniel E.E., Paton D.M. (eds) Smooth Muscle. Springer, Boston, MA

Weisskopf, M. et al. (1994) ‘Mediation of hippocampal mossy fiber long-term potentiation by cyclic AMP’, Science, 265(5180), pp. 1878–1882.

Wilms, C. D. and Eilers, J. (2007) ‘Photo-physical properties of Ca^{2+} -indicator dyes suitable for two-photon fluorescence-lifetime recordings’, Journal of Microscopy, 225(3), pp. 209–213.

Wojciech K. C., et al. (2006) ‘The Future Prospects of Microbial Cellulose in Biomedical Applications’. American Chemical Society . 8(11), pp.1-12.

Wolf, S. A. et al. (2006) ‘Cognitive and Physical Activity Differently Modulate Disease Progression in the Amyloid Precursor Protein (APP)-23 Model of Alzheimer’s Disease’, Biological Psychiatry, 60(12), pp. 1314–1323.

Wu, J. W. et al. (2016) ‘Neuronal activity enhances tau propagation and tau pathology in vivo’, Nature Neuroscience. 19(8), pp. 1085–1092.

Xia, Y., Sun, K. and Ouyang, J. (2012) ‘Solution-Processed Metallic Conducting Polymer Films as Transparent Electrode of Optoelectronic Devices’, Advanced Materials. 24(18), pp. 2436–2440.

Xia, Y. and Whitesides, G. M. (1998) ‘Soft Lithography’, Angewandte Chemie International Edition. 37(5), pp. 550–575.

Xie, C. et al. (2015) ‘Identification of key amino acids responsible for the distinct aggregation

properties of microtubule-associated protein 2 and tau', Journal of Neurochemistry. 135(1), pp. 19–26.

Xu, B. et al. (2000) 'The role of brain-derived neurotrophic factor receptors in the mature hippocampus: modulation of long-term potentiation through a presynaptic mechanism involving TrkB.', The Journal of neuroscience . 20(18), pp. 6888–97.

Yamada, K. et al. (2014) 'Neuronal activity regulates extracellular tau in vivo.', The Journal of experimental medicine. 211(3), pp. 387–93.

Yanamandra, K. et al. (2013) 'Anti-Tau Antibodies that Block Tau Aggregate Seeding In Vitro Markedly Decrease Pathology and Improve Cognition In Vivo', Neuron. 80(2), pp. 402–414.

Yang, Hui et al. (2013) 'Human umbilical cord mesenchymal stem cell-derived neuron-like cells rescue memory deficits and reduce amyloid-beta deposition in an AβPP/PS1 transgenic mouse model', Stem Cell Research & Therapy, 4(4), p. 76.

Yang, J. et al. (2018) 'Bacterial Cellulose as a Supersoft Neural Interfacing Substrate', ACS Applied Materials & Interfaces. 10(39), pp. 33049–33059.

Yoshida, H. and Goedert, M. (2006) 'Sequential phosphorylation of tau protein by cAMP-dependent protein kinase and SAPK4/p38? or JNK2 in the presence of heparin generates the AT100 epitope', Journal of Neurochemistry. 99(1), pp. 154–164.

Yoshiyama, Y. et al. (2007a) 'Synapse Loss and Microglial Activation Precede Tangles in a P301S Tauopathy Mouse Model', Neuron, 53(3), pp. 337–351.

Yoshiyama, Y. et al. (2007b) 'Synapse Loss and Microglial Activation Precede Tangles in a P301S Tauopathy Mouse Model', Neuron. 53(3), pp. 337–351.

Yu, J.-Z. and Rasenick, M. M. (2006) 'Tau associates with actin in differentiating PC12 cells', The FASEB Journal, 20(9), pp. 1452–1461.

Zempel, H. et al. (2010) 'Aβ Oligomers Cause Localized Calcium Elevation, Missorting of Endogenous Tau into Dendrites, Tau Phosphorylation, and Destruction of Microtubules and

Spines', The Journal of Neuroscience, 30(36), pp. 11938 – 11950.

Zempel, H. et al. (2017) 'Axodendritic sorting and pathological missorting of Tau are isoform-specific and determined by axon initial segment architecture.', The Journal of biological chemistry. 292(29), pp. 12192–12207.

Zhang, W. et al. (2014) 'Effects of neural stem cells on synaptic proteins and memory in a mouse model of Alzheimer's disease', Journal of Neuroscience Research, 92(2), pp. 185–194.

Zhang, W. et al. (2018) 'Heparin-induced tau filaments are polymorphic and differ from those in Alzheimer's and Pick's diseases', bioRxiv. 5(8), pp. 468892.

Zhang, Y.-Q. et al. (2012) 'Identification of CSPα clients reveals a role in dynamin 1 regulation', Neuron, 74(1), pp. 136–150.

Zhang, Y. and Bhavnani, B. R. (2006) 'Glutamate-induced apoptosis in neuronal cells is mediated via caspase-dependent and independent mechanisms involving calpain and caspase-3 proteases as well as apoptosis inducing factor (AIF) and this process is inhibited by equine estrogens', BMC Neuroscience. 7(1), pp. 49.

Zhao, C., Deng, W. and Gage, F. H. (2008) 'Mechanisms and Functional Implications of Adult Neurogenesis', Cell. 132(4), pp. 645–660.

Zhou, L. et al. (2017) 'Tau association with synaptic vesicles causes presynaptic dysfunction', Nature Communications. 11(8), pp. 15295.

Zhou, Y. et al. (2018) 'Relevance of Phosphorylation and Truncation of Tau to the Etiopathogenesis of Alzheimer's Disease', Frontiers in Aging Neuroscience 6(10), pp. 27.

Yun, C. et al. (2019) 'Generating semi-metallic conductivity in polymers by laser-driven nanostructural reorganization', Materials Horizons. Royal Society of Chemistry. 6, 2143-2151

Zhu, S.-E., Yuan, S. and Janssen, G. C. A. M. (2014) 'Optical transmittance of multilayer graphene', EPL 108(1), pp. 17007.